Role of the planar polarity pathway in cognitive functions in the context of postnatal development and aging

Noémie Depret

université de BORDEAUX

THÈSE PRÉSENTÉE POUR OBTENIR LE GRADE DE

DOCTEUR DE L'UNIVERSITÉ DE BORDEAUX

ÉCOLE DOCTORALE DES SCIENCES DE LA VIE ET DE LA SANTE

Par Noémie Depret

Role of the planar polarity pathway in cognitive functions in the context of postnatal development and aging

Sous la direction de : Dr Nathalie SANS

Soutenue publiquement le 18 Novembre 2022

Membres du jury :

Pr. Marc LANDRY	Université de Bordeaux	Président
Dr. Claire RAMPON	Université de Toulouse	Rapportrice
Pr. Fadel TISSIR	Hamad Bin Khalifa University	Rapporteur
Dr. Cordelia IMIG	University of Copenhagen	Examinatrice
Dr. Nelson REBOLA	ICM Paris	Examinateur
Dr. Nathalie SANS	Université de Bordeaux	Directrice de thèse

La science, mon enfant, est faite d'erreurs, mais d'erreurs qu'il est bon de commettre, car elles mènent peu à peu à la vérité.

Jules Verne

What's the use of all this work if we don't get some fun out of this?

Rosalind Franklin

Table of contents

Acknowledgements / Remerciements

First I would like to thank Claire Rampon, Fadel Tissir, Nelson Rebola, Cordelia Imig and Marc Landry for their participation in this thesis jury and for the time they took to read the manuscript. I want to thank the Ministère de l'Enseignement Supérieur, de la Recherche et de l'Innovation (MESRI) for the 3-year PhD fellowship and the 6-months prolongation that made this work possible.

Of course, I want to thank Nathalie Sans, my PhD supervisor. From the master until now you taught me how to create, write, handle and promote a research project. Your scientific rigor and curiosity pushed me to always do my best and strive for better. I knew your door was always open to discuss experiments and ideas, despite being one of the busiest people I know. I am also grateful for the many opportunities you gave me to present my work in front of the scientific community. Thanks to you, I've become a more assured, independant and resilient scientist.

Many thanks to Mireille Montcouquiol, my second boss. I deeply value your involvement and support during these four and a half years, and our conversations helped me grow as a scientist and as a professional in general. Thank you for being here every time I needed it, especially during this last year, even if I was not officially your student. You taught me the power of clear explanations, and how a well crafted sentence can make all the difference. You are at the origin of the Vangl2 story in this lab, and I hope that this work achieves to continue what you started.

Maïté, you are the one who made me come to Bordeaux and to this lab, and I am forever grateful for it. You taught me most of what I know, from surgery to data analysis, and you passed on your love for science and your work ethics to me. You were always here to answer my questions and to help solve my problems, scientific or technical. You have been an indefectible support during the master and the PhD, and I don't know how to thank you for everything you did, from those long hours at the radial maze to our discussions around coffee and cramique. I am proud to be "une des filles de Maïté" as Nath Aubailly likes to say!

Speaking of whom, thank you Nathalie Aubailly for your endless cheerfulness and energy. Thank you for your help with the saisines and the experiments, you've been a precious help. Thank you for checking on me all the time during the late nights and for

putting up with my endless complaints about the weather (Bordeaux's heat can be tough for a northerner!).

Thank you to my blue office partners, Marie and Charlotte. Marie, you are one hell of a scientist and I really admire your strength and resilience, thank god you were here for electrophysiology! Charlotte, you are a biochemistry fairy, thank you for everything you did for the project. Thank you both for your incredible kindness and support during this last year. Thank you so much for our discussions, the serious ones and the less serious ones (between "Robiiiin ça va nous muscler les mollets" to the Bec en sabots du Nil and your sudden passion of ornithology, the choice is large), and for putting every song you know into my head! I can tell with confidence that our lunch breaks are the best in the whole Neurocampus, and I will never find better partners for blindtests and games.

Thank you to my fellow PhD students from the yellow office during those 4 years. Shri, thank you for your kindness and our conversations about data analysis and writing (and also our shared obsession with food). Eloïse, thank you for your help this past year and for those good moments spent together when you were not buried somewhere at the R+2! I am happy to have found someone that shares my passion for dark chocolate, and your geography knowledge is truly amazing. I wish you the best for the rest of your thesis. See you in a few years to make our mobile lab in St Vincent les Grenadines!

Thank you Jérôme for all the wisdom and incisive questions about the project during those 4 years. Also your talent for crosswords puzzles will forever impress me!

Thank you Sonia for your help with the cell culture experiments (and for bringing so many delicious brioches to the lab).

A big thank you to all the past members of the lab that I've met: Léa, Steve, Camille, Jen, Anne, Sybille, Stéphanie, Isa, Audrey, Arnaldo, Mehdi… It was a pleasure to learn and work with/around you.

A special thanks to Ana. You've been here for every single moment of this PhD journey and I consider you not only as a friend and colleague, but as a mentor. Since my arrival in the lab, you've been here to discuss absolutely everything (I still miss those "Good morning no?" coffees in the lunchroom). We got through all the ups and downs of this peculiar path together, and your scientific curiosity, enthusiasm and your endless energy and will pushed me to do the best science I could. Thank you for those conversations

that still continue from across the Channel, for your humor, for listening to all my complaints and ideas and for all of your advice on academia and life in general. You have been a crucial support for me, talking me through the rough patches and celebrating when it was due. I am extremely lucky to have you as a friend.

Thanks to Vasika and Nicolas, “my” students who helped me a lot for the project. Despite my initial fear of becoming a supervisor, it was a pleasure to accompany you during your first steps in the research world. I hope I didn’t scare you away from science!

I want to sincerely thank our collaborators for the project starting with Dr. Claudia Racca, who taught me everything about SBFSEM with patience and kindness. Thank you to Dr. Aline Marighetto, Dr. Azza Sellami and Dr. Shaam Al Abed for the help with the radial maze experiments, from the experimentation to the analysis and adding many ideas to the behavioural part of the project. I thank Dr. Christophe Mulle and Dr. Gael Barthet for their help on the electrophysiology part of the project. I also thank Pr. Joris de Wit who provided us plasmids for the *in vitro* experiments.

A huge thanks to the team handling the Neurocentre Magendie’s animal facilities, especially Ruby and JB who took such good care of my mice at the R+2, Melyssa who handled the reproductions, Julie and Sara. And thank you to the people of the genotyping facility of Magendie for their efficiency.

I also want to thank the people from the transcriptomic and bioinformatic facilities that helped us a lot for the project: Thierry, Hélène, Alexandre Brochard, Alexandre Favereaux and Vanessa.

I also thank the people from the Bordeaux Imaging Center especially Sébastien, Christel and Jérémie. Thank you for accommodating all my demands for my 3D reconstructions, the BIC has been my second home for quite some time!

A big thanks to all the people in the institute and in the Neurocampus with which I enjoyed Neurosocials, afterworks at a bar, parties, or just spontaneous conversations at the corridors: Imane, Dana, Lyes, Nicolas, Stéphane, Pierre-Louis, Juliette, Ha Rang, Cloé, Mario, Unai, Claudia, Sophie, Céline, Camille, Vincent, Marie, Franck, Thibault… I’m sure I’m forgetting people but it was a pleasure to be around you all this time.

Je vais passer au français pour ces derniers remerciements.

Je suis arrivée à Bordeaux il y a 4 ans et demi sans connaître personne et j'ai la chance d'avoir fait la connaissance de personnes extraordinaires que je suis fière d'appeler mes amis (et de fournir en foccacia et gâteaux !). Alexia, merci pour les restos, les cafés, les bières, merci de m'avoir transmis la passion du blind test, de me laisser casser des murs chez toi et globalement de toujours savoir quoi dire. Valentine, merci de m'avoir adoptée en master 2 alors que je débarquais juste, merci pour les dates au ciné, les grandes discussions, les pisco sours, les innombrables soirées chez toi et tant d'autres choses. Léonie, ma Vang-girl, merci pour ton déhanchement cosmique sur Just An Illusion, pour les brunchs à Toulouse, pour ta bonne humeur et ta gentillesse sans faille. Claire, merci pour les moules, les soirées au Back To et les après-midi à la piscine, et pour être un modèle de résilience et de tenacité. Thank you Paula, for your energy, your optimism and your great music tastes (I blame you for my reggeaton obsession now). Pierre F, merci d'être venu voir tous ces films avec moi, pour tous les cafés chez les Herry et pour re-découvrir l'origine des clémentines avec moi tout les quinzes jours. Pierre M, merci pour les pauses café dans le patio, merci pour ta gentillesse et ton soutien. Tom, merci pour les dîners de grands personnes et les recommandations culinaires. Louison, merci pour ton humour et tes expressions hilarantes, merci pour les pauses pendant les weekends au labo et les moments chez Alexia. Merci à Yoni, Sara, Camille, Seb, Jeremy, Alison, Marie-Lou, Jeanne… La liste est longue et j'en oublie sûrement mais je n'oublie pas les bons moments passés ensemble.

Avant la team de Bordeaux, il y a eu mes nordistes qui me soutiennent toujours de loin. Merci Lèche Mousse, Florine, Julie, Clémence, May et tous les copains du groupe Biolingues. Depuis les bancs du SN1 jusqu'aux soirées rue Solfé, vous faites partie de mes meilleurs souvenirs de fac. Vivement nos prochaines retrouvailles. Merci à mes ardennais, et surtout à Chloé, ma quoy qoyi qui partage toutes mes obsessions musicales et autres depuis le collège. Loin des yeux, près du cœur.

Je remercie du fond du cœur ma famille, qui m'a donné la liberté et l'opportunité de faire ce que je voulais et qui m'ont toujours soutenu dans mes choix. Merci pour les "encore un petit quart d'heure", merci pour tous ces moments de pause, pour les vacances, les randos, la musique, les repas, les petit colis, les appels et les messages même quand je ne prenais pas de nouvelles... Merci pour votre amour et votre soutien. Désolée de vous décevoir pour ma carrière de pâtissière itinérante, le camion de cupcakes ça sera peut être pour plus tard !

Et enfin je veux remercier Alix, sans qui j’aurais du mal à avancer. Ton soutien et ta présence à mes côtés me sont précieux et indispensables, et les mots me manquent pour exprimer ma gratitude et mon amour.

Scientific Production

Publications

- Depret N (…) Montcouquiol M & Sans N. Core PCP protein Vangl2 shapes the temporal connectivity of the hippocampal mossy fiber synapse and modulates declarative memory processes. (in preparation)

- Depret N (…) Montcouquiol M & Sans N. PCP protein Vangl2 participates in hippocampal degradation during physiological aging. (in preparation)

Posters

- The temporal connectivity of Mf and CA3 pyramidal neurons during development that determined reference memory representations is controlled by the planar cell polarity protein Vangl2. FENS 2022, Paris, France (2022)

- Core PCP protein Vangl2 shapes the temporal connectivity of the hippocampal mossy fiber synapse and modulates declarative memory processes. Neurodev Meeting, Bordeaux, France (2022)

- Core PCP protein Vangl2 shapes the maturation of the hippocampal mossy fiber synapse and modulates hippocampal-dependent memory. Neurocampus Day, Bordeaux,France (2021)

- PCP protein Vangl2 organizes hippocampal mossy fiber connectivity and structural development. Virtual Forum of the Federation for European Neuroscience (FENS) 2020

- The planar polarity protein Vangl2 is involved in the morphological development and plasticity of the DG-CA3 network in mice hippocampus. Neurotechnologies Symposium, Québec, Canada (2019)

- The planar polarity protein Vangl2 is involved in the morphological development and plasticity of the DG-CA3 network in mice hippocampus. Annual symposium of Neurocentre Magendie, Bordeaux, France (2019)

- Vangl2 controls the development of the morphological complexity of the mossy fibers buttons in mice hippocampus. Neurocampus Day, Bordeaux,France (2018)

Talks

- *Morphofunctional role of Vangl2 in the DG-CA3 circuit during postnatal development and aging*. Bordeaux Neurocampus Doctoral Research Award Day, Bordeaux, France (2022)

- *The planar cell polarity protein Vangl2 regulates the mossy fiber-CA3 connectivity in the hippocampus,* 9th annual Symposium of Neurocentre Magendie, Bordeaux, France (2022)

- *Vangl2 regulates hippocampal mossy fiber-CA3 synapse formation and morphofonctional plasticity,* Synapse and Network Day, Bordeaux, France (2021)

- *Vangl2: a key player in the morpho-functional development of hippocampal network,* Hot Topics, the internal seminars of Neurocentre Magendie, Bordeaux, France (2019)

- *The planar polarity protein Vangl2 is involved in the morphological development and plasticity of the DG-CA3 network in mice hippocampus,* Flash Talk, Neurotechnologies Symposium, Québec, Canada (2019)

List of abbreviations

Aβ	β-amyloid
AD	Alzheimer’s disease
AMPAR	α-amino-3-hydroxy-5-methyl-4-isoxazolepropionic acid receptor
Ankrd6	Ankyrin Repeat Domain 6
APP	β-amyloid precursor protein
ASD	Austim Spectrum Disorder
AZ	Active zone
CA	*Cornus Ammonis*
cAMP	Cyclic adenosine monophosphate
Celsr	Cadherin EGF LAG seven-pass G-type receptor
CE	Convergent extension
CNS	Central nervous system
Cter	C-terminus
Ctl	Control
DCX	Doublecortin
DG	Dendate gyrus
Dia	Diaphanous
DIV	Days in vitro
DS	Down syndrom

Dsh/Dvl	Dishevelled
EE	Enriched environment
E(x)	Embryonic day (x)
ECM	Extracellular matrix
EPSC	Excitatory Post-Synaptic current
Fmi	Flamingo
Fz/Fzd	Frizzled
GABA	Gamma-Aminobutyric Acid
GAG	Glycosaminoglycan
GC	Granule cell
GPC4	Glypican
GPR158	G-protein-coupled receptor 158
HC	Hair cell
HF	High frequency
HSPG	Heparan sulfate proteoglycan
ID	Intellectual disability
IN	Interneuron
ITI	Inter-trial interval
JNK	c-Jun NH2-terminal Kinase
KCl	Potassium chloride
KAR	Kainate receptor

KCl	Potassium chloride
kDa	Kilodalton
KO	Knockout
Lp	Looptail
LTD	Long term depression
LTP	Long term potentiation
MF	Mossy fiber
MFB	Mossy fiber bouton
MFB/TE	Mossy fiber bouton/Thorny excrescense
mGlur	Metabotropic glutamate receptor
MMP	Matrix-metalloproteinase
MTLE	Mesial temporal lobe epilepsy
Mwh	Multiple Wing Hairs
MWM	Morris Water Maze
NMDAR	N-methyl-D-aspartate receptor
mRNA	Messenger RNA
mV	Milivolts
Nter	N-terminus
NTD	Neural tube disorder
OC	Organ of Corti
P(x)	Postnatal day (x)

PC	Pattern completion
PCP	Planar cell Polarity
PDZ	PSD95/ Dlg1/ ZO-1
PDZ-BDM	PDZ - Binding Domain Motif
Pk	Prickle
PPR	Pair-pulse ratio
RM	Reference memory
SBFSEM	Serial block face scanning electron microscopy
Sl	*stratum lucidum*
Sr	*stratum radiatum*
Sm	*stratum moleculare*
Vang	Van-gogh protein
Vangl	VANGL planar cell polarity protein 2
WM	Working memory
WT	Wild-type
Wnt	Wingless

Abstract

Lack of knowledge on the mechanisms of development and function of the central nervous system are slowing our efforts to take care of people suffering from cognitive disorders. Understanding those mechanisms and their role in the modification of neuronal and synaptic properties induced by the environment during life and aging is therefore necessary.

My PhD research project tackles this issue through the study of the planar cell polarity protein Vangl2, which is known to regulate cytoskeleton dynamics during development. I study the role of this protein in the hippocampus, a cerebral structure involved in episodic memory and context discrimination, which is known to be affected in some cognitive disorders. Preliminary data from the lab showed that Vangl2 is enriched postnatally in the network formed by 2 sub-regions of the hippocampus: the dentate gyrus and the CA3. My work shows that Vangl2 plays a crucial role in the development and maintenance of a specific synaptic connection in this network: the synapse formed between the granular cell of the DG and the pyramidal neurons of the CA3. Using a mice model for an early deletion of Vangl2 and techniques of virus injections and microscopy, I show that the early loss of Vangl2 delays the development of the synapse and affects its structural plasticity in adults. Using behavioural experiments, I show that the early loss of Vangl2 induces defects in some memory processes involving the hippocampus in adult mice. Interestingly, data in aging mutant mice show that the early loss of Vangl2 in the hippocampus has protective effects against the functional and morphological degradation of the DG/CA3 network linked to aging.

These results show the importance of Vangl2 in the morphofunctional properties of the DG/CA3 network across development and aging and establish a link between the planar cell polarity pathway, the synaptic development and function in the hippocampus, and cognitive processes through life.

Keywords : hippocampus, memory, planar polarity, plasticity, cognitive processes

Résumé

La mauvaise compréhension de la formation et du fonctionnement du système nerveux central nous freine dans la prise en charge des troubles cognitifs. Comprendre ces mécanismes et comment ils modifient les propriétés des neurones et de leurs synapses en fonction de l'environnement et de l'âge est donc essentiel.

Mon projet aborde cette problématique par l'étude originale de la protéine de la voie de la polarité planaire cellulaire (PCP) Vangl2, qui régule les dynamiques du cytosquelette pendant le développement et participe à la morphogenèse de nombreux tissus. J'étudie son rôle dans le circuit hippocampique, structure cérébrale impliquée dans la mémoire épisodique et la discrimination de contexte, dont le dysfonctionnement entraine des troubles cognitifs. Je montre que Vangl2 joue un rôle dans le développement et le maintien d'une connexion spécifique au sein de l'hippocampe : la synapse formée entre les cellules granulaires du DG et les neurones pyramidaux du CA3. A l'aide d'un modèle murin de délétion précoce de Vangl2 et de techniques d'injections virales et d'imagerie, je montre que l'absence de Vangl2 retarde le développement de la synapse et affecte sa plasticité structurale chez l'adulte. De plus, à l'aide de tests comportementaux, je montre que l'absence de Vangl2 induit des troubles de certains processus mnésiques hippocampaux dépendant chez la souris adulte. Mes résultats préliminaires montrent également un rôle de Vangl2 dans les effets du vieillissement physiologique sur le circuit DG/CA3, avec un potentiel effet protecteur de la délétion précoce de vangl2 vis à vis des altérations morphofonctionelles dues au vieillissement.

Les résultats obtenus au cours de ce projet de thèse permettent donc d'établir un premier lien entre la voie de la PCP, le développement et la fonction synaptique de l'hippocampe, et la régulation des processus cognitifs au cours de la vie.

Mots clés : hippocampe, mémoire, polarité planaire, plasticité, processus cognitifs

Chapter I : Introduction

1- Hippocampus

1.1- Anatomy of the hippocampus

Spatial organization of the hippocampus

First mention of the hippocampus as a brain structure dates back to 1564, when the Bolognese anatomist Julius Caesar Aranzi compared its curved shape to a seahorse (from the Greek ιππος = horse, and καμπος = sea monster). The anatomy of the hippocampus was reported in the famous drawings of neuroanatomists Camillo Golgi and Santiago Ramón y Cajal in 1903 and 1911 respectively (Golgi, 1903; Ramon y Cajal, 1911). Their works depict the peculiar organization of hippocampal connectivity, and Ramón y Cajal, who described with great precision the dendritic and axonal projections and the spines, even hypothesized a functional circuit that is still relevant to today's studies.The hippocampus is a bilateral brain structure located in the medial temporal lobe. It is composed of several sub-regions like the dentate gyrus (DG), the *cornus ammonis* regions (CA1, CA2 and CA3). These regions are highly interconnected and with the other brain structures linked to the hippocampus such as the entorhinal cortex, the amygdala or the subiculum, they form the hippocampal formation. In mammals, both hippocampi are linked by a fibrous structure, the hippocampal commissure, which is located under the corpus callosum linking the brain hemispheres.

On top of the different sub-regions, the hippocampus is also organized through three axes: the dorso-ventral axis (also called antero-posterior axis in primates), the proximo-distal axis (also called transverse axis) and the superficial-deep radial axis. Inside a subregion, the connectivity and physiology will change along those two axes, resulting in different functional consequences **(Figure 1)** (reviewed in Fanselow and Dong, 2010; Moser and Moser, 1998). The most prominent distinction that can be made is between the ventral hippocampus and the dorsal hippocampus. The dorsal hippocampus performs primarily cognitive functions while the ventral hippocampus is more involved in mood regulation and emotional response. This is supported by differences in the afference received by the two regions (mainly dorsolateral entorhinal cortex for the dorsal hippocampus; ventromedial entorhinal cortex, amygdala and prelimbic cortex for the ventral hippocampus) as well as their projections. The dorsal hippocampus projects to the retrosplenial area (RSP) of the anterior cingulate cortex, to the ventral tegmental area

(VTA) via the septum as well as to the ventral hippocampus. On the other hand, the medial prefrontal cortex (mPFC), hypothalamus, amygdala, bed nucleus of the stria terminalis (BNST), and the VTA via the nucleus accumbens (nACC). All of these regions are involved in fear response, anxiety and motivation, explaining the role of ventral hippocampus activity in emotional response. Differences in gene expression between the dorsal and the ventral hippocampus have also been reported throughout development, allowing the definition of a shifting molecular signature along the dorso-ventral axis (Lee et al., 2017; O'Reilly et al., 2015). Another interesting difference: studies suggest that dorsal and ventral hippocampal structures are differently impacted during aging and in pathology. The dorsal hippocampus seems to be more impacted by aging-related changes in connectivity and function than the ventral hippocampus (Reichel et al., 2017; Schreurs et al., 2017).

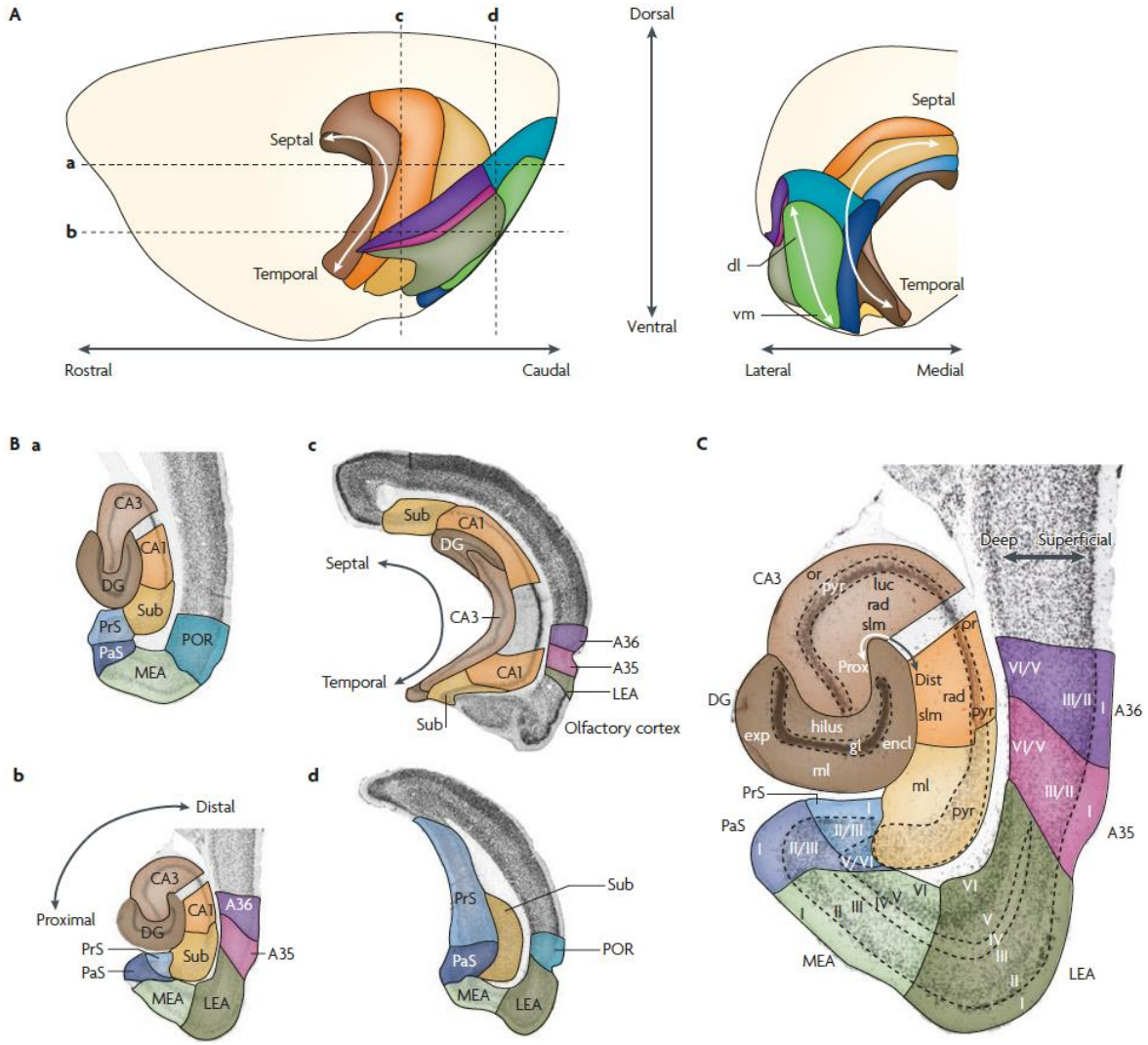

Figure 1: Detailed representation of the rat hippocampus. **(A)** Lateral and caudal views. Three axes are indicated for orientation in the hippocampal formation: the dorsoventral axis, the proximodistal axis,and the

radial axis. In the parahippocampal region, a similar superficial-to-deep axis is used. Additionally, the presubiculum and parasubiculum are described by a septotemporal and proximodistal axis. The entorhinal cortex, which has a lateral and a medial aspect, is described by a dorsolateral-to-ventromedial gradient and a rostrocaudal axis. The perirhinal cortex and the postrhinal cortex share the latter axis with the entorhinal cortex and are additionally defined by a dorsoventral orientation. The dashed lines in the left panel indicate the levels of two horizontal sections (a,b) and two coronal sections (c,d), which are shown in part B. All subfields of the parahippocampal–hippocampal region are colour-coded : dentate gyrus (DG; dark brown), CA3 (medium brown), CA1 (orange), the subiculum (Sub; yellow), presubiculum (PrS; medium blue), parasubiculum (PaS; dark blue), entorhinal cortex (LEA; dark green and MEA; light green), perirhinal cortex (consisting of Brodmann areas (A) 35 (pink) and 36 (purple)), postrhinal cortex (POR; blue-green). **(B-C)** A Nissl-stained horizontal cross section (enlarged from part Bb) in which the cortical layers and three-dimensional axes are marked. The Roman numerals indicate cortical layers. CA, *cornu ammonis*; dist, distal; dl, dorsolateral part of the entorhinal cortex; encl, enclosed blade of the DG; exp, exposed blade of the DG; gl, granule cell layer; luc, *stratum lucidum*; ml, molecular layer; or, *stratum oriens*; prox, proximal; pyr, pyramidal cell layer; rad, *stratum radiatum*; slm, *stratum lacunosum-moleculare*; vm, ventromedial part of the entorhinal cortex. Adapted from van Strien et al., 2009.

Compared to the cerebral cortex, which has a characteristic anatomical organization in 6 layers, the neuronal cells in the hippocampus are organized in a simpler 3-layers architecture. The deepest layer contains afferent and efferent axonal projections, as well as interneurons. In the DG it is called the hilus, while it is called the *stratum oriens* in the CA regions. The layer above it contains the principal excitatory cells and some inhibitory interneurons, it is known as the granule cell layer in the DG and as the *stratum pyramidale* in the CA regions. In the DG, the granule cell layer is divided in two, with the addition of the subgranular zone where the progenitor cells involved in adult neurogenesis can be found. The most superficial layer contains the dendritic ramifications of the principal cells and is called the *stratum moleculare* in both DG and CA regions. In the CA regions, the *stratum moleculare* is divided into three: the *stratum lucidum* (found only in the CA3 region), *stratum radiatum* and *stratum lacunosum*. Similarly, the *stratum moleculare* in the DG is divided into the outer-, middle- and inner-molecular layers. The frontier between the CA layers and the DG layers is called the hippocampal sulcus (Chauhan et al., 2021). In the CA3 region, on top of the radial layers, there is also a transversal subdivision defining the CA3a (closer to the CA2), CA3c and CA3c (close to the hilus). These regions have different connectivity patterns, such as the absence of recurrent connections and the presence of back-connections to the DG in the CA3c. Along those connective specificity, the different subregions of the CA3 are involved in different behavioral functions (reviewed in Kesner, 2013).

Cellular diversity in the hippocampus

With more than 600 000 cells in mice, the hippocampus is a place of great cellular diversity (Attili et al., 2019). Many studies have reported a wide variety of neuronal and glial subtypes in the different hippocampal subregions, differing in their morphological and physiological properties. We will briefly summarize the different types of cells classically found in the healthy adult rodent hippocampus.

Excitatory neurons in the hippocampus can be divided into two principal categories: pyramidal cells, which are found in the CA regions, and granule cells, found in the DG (Spencer and Bland, 2019). Pyramidal cells get their names from the distinctive shape of their cell body, from which apical and basal dendritic trees emerge. Pyramidal neuron's orientation is homogeneous across substructures, with their basal dendrites and axons projecting in the *stratum oriens* and their apical dendrites projecting to the *stratum radiatum*. However many differences exist between CA1, CA2 and CA3 pyramidal neurons, in terms of morphology (smaller cells bodies in the CA1 than in the CA3), molecular signature, connectivity (presence of complex dendritic spines in the CA3 and not in the CA1 and CA2) and functional properties (lower resting potential in CA2 than CA3). Such discrepancies exist also along the different hippocampal axes defined previously (reviewed in Cembrowski and Spruston, 2019). A good example is the differences between the pyramidal neurons of the CA3a, CA3b and CA3c regions with a gradient of excitability from the CA3c to the CA3a, and the absence of recurrent synapses in the CA3c (Sun et al., 2017). Granule cells have small circular cell bodies, an arborized apical dendritic tree that projects into the *stratum moleculare* and an axonal projection called mossy fiber. Discrepancies between granule cells can be found along the radial axis of the DG, notably in terms of maturation which will be discussed in the sections 1.2 and 1.3. To be noted, the hilus of the DG also contains excitatory neurons called mossy cells that project back to the granule cells.

The hippocampus is also characterized by a great variety of GABAergic inhibitory interneurons (IN) scattered throughout the different regions. They are involved in feedforward and feedback regulation mechanisms of the synaptic transmission and their variability might be key in fitting the computational needs for appropriate cognitive responses in different situations. Currently, 29 different types of IN have been identified in the CA1 region based on their morphology, functional properties, molecular signature

developmental origin and connectivity (reviewed in Booker and Vida, 2018). Contrary to pyramidal cells, hippocampal INs have very diverse morphological properties, with as many as 16 morphological types identified in the CA1 (Parra et al., 1998). One commonality is that IN contact mainly local cells, and their dendritic and axonal prolongation are rarely spreading outside of their local area. Regarding connectivity, hippocampal IN can be divided into different categories depending on which structure they project. It has been extensively reviewed by Booker and Vida in 2018 and Pelkey et al. in 2017. Perisomatic IN are the most common such as basket cells that project onto the soma and perisomatic dendritic region of pyramidal neurons, and axo-axonic IN that project onto the axon initial segment. Dendritic IN project onto the dendrites of pyramidal neurons and other IN and can project their axons to contact long-range targets. Among them are SOM expressing IN, and CCK expressing IN. A large set of CR and/or VIP expressing IS-INs form a unique niche among INs, as they selectively inhibit other INs. These different types of projections allow for specific inhibition onto specific pathways and fine spatial and temporal regulation of circuit response depending on the demand.

Glial cells are also a big part of the hippocampal circuits. They participate in the shaping and maintenance of synaptic connections. Astrocytes are the most numerous glial cells in the hippocampus, with up to 25 000 cells. They can be GFAP or S100β reactive. In healthy conditions, they participate to synaptic transmission and also have a support role to neuronal cells. Microglial cells are less numerous than astrocytes, with an average of 5000 cells. They display a very ramified morphology when in their quiescent state. On top of their primary function in “silent” clearing of the healthy brain and immune response in pathological context, microglia also has a developmental role in the hippocampus. During development they participate in the refinement of synaptic connectivity via some pruning mechanisms and are also involved in adult neurogenesis in the DG (Gemma and Bachstetter, 2013). Astrocytes and microglial cells are dispersed quite evenly throughout the hippocampus. The last type of glial cells found in the hippocampus are oligodendrocytes, which myelinate the axons to facilitate signal transmission. Three types of oligodendrocytes have been described in the hippocampus based on their morphology. Ramified oligodendrocytes have the most numerous processes, the largest cell body, occupy the largest area and form beaded-like structures, due to mitochondria aggregates, along the processes. Stellar-shaped oligodendrocytes have smaller cell bodies and their processes cover a significantly smaller area. Those of the smooth subtype have a small

cell body with at most two processes. The oligodendrocytic density varies depending on the hippocampal region with the highest density found in the hilus. There are also specific subtypes enrichment depending on the layer as reported by Vinet et al. in 2010.

Trisynaptic circuit

The most studied circuit in the hippocampal formation is the trisynaptic pathway forming the cortico-hippocampo-cortical circuit **(Figure 2)** (Yeckel and Berger, 1990). It is composed of the perforant pathway, the mossy fiber pathway and the Schaffer collateral pathway. The perforant pathway is formed by the axonal projections from the layers II/III of the entorhinal cortex that form excitatory synapses onto the granule cells of the DG. The mossy fiber pathway forms the connection allowing the transmission of information between the DG and the CA3 and will be described in length later in section 2.2. Lastly, the CA3 pyramidal neurons project onto the pyramidal neurons of the CA1 via the Schaffer collaterals. The loop is completed with the axonal projections of the CA1 back onto the layer V of the entorhinal cortex via the subiculum (Blackstad and Kjaerheim, 1961). The CA3 also forms non canonical projections onto other CA3 cells called recurrent synapses, as well as contralateral projections onto the CA1 and CA3 of the other hemisphere (Knierim, 2015; Lin et al., 2021; Witter et al., 2017).

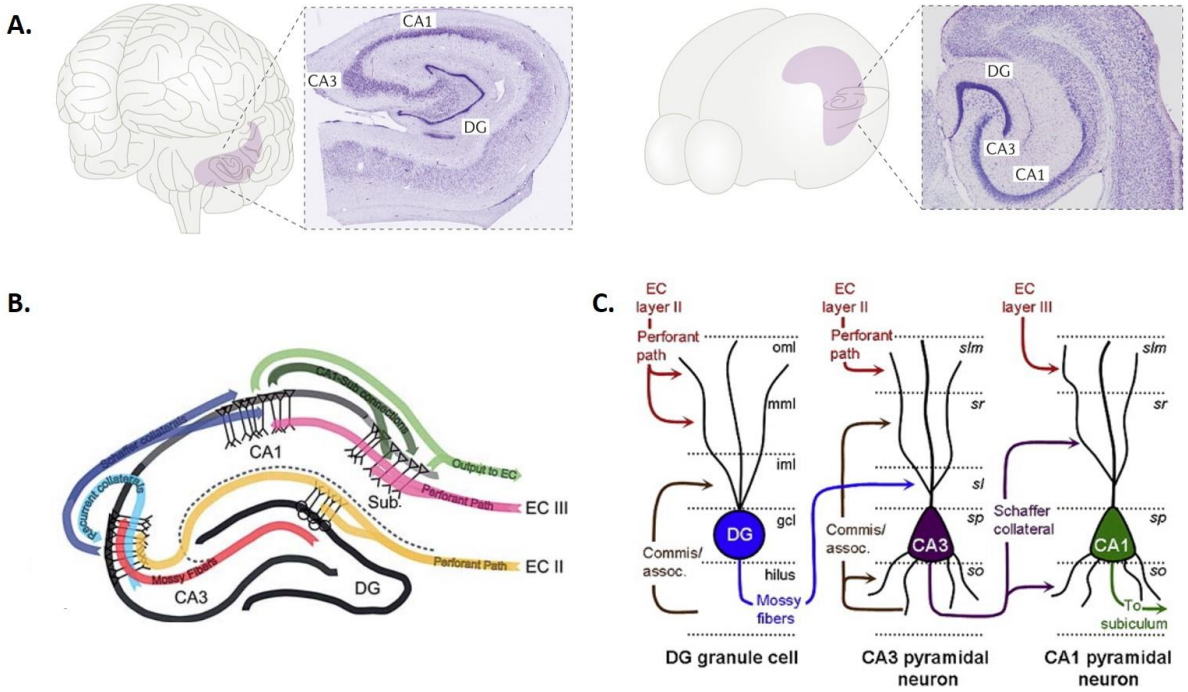

Figure 2: Anatomy of the hippocampus. **(A)** Nissl-stained section through the human hippocampus and the mouse hippocampus. **(B)** The traditional trisynaptic pathway comprising the entorhinal-dentate

perforant path synapse (yellow and pink), the dentate gyrus (DG)-*cornu ammonis* CA3 mossy fiber synapse (red), and the CA3-CA1 Schaffer synapse (navy). Also indicated are the strong intrinsic CA3 auto-associational connections (blue) as well as the subiculum and CA1 and subicular projections to the EC (green). **(C)** Representation of the projections of the principal hippocampal cells throughout hippocampal layers. Abbreviations: commis/ assoc.: commissural/associational input; DG: dentate gyrus; EC: entorhinal cortex; gcl: granule cell layer; iml: inner molecular layer; mml: middle molecular layer; oml: outer molecular layer; sl*: stratum lucidum*; slm: *stratum lacunosum/moleculare*; so: *stratum oriens*; sp: *stratum pyramidale*; sr: *stratum radiatum*. (Adapted from Hainmueller and Bartos, 2020; Hara and Morrison, 2014; Witter et al., 2017).

1.2- Neurogenesis and development

Hippocampal development spans from early embryonic stages to the perinatal period in rodents, and well into adolescence in humans. This section will address the mechanisms leading to the formation of a mature hippocampal structure in mice, focusing on the DG and the CA3 regions **(Figure 3)**.

The formation of the hippocampus happens in the dorso-medial region of the telencephalon, starting at E8.5. The formation pattern of the future hippocampus is dictated by the numerous morphogenetic factors secreted by the cortical hem (Khalaf-Nazzal and Francis, 2013). Expression of genes from the Wnt family, such as Wnt3a, Wnt5a and Wnt2b, is essential to the correct formation of the hippocampus and alteration of their expression leads to altered cell proliferation and specification (Lee et al., 2000). In rodents, hippocampal postmitotic neurons are mainly produced from E10 to E18 in the neuroepithelium of the ventricular zone neighboring the cortical hem. Most of the cells produced in the early stages of this period (E10-E16) will form the CA regions, while the neurons forming the DG are mainly produced later (E16-E18) (Angevine Jr., 1965; Bayer, 1980). The hippocampal neurons then undergo different phases of migration, which varies depending on the subregion.

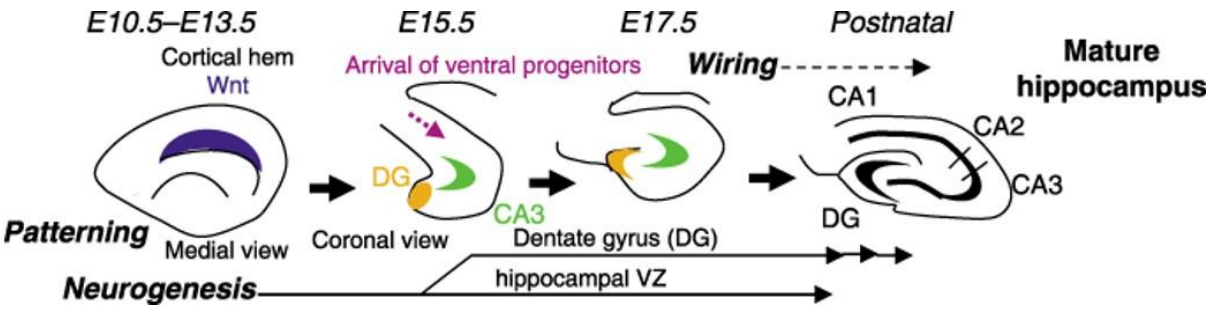

Figure 3: Developmental steps during the formation of the hippocampus. Patterning of the hippocampus is regulated by Wnt signaling (purple) as early as E10. Progenitor cells in the hippocampus ventricular zone migrate to become hippocampal pyramidal neurons to form CA3 (green). At around E15.5, a subtraction of

the progenitor cells migrates to form prospective DG (orange) and differentiates to become granule cells at early postnatal weeks.(Adapted from Iwata and Hevner, 2009).

Studies have demonstrated that CA3 neurons possess a specific molecular signature present from neurogenesis and sustained in adults, allowing their identification very early during hippocampal development. CA3 pyramidal cells specifically express KA1 and Py antigen (Grove and Tole, 1999).The CA3 pyramidal cells are generated from E11, with a peak of neurogenesis at E15 (Bayer, 1980). They leave the ventricular zone and stay in pause in the intermediate zone for 5 days before starting to acquire their pyramidal shape and migrating to their final position in the *stratum pyramidale* (Nakahira and Yuasa, 2005). The reason underlying this delay of migration of the CA3 pyramidal cell might be that the cells wait in order to coordinate with DG granule cells, which are generated later, in order to facilitate the connection of those 2 regions during postnatal development (Altman and Bayer, 1990). Indeed, it has been shown neurons preferentially connected other cells with similar neurogenesis windows, even if they were generated in other subregions (Deguchi et al., 2011). The radial position of pyramidal cells in the sp depend on their generation and migration timing, the pyramidal cells born early constituting the deepest layer of the *stratum pyramidale* while the lastest born cells are in the superficial layer in an “inside-out” lamination process. Once the pyramidal cells of the CA3 have reached their final position, they continue to undergo maturation during the postnatal period, notably via the establishment of the DG-CA3 connectivity in the *stratum lucidum* which will be discussed in the section 2.3.2. The CA3 is considered mature by P23, where adult-like markers are starting to be expressed (Lee et al., 2017) .

DG cells are initially generated in a specific part of the ventricular zone located next to the fimbria, from progenitors called radial glial cells which specifically express the transcription factors Sox2 or Pax6. Starting at E10, these radial glial cells can differentiate in either a progenitor cell or into an immature neuron with a peak of neurogenesis around E16. The migration of the newly generated cells to the future DG happens in two steps : first the progenitors and immature neurons migrates to form the hilus and the supra-pyramidal blade of the DG which becomes visible around E18, then later the migration flux is reoriented and the cells will accumulate to form the infra-pyramidal blade of the DG (Rickmann et al., 1987). During the first postnatal days, the progenitors that have migrated to the DG continue to differentiate and generate new granule neurons to finish the formation of the DG blades. Around P3, they relocate to form the subgranule cell layer

directly under the granule cell layer. Interestingly the organization of the granule neurons in the granule cell layer follows a “outside-in” pattern opposite to the “inside-out” one observed in the *stratum pyramidale* of the CA regions, with the “oldest” neurons located in the superficial layer while the “newest” neurons are in the deeper layers (Hayashi et al., 2015). The maturation period of the granule neurons of the DG continues until P28, during which they develop their dendritic tree and their axonal projections.

1.3- Adult neurogenesis

The hippocampus is one of the only brain structures capable of producing new neurons at the adult stage via a process called adult neurogenesis (reviewed in Abrous et al., 2005; Altman and Das, 1965; Jin, 2016).The generation of a newborn neuron through adult neurogenesis can take up to 7 weeks, from their exit from the proliferative phase to the final integration of the neuron in the DG network **(Figure 4)** (reviewed in Ehninger and Kempermann, 2008; Gonçalves et al., 2016).

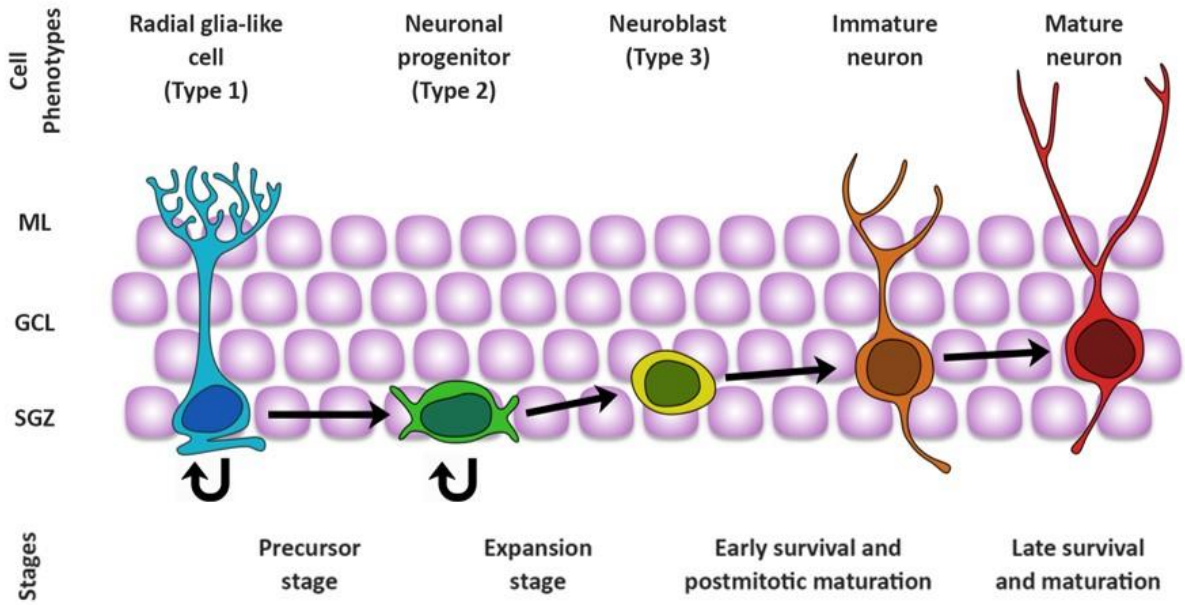

Figure 4: Schematic representation of neuronal differentiation during adult hippocampal neurogenesis. ML: molecular layer; GCL: granule cell layer; SGZ: subgranular zone. (Adapted from Kozareva et al., 2019).

The process starts with a precursor cell phase during which the pool of cells that can differentiate into mature neuronal and glial cells increases greatly. Type I neural stem cells located in the subgranular layer of the DG proliferate and form type II neural progenitor cells that will, in turn, form type III progenitors also called neuroblasts that can turn into new neurons or glial cells. During this phase, the molecular signature of the

different progenitors switch during this division/proliferation process, allowing their identification. Once the neuroblasts have exited the cell cycle and differentiated into postmitotic neurons, they start migrating up in the DG and undergo a maturation phase during which they acquire their morphological and functional properties. During the first 3 weeks of this maturation phase, they will establish their dendritic arborization in the molecular layer and their axonal projection towards the CA3 (Hastings and Gould, 1999). During this period, the pool of newborn neurons also undergo a selection phase, where a large proportion of those neurons die (Tashiro et al., 2006). After that, they develop their dendritic spines and start receiving afferences around 4 weeks after the start of the maturation period, completing their integration in the network as newborn granule cells (Toni and Schinder, 2016; Zhao et al., 2006). Adult-born neurons are thought to be important for memory formation, especially for context discrimination (Tronel et al., 2012). Enhancement or alteration of adult neurogenesis in rodents have been shown to impact the behavioural performance of the animals (Dupret et al., 2008; Lods et al., 2021; Nakashiba et al., 2012). Reciprocally, integration of newborn granule cells in the network is accelerated by learning (Gould et al., 1999; Tronel et al., 2010). In summary, adult neurogenesis is a very important process in the hippocampal formation which has a great functional and behavioural significance. We will come back to adult neurogenesis in the context of our structure of interest, the mossy fiber synapse, in a subsequent section.

1.4- Role in memory

Memory is a fascinating subject that has been at the center of many studies across the centuries. It encompasses different types of processes that have been determined by their temporality, the nature of information that are treated and their expression. Different subtypes of memory involve different kinds of processes and different cerebral structures **(Figure 5)**. Nowadays, it is widely accepted and demonstrated that the hippocampus and other associated structures of the medial temporal lobe play a key role in the encoding and retrieval of certain types of memory. In this section, I will briefly summarize the different roles of the hippocampus in memory formation, consolidation and recall, with a focus on the dorsal hippocampus, as it is our structure of interest.

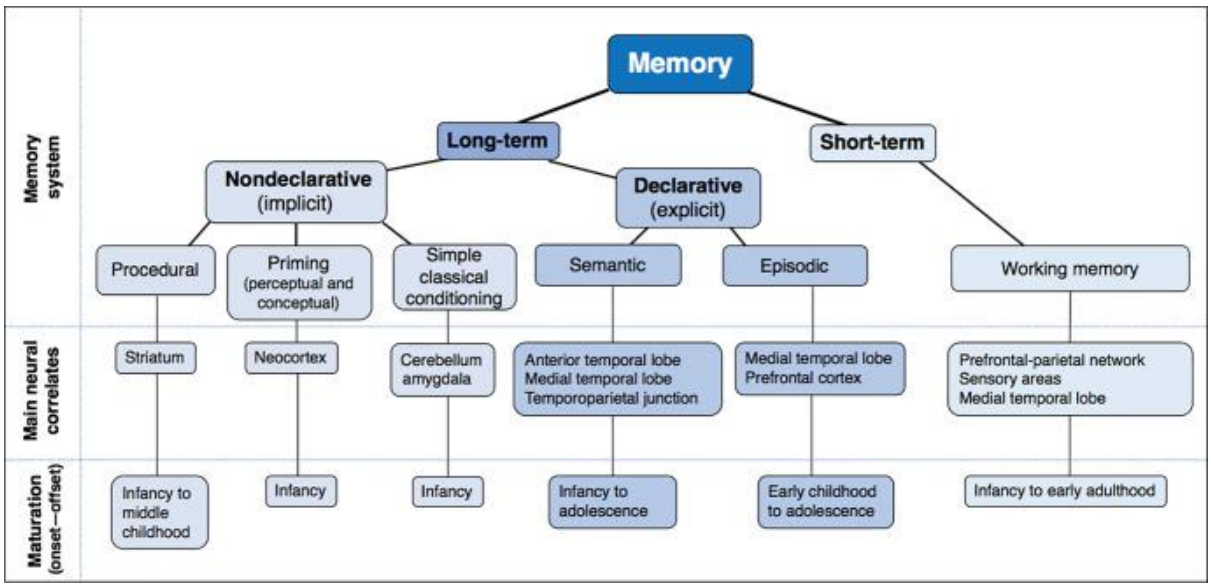

Figure 5: Classification of the different types of memory in humans. From Bouyeure and Noulhiane, 2020, adapted from a taxonomy model from Squire and Zola, 1996.

Long-term memory, pattern completion and pattern separation

Long-term memory allows the storage of information over a long time period (from hours up to years) with virtually no limit of storage capacity. Long-term memory is divided into declarative and nondeclarative memories. Non-declarative memory is not conscious and can't be verbalized, but is expressed through the performance of an action or a skill learned by experience. An example of it is procedural memory (for example: tying your shoelaces, writing) which relies on the striatum, the cerebellum and basal ganglia. On the contrary, declarative memory concerns general facts and personal information that can be consciously retrieved and verbalized. The recollection of general facts without ties to personal experience ("the hippocampus is involved in memory") is called semantic memory. The recollection of associative memories tied to the spatial and temporal context of personal experiences ("to go to the bakery, I have to turn left then walk 2 minutes") is called episodic memory (Tulving, 2002). In humans, studies such as the famous H.M case demonstrated that damage to the hippocampal formation led to the inability to form and store new episodic memories, indicating the necessity of the hippocampal integrity for the encoding and retrieval of declarative memory (Scoville and Milner, 1957). Similar results were obtained in a variety of animal models, where spatiotemporal episodic-like memory performances were altered when the hippocampus was damaged (Chiba et al., 1994; Eichenbaum, 1999; Etchamendy et al., 2003; Kesner and Novak, 1982).

In humans declarative memory can be easily evaluated. However, in animal models, the inability to communicate makes the evaluation process obviously different. One of the expressions of declarative memory in animal models that can be evaluated is spatial memory. Spatial processing has been tightly associated with the hippocampus since the discovery of “place cells”, which are ensembles of cells in some hippocampal subregions that fire specifically in particular locations and this firing pattern is conserved for long periods of time (O’Keefe and Dostrovsky, 1971; Thompson and Best, 1990). The evaluation of declarative memory is mostly done via the evaluation of the spatial and the temporal components using spatial tasks such as the Y maze, the Morris water maze (MWM) or the radial maze for rodents (Kraeuter et al., 2019; Vorhees and Williams, 2014). Alterations of spatial learning and memory in WMW have been reported in animal models with hippocampal damage (Moser et al., 1995). In spatial memory and reference memory tasks in the radial maze, hippocampal lesions have also been correlated to altered performances (Brayda-Bruno et al., 2013; Kesner and Novak, 1982).The associative aspect of episodic-like memory can also be studied with a classic fear conditioning paradigm, which relies on pavlovian conditioning by associating contextual and cued stimuli with a light footshock. Studies with hippocampal lesions show that the hippocampus participates in the contextual conditioning only (Phillips and LeDoux, 1992).

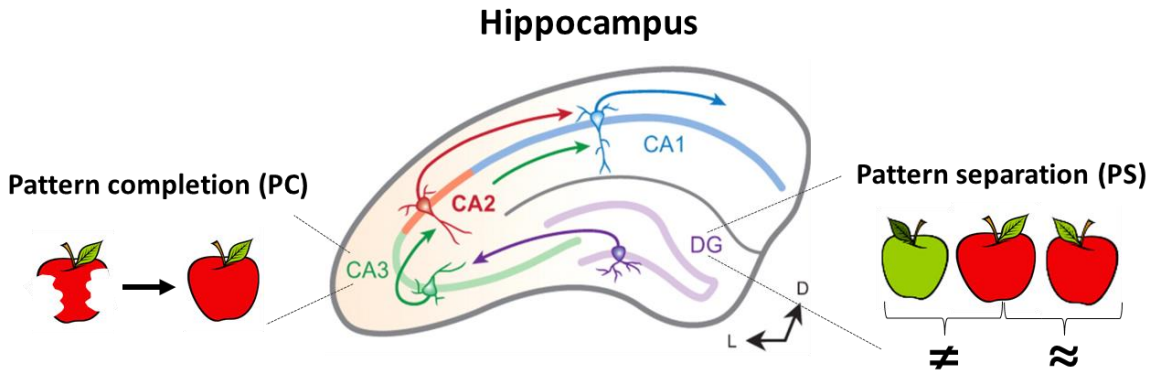

Figure 6: Schematic representation of pattern separation (PS) and the pattern completion (PC) processes. Mechanistically, the PS is mostly supported by the DG whereas the PC mainly relies on the CA3 area. The PS enables the discrimination of one memory from a very similar one and the PC allows the “reconstruction” of a memory from partial sometimes information.

Specific encoding and recalling roles have been associated with the DG and CA3 subregions of the hippocampus. Indeed, computational theories suggest that in order to allow the retrieval of complete information from the activation of a small number of cells,

the hippocampus has to carry out two competitive and complementary processes, called pattern separation and pattern completion **(Figure 6)**. The pattern separation allows the encoding and separation of similar contextual information in order to distinguish them before storing them. This process reduces the overlap between similar events and decreases the probability of interference during memory retrieval. In the hippocampus, the subregion engaged in pattern separation processes is the DG. The number of GCs in the DG is five-fold the number of neurons in the entorhinal cortex and have distinct connectivity patterns along with a sparse firing profile. This enables each granule cell to carry only a small and distinct fraction of the total input, expanding the relatively few entorhinal cortex neurons inputs onto many more GCs. Because of that, entorhinal-granule cell connections can separate and amplify even the smallest, but relevant, difference present in the afferent information (McNaughton and Morris, 1987). Therefore, two memories acquired in an environment could be encoded by statistically independent populations of neurons, with independent firing locations in the DG for each memory (R. P. Kesner, 2013). The now separated patterns are transmitted to the CA3 via the mossy fibers that allows the distinct storage of similar events (Rolls, 2018). The memories are temporarily stored in the hippocampus (from hours up to months) where they are consolidated with recurrent activation of the correct hippocampo-cortical networks. With time, the cortical connections are strengthened and memories are shifted to the cortex for a more permanent storage (Frankland and Bontempi, 2005). On the other hand, pattern completion is the ability of the network to recall stored patterns when partial or degraded information is presented during memory retrieval. Pattern completion relies on the CA3 and its autoassociative characteristic, given by the numerous recurrent connections between CA3 pyramidal neurons. The CA3 receives an incomplete stimulus directly from the entorhinal cortex via the perforant pathway, recruiting some pyramidal neurons that will activate other pyramidal neurons thanks to the recurrent synapses. This allows the transmission of a more complete signal and allows the retrieval of a complete memory (Hunsaker and Kesner, 2013; R. P. Kesner, 2013). Pattern separation and completion processes can be evaluated in animal models with spatial tasks (radial maze, WMW) and with contextual tasks (context discrimination, fear conditioning) (Nakashiba et al., 2012; Robert et al., 2020). Studies showed that damaging the DG and the CA3 could impair pattern separation and pattern completion performances (Lee and Lee, 2020; Nakashiba et al., 2012; Robert et al., 2020). A lot of these studies suggest that, even though pattern separation and completion happen in the same network, they are in

competition and coexist in an ever-changing balance (Nakashiba et al., 2012; Newman and Hasselmo, 2014; Robert et al., 2020; Yassa et al., 2011).

Short-term memory

Short-term memory, also called working memory (WM), is the ability to store, recall and manipulate information for a limited time before it fades or is consolidated into a more permanent type of memory. For a long time, the hippocampus role in WM was disregarded, mainly because of the famous H.M. study where a patient with hippocampal lesion had total anterograde amnesia but was capable of retaining information for a few minutes before forgetting about it (Scoville and Milner, 1957). However, a number of studies describe defects of WM in patients with hippocampal damage, specifically for visuospatial and relational working memories (Olson et al., 2006a, 2006b; Piekema et al., 2007). This showed the relevance of studying the hippocampus for better understanding WM processes.

In 1972, Olton and Samuelson showed that working memory also existed in rodents as the storage of relevant information for a task in radial maze was erased the day after (Olton et al., 1979; Olton and Samuelson, 1976). In rodents, hippocampus-dependent WM can be evaluated with a variety of spatio-temporal tasks, including classic radial maze working memory task, Y maze working memory task and every-day like working memory task in radial maze (Al Abed et al., 2016; Dudchenko, 2004; Mingaud et al., 2008). The Y-maze WM task relies on spontaneous alternation behavior based on spatial clues, and rats with hippocampal lesions show deficits of performance in this test (Hughes, 2004). In the classical radial maze WM, when retrieving food rewards at the end of baited arms, the animals would remember the arms already visited and not re-enter those after a short delay. This memory lasts a few minutes and is definitely impaired after a 60 min delay (Bolhuis et al., 1986). The everyday-like memory task adds some complexity to the classic radial maze task, as it allows the evaluation of working memory performances depending on retention and organization difficulties. Mice with hippocampal lesions had impaired performance in a delay-dependent manner, showing the importance of the structure for the retention component of working memory, and their performance was also impaired when the organizational demand was increased with the introduction of proactive interferences (Al Abed et al., 2016). As for the subregions specifically involved in working memory processing, a clear answer is yet to be

established. However, a study from Al Abed and colleagues from 2016 showed that the DG and the CA3 were activated by the everyday-like working memory task for young and aged individuals, while the CA1 level of activity was not particularly activated. This suggests that the DG-CA3 circuit might be of importance for hippocampal processing of working memory.

1.5- Hippocampal modifications during physiological aging

With age, the functional and physical properties of the brain are affected, leading to cognitive impairments and vulnerability to pathology. Due to its importance in cognitive processes and its sustained adaptability throughout adulthood, it is particularly interesting to study the hippocampus in the context of aging. Many studies report a number of structural and functional changes in the hippocampus during aging, which we are going to recapitulate in this section **(Figure 7)**.

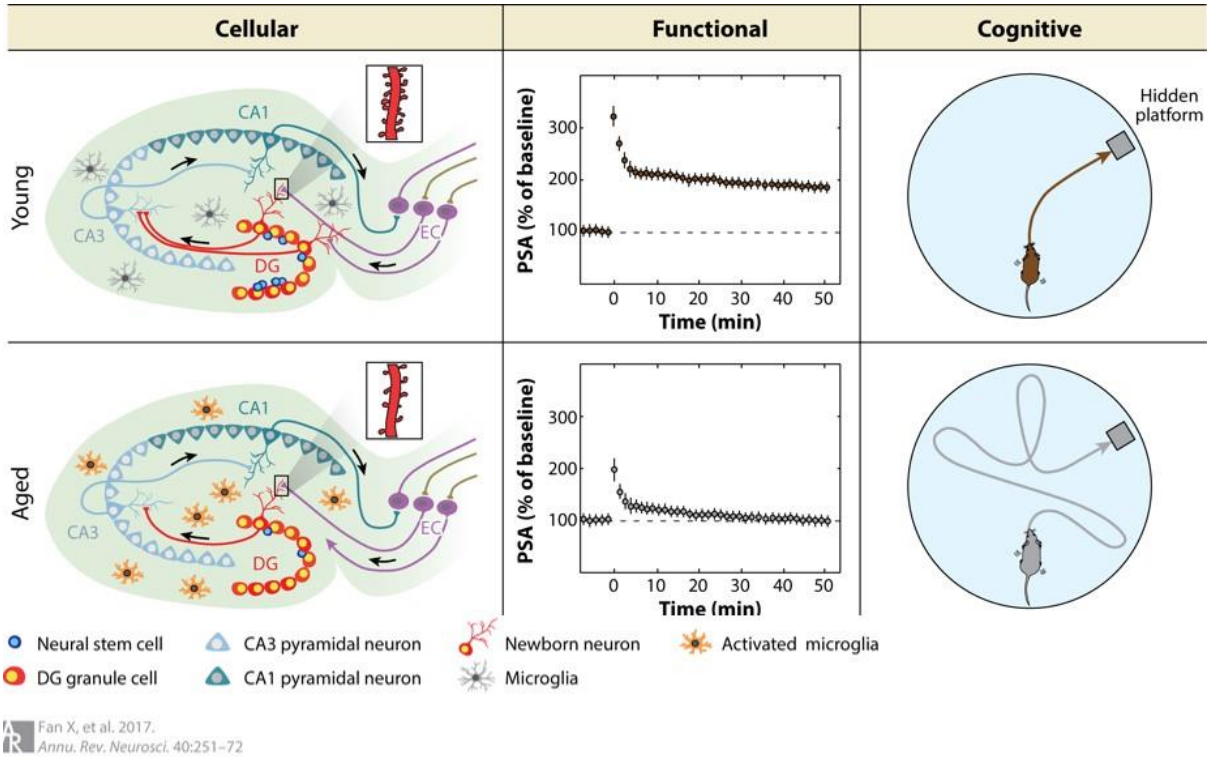

Figure 7: Age-related hippocampal changes. Aged hippocampus display alterations at the global, cellular and functional levels. Reduction of adult neurogenesis, synaptic density and neuroinflammation impact the connectivity and function of the hippocampal network, shown here by reduced LTP. These changes result in a decline of hippocampal-dependent cognitive performances such as spatial memory. DG, dentate gyrus; EC, entorhinal cortex; PSA, population spike amplitude. (Adapted from Fan et al., 2017).

Age-related systemic changes

Changes in the global morphological properties of the hippocampus have been reported in both aged humans and animal models. In humans, age-related hippocampal atrophy has been repeatedly reported in longitudinal MRI studies (Nadal et al., 2020; Nobis et al., 2019; Veldsman et al., 2021). A study from 2020 done in healthy subjects showed a gradient of vulnerability to aging between the different hippocampal subregions, the DG being the most vulnerable, followed by the hilus then the CA3 and CA1 (Feng et al., 2020).Recently, Nadal and colleagues studied the annual rate of reduction in the hippocampal subregions, and they report a higher rate of reduction in the DG while the CA3 and CA1 are less affected. The reduction rate is also higher in the hippocampus compared to the overall reduction in cerebral grey matter (Nadal et al., 2020). In animal models, the existence of such hippocampal atrophy is debated. In rats, age-related hippocampal atrophy has been observed (Driscoll et al., 2006) but in mice some studies show no significant changes in hippocampal volume (Von Bohlen und Halbach and Unsicker, 2002), while others show a specific reduction in the dorsal hippocampus (Reichel et al., 2017). The mechanical properties of the hippocampus are also modified during aging. Magnetic Resonance Elastography (MRE) and MRI studies in humans and mice show that mechanical properties such as stiffness or viscoelasticity vary according to age, with a reduction of stiffness and an increase of viscoelasticity in the hippocampus of older individuals (Delgorio et al., 2021; Palotai et al., 2022).

These global changes are the reflection of other changes happening at a lower scale (reviewed in Blinkouskaya et al., 2021). Aging has been linked to a decrease in the number of neurons in the hippocampus, though those results are debated as some studies report no significant change in neuron numbers (Edler et al., 2020; Fu et al., 2015; West, 1993). The putative reduction of neuron numbers can be due to normal neuronal death, and also to a reduction of adult neurogenesis in the DG in older individuals (Knoth et al., 2010; Kozareva et al., 2019; Kuhn et al., 1996). Aging is also linked to demyelination of axons in the brain, and the hippocampus is no exception. Studies report lower levels of markers of oligodendrocytes and myelin, suggesting an alteration of myelinated axons in the aging hippocampus (Ahn et al., 2017; Tanaka et al., 2005). In humans, this is reflected by the reduction of white matter observed in older individuals.

Aging is also associated with an increase of neuroinflammatory hallmarks in the hippocampus, even during healthy aging (reviewed in Barrientos et al., 2015; Di Benedetto and Müller, 2019). Levels of proinflammatory cytokines such as IL-6 and IL-1β in aged mice (Porcher et al., 2021). Studies report an increase of glial markers in aged mice, such as markers of primed microglia and reactive astrocytes (Barrientos et al., 2015; Cerbai et al., 2012; Rodríguez et al., 2014). This priming and activation of glial cells is accompanied by morphological changes typical of a proinflammatory activation (Cerbai et al., 2012; Sierra et al., 2007). These changes can participate in the dysregulation of hippocampal function in aging.

Age-related synaptic changes

Synaptic alterations have been observed in the hippocampus of aged animals. However, the changes seem to vary depending on the species. Several studies report a significant reduction of synaptic density in the hippocampus of aged mice, in all subregions. On top of the reduction of synaptic numbers, a modification of synaptic types is observed in the CA3 region, with an increase of perforated synapses in the *stratum radiatum* which leads to a modification of the inputs (Buss et al., 2021). Other specific changes are reported in the CA3 at the level of the mossy fiber/thorny excrescences (MFB/TE) synapse and we will detail them in section 2.2.7. Alterations of synaptic proteins that have a role in synaptic maintenance and function such as PSD95, synaptophysin, synapsin and glutamate receptors were observed during aging (VanGuilder et al., 2010). The alteration of synaptic structure and protein content have functional consequences. We observe a reduction of excitatory synaptic transmission with age in both rodents and non-human primates. Moreover, synaptic plasticity is also affected in the hippocampus of older individuals with reduced levels of long term potentiation (LTP) and facilitated long term depotentiation (LTD). The alteration of LTP is due, at least partly, to the modification of NMDA levels and composition with age which leads to a disruption of Ca2+ signaling (Barnes et al., 2000, 1992; reviewed in Kumar and Foster, 2019). These impairments of hippocampal synaptic function are correlated with cognitive decline.

Age-related behavioural changes

Cognitive decline is mostly associated with pathological aging and neurodegenerative disorders. However, all the structural and functional alterations that we listed previously

have some consequences on hippocampal function and physiological aging has been associated with significant impairments of cognitive function. Healthy aged individuals show loss of hippocampal-dependent processes such as declarative memory and working memory (Driscoll et al., 2003; O'Shea et al., 2016). Similar defects in hippocampal-dependent cognitive processes have been observed in animal models of physiological aging. Old rats and mice present impaired spatial memory and pattern separation (Barnes, 1979; Burke et al., 2010; de Fiebre et al., 2006). Several studies using radial maze paradigms show that aged mice have alteration of short-term/working memory and reference memory performances (Al Abed et al., 2020, 2016; Marighetto et al., 1999; Mingaud et al., 2008).

2- DG-CA3 circuit / MF-TE synapse

2.1- Classic Glutamatergic Synapse

The functional contact by which a presynaptic and a postsynaptic neuron communicate in the brain is called a synapse. Chemical synapses require the synthesis and release of a neurotransmitter stocked in presynaptic vesicles following depolarization of the presynaptic bouton. At the postsynaptic site, the released neurotransmitter transiently binds to its specific receptors to generate a postsynaptic electric signal that can either be inhibitory or excitatory, depending on if it induces a postsynaptic hyperpolarization or depolarization. Here we will focus on glutamatergic synapses as they are the main type of chemical synapse found in the hippocampus. Glutamatergic synapse is an asymmetric structure composed of a presynaptic bouton and a postsynaptic dendritic spine separated by the synaptic cleft (~20 nm).

The presynaptic compartment of a glutamatergic synapse, also called presynaptic bouton, is formed by an axon terminal onto a spine. It contains everything allowing the storing and release of glutamate-filled synaptic vesicles, as well as signaling and scaffolding proteins maintaining the structure and function of the bouton. Three distinct functional zones can be found in the presynaptic bouton. The first is the active zone where vesicles dock to the cell membrane and undergo exocytosis to release the glutamate in the synaptic cleft upon the arrival of an action potential. The second zone close to the

active zone is the synaptic vesicle domain where we find 3 populations of synaptic vesicles: the readily releasable pool ready for exocytosis, the recycling pool and the reserve pool that is the furthest away from the active zone. The final zone of the presynaptic bouton is the mitochondrial domain that is involved in protein synthesis and Ca2+ regulation.

The size of a classic presynaptic bouton varies depending on the structure observed, but in the *stratum radiatum* of the CA3 and the CA1 of mice, the average presynaptic volume is around 0.07-0.2 μm^3 but can span over a 30 fold range (Pasaoglu and Schikorski, 2016). The boutons contain in average 200-350 synaptic vesicles, with a mean of 10 synaptic vesicles docked onto the active zone. Typical glutamatergic boutons possess only one active zone of mean surface of 0.03 μm^2 (Harris and Stevens, 1989; Pasaoglu and Schikorski, 2016; Shepherd and Harris, 1998).

The common postsynaptic target of the presynaptic glutamatergic bouton is a dendritic spine. A dendritic spine consists of a 0.5-2 µm head that is connected to the dendritic shaft by a narrow neck of ~0.2 µm (Calabrese et al., 2006). A characteristic of the dendritic spine is the presence of the postsynaptic density (PSD), an electron-dense structure that contains a wide variety of proteins such as glutamate receptors, adhesion molecules, scaffolding proteins, cytoskeleton proteins, etc. The glutamate released by the presynaptic bouton acts on ionotropic glutamate receptors such as postsynaptic a-amino-3-hydroxy-5-methyl-4-isoxazolepropionic acid sensitive receptors (AMPAR), N-methyl-D-aspartate-sensitive glutamate receptors (NMDAR) and kainate receptors (KAR) (Baude et al., 1995; Castillo et al., 1997b; Jonas et al., 1993a). The precise composition of glutamate receptors at the PSD can vary and affect synaptic function.

2.2- MFB/TE synapse

2.2.1- Morphology

The granular cells of the DG form axons named mossy fibers (MF), were first described by Golgi and then named by Cajal (Golgi, 1886; Ramon y Cajal, 1911). Their name is due to the presence of numerous varicosities and filopodia on the axona projections, reminiscent of moss filaments. These MFs first create connections with mossy cells and interneurons in the hilus of the DG (Acsády et al., 1998). Then they exit the hilus and project into the *stratum lucidum* region of the CA3, where create contacts with

postsynaptic structures named thorny excrescences (TE) formed on the proximal part of both basal and apical dendrites of pyramidal neurons of the CA3 (Henze et al., 2000; Rebola et al., 2017). Amaral discovered and described the synaptic terminals present on those mossy fibers: small “en passant" synapses on hilar cells, giant mossy fiber synapses on CA3 dendrites in the *stratum lucidum*, and filopodial extensions from these giant synapses that connect interneurons (Amaral, 1979; Amaral and Dent, 1981).The MF can form up to 15 presynaptic boutons along its shaft. The boutons have different complexities, with a tonotopic repartition of the MFB size along the different CA3 sub-regions. The largest and most complex MFB synapses are found in the CA3b, whereas the MFB synapses of the CA3a and CA3c are less complex (Galimberti et al., 2010, 2006).

Compared to “classical” facing synapses, the MFB/TE synapse is characterized by a convoluted structure. The pre-synaptic structure formed by MF (called mossy fiber bouton or MFB) completely enfolds the postsynaptic TE, instead of only facing it like in “classical” synapses. Both pre- and postsynaptic structures are anchored to one another thanks to *puncta adherentia*, composed of different adhesion molecules such as nectins (Mizoguchi et al., 2002), or N-Cadherin (Takai et al., 2003). Puncta adherentia are quite small (0,07µm² in rats) and can be found in the zone where the presynaptic bouton joins the dendritic shaft of the CA3 pyramidal neuron. In rodents, a single mossy fiber can contact up to 18 CA3 pyramidal neurons to form a synapse (Henze et al., 2000). A single MFB can also contact several TEs, either on different dendritic segments from the same pyramidal neurons or from different pyramidal neurons (Chicurel and Harris, 1992; Galimberti et al., 2006). In total a pyramidal cell can receive up to 50 MFB/TE synapses from different mossy fibers (Amaral et al., 1990). In mice, the mature MFB is characterized by its large size (from 2 to 14µm^3 volume) and its capacity to create 1 to 6 filopodias that can contact inhibitory interneurons (Wilke et al., 2013). The length of the filopodias vary during development. Moreover, these presynaptic boutons often present presynaptic “satellites”. All these satellites display the same features as a presynaptic bouton: they possess filopodia and contact CA3 pyramidal neurons. However, they are often smaller than the MFB they originated from.

This complex synapse contains multiple active zones, which are defined by the dense accumulation of synaptic vesicles in symmetry with the postsynaptic density, with an average of 6 active zones per synapse (Wilke et al., 2013). Actives zones at the MFB/TE

synapse are in majority perforated with interruption of the pre- and the postsynaptic densities (Rollenhagen et al., 2007). The active zones found at MFB/TE synapse cover a large range of volume, from very small to very large structures (0,07µm² to 0,17µm² in rats). They are also close to each other, which can cause spillover of neurotransmitter and synaptic crosstalk (Barbour and Häusser, 1997). The high number of pres-synaptic active zones and PSDs participates in the unique functional characteristics of this giant synapse (Urban et al., 2001).

MFB/TE synapses contain a large pool of synaptic vesicles (up to 25 000), evenly distributed throughout the synapse in young individuals and more concentrated around active zones in adults (Rollenhagen et al., 2007). The number of synaptic vesicles at an active zone is estimated at 850 vesicles which is much more than in “classical” synapses. Recent electron microscopy studies also distinguish 3 types of synaptic vesicles in the near vicinity of active zones : small clear-core SVs (diameter = 33–55 nm), giant clear-core vesicles (GVs; diameter = 60–120 nm), and (3) dense-core vesicles (DCVs, diameter = 46–91 nm) (Maus et al., 2020). The realizable pool of a MFB has been estimated to ~1400 vesicles for a 30 ms pulse stimulation (Hallermann et al., 2003).

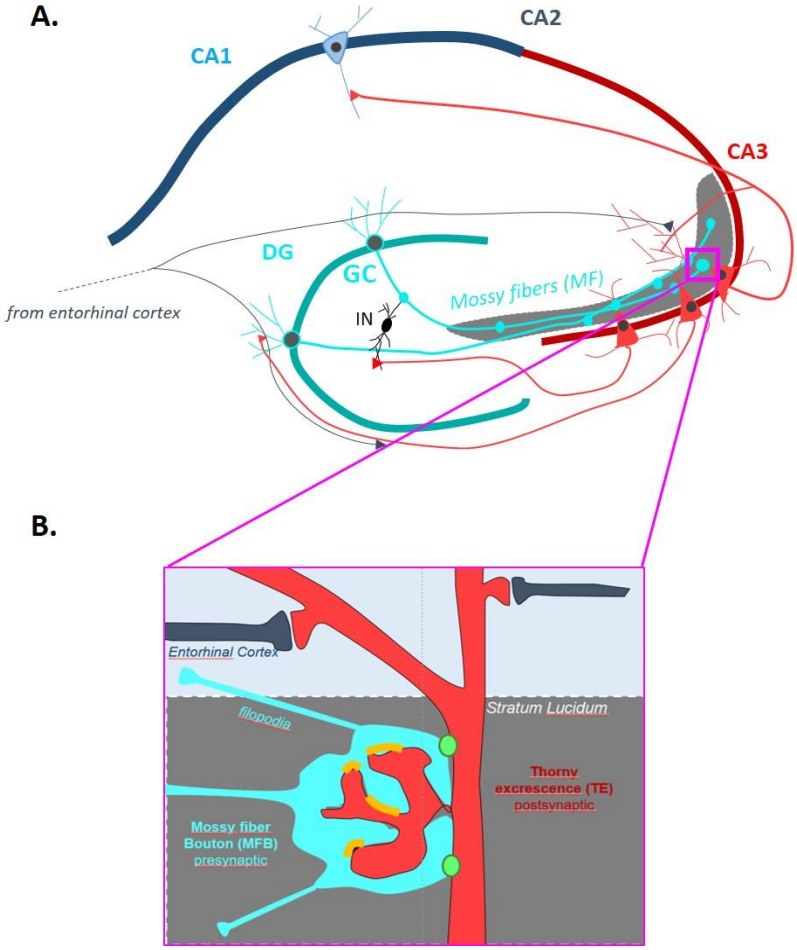

Figure 8: Schematic representation of the MFB/TE synapse. **(A)** The mossy fibers (MF) (turquoise) project from the DG to the *stratum lucidum* (grey) of the CA3 to make synapses with the thorny excrescences (TE) of the pyramidal neurons (red). **(B)** The magnification of the synapses made by the MF and the TE in the *stratum lucidum* shows the complexity of their structure, with the MF bouton engulfing the TE, creating multiple active zones (light green dots) and associated PSDs (yellow). Outside of the stratum *lucidum*, classical facing synapses can be found.

The majority of the glutamatergic synapses of the brain are “tripartite” synapses, with close apposition of astroglial processes to the synaptic cleft that can regulate glutamatergic transmission (Perea et al., 2009). Interestingly, electron microscopy studies showed that in MFB/TE synapses, astroglial prolongations do not reach in the synaptic cleft and are not observed near active zones, and the postsynaptic element is almost completely covered by the MFB. However the MFB were largely covered by glial processes, isolating individual MFB/TE synapses from surrounding synapses (Rollenhagen et al., 2007; Wilke et al., 2013). This might contribute to the efficacy of the MFB/TE synapse by allowing glutamate spillover between active zones of the same synapse, while avoiding contamination of the signal by neighboring synapses.

All of those morphological characteristics make the MFB/TE synapse unique in the hippocampal formation and the brain.

2.2.2- Development

In the previous section, we described the unique morphological features of the MFB/TE synapse. Equally unique developmental processes are required for the formation of this synapse in the CA3.

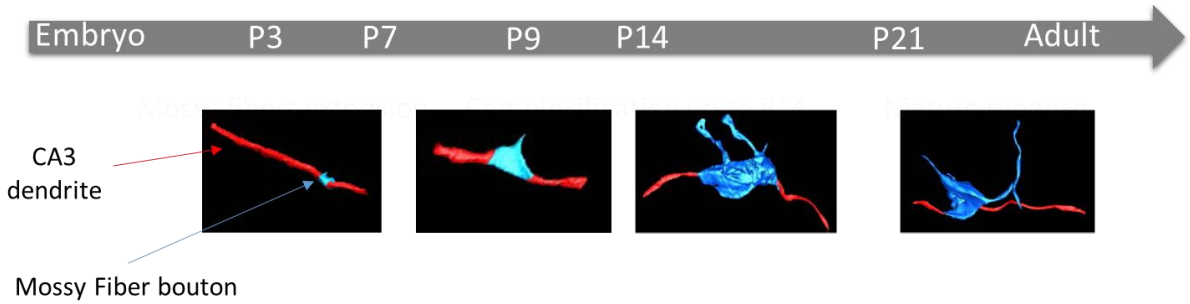

Figure 9: Timeline recapitulating the postnatal development of the MFB/TE synapse. First contact between mossy fibres and CA3 dendrites happens around P7, complexifying until P14 and are considered mature by P21.(Adapted from Wilke et al., 2013).

Development timing

The development of this MFB/TE synapse is progressive and occurs in postnatal stages, as all DG cells have exited the cell cycle by P15 (Yu et al., 2014). In mice, the first MFs of DG granular cells reach the *stratum lucidum* at P3. MFs make the first contacts with CA3 pyramidal cells at P7, creating “en passant" synapses with the proximal part of apical dendrites. The presynaptic terminals of the mossy fibers complexify themselves until P14 (Amaral and Dent, 1981; Lanore et al., 2012). The first post-synaptic TEs emerge from the proximal dendrites of pyramidal neurons between P7 and P9 and the structural and functional complexity of the MFB synapse increases until P21 (Wilke et al., 2013). From P21, the synapse is considered mature as little changes are observed until the adult stage (P420) (Amaral and Dent, 1981). MFB/TE synapse development has also been observed in *in vitro* cultures of hippocampal neurons (Grosse et al., 1998) and *ex vivo* organotypic slices (Dailey et al., 1994; Koyama et al., 2004; Robain et al., 1994). The MFB/TE synapses formed in vitro have similar molecular composition and ultrastructural characteristics to those formed in vivo (Dailey et al., 1994; Robain et al., 1994). These studies show that it is the presynaptic mossy terminals that induce the formation and

complexification of thorny excrescences from the CA3 pyramidal dendrites (Robain et al., 1994). They also suggest that the maturation of presynaptic elements, the dendritic targeting and subsequent postsynaptic complexification might rely on an intrinsic program of dentate gyrus granule cells, which can differ between models (Grosse et al., 1998; Vaughn et al., 1977).

Protein interactions involved in MFB/TE synaptic development

These multiple developmental steps, along with the peculiar morphological features of the synapse, demonstrate the elevated complexity of this circuit. Complex protein interactions might be involved in its establishment and development, with a precise organization in both time and space.

One of the key mechanisms involved in the development of MFB/TE synapses is the quasi-unidirectional projection of the mossy fibers in the *stratum lucidum*. This precise control of the projections relies on the involvement of different proteins that can act as guidance cues or adhesion proteins. Classical axonal guidance proteins such as ephrins, semaphorins and plexins have been reported to play a role in the addressing of the mossy fibers during postnatal development. Semaphorins are repulsive proteins that can be either secreted in the ECM or attached to the membrane. Once linked with their plexin receptors, they trigger an intracellular signalisation cascade that, through GTPases activation, results in actin reorganization and axon retractation. Mossy fibers express Plexins A2 and A4, receptors for the Semaphorins 6A and 6B, which prevent their migration in the *stratum radiatum* and *stratum pyramidal* of the CA3 (Suto et al., 2007; Tawarayama et al., 2010).

Specific cell adhesion molecules (CAMs) are also involved in the MFB/TE synapse development, notably in the anchoring of the pre- and postsynaptic elements via the puncta adherentia. Nectin-1 and -3, N-Cadherin, Cadherin-8 and -9, Catenins and Afadins form puncta adherentia when the mossy fiber contact the CA3 pyramidal dendrite during the first postnatal week, and participate to the maturation of the MFB/TE synapse (reviewed in Mizutani et al., 2021). Alteration of CAMs expression in mice leads to disruption of the MFB/TE synaptogenesis et to abnormal connectivity, with decreased numbers of MFB/TE synapses, altered morphology and function (Sai et al., 2017; Toyoshima et al., 2014; Williams et al., 2011).

The development of MFB/TE synapses relies also on membrane heparan sulfate proteoglycans (HSPG). HSPG are proteins with long heparan sulfate glycosaminoglycan chains attached to their principal domains (Sarrazin et al., 2011). They are involved in a variety of processes via their interaction with different binding partners, and their role in brain development, function and pathology has been a topic of interest since the 1980s (Condomitti and de Wit, 2018; Kamimura and Maeda, 2021; Mashima et al., 2022; Saied-Santiago and Bülow, 2018). Recents studies showed the involvement of two types of HSPG in the MFB/TE synapse development: neurexins and glypicans (Condomitti et al., 2018; Zhang et al., 2018). Zhang et al. showed that Neurexins are HSPG with long HS chains that are necessary for synaptic differentiation both *in vitro* and *in vivo*. Neurexin-binding partners Neuroligins (NL1-4) and LRRTM2 bind trans-synaptically to the HS chains during synaptic development and disturbing these interactions prevent presynaptic differentiation and function. Suppressing HS chains on Neurexin1 in mice results in smaller and less complex MFB/TE synapses with fewer PSDs, along with altered synaptic transmission (Zhang et al., 2018). The importance of neurexins, LRRTM and neuroligins in synaptic development was already established, but it was the first study that showed the importance of HS in this interaction. Glypican 4 (GPC4) is another HSPG particularly important for MFB/TE synapse development. It is enriched in the DG GCs and is present in the mossy fibers as early as P7. In association with its co-receptor LAR, GPC4 binds the orphan receptor GPR158 trans-synaptically via its HS chains, and this interaction is necessary for presynaptic differentiation and specificity of MFB/TE synapses. Deleting *GPR158* affected the formation of MFB/TE synapses in mice, resulting in synapses with altered morphology and function (Condomitti et al., 2018). The molecular mechanisms via which HSPG regulates MFB/TE synapse development are still widely unknown. However a recent study showed that GPC4 is also involved in pathological MFB/TE synapse sprouting after seizures and explored the possible downstream pathway involved (Ma et al., 2022). They showed that GPC4 expression was increased after pilocarpine-induced seizures and activates the mTOR pathway, which is known to induce MF sprouting after epileptic seizures (Shima et al., 2015). However more studies are needed to see if the mTOR pathway is also involved in the development of MFB/TE synapse during the postnatal period, and to explore the other possible pathways involved in HSPG regulation of MFB/TE synapses development.

2.2.3- MFB/TE synapse and adult neurogenesis

As stated previously, the hippocampus is known for its high levels of adult neurogenesis, leading to the generation of new dentate granule cells. These adult newborn GCs can develop mossy fiber synaptic input and create MFB/TE synapses onto CA3 pyramidal dendrites in the *sl* within 4 weeks after their generation, matching the rate of initial MFB/TE synaptogenesis during postnatal hippocampal formation (Faulkner et al., 2008; Gu et al., 2012; Toni et al., 2008). This developmental process involves CAMs, just as in the initial postnatal development of MFB/TE synapses. SynCAM1 and Neuroligin2 in particular have been shown to play a crucial role in the maturation of newborn MFB/TE synapses, regulating the number and size of MF terminals in the CA3 (Krzisch et al., 2017). The newly formed MFB/TE synapses have similar structural properties as the mature ones, with large presynaptic boutons engulfing complex TE with several PSDs and filopodias connecting interneurons (Faulkner et al., 2008; Toni et al., 2008). Newly formed MFB/TE synapses are capable of triggering post-synaptic responses in CA3 pyramidal cells (Toni et al., 2008). The EPSCs evoked after stimulation of adult born MFB/TE synapses reach their maximal value at around 4 weeks after differentiation, and can be blocked by specific AMPAR antagonists and mGluR agonists (Gu et al., 2012). These studies show that MFB/TE synapses formed by adult-born GCs are functional mossy fiber synapses that are fully incorporated in the DG-CA3 network at the same rate as mature MFB/TE synapses. Integration of those newborn MFB/TE synapse participate in cognition, as it has been shown that impairments of the formation of MFB/TE synapses by newborn GCs lead to memory impairments (Gu et al., 2012; Krzisch et al., 2017) and blocking adult neurogenesis impairs pattern separation, a process heavily relying on DG-CA3 connectivity (Nakashiba et al., 2012).

This phenomenon of integration of new MFB/TE synapses is sustained throughout life, even though neurogenesis is reduced in older adult stages. A recent study by Murray et al. recently explored the specifics of integration of newly born MFB/TE synapse in young and aged adult mice. They showed that the new MFB/TE synapses formed in aged brains displayed the same structural features as the ones formed in young adults. However some discrepancies have been observed between the integration of new MFB/TE synapse in young adult mice and their integration in old mice. Newborn GCs generated in young adult mice (3 months old) form a lot of smaller MFB/TE synapses initially but the majority of them are pruned with time, resulting in a smaller number of fully mature MFB/TE synapses. These new synapses formed in young adult stages can share

postsynaptic elements with preexisting MFB/TE synapses formed during the postnatal period. They can eventually replace those mature synapses but it is rare in young adult mice, and creation of *de novo* synapses is the principal mode of integration observed in young adult stages. In contrast, a smaller population of newborn GCs from the hippocampus of aged mice (18 months old) form MFB/TE synapses but those synapses are not pruned with time and acquire mature characteristics quickly, leading to a higher density of newborn MFB/TE synapses with time (Trinchero et al., 2019). Another difference is that the newly formed MFB also shares postsynaptic elements with pre-existing ones. However, integration of those new MFB/TE synapses in aged hippocampus is rather done through synaptic replacement of those old preexisting MFB, as de novo synaptogenesis is rare at this stage. These differences between sharing and remplacement could have interesting implications for hippocampal function across stages, and ultimately might be involved in the decline of cognitive processes in aging (Murray et al., 2020).

2.2.4- Structural plasticity

MFB/TE synapses can undergo structural plasticity throughout life. Many studies report a diversity of changes of the MFB/TE synapse's morphology and organization following a change in activation or environment **(Figure 10)**. Several studies from Pico Caroni's team showed that a sustained enrichment of the environment induced an increase in size and complexity of the presynaptic MFB in adult mice (Galimberti et al., 2006). Interestingly, all synapses formed by the same mossy fiber will not have the same rearrangements following EE, meaning the plastic properties are specific to individual MFB/TE synapses and are regulated locally (Galimberti et al., 2006).

Using organotypic slice cultures, it has been shown that these anatomical modulations of MFB/TE synapses are activity-dependent. Several studies showed that blocking activity of granule cells with inhibitors such as TTX, GABA or DCG IV induced a reversible reduction of size and complexity of the MFB in organotypic slices (Chierzi et al., 2012; Galimberti et al., 2006). Interestingly, filopodial extensions are not affected by suppression of granule cells spiking, suggesting that they remodel independently from the MFB (Chierzi et al., 2012). Conversely, high frequency stimulation and chemical LTP induce an increase of size and complexity of both the presynaptic MFB and the postsynaptic TE (Maruo et al., 2016; Orlando et al., 2021; Zhao et al., 2012). This

structural remodeling requires the activation of postsynaptic NMDAR, KAR and mGluR to happen, but not the AMPAR (Galimberti et al., 2006; Maruo et al., 2016). The dialogue between the pre- and the postsynaptic elements is also a key element of this plasticity, as blocking the calcium mediated release of intercellular messenger such as arachidonic acid and nitrid oxide blocks the morphological changes in MFB after HFS (Maruo et al., 2016). Functionally, the increased morphology of the MFB/TE synapse after activity dependent structural plasticity has been correlated with increased amplitude of EPSCs (Galimberti et al., 2006; Maruo et al., 2016). This can be attributed to the increase of active zones as well as the rearrangement of synaptic vesicles observed after structural plasticity events (Orlando et al., 2021; Zhao et al., 2012).

Several studies make the link between MFB/TE synapses structural plasticity and performances in hippocampal-dependent memory tasks. Increase of MFB size has been observed in rats who were trained for spatial learning in a water maze paradigm and for mice trained for context discrimination in a fear conditionning paradigm (Carasatorre et al., 2015; Holahan et al., 2006; McGonigal et al., 2012; Ruediger et al., 2011; Weng et al., 2018). This training-induced structural plasticity has been correlated with better performances in subsequent hippocampal-dependent tasks, such as pattern separation (Carasatorre et al., 2015; Ruediger et al., 2011). Holanhan and Routtenberg showed that local inactivation of CA3 activity during a learning task blocked the learning induced remodeling of MFB/TE synapses and impaired spatial learning and memory in rats (Holahan and Routtenberg, 2011). Though it might be tempting to deduce that blocking MFB/TE structural plasticity affects memory, the study only highly highlights the importance of circuit activity in the regulation of structural plasticity. However, it is clear that activity-driven MFB/TE structural remodeling is a key element in mechanisms of learning and memory.

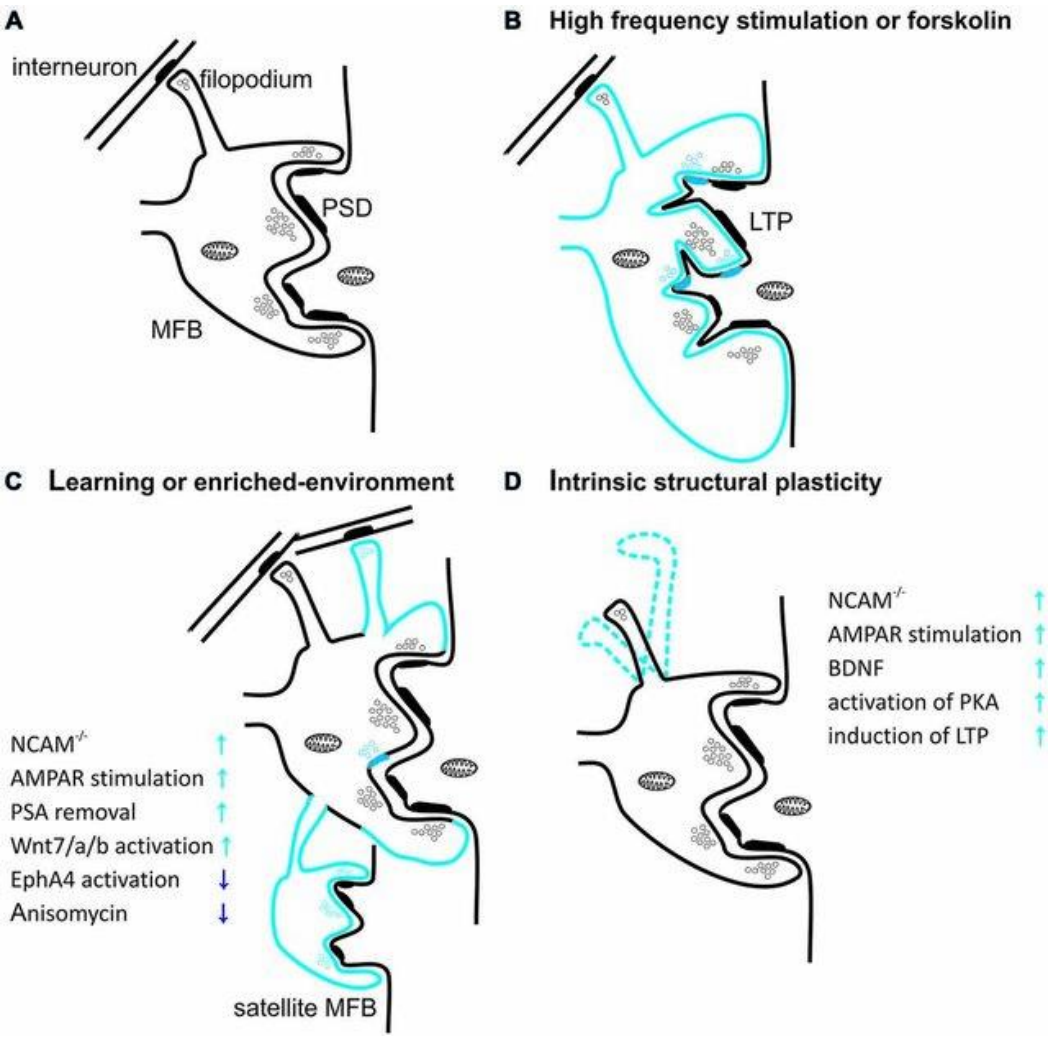

Figure 10: Different types of structural plasticity at the MFB/TE synapse. **(A)** Schematic diagram showing mossy fiber bouton (MFB) contacting thorny excrescences of CA3 pyramidal neuron. Thick postsynaptic lines reflect postsynaptic densities. **(B)** Induction of long-term potentiation (LTP) in MFB/TE synapses with high-frequency stimulation or forskolin leads to increase in MFB volume and in the number of release sites per MFB. Blue color reflects structural plastic changes. **(C)** Spatial learning or enriched-environment promotes an expansion of mossy fibers terminals in the *stratum lucidum*. Furthermore, housing mice in an enriched environment leads to an increased local complexity of MFBs with frequent appearance of satellite boutons with functional release sites. Additionally hippocampus-dependent learning increases the number of filopodia protruding from MFBs and contacting feedforward projecting PV+ interneurons. **(D)** MFB filopodia are characterized by a dynamic intrinsic structural plasticity in the adult hippocampus ex vivo. Filopodia undergo spatial rearrangement in shape in mature hippocampal slice cultures. Plasticity processes that increase MF transmission affect also filopodia motility. (From Wiera and Mozrzymas, 2015).

Molecular mechanisms underlying the structural plasticity of the MFB/TE synapse are numerous and widely unknown. Several families of proteins are involved in the structural plasticity of the MFB/TE synapse. Gradients of expression of morphogenic proteins in the CA3 and DG are key for the plastic properties of individual MFB/TE synapses. Galimberti et al. showed that the gradient of expression of EphA4 (higher in the lower blade of the

DG) during a sensitive period in juvenile mice is responsible for the establishment of specific plasticity levels in a topographic manner along the CA3 (Galimberti et al., 2010). One possible explanation is the establishment of opposite gradients of ephrin receptors in the CA3, which could induce the creation of less repulsive zones allowing the morphological changes for the mossy fiber boutons (Klein, 2009; Tremblay et al., 2009). The Wnt family, already involved in the development of the hippocampus, plays a role in the structural plasticity in the CA3. Wtn7a/b has been shown to be express in the CA3 after bursts of activity of GCs induced by EE, and is necessary and sufficient to induces the subsequent complexification of MFB in the CA3 (Chen et al., 2006; Gogolla et al., 2009).

Several proteins involved in synaptic vesicle dynamics are involved in structural plasticity. Rab3a is a small vesicle binding protein that is necessary for LTP at the mossy fiber (Castillo et al., 1997a; Lonart et al., 1998). Rab3a-deficient mice do not present any structural plasticity following EE, HFS or learning of a task, probably because of the activity dependent nature of this plasticity (Gogolla et al., 2009; Ruediger et al., 2011). Munc13-1 is a known interactor of Rab3a and necessary for synaptic docking and fusion to the membrane. HPF electron microscopy data shows that Munc13-1 deficient mice have no relocalisation of vesicles and change of presynaptic MFB surface, meaning that the fusion of vesicle regulated by Munc13-1 is responsible for some of the morphological changes observed during activity-induced structural plasticity (Zhao et al., 2012).

Other factors linked to synaptic activity have been linked to structural plasticity in MFB/TE synapse. Deletion of the activity-dependent transcription factor Npas4 prevents plasticity at the MFB/TE synapse following contextual learning (Weng et al., 2018). The EE-induced plasticity observed by Galimberti et al. is regulated by PKC activation (Galimberti et al., 2006).

2.2.5- Synaptic Transmission and plasticity

Along with their structural, developmental and molecular peculiarities, mossy fiber synapses also possess unique electrophysiological properties.

Molecular players in the MFB/TE synaptic transmission

Like most excitatory synapses in the central nervous system, the MFB/TE synapse is glutamatergic and relies on the ionotropic receptors AMPA, NMDA and KAR (Conner-Kerr et al., 1993; Crawford and Connor, 1973). Studies report the presence of 2 types of AMPAR at the synapse: The GluR2 lacking Ca2+ permeable AMPAR, present at the MF-interneurons synapses, and the GluR2 lacking CA2 impermeable AMPAR (Lei and McBain, 2002; Toth et al., 2000). These two types of AMPAR are associated with different features of transmission with Ca2+ impermeable AMPAR playing a role in rapid and precise transmission while Ca2+ permeable AMPAR are required robust transmission and multiple action potential firing (McBain, 2008). In mice, Ca2+ impermeable synapses are significantly more present than Ca2+ permeable synapses (McBain, 2008).

One particularity of the MFB/TE synapse compared to other glutamatergic synapse is the low levels of NMDA receptors. Several studies report a significant difference in the NMDAR/AMPAR ratio at the MFB/TE synapse compare to other hippocampal glutamatergic synapses (Kakegawa et al., 2004; Rebola et al., 2011; Takumi et al., 1999). NMDAR found at the MF synapse are in majority composed of the GluN1-GluN2A subunits, as very low levels of GluN2B were reported in the *stratum lucidum* of the CA3 (Fritschy et al., 1998; Watanabe et al., 1998). However, studies showed that more GluN2B-containing NMDAR are recruited in the post-synapse after LTP (Carta et al., 2018). The NMDAR found in the postsynaptic part of the MF synapse can trigger postsynaptic currents and are involved in enhancement of the synaptic transmission as well as in the regulation of synaptic plasticity in recurrent CA3-CA3 synapses (Hunt et al., 2013; Kwon and Castillo, 2008; Rebola et al., 2011).

KAR in MFB/TE synapses can be found both pre-synaptically and post-synaptically. Granule cells predominantly express the GluK1, GluK3, GluK4 and GluK5 sub-units of the KAR (Wisden and Seeburg, 1993). Post-synaptic KAR are composed of the sub-units GluK2, GluK4 and GluK5 and play a role in the generation of postsynaptic EPSC of low amplitude (Castillo et al., 1997b; Fernandes et al., 2009; Mulle et al., 1998). High affinity KAR can be found in the presynaptic compartment of the MFB/TE synapse and can be activated by the glutamate released from their cell (autoreceptors) or from neighboring cells (heteroreceptors) (Kamiya and Ozawa, 2000). They can have a role in the release

of GABA from the MFB/TE synapse, but also enhance the synaptic transmission and participate in paired pulse facilitation and frequency facilitation.

On top of the activation of ionotropic receptors, the glutamate of the MFB/TE synapse acts on metabotropic receptors (mGluRs). These G protein-coupled receptors have a slower action than ionotropic receptors that rely on ionic flux, as they act by activation of g-proteins and secondary messengers. Type II and III mGluRs are mainly expressed in the presynaptic mossy fiber bouton, while type I mGluRs can be predominantly found in the postsynaptic part of the synapse on the CA3 pyramidal neurons (Baude et al., 1993; Luján et al., 1996; Shigemoto et al., 1997). Type II mGluRs are extrasynaptic receptors while Type III receptors are specific to the synaptic cleft (Corti et al., 2002). mGluR1 and mGluR5 seem to be enriched in the dendrites of the CA3 pyramidal neurons while mGluR2, mGluR2/3 and mGluR7b are enriched in the presynaptic mossy fiber (Shigemoto et al., 1997). Type I mGluRs regulate the intrinsic excitability of the CA3 pyramidal neurons, however their role in LTP/LTD is still discussed. Type II mGluRs are also regulators of the intrinsic excitability of the synapse and they are involved in plasticity mechanisms such as LTP/LTD and synaptic depotentiation. Type III mGluRs are also involved in the inhibition of synaptic transmission at the MFB/TE synapse (Griego and Galván, 2020; Shigemoto et al., 1997).

Although adult MFB/TE synapses have a glutamatergic synaptic transmission, they have also been described as GABAergic. Adult mossy fiber synapses are found immunoreactive for GABA at their synaptic contacts with CA3 TE in humans, primates, and rats (Bergersen et al., 2003; Sandler and Smith, 1991). The GABA colocalizes with glutamate at those synapses, though less abundant (Bergersen et al., 2003). Other proteins linked to GABAergic transmission have been identified in the MFB/TE synapse: GAD_{67}, the synthetizing enzyme of GABA (Sloviter et al., 1996), GAT-1, the GABA membrane transporter (Frahm et al., 2000; Gómez-Lira et al., 2002) and VGAT, the vesicular transporter of GABA, although it still have to be confirmed for the latter (Boulland and Chaudhry, 2012; Chaudhry et al., 1998). The GABAergic/glutamatergic duality of the MFB/TE synapse varies throughout its development.

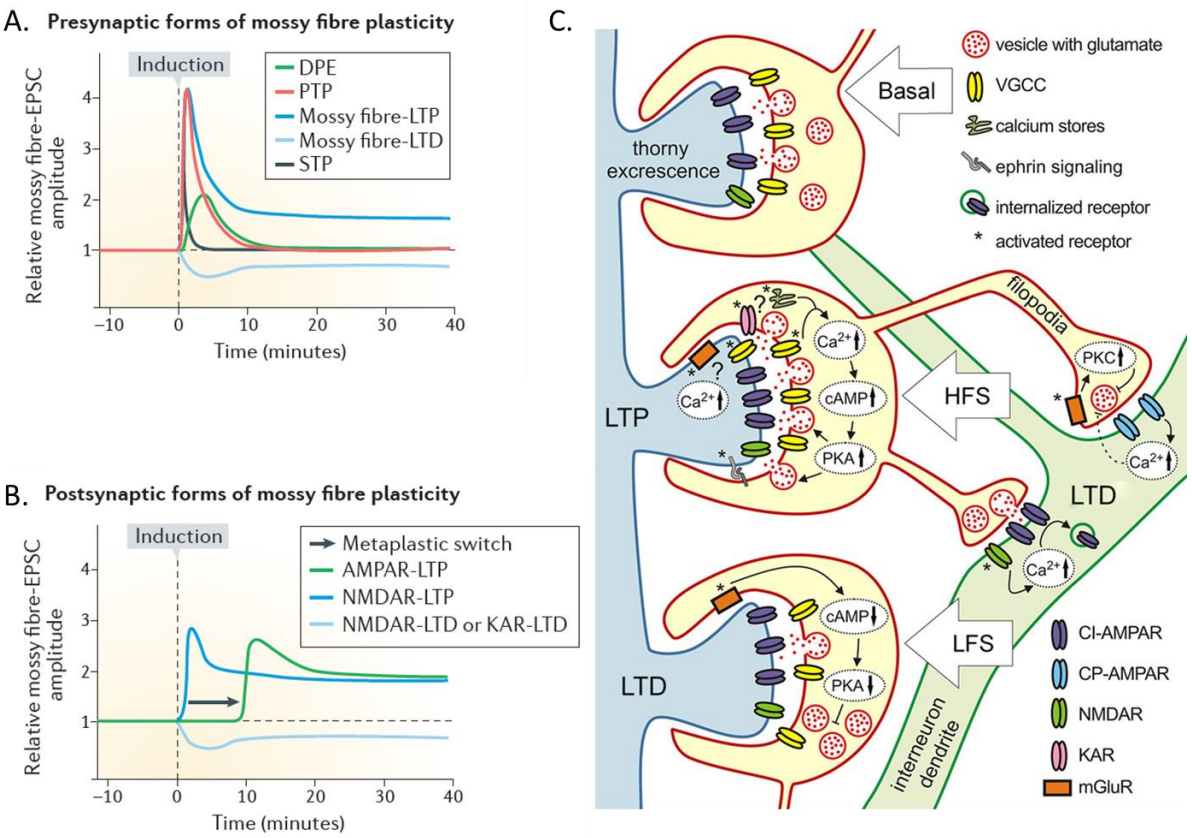

Figure 11: Functional synaptic plasticity at the MFB/TE synapse. **(A)** The typical time course of different types of mossy fibre presynaptic plasticity. These include short-term plasticity (STP; including frequency and burst facilitation), intermediate forms of plasticity (depolarization-induced potentiation of excitation (DPE) and post-tetanic potentiation (PTP) and mossy fibre long-term potentiation (LTP) and long-term depression (LTD). **(B)** Typical time course of different types of MFB/TE postsynaptic plasticity. A brief burst of mossy fibre stimulation induces selective NMDAR-LTP which acts as a metaplastic switch that makes the synapses amenable to subsequent AMPAR-LTP. Both synaptic KAR-mediated EPSCs and NMDAR-mediated EPSCs are also subject to LTD. **(C)** Illustration of the molecular mechanisms underlying long term plasticity events at the MFB/TE synapse. (Adapted from Evstratova and Tóth, 2014; Rebola et al., 2017).

On top of glutamate and GABA, the MFB/TE synapse's activity can be regulated by neuropeptides released from the MFB. Opioid peptides such as dynorphin and enkephalin and their receptors are found at the MFB/TE synapse. Dynorphin is released after high frequency stimulation and can inhibit synaptic transmission and plasticity (Salin et al., 1995; Weisskopf et al., 1993). Other peptides such as neuropeptide Y have inhibitory effects on the MFB/TE synapse activity (McCarthy et al., 1998). The regulation of MF neurotransmission by neuropeptides is particularly studied in the context of epilepsy, as their inhibitory function has been shown to be neuroprotective (reviewed in Kovac and Walker, 2013).

Short-term plasticity events at the MFB/TE synapse

MFB/TE synapses are characterized by a very low release probability at their release sites (Pr = 0.01-0.05) (Jonas et al., 1993b). Because of that, synaptic transmission at low frequency stimulations mostly end up failing in those conditions. Despite this low release probability, a huge rise of synaptic transmission efficacy is observed when the activity is switched to high frequency stimulation (post-tetanic potentiation or PTP, can last a few minutes) and/or bursts of activity (synaptic facilitation, can last a few hundreds of milliseconds) **(Figure 11)** (Henze et al., 2002b; Salin et al., 1996; Toth et al., 2000; Zucker and Regehr, 2002). Following these plasticity events, unitary MFB/TE synapses are able to induce action potentials in CA3 pyramidal neurons and strongly drive CA3 network activation, giving the synapse its “conditional detonator” phenotype. These strong short-term enhancements of synaptic transmission are mainly driven by presynaptic mechanisms. Recent findings show that the distribution of synaptic vesicles in MFB contribute to the short-term plasticity of the synapse. Using high-pressure cryoEM tomography, they showed that the level of synaptic vesicles docked at AZ were smaller in MFB/TE synapses than in “classical” synapses but was increased during post tetanic potentiation, and MFB also had a pool of tethered vesicles close to the AZ that could be recruited during short-term plasticity events (Maus et al., 2020; Vandael et al., 2020). Moreover, several studies report the presence of giant vesicles among those pools of docked and tethered vesicles, which are involved in the induction of giant EPSCs (Henze et al., 2002a; Imig et al., 2020; Rollenhagen et al., 2007). This might be one explanation for the huge plasticity range observed at the MFB/TE synapse, due to the prevention of vesicular depletion upon multiple stimulations as well as the capability of releasing huge quantities of neurotransmitter. Post tetanic potentiation and presynaptic facilitation also rely on presynaptic Ca2+ influx. Repeated stimulations induce an important influx of Ca2+, activating CAMKII and allowing short term facilitation (Salin et al., 1996). Moreover, the release of intracellular Ca2+ from mitochondrias and the endoplasmic reticulum have been shown to participate in PTP and facilitation at the MF/tE synapse (Lee et al., 2020). Presynaptic KARs and NMDARs are also involved in presynaptic short-term plasticity. Reduced facilitation is observed when specific inhibitors such as CNQX and MK-801 are applied on slices, and is also found in mutant mice models lacking GluR6 and Grin1 (Contractor et al., 2001; Lituma et al., 2021). Despite all those presynaptic mechanisms, the regulation of MFB/TE short-term plasticity might not be entirely presynaptic. A recent

study by Vandael and associates show that postsynaptic mechanisms relying on Ca2+ signaling contribute to the regulation of PTP via transsynaptic feedback mechanisms (Vandael et al., 2020). This challenges the model of presynaptic regulation of plasticity of the MFB/TE synapse, and implies that much more remains to be explored in the regulation of the MFB/TE synaptic transmission.

Long-term plasticity events at the MFB/TE synapse

Long-term plasticity events include long-term potentiation (LTP) and long-term depression (LTD) **(Figure 11)**. LTP in the MFB/TE synapse takes a unique NMDA-independent form, which is not found in “classical” synapses in which LTP happens via NMDAR activation and the ensuing increase of AMPAR response (Harris and Cotman, 1986). This can be explained by the low levels of expression of NMDAR in the TE (Watanabe et al., 1998). The induction of LTP at the MFB/TE synapse involves mainly presynaptic mechanisms leading to an increase of neurotransmitter release. It requires the increase of presynaptic Ca2+ via the activation of Ca2+ channels, notably R-type channels; and the activation of cAMP-dependent pathways (Henze et al., 2000; Nicoll and Schmitz, 2005). Presynaptic glutamate receptors are also involved in LTP formation and regulation at the MFB/TE synapse. The involvement of mGluR in the LTP formation has been debated, as some studies show that the application of mGluR antagonists on slices abrogate LTP (Bashir et al., 1993; Ito, 1991), while some others do not observe any effect of these antagonists on plasticity (Hsia et al., 1995; Manzoni et al., 1994). However, the role of KARs has been thoroughly demonstrated, as they facilitate the formation of LTP by enhancing Ca2+ influx. Despite being described as presynaptic, LTP at the MFB/TE synapse relies also on postsynaptic mechanisms. Postsynaptic NMDAR can be activated by repetitive stimulation of the MFB/TE synapse and can participate in the formation of action potentials in the pyramidal cells, in a mechanism called NMDAR-LTP (Kerr and Jonas, 2008). NDMAR-LTP depends on the activation of NMDAR, on postsynaptic calcium levels, activation of PKC, mGlur5 and adenosine receptors (Kwon and Castillo, 2008; Rebola et al., 2011, 2008). These shed a light onto the complex nature of LTP at the MFB/TE synapse.

LTD in the MFB/TE synapse is also induced presynaptically **(Figure 11)**. Trains of low frequency stimulation are able to induce NMDAR-independent LTD. This relies on the activation of presynaptic mGluR2 along with increased levels of Ca2+, induced by the

repeated stimulations (Kobayashi et al., 1996; Yokoi et al., 1996). Activation of mGluR2 reduces the levels of cAMP, reducing PKA activity and the release of neurotransmitters. Expression of other factors have been shown to reduce activity in MFB/TE synapses and participate in LTD, such as BDNF (Garad et al., 2021).

2.2.6- Functional roles of the DG-CA3 circuit and the MFB/TE synapse

In terms of behavior, the DG-CA3 circuit is responsible for encoding and retrieval of episodic memory processes such as contextual memory and novelty encoding (R. Kesner, 2013). MFB/TE synapse is particularly important in DG-CA3 circuit function in pattern separation and pattern completion. Studies have shown that the MFB/TE synapse was essential for pattern separation, due to the sparse firing of GCs and the low probability of pyramidal cells to receive input from an identical subset of GCs. Inhibition of MFB/TE synaptic transmission and/or lesion of the DG result in pattern separation deficits in different paradigms (R. P. Kesner, 2013; Lee et al., 2017; Lee and Lee, 2020; Nakashiba et al., 2012; Rebola et al., 2017). Conversely, increased MFB/TE coverage has been associated with better performances in spatial pattern separation (Carasatorre et al., 2015). A study also shows that MFB/TE synapses participate in pattern completion and recall of contextual memory, and that their function switches from pattern separation to pattern completion depending on their age (Nakashiba et al., 2012).

2.2.7- MFB/TE synapse in pathology and aging

Neurodevelopmental pathologies

Alterations of MFB/TE synapse have been reported in several models of neurodevelopmental disorders linked with deficits in memory processes.

A number of studies using single-gene mouse models of ASD show morphological and functional deficits of the MFB/TE synapse. Earlier studies showed that the *frm1*-KO mouse used to model Fragile X Syndrome, a monogenic mutation leading to ASD and intellectual disabilities, presents reduced mossy fiber bundles with a lot of errors of migration with synapses formed in the *stratum pyramidale* (Ivanco and Greenough, 2002; Mineur et al., 2002). This suggests an alteration of MFB/TE synapse development and maturation, which was confirmed by a study showing that actin dynamics are affected in *frm1*-KO mice resulting in decreased MFB size and increased TE size was increased,

which is typical of immature synapses (Scharkowski et al., 2018). The function of the synapse is also altered, with increased frequency of mEPSCs, hyperexcitability, impaired activity-dependent presynaptic plasticity and protein synthesis at the MFB, which can be of significant importance for synaptic function and behaviour (Monday et al., 2022). Similar phenotypes of morphological and functional immaturity were observed in other monogenic models of ASD/ID, the Kirrel3-KO and GluK$^{-/-}$ mice (Lanore et al., 2012; Martin et al., 2017, 2015; Micheau et al., 2014; Roh et al., 2017). The maturation of the MFB/TE synapse seems to be a particularly relevant target in ASD/ID pathology, and disruption of this connection could explain some symptoms observed in patients such as the difficulty to recognize patterns.

Another neurodevelopmental disorder linked to MFB/TE synapse dysfunction is Down's syndrome. Abnormal morphology and synaptic transmission have been reported in two mice models of DS, the Ts65Dn mouse and the Tc1 mouse. They both had a reduced MFB/TE synapse density in the CA3, and the remaining TE were smaller (Popov et al., 2011; Witton et al., 2015). MF-driven EPSCs were reduced in both mice models and Tc1 mice also had impaired presynaptic facilitation, however LTP remained intact in both mice models (Hanson et al., 2007; Witton et al., 2015). This functional deficit might alter information transmission in the hippocampal circuit, and it could explain the DG-dependent deficits in spatial and contextual information processing (Smith et al., 2014; Witton et al., 2015). This suggests that specific dysfunction of the DG-CA3 circuit, and by extension of the MF-TE synapse, strongly contributes to the cognitive symptoms of DS and must be considered as a potential therapeutic target. Indeed a study reports that the morphological and functional phenotype seems to be reversible with fluoxetine treatment in Ts65Dn mice (Stagni et al., 2013). However other studies are needed to check if rescuing the MFB/TE synapse is sufficient to alleviate the cognitive deficits in DS models.

Abnormal MFB/TE maturation has been linked to schizophrenia. Post-mortem studies on schizophrenic patients show a reduction of MFB/TE synapse density and volume, which is also found in mice models of the disease along with aberration of mossy fiber targeting (Abulaiti et al., 2022; Faulkner et al., 2008; Kolomeets et al., 2007, 2005; Kvajo et al., 2011). Studies in monogenic mice models such as DISC1-KO, showed that MFB/TE synapse excitability was altered, with reduced facilitation and excitability in the presynaptic element (Kvajo et al., 2011). This suggests that problems of maturation and reduced synaptic input from mossy fibers to CA3 neurons in schizophrenia contributes to

the pathology, notably to the hippocampal-dependent cognitive impairments (Kobayashi, 2009; Weinberger, 1999).

A strong association is made between hippocampus and one of the most common forms of epilepsy: mesial temporal lobe epilepsy (MTLE). One specific symptom identified in the hippocampus of MTLE patients and models is the development of aberrant MFB/TE synapse in the inner molecular layer of the DG, a phenomenon also known as mossy fiber sprouting, as well as ectopic dispersion of GCs and reorganization of existing MFB/TE synapse (Kienzler et al., 2009; Sutula et al., 1989). The origin of MFB/TE synapse sprouting is multiple. Among the proposed mechanisms, the downregulation of chemorepellent molecules such as Sema3A, as well as the upregulation of growth factors such as BDNF after seizure-induced hippocampal injuries is thought to participate in the ectopic growth of new MF (Binder et al., 2001; Holtmaat et al., 2003). Some studies also propose that the death of hilar mossy cells after seizure leaves vacating synaptic sites on the GC, giving free space for the new MF to form abnormal retrograde connections (Longo et al., 2003). The role of MFB/TE sprouting in epileptic pathology is a debated subject. For a long time, the formation of de novo recurrent excitatory synapses by the aberrant MF was thought to be the cause of the hippocampal hyperexcitability observed in epileptic patients and animal models (Cavazos et al., 1991; Hendricks et al., 2019). However, this hypothesis has been more and more challenged, as studies show that MFB/TE sprouting is not found in every case of MTLE and that it is not a necessary phenomenon in the maintenance of hippocampal hyperexcitability. Moreover, sprouting can be blocked without affecting the occurrence of seizures (reviewed in Buckmaster, 2014). It suggests that MFB/TE synapse sprouting might be an adaptive mechanism that becomes pathogenic, in an attempt to compensate for the loss of synaptic input due to neuronal death and that it is a phenomenon unrelated to seizure genesis.

Physiological and pathological aging

Among the connective changes observed during aging, the DG-CA3 circuit is particularly affected, resulting in diverse behavioural consequences, from loss of episodic memory to disorientation. While the recurrent synapses of the pyramidal neurons of the CA3 are increased, the number of synapses from the entorhinal cortex onto the DG are reduced during aging, as well as the number of synapses of the molecular layer in the DG (Buss et al., 2021; Scheff et al., 2006). MFB/TE synapses formed between the mossy fibers of

the DG and the pyramidal cells of the CA3 seem to be particularly affected during normal and pathological aging. There is a huge reduction of MFB/TE synapse number in the CA3 of aging rats (Ojo et al., 2013). They present structural changes such as reduced volume and reduction of the filopodia's length in aged humans (Das et al., 2019). As discussed previously in the section 2.2.3, integration of newborn MFB/TE synapses is also affected, with no more formation of *de novo* synapses. Interestingly, despite all those structural deficits observed in MFB/TE synapses in aged mice, EE and LTP still elicit strong structural plasticity in the remaining MFB/TE synapses with increased size and new filopodial extensions (Gogolla et al., 2009; Trinchero et al., 2019). On top of synaptic morphology modifications, deficits of synaptic functional properties and plasticity have also been reported. Studies done in aging rats show increased stimulations are needed to elicit LTP in the DG and that CA3 firing rates are increased (Barnes et al., 2000; Villanueva-Castillo et al., 2017; Wilson et al., 2005). It was also shown that stimulation-evoked glutamate release and clearance was affected in the DG-CA3 circuit in aging rats, affecting the neurotransmission in the circuit and thus potentially affecting memory and behaviour (Stephens et al., 2011). Several studies report loss of episodic memory, with diminished performances in pattern separation tasks and attenuated response to novelty, which are processes that rely heavily on the DG-CA3 circuit (Burke et al., 2010; Cès et al., 2018; Dillon et al., 2017; Yassa et al., 2011).

Alteration of MFB/TE synapses are also present during pathological aging and neurodegenerative disorders. Mouse models of AD present a degradation of the size and complexity of the MFB/TE synapse, with reduced synaptic contact zone in mice model of AD (Wilke et al., 2014). Accumulation of abnormal proteins may participate in the deterioration of the MFB/TE synapse. It has been shown that markers of tauopathies accumulate in the mossy fibers of human patients before the onset of cognitive decline (Christensen et al., 2019). Structural plasticity is also affected in models of neurodegenerative disorders with Tau abnormalities, as soluble Tau has been shown to prevent structural plasticity of mossy fibers (Bolós et al., 2017; Decker et al., 2015). It is probable that models of neurodegenerative disorders such as AD display altered structural plasticity alterations on top of the morphological degradation observed in basal conditions. Studies in mice models of AD showed that even though basal synaptic properties are unaltered, presynaptic LTP, short term synaptic plasticity depending on membrane lipids and LTP of NMDAR dependent EPSCs were strongly impaired in

MFB/TE synapses (Jin et al., 2022; S. H. Lee et al., 2012; Maingret et al., 2017; Silva et al., 2019; Viana da Silva et al., 2016).

3- The Planar Cell Polarity pathway and VANGL planar cell polarity protein 2

3.1- Planar Cell Polarity basics

In epithelial tissues, Planar Cell Polarity (PCP) is the coordinated orientation of cells/cellular structures within the plane of the tissue, perpendicularly to the apico-basal polarity axis. The signaling pathway controlling this organization is highly conserved throughout evolution, from invertebrates to mammals, via core PCP proteins that are asymmetrically polarized within the plane of the epithelium to establish a correct PCP axis. This establishment of the polarity axis within the tissue involve the regulation of cytoskeleton and adhesion protein dynamics. More globally, the proteins participating in PCP signaling are necessary for the morphogenesis and organization of most tissues and organs in many species. They are involved in 2 types of PCP mechanisms: the non-autonomous PCP and the autonomous PCP. The non-autonomous PCP allows the establishment of a global polarity axis within the whole tissue. The autonomous PCP establishes a cellular planar polarity axis within cells. Both mechanisms are interconnected and necessary for the correct polarization and morphogenesis of tissues.

Our knowledge about PCP signaling in epithelia initially arises from studies done in the fruit fly *Drosophila melanogaster* and the regulation of the coordinated organization and orientation of actin-based hair-like structures called trichomes that are found at the apical surface of the wing's epithelial cells (Adler, 2002). In mammals, the actin-rich hair bundles found in the inner ear epithelia have been used as a model for PCP study for more than 20 years now (Montcouquiol et al., 2008, 2003; Montcouquiol and Kelley, 2020). In both models, the abnormal orientation of the actin enriched hair structures is used as a readout to identify PCP mechanisms **(Figure 12)**. Many other epithelia in drosophila and mammals are used as PCP models, but we will focus mainly on the two first structures as examples in the following sections (Davey and Moens, 2017; Henderson et al., 2018; Singh and Mlodzik, 2012).

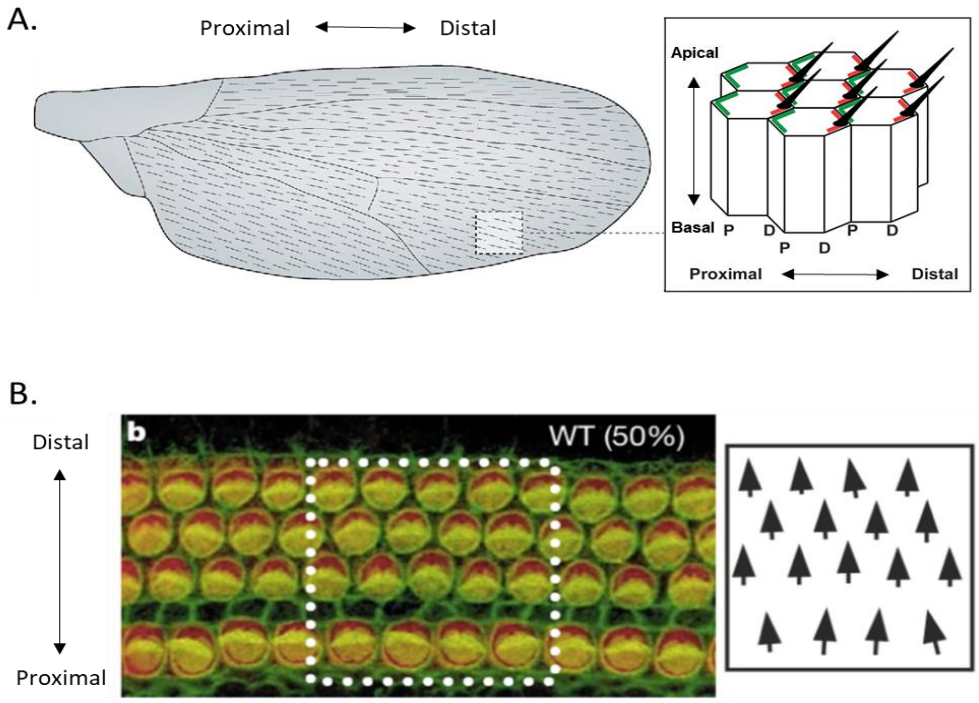

Figure 12: Models of Planar Cell Polarity. **(A)** Drosophila wings are epithelia composed of epidermal cells bearing each an actin-rich hair, with the particularity that all of the hairs point in the same direction within the epithelial plane, defining the PCP axis. **(B)** Surface view of the auditory epithelium, with the auditory cells labeled with myosin VI (red) and the actin-rich hair bundle at the apical surface labelled with phalloidin (green). In the wild-type (WT) tissue, the hair bundles have a uniform orientation, pointing in the same direction defining the PCP axis of the tissue. (Adapted from Devenport, 2014; Montcouquiol et al., 2003; Xie et al., 2018) .

3.1.1- Core PCP proteins & associated PCP proteins in mammals

Core PCP proteins

The core PCP signaling pathway is composed by six core proteins and their isoforms : the cytosolic proteins Ankyrin Repeat Domain 6 (Ankrd6 ; known as Diego, Dgo, in invertebrates), Prickle 1-2 (Pk1-2) and Dishevelled 1-3 (Dvl1-3 ; or Dsh in invertebrates) the transmembrane proteins Van Gogh-like 1-2 (Vangl1-2 ; known as Van Gogh, Van, or Strabismus, Stbm, in invertebrates), Cadherin EGF LAG seven-pass G-type receptor 1-3 (Celsr1-3 ; known as Flamingo, Fmi, or Starry Night, Stan, in invertebrates), and Frizzled (Fz, the number of isoforms varies across species). Mutations of the genes coding for these proteins result in abnormal cellular organization and tissue malformations in drosophila wing epithelia (Wong and Adler, 1993).

Preferential complexes are formed during PCP establishment at the single cell level: Pk, Vang are accumulating at one side of the cell, while Diego, Dsh and Fz accumulate at the opposite side. Fmi is found on both sides and stabilizes Vang and Fz at the membrane. This segregation is regulated by intracellular feedback mechanisms such as the inhibitory interaction between Pk and Dsh, which prevents their uniform accumulation across the cell and strengthens the formation of the preferential complexes (Das et al., 2004). The planar segregation of PCP protein complexes is thought to regulate the recruitment of cytoskeleton proteins, determining the sublocalisation of a structure (such as the hair of a cell) at the single cell level, in a cell autonomous (also called cell-autonomous PCP). The regulation of cytoskeleton by PCP will be discussed in the following section.

The establishment of PCP in epithelial cells and tissue relies on the planar and asymmetrical distribution of these core proteins along opposite domains at the cell apices **(Figure 13)**. This asymmetric repartition of the core PCP proteins relies on their level of expression and subsequent formation of protein complexes. The core PCP proteins can form a quite dense interactome: Vang, Pk, Dsh, and Diego can all interact with one another, and Fmi may interact directly with Fz or Vang, while Fz may interact with Vang and Dsh (Harrison et al., 2020). The consequence of those many interactions is that the absence of one core PCP protein is sufficient to affect the planar distribution of the remaining five, with a specific importance of Fmi and Fz since their absence completely prevents the recruitment of the remaining proteins (Struhl et al., 2012; Strutt and Strutt, 2007).

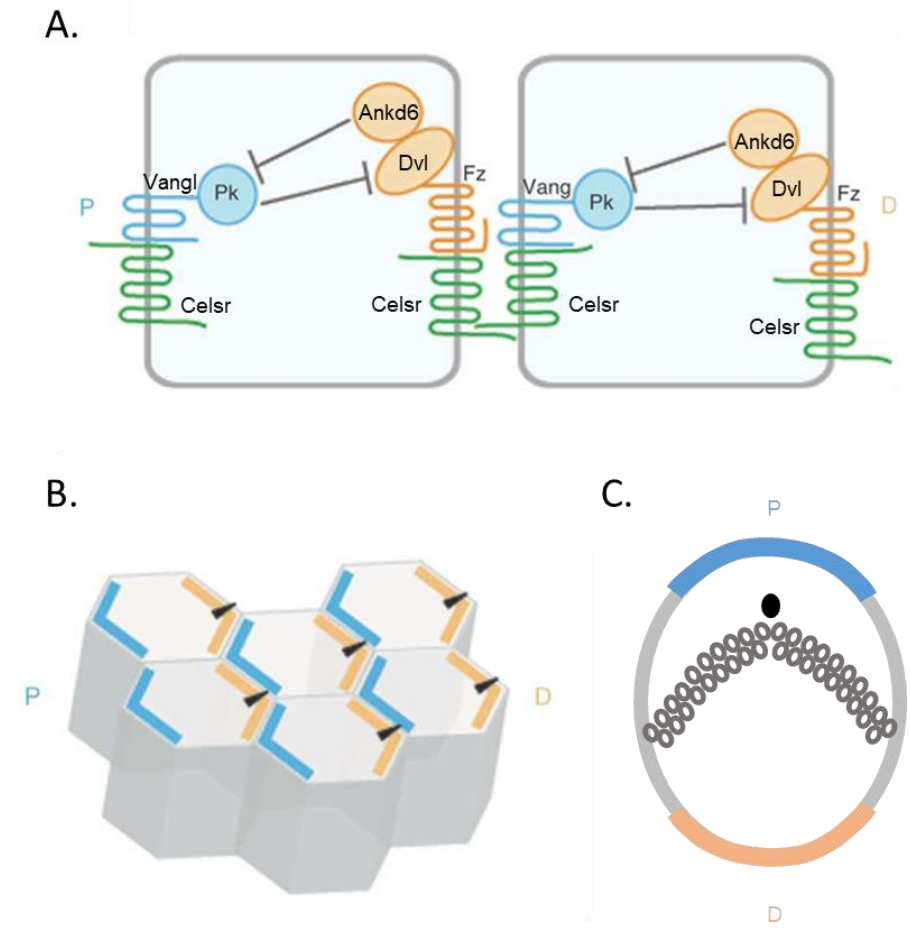

Figure 13: (A) Representation of asymmetric distribution of core PCP proteins: in orange, Ankd6, Dvl, and Fz are restricted to the distal side. In blue, Pk and Vangl localize to the proximal. Celsr (green) can be found on both sides. **(B-C)** Asymmetric repartition in the drosophila wing epithelia and in the mammalian hair cell. (Adapted from Singh and Mlodzik, 2012).

The asymmetric organization of PCP proteins allows the establishment of polarity within a cell, but it also participates in the common polarization of ensembles of cells in tissues (also called non-cell autonomous PCP). The non-cell autonomous PCP has been first described in the drosophila using chimeras where normal wing cells surround mutant cells lacking *Fz* or *Vang* (Taylor et al., 1998; Vinson and Adler, 1987). The orientation of the trichoma was used as a readout for a PCP phenotype. The results showed that the orientation of the trichoma of normal cells surrounding the mutant cells was modified (toward the *Fz*-lacking cells and away the *Vang*-lacking cells). This demonstrated the existence of a tissue-level PCP signal that relied on cell-cell contacts for the transmission of a polarized signal across the tissue. Importantly, this polarization transmission does not require the cytosolic core PCP proteins but only the transmembrane ones: Fz, Vang

and Fmi. The atypic adhesion protein Fmi is particularly important for the cohesive establishment of PCP within a tissue, as it will form cell-cell junctions by forming homophilic transcellular bonds with other Fmi molecules. Fmi molecules associated with Fz are more likely to stably associate with a junctional Fmi molecule of an adjacent neighbouring cell that is not bound to Fz (either bond to Vangl or bond to neither Vangl or Fz). The establishment of non-cell autonomous PCP is thought to happen first, before the cell-autonomous one (Wong and Adler, 1993). This is confirmed in studies on Fmi mutants, in which the formation of PCP complexes was reduced, with lower levels of Vang and Fz at the cell wall and no recruitment of the cytosolic PCP proteins (Axelrod, 2001; Harrison et al., 2020; Shimada et al., 2001; Strutt, 2001). Importantly, this signal transmission does not require the cytosolic core PCP proteins Pk, Dsh or Dgo, but only the transmembrane ones, Fz, Vang and Fmi. It has to be noted that the core PCP pathway is not the only one involved in the establishment of tissue level PCP. The Fat/Dachsous pathway is known to also participate in the asymmetrical repartition of proteins within cell ensembles (reviewed in Strutt and Strutt, 2021; Thomas and Strutt, 2012).

Associated PCP proteins

Associated PCP genes have been named as such and identified in mammals, as new regulators of PCP, because the mutation of the genes did not induce a known PCP deficit at the time. These PCP associated proteins can be differentiated from core PCP proteins because they are not segregated in a polarized manner in the cell, their mutation/deletion does not result in the loss of asymmetry of other core PCP proteins, and their mutation/deletion often result in mild PCP phenotypes in epithelial tissues such as the cochlea, although it can be worsened by the partial loss of expression of one of the core PCP genes. Most of those PCP-associated proteins have been discovered using the cochlear model of PCP, or via their link to neural tube defects (Lu et al., 2004; Montcouquiol et al., 2003). Among the PCP-associated proteins, there are proteins involved in apico-basal polarity, cell adhesion and protein trafficking such as Scribble (Scrib, Montcouquiol et al., 2003), Ptk7 (J. Lee et al., 2012; Lu et al., 2004), Sec24b (Merte et al., 2010; Wansleeben et al., 2010) and Ror2 (Martinez et al., 2015; Schambony and Wedlich, 2007) to cite a few.

PCP is also known as the “non-canonical Wnt pathway” (Eisenmann, 2005). Wnts are lipid-modified morphogens that act in a wide range of biological processes across life, controlling cell proliferation, differentiation, growth and migration among others (reviewed in Nusse, 2005). There is a large number of Wnts, particularly in mammals, with up to 19 Wnt genes identified in mice so far, involved in different pathways among which we find the canonical Wnt/β-catenin pathway and our pathway of interest, the non-canonical Wnt/PCP pathway. The major difference the two pathways is that while the canonical one involves a regulation of ß-catenin levels and transcriptional changes (reviewed in Buechling and Boutros, 2011; Nusse and Clevers, 2017), the PCP pathway mostly controls cytoskeleton reorganization in absence of transcriptional activity (reviewed in Adler, 2012). Both pathways share a common starting point: a Wnt molecule will bind to a Fz receptor and activate downstream effectors. Because of their overlapping expression patterns, the specificity of Fz-Wnt interactions is still blurry but some Fz can be specific to the activation of one pathway or the other. Similarly, the specificity of Wnt ligands for Fz are not strictly defined and can be modified by many parameters, giving rise to a very complex network that is still being deciphered (Cadigan and Liu, 2006; Wu et al., 2004).

3.1.2- Effectors and Cytoskeleton regulation

The identification and description of PCP effectors is a complex complex topic, even in *Drosophila*. Many proteins have been identified as PCP effectors but a common effector to all systems is yet to be discovered. Here we will focus on a few proteins that have a role in PCP signalling but which role can’t be generalized to all PCP models.

The asymmetric distribution of the core PCP proteins is thought to regulate cytoskeleton organization and adhesion molecules presence at the membrane within the cell, leading for example to the specific localization of the trichome only at the distal apex of the epithelial cell in *Drosophila*’s wings. Studies propose that proteins that inhibit actin hair formation such as Inturned (Int), Fuzzy (Fuzz) and Fritz (Frtz) are recruited and regulated by Vang at the proximal side (reviewed in Adler and Wallingford, 2017; Strutt and Warrington, 2008). Int, Fuzz and Fritz are known to regulate the recruitment of the Multiple-wing-hairs (Mwh) protein, which repress actin polymerisation. As a result, the

actin polymerization leading to hair development is restricted to the distal side. Knocking out those regulators leads to the formation of multiple hairs in aberrant position, confirming their role in the restriction of actin polymerization, without disrupting the asymmetric PCP organization (Wong and Adler, 1993).

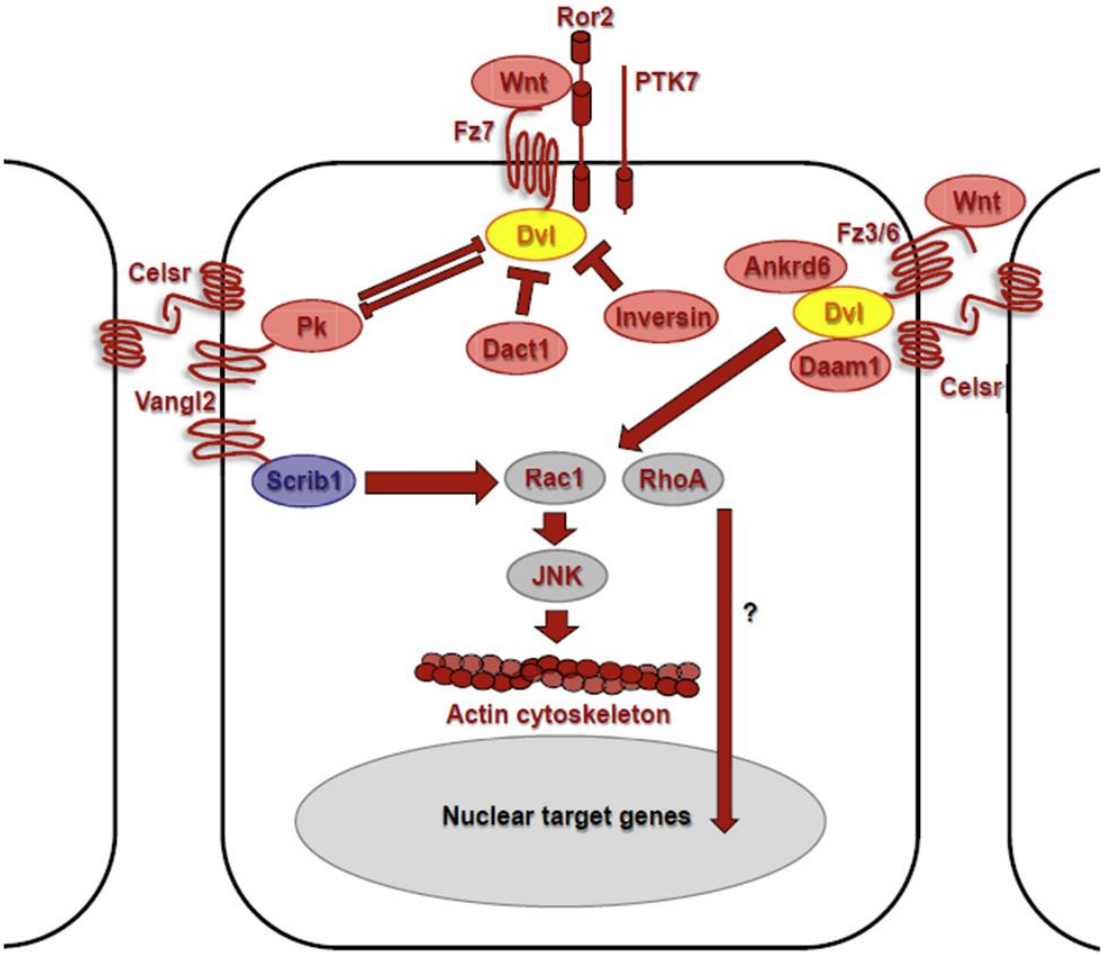

Figure 14: Planar cell polarity signaling cascade. Interactions within core PCP proteins and with associated PCP proteins regulate the activity of effectors (grey) that will allow the control of cytoskeleton dynamics and possibly transcriptional regulation. Arrows indicate activation; blunted arrows indicate inhibition. (From Sans et al., 2016).

The Rho kinase RhoA and the formin Diaphanous (Dia) are notable actin regulators, and mutations in the genes coding for these proteins also affect trichome formation and orientation. RhoA mutant clones present aberrant trichome orientation and number, in a cell-autonomous manner (Strutt et al., 1997). Similarly, genetic depletion or expression of a constitutively active Dia affect the orientation and the number of hairs per cell. Because of this overlap with RhoA's role, it is believed that Dia (and by extension other formins) are Rho effectors (Lu and Adler, 2015). RhoA is thought to activate and boost

the accumulation of Mwh via a direct interaction, and thus driving the specific formation of the hair at the distal side of the cell (Yan et al., 2009). In addition, Dia is thought to interact genetically with Mwh and restrict its localization proximally (Lu and Adler, 2015). Mutations in Dia coding genes results in abnormalities often associated with PCP defects, such as alteration of the inner ear hair cells and abnormal cytoskeleton dynamics leading to altered development (Labat-de-Hoz and Alonso, 2021; Lau et al., 2021).

Other notable downstream PCP effectors are JNK proteins (reviewed in Roszko et al., 2009). Disruption of the JNK signaling can induce polarity defects. Studies using the organization of ommatidia in the drosophila's eye, showed that Dsh activates JNK cascades via its DEP domain, which is the region essential for its activity in PCP signaling and that activating the JNK pathway can rescue the PCP phenotype in Dsh mutants (Boutros et al., 1998).

3.1.3- PCP in vertebrates/mammals

Convergent extension

Convergent-extension (CE) is a crucial developmental process that has been demonstrated to occur during gastrulation in xenopus and zebrafish, and in neural tube closure in xenopus, zebrafish and mice (reviewed in Wallingford, 2012). During CE, the cells composing a tissue converge along a developmental axis, while elongating perpendicularly to this axis **(Figure 15)**.

Disruption of CE is accepted as a readout for PCP signalling disruption in vertebrates, including mammals. Because of the importance of coordinated and polarized migration, PCP signaling has been shown to be critical for CE (Roszko et al., 2009; Vichas and Zallen, 2011). The end result of the disruption of CE is a deficit in anteroposterior elongation, resulting in shorter structures within a tissue and animals with short trunks, which is the typical readout of non-canonical Wnt/PCP deficit in zebrafish and *Xenopus laevi* (Wallingford, 2012; Wang and Nathans, 2007). In constrast, the alteration of the canonical Wnt pathway affect the patterning of the xenopus embryo, without affecting the CE mechanisms in itself. The readout of the canonical Wnt/βcatenin deficits is the development of duplicated, but well proportioned structures in embryos (Funayama et al., 1995). In mammals, aberrant CE associated with core PCP genes mutations results in neural tube defects with various degrees of severity from spina bifida to

craniorachischisis. This has been notably shown in *Vangl*, *Celsr* and *Fz* mutants and is recognized as a PCP related phenotype.

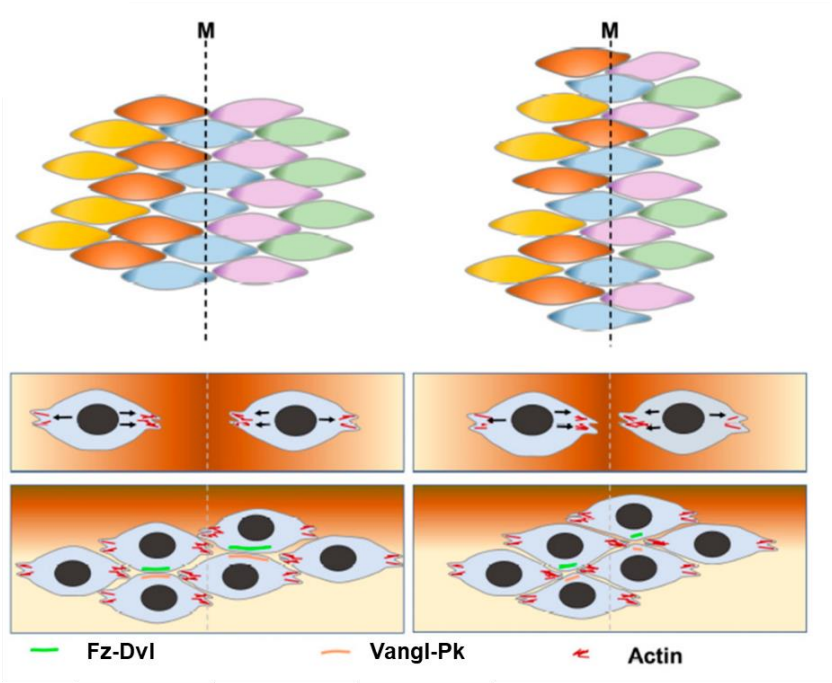

Figure 15: The process of convergent extension. Cells elongate along the mediolateral axis, move and intercalate with neighboring cells resulting in the anteroposterior axis, which leads to the narrowing and lengthening of the body axis. During this process, Pk and Vangl localize anteriorly whereas Fz and Dvl localize posteriorly, and participate to the regulation of CE via the control of actomyosin dynamics. (Adapted from Wang et al., 2019)

Mechanistically, convergence relies on the capacity of cells to extend protrusions between them. The cells create these protrusions randomly, but they eventually respond to cues in the environment to orient and start intercalation within the neighboring cells. The lamellipodia then exert actomyosin-based tractions that will shrink mediolaterally oriented cell-cell junctions, driving cell movement and finishing their intercalation in the media-lateral axis (Shindo, 2018). The first paper linking PCP and CE showed that the non-canonical Wnt/PCP ligand Wnt5a regulates CE mechanisms via the elongation of filipodial structures (Moon et al., 1993). Shortly after that, a study showed that blocking Dvl function in *Xenopus* embryo led to shortened trunk development (Sokol, 1996). Later studies identified the role of Vangl in CE in *Xenopus* (Darken et al., 2002; Goto and Keller, 2002; Jessen et al., 2002). Both up- and downregulation of Vangl expression inhibited CE during gastrulation and neural tube closure processes, resulting in a trunk shortening and open neural tube. Similarly for Fmi, the expression of a truncated form of the protein

leads to disrupted CE dynamics (Carreira-Barbosa et al., 2009). More recent studies also linked Vangl and Pk to the regulation of actomyosin traction during CE (Butler and Wallingford, 2018; Shindo et al., 2019).

Taken together, these studies show the importance of PCP signaling for the establishment and regulation of cell movement during convergent-extension, with a fairly conserved mechanism throughout evolution.

PCP in the inner ear

As stated previously, one of the best and the first model of PCP in mammals is the organization of hair cells in the inner ear and more precisely in the cochlea. The organ of Corti (OC), the sensory epithelium of the cochlear duct, comprises tightly organized rows of hair cells (HCs) interlaced with similarly ordered rows of supporting cells. Each HC is topped with an actin-rich stereociliary bundle that has a V shape. The vertices of all HCs are uniformly aligned along the proximal to distal axis displaying a perfect example of PCP organization. This polar organization of the hair bundles is crucial for cochlear function, as each bundle is directionally sensitive and can only respond to deflections along the PCP axis (reviewed in Montcouquiol and Kelley, 2020). Montcouquiol and colleagues showed that the core transmembrane protein Vangl2 is necessary for the proper orientation of the hair bundles (Montcouquiol et al., 2003). The PCP phenotype observed in these Vangl2 mutant hair cells was very similar to the one observed in the wing cells in Drosophila, validating the conservation of PCP function between species and highlighting this epithelium as a valid one to identify and study core PCP in mammals **(Figure 16)**. Other studies showed that the other transmembrane PCP proteins are involved in the orientation of HC: Celsr1 the same year (Curtin et al., 2003) then the Fz isoforms Fz3 and Fz6 (Wang et al., 2006). Later studies showed that deletion of the three cytosolic core PCP proteins have only mild or no effects, which could be due to compensatory mechanisms or a difference in the signalling cassette. Ankrd6 (Diego) mutants had little to no impact on the HC polarity (Etheridge et al., 2008; Jones et al., 2014). Various combinaison of *Dvl1/2/3* deletion in compound mutants had also mild PCP defects in the hair bundle orientation(Wang et al., 2006). Finally, the Pk2 isoform seem to be not involved at all in the orientation of the hair bundle in the cochlea as it is not present in the auditory sensory epithelium, but there is not study on Pk1 (Yang et al., 2017). Thanks to its easily identifiable PCP phenotype, a lot of the PCP associated genes

have been identified in the mammalian cochlea. Montcouquiol et al showed that *Scrib* mutation resulted in misorientation of the hair bundles in circletail mutants mice (Montcouquiol et al., 2003). Similar phenotypes were used to identify Ptk7 (J. Lee et al., 2012; Lu et al., 2004) , Sec24b (Merte et al., 2010; Wansleeben et al., 2010) and Ror2 (Martinez et al., 2015; Schambony and Wedlich, 2007) as PCP-associated proteins among others. The cochlear model can also be used to detect PCP genes involved in CE mechanisms, as anomalies during this developmental process result in shortened cochleas. Such phenotypes have been reported in mutant mice carrying Vangl2 and Dvl mutations while Fz and Celsr have not been associated with cochlear length changes.

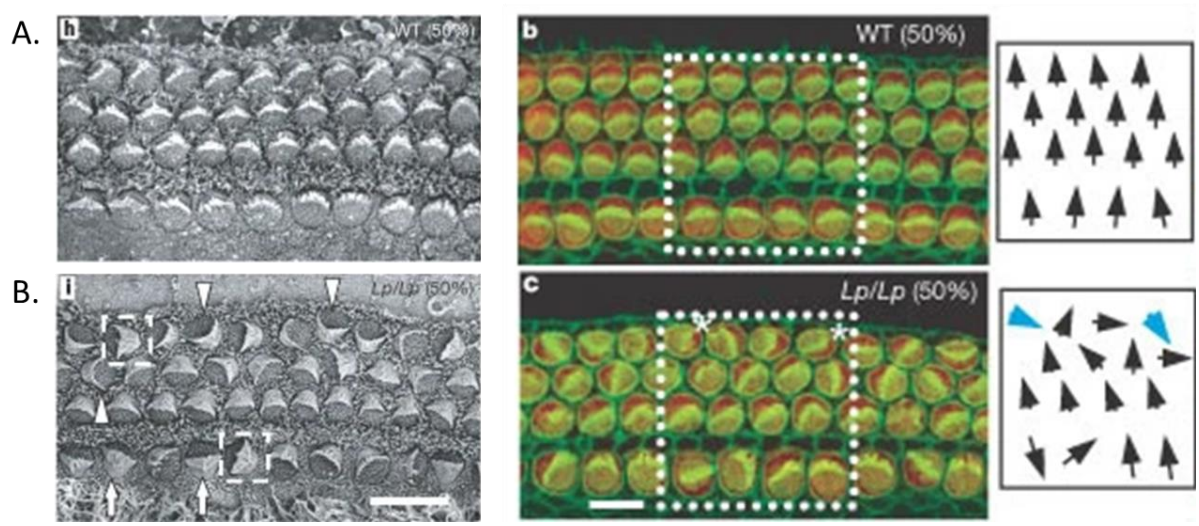

Figure 16: Example of a PCP phenotype in the mammalian cochlea. **(A)** SEM and immunofluorescence images of the surface of the organ of Corti in wild type E18.5 mice. You can appreciate the uniform orientation of the hair bundle along the PCP axis (black arrows on the right panels). **(B)** SEM and immunofluorescence images of the surface of the organ of Corti in E18.5 looptail mutant mice. The hair bundles are misoriented (white arrows and stars on the left panels). (from Montcouquiol et al., 2003).

Core PCP signaling has been shown to play a decisive role in the morphogenesis of many other tissues in mammals, ciliated or not. PCP participates to the polarization of ciliated cells in brain ventricles and the trachea, to cardiac and renal development and maturation as well as neuronal progenitor regulation (Henderson et al., 2001; Lake and Sokol, 2009; Tissir et al., 2010; Yates et al., 2010). The best demonstration of the importance of PCP signaling in cilia control came from a study in 2010, where Wong and collaborators showed that the deletion of both *vangl1* and *vangl2* lead to a loss of the left-right axis patterning in embryos, a mechanisms controlled by a small set of ciliated cells, the node cells (Wong et al., 2010).

More generally, PCP signalling seems to be crucial in most tissue morphogenesis in mammals, which supports a link between the dysfunction of these proteins and the onset of developmental disorders and pathology.

3.2- The core PCP protein Vangl2 in the CNS

In this section, we will focus on the protein of interest to our study, Van Gogh like 2 (Vangl2), in the context of the mammalian central nervous system.

3.2.1-Vangl2 and its function in PCP pathway

Protein structure

Van Gogh like 2 (Vangl2) is a vertebrate homologue of the Van Gogh/Strabismus (Vang/Stbm) protein discovered in Drosophila. Mutations of the gene coding for Vang/Stbm are associated with PCP defects in epithelial tissues, notably in the wing hairs and the eye (Taylor et al., 1998; Wolff and Rubin, 1998). In mice it was identified using the looptail mutant, in which missense mutations of the gene cause PCP defects and lead to severe neural tube defects (NTD) (Kibar et al., 2001). This gene is highly conserved throughout evolution and homologues have been identified in fish (Jessen et al., 2002), in amphibians (Darken et al., 2002). In vertebrates, 2 homologues of Vang have been identified: Vangl1 (Stbm2) and Vangl2 (Stbm1), both found on chromosome 1 in humans and mice (Kibar et al., 2001). The 2 homologues have a very similar structure and have many interactors in common, but their expression pattern can be either overlapping or be mutually exclusive depending on the developmental stage and organ (Nagaoka et al., 2014a; Tissir and Goffinet, 2006; Torban et al., 2012). Alterations in the balance of expression between Vangl1 and Vangl2 have been linked to development of neural tube disorders (NTD) both in murine animal models and in humans (Doudney et al., 2005; Torban et al., 2008).

Vangl2 encodes for a 521 amino acids (~60kD) tetraspanin protein containing four transmembrane domains and its Cter and Nter are both located in the intracellular part. Two Ser/Thr phosphorylation clusters are located in the Nter region of Vangl2 (Gao et al., 2011) while its Cter region contains the known interaction domains: a PDZ-binding motif and a protein interaction domain. The long Cter region is also where the 2 missense

mutations leading to the *looptail* phenotype are found (Torban et al., 2004b). The structure of the protein is detailed in **Figure 17**.

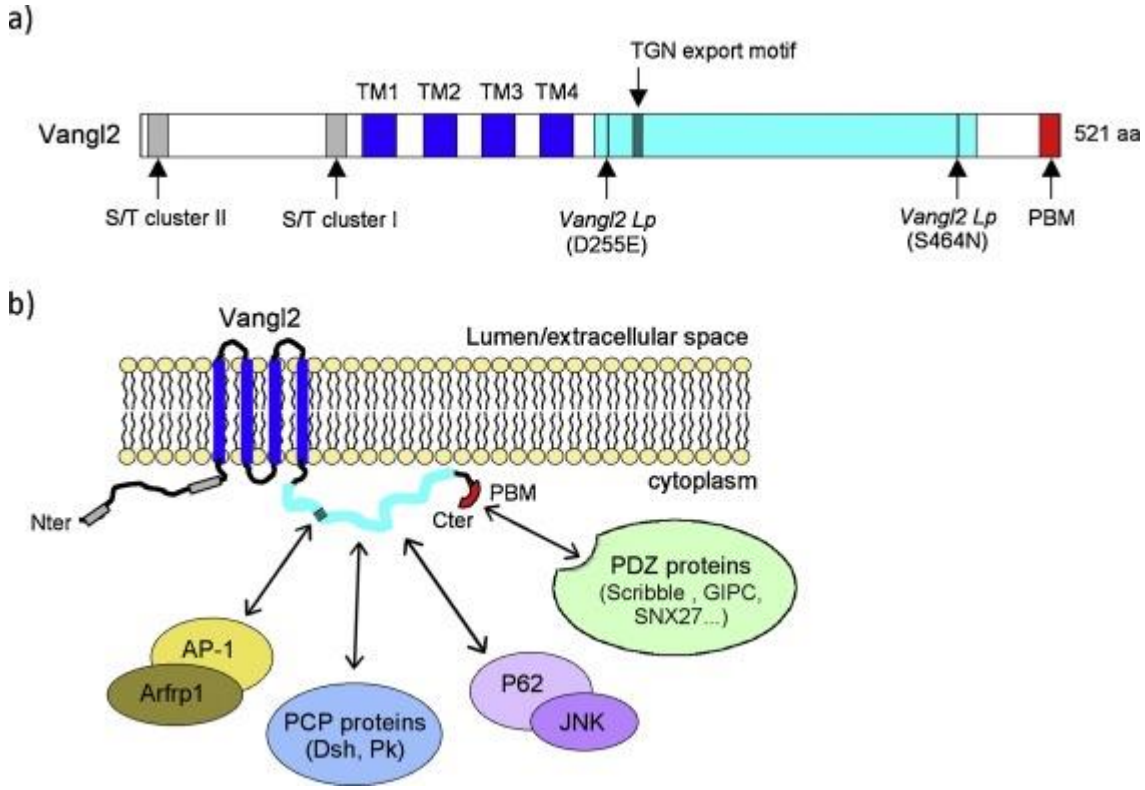

Figure 17: Structural and topological organization of Vangl2. **(a)** Structural organization of Vangl2 with the positions of the four transmembrane (TM) domains (dark blue), the two Ser/Thr phosphorylation site clusters (grey), the Dvl/Pk interacting region (cyan), the C-terminal PDZ binding Motif (PBM)domains (red) and the TGN sorting motif (grey box in the C-terminal region). Positions of the two Lp mutations are also indicated by arrows. **(b)** Schematic representation of Vangl2 topology and some of the potential interactions it can create with other proteins. (From Bailly et al., 2018).

Vangl2 Interactors

In *Drosophila*, Vangl2 and other proteins interact both intracellularly and intercellularly, leading to the transmission of the specific organization of the PCP proteins from cell to cell and to the establishment of the planar polarity through the entire tissue. These inter-intracellulars interplays also provide a molecular basis for the cell autonomous and cell non-autonomous actions of the transmembrane core proteins. By associating with transmembrane proteins, Vangl2 can promote proper assembly and targeting of the PCP complexes. We know for exemple that Vangl/Pk accumulates in an apical-proximal position while Fz/Dsh locates at the apical distal side (Bastock et al., 2003). But by associating with cytoplasmic proteins such as Dsh and Pk, Vang2 can recruit and regulate the activity of downstream effectors such as RhoA, Rac1 or Daam1

(Lindqvist et al., 2010; Seo et al., 2017; Strutt et al., 1997). The regulation of these downstream effectors allows the modulation of cytoskeleton dynamics. This organization is very sensitive to alterations of expression of the PCP genes, explaining why the loss of expression or overexpression of one of them leads to disruption of the interactions and loss of the organization of the other PCP proteins, inducing disruption of epithelial tissue development, organization and function.

In mammals, Vangl2 is known to interact with the different isoforms of Dishevelled (Dsh), and Torban et al. showed alterations of Dsh binding in Vangl2 mutants (Torban et al., 2004b). It is also known to interact with some Frizzled (Fzd) and Prickle (Pk) isoforms (Nagaoka et al., 2019). Vangl2 also interacts with associated PCP proteins, such as Scribble 1 (Scrib1) (Montcouquiol et al., 2003) and Celsr1 (Stahley et al., 2021). Vangl1 and Vangl2 can associate to form heterodimers at the plasma membrane (Belotti et al., 2012). In epithelial cells, such as *Drosophila* wings or mouse cochlea, Vangl2 and its interactors show a capacity to segregate in an asymmetric and stereotypical manner, typical from *drosophila* core PCP proteins (Adler, 2012; Devenport, 2014; for rewiew see Montcouquiol and Kelley, 2020). Vangl2/Pk accumulates in an apical-proximal position while Fz/Dsh locates at the apical distal side (Bastock et al., 2003).

Vangl2 also interacts with many non-PCP-related proteins (reviewed in Bailly et al., 2018).The intracellular PDZ-binding domain located in Cter allows interactions with numerous PDZ proteins such as the PCP-associated protein Scribble, GIPC1 and SNX27 which participates to Vangl2 trafficking, MAGI-3 which regulates Vangl2 activation of effectors, and DLG/SAP97 and PSD95 (Courbard et al., 2009; Giese et al., 2012; Yao et al., 2004; Yoshioka et al., 2013). The interaction found between Vangl2 and PSD95 in the postsynaptic densities of dendritic spines of neurons is thought to be necessary for the clustering of postsynaptic molecules, but has little to no role in the localization of Vangl2 in the postsynapse (Nagaoka et al., 2015).
In the same structure, Vangl2 is found interacting with the adhesion molecule N-cadherin (Nagaoka et al., 2014b), reminiscent of what was showed in drosophila epithelial cells with E-cadherins ,suggesting a role of Vangl2 in the formation/maintenance of this structure. Our group recently showed that Vangl2 regulates the levels of N-cadherin at the membrane engaging in the clutch mechanism to modulate axonal outgrowth in young hippocampal neurons (Dos-Santos Carvalho et al., 2020).

Other putative Vangl2 interactors could be found in the vast family of heparan sulfate proteoglycans (HSPG). A recent study has shown that Vangl2 and a key component of HSPG, the glycosaminoglycans (GAGs) chains, are co-expressed in mouse embryos (Nychyk et al., 2022). The combination of the loss of GAGs chains with heterozygote looptail mutation also give rise to severe NTD, which would be normally absent in heterozygote looptail mice. These results suggest a possible interaction between Vangl2 and proteoglycans, which could work together for neural tube closure. One candidate of interest for Vangl2 interaction is Syndecan4 (Sdc4), from the transmembrane HSPG family of syndecans. Sdc4 has been shown to participate in PCP-dependent CE mechanisms during *Xenopus* gastrulation phase, and has a partially overlapping expression pattern with Vangl2 (Muñoz et al., 2006; Torban et al., 2007). A study using looptail mutant mice showed that Vangl2 interacts genetically with Sdc4, as the PCP phenotypes of Vangl2lp mice are worsened when Sdc4 is also mutated. In the same study, they showed that the stability of Sdc4 levels seem to be regulated by Vangl2, as shown in looptail mutant mice where Sdc4 expression can't be detected in otic vesicles and non-neural ectoderm (Escobedo et al., 2013). However, despite both proteins having a PBM, the proof of a physical interaction between the two remains to be established. Another interesting HSPG candidate as Vangl2-interactor is Glypican 4 (GPC4), which is a GPI-anchored HSPG protein. Studies in the zebrafish embryo showed that Vangl2 and GPC4 both participate in mesoderm and endoderm CE mechanisms (Marlow et al., 1998; Ohkawara et al., 2003). Several studies have shown that GPC4 is needed for planar polarization of mesodermal and endodermal cells, and GPC4 mutations result in PCP phenotypes in those cells, even aggravating those present in Vangl2 mutants (Balaraju et al., 2021; Jessen et al., 2002; Topczewski et al., 2001). However other studies report that GPC4 mutants do not induce PCP phenotypes, notably in the hair cells of the sensory lateral line system of zebrafish (Navajas Acedo et al., 2019). The PCP role of GPC4 and putative Vangl2 interaction might be tissue- and stage-dependent. A lot is yet to be discovered about the relation between Vangl2 and HSPG.

3.2.2- Vangl2 expression in the central nervous system

Among other PCP proteins, Vangl2 expression in the CNS through the embryonic development until the adult stage has been thoroughly studied in mice. Vangl2 has been

shown to be expressed in the whole embryo at low level during the very early development (E7). Its expression level then increases to reach a peak at E11 and remains high during the end of development and postnatally (Kibar et al., 2001). More specifically, at E7-7.5, Vangl2 is expressed within the presumptive neuroectoderm and persists at the neuroepithelium through the late stages of neural tube closure. Interestingly, at E10.5 vangl2 is found enriched in the entire CNS and the otocyst, a structure that will give rise to the inner ear system, both auditory and vestibular (**see Figure 18A**).

Later in the development, at E12.5, Vangl2 mRNA is highly expressed in mindbrain, retina and in telencephalon, specifically in precursor neurons in the ventricular zone (VZ), with a caudal-rostral expression gradient (Tissir and Goffinet, 2006). In newborn mice, Vangl2 expression stays abundant in VZ, rostral migratory stream (RMS) and in the external granular layer of the cerebellum. Its expression is moderate at this stage in the telencephalic cortical plate (CP), cortex and in the hippocampus, specifically in the dental gyrus (DG). These expression levels stay stable during brain maturation (around P10). Vangl2 expression in hippocampus has been also seen in mouse hippocampus and in rat hippocampal cultured neurons, and more precisely, Vangl2 colocalized with severals synaptic markers, mainly with PSD95 (Nagaoka et al., 2014b; Thakar et al., 2017; Yoshioka et al., 2013).

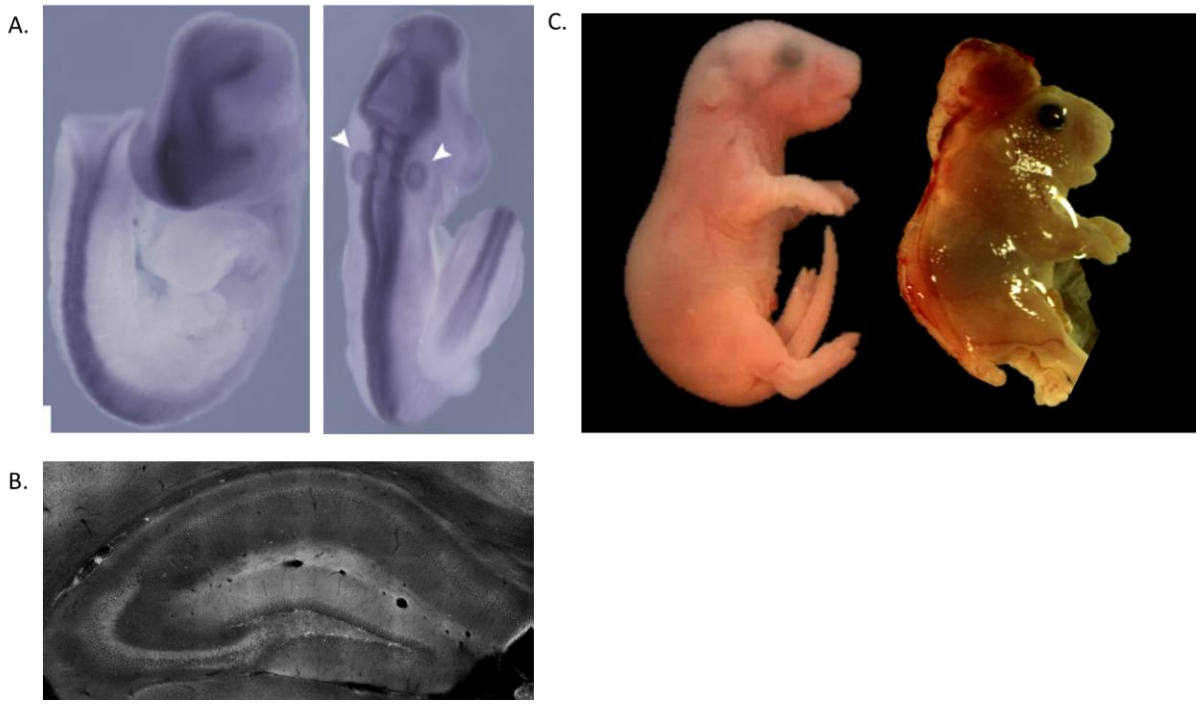

Figure 18: Vangl2 in the central nervous system. **(A)** In situ hybridization of Vangl2 mRNA in E10.5 mouse embryos, showing the enrichment of Vangl2 in the neural tube and in the otocyst (white arrows). **(B)**

Immunofluorescence image of Vangl2 expression in the adult mouse hippocampus, showing an enrichment in the DG and the CA3. **(C)** Exemple of NTD caused by Vangl2 looptail mutation, images from Montcouquiol Sans' lab. (Adapted from Kibar et al., 2001; Robert et al., 2020).

At a more mature stage, around P21, Tissir and Goffinet found a more diffused expression level of Vangl2, which remains significant in the DG and around lateral ventricles. This was confirmed in adult mice (10 weeks old), where Vangl2 is present in the hippocampus with specific enrichment in the granule cells of the DG and in the *stratum lucidum* of the CA3 **(Figure 18B)** (Robert et al., 2020). Vangl2 has recently been shown to be expressed in mice oligodendrocytes cell bodies and processes (Jarjour et al., 2020).

3.2.3-Vangl2 developmental role in the CNS

Convergent extension and neural tube closure

As described precedently, Vangl2 is expressed in the central nervous system during embryonic development as well as postnatally. Indeed, studies show that Vangl2 plays a key role in the correct formation of the CNS, notably in the closure of the neural tube as well as in neuronal migration. Formation of the CNS begins in the vertebrate embryo during the neurulation phase, where the mediolateral axis of the neural plate is converted into the dorsoventral (DV) axis of the neural tube. Then the neural tube starts closing, starting with the elevation of the neural folds, which will join and fuse at three points of the embryo. From these three points, the neural fold fusion is initiated and tube closure spreads in both a rostral and caudal direction (Colas and Schoenwolf, 2001; Copp et al., 2003). Failure of these closure steps induces several disorders with varying severity, grouped in the family of the Neural Tube Defects (NTD).

Vangl2's role in the neural tube closure mechanism was discovered using the Looptail mutant (Lp) in which the *vangl2* gene carries a missense mutation (S463N) (Kibar et al., 2001). The Lp mutant is characterized by severe NTD (craniorachischisis) and embryonic death when the mutation is homozygote (Strong and Hollander, 1949), proving the importance of Vangl2 expression for the correct development of the CNS. Lp mutants display an enlargement of the gap formed by the ventral neural plate in between the neural folds at E8.5 compared to the controls, which disrupt the subsequent closure of the neural tube by preventing the fusion of the neural folds (Greene et al., 1998). Later, a study showed that Vangl2 is asymmetrically expressed in the floor plate of the neural

tube where, along with the protein Sonic hedgehog (Shh), it contributes to the neurulation (Murdoch et al., 2001). The importance of Vangl2 in the neurulation mechanism is due to its role in convergent extension (reviewed in Torban et al., 2004a). Convergent extension is the process by which the tissue of an embryo is restructured to converge along one axis and extend along a perpendicular axis by cellular movement, which we found in the context of neurulation and neural tube closure. Vangl2 has been shown to be involved in this mechanism in several vertebrate models and that alteration of Vangl2 expression lead to the inhibition of convergent extension (Darken et al., 2002; Goto and Keller, 2002; Park and Moon, 2002; Torban et al., 2004b). Later it was shown that the phosphorylation of Vangl2 by Wnt5a and Ror2 was necessary for its role in neural tube development (Gao et al., 2011; Yang et al., 2017). Wtn5a asymmetric expression in the neural tube induces the formation of a complex with Vangl2 and Ror2, inducing a gradient of Vangl2 phosphorylation (Gao et al., 2011). Using phospho-Vangl2 mutants and Ror2 mutants, it was shown that the absence of Vangl2 phosphorylation resulted in development of NTD in the embryo and a loss of the asymmetric repartition of Vangl2 (Yang et al., 2017). The same study showed that Dvl and CK1ε/δ were involved in the mechanisms of phosphorylation of Vangl2 during neural tube formation.

Asymmetric cell division and neurogenesis

In the vertebrate brain, Vangl2 is also involved in neurogenesis and cell fate determination (reviewed in Hakanen et al., 2019; Smith et al., 2017). In Drosophila, Vang is necessary for the recruitment of the associated PCP protein Partner of inscuteable (Pins) at anterior localization, which enables the correct asymmetric division of the sensory organ precursor cells (Bellaïche et al., 2004; Montcouquiol and Kelley, 2020). In mammals, the development of the complex brain cell organization is thought to depend on the balance between symmetric and asymmetric divisions of neural progenitors occupying the ventricular zone. The asymmetric cell division of neural progenitors allows them to renew as well as to produce daughter cells who will become excitatory neurons or glial cells. This is enabled by a mechanism called spindle size asymmetry, during which the mitotic spindle is positioned asymmetrically in the cell leading to the formation of one small daughter cell which will become a self-renewed precursor, and a big daughter cell which will become the neuron or glial cell. Vangl2 participates in the asymmetric cell division of neural progenitors during corticogenesis in embryos (Delaunay et al., 2014; Lake and Sokol, 2009). It has been shown that Vangl2, along with its activator Wnt7A,

determines the position of the metaphase plate and the size of the spindles. High Vangl2 and Wnt7A levels lead to the suppression of spindle size asymmetry in dissociated neurons (Delaunay et al., 2014). Looptail mice precursors had an increased level of spindle size asymmetry and asymmetric cell division in vivo at E11.5 and E14.5 (Delaunay et al., 2014; Lake and Sokol, 2009). However little to no effect of Vangl2 was observed on the orientation of the plane of division. The impact of Vangl2 on neurogenesis subsits even in later stages. The same study showed that Vangl2 downregulation in vivo induced an early exit of the cell cycle in the neural cell progenitors, leading to a reduction of the size of the precursors pool still available after birth and therefore inducing a decrease of late born neurons generation (Delaunay et al., 2014). A recent study from Koehl et al. in collaboration with our lab showed that the looptail mutation of Vangl2 affects the survival of adult-born neurons in the DG of adult mice, suggesting a role for Vangl2 in adult neurogenesis (Koehl et al., 2022).

3.2.4- Vangl2 implication in cellular mechanisms in the CNS

Vangl2 and adhesion

As stated previously, Vang, along with Fz and Fmi, are essential for the intercellular organization and cell-cell junctions during Drosophila wing patterning (Strutt and Strutt, 2007, 2009; Strutt, 2001). Since then, several studies have been made about possible interactions between Vangl2 and adhesion molecules in the CNS.

So far, most of the data linking Vangl2 and adhesion molecules are on N-Cadherin. In 2014, Nagaoka et al. managed to coimmunoprecipitate Vang2 with N-cadherin using purified PSD fraction. This physical interaction would require Pk binding domain on the Cter of Vangl2 and the b-catenin binding site in N-cadherin (Nagaoka et al., 2014b). Experiments on hippocampal neuron cultures show that this Vangl2-N-Cadherin interaction is essential for Vangl2 function, and that Vangl2 regulates at least partially N-cadherin internalization at the synapse. Our group supported a functional link between Vangl2 and N-cadherin in young hippocampal neurons (Dos-Santos Carvalho et al., 2020). This study further show that the environment, for exemple the composition of tge extracellular matrix (ECM), can reciprocally modulate the axonal outgrowth.

A similar interplay between componants of the ECM and Vangl2 at the membrane has been observed in other systems. Recently, Jessen and Jessen showed in a

fibrosarcoma cell line as well as in zebrafish embryos, that the presence of αv integrins, which are known to interact with ECM proteins, modulate the levels of Vangl2 available at the membrane (Jessen and Jessen, 2019). Moreover they showed that altering the integrin-ECM interactions reduced the Vangl2 levels, suggesting that directly or indirectly stabilizes plasma membrane Vangl2 by preventing its internalization. ECM proteins also regulates Vangl2 through fibronectin, which has been shown to be necessary for Vangl2 translocation to the plasma membrane (Love et al., 2018), but rescue of fibronectin expression rescues Vangl2 membrane protrusion phenotype but not its PCP pathway functions. Matrix metalloproteinases and especially MMP14 could be involved in this ECM degradation regulation as Vangl2 has been shown to regulate MMP14 endocytosis downstream of focal adhesion kinase (Williams et al., 2012).

Role in axonal guidance

PCP has a well known influence on axonal guidance, through different proteins such as Celsr3 and Fzd3 (Chai et al., 2014; Hua et al., 2014; Lyuksyutova et al., 2003). The function of Celsr in axonal guidance is conserved from *Drosophila*, where Fmi also controls axonal guidance. Fz isoforms in axonal growth is conserved from invertebrates to mammals (Lyuksyutova et al., 2003; Pan et al., 2006; Shimizu et al., 2011). The role of Vangl2 on this axonal guidance is more controversial, as it was not reported in *Drosophila*.

At embryonic stage, Looptail mutant mice (Lp) shows monoaminergic axon guidance defects in the brainstem and a hyperfasciculation phenotype that can suggest a Vangl2 implication on axon-axon interactions (Fenstermaker et al., 2010). In Shafer et al., 2011, it's shown that the anterior-posterior commissural axons defects that is observed in Lp mutant embryos is due in part by the fact that Vangl2 mediate Wnt-stimulated commissural axon outgrowth, as it has been shown for Fzd3. This implication of Vangl2 on axon guidance is consolidated with their observations of commissural neuron filopodia: the filopodia that are elongating or stable tend to have higher levels of Vangl2 expression than the shortening filopodia. In Vivancos et al., 2009, it's in the facial branchiomotor neurons distribution that Lp mutant embryos show abnormalities. Significant axonal guidance defect has been also observed later in retinal ganglion cells of Lp mutant embryos (Leung et al., 2016). More recently, we showed that the conditional mutant Emx1-Vangl2$^{-/-}$ cKO mice have an agenesis of both the corpus callosum and the

hippocampal commissure (Dos-Santos Carvalho et al., 2020) that we argued was du to a disruption of axonal outgrowth but not axonal guidance. We failed to observe in these mutants the massive axonal deficits reported in Celsr3 or Fz3 mutants (Tissir et al., 2005; Wang et al., 2002). A compensatory mechanism via Vangl1 can be excluded as ta conditional mutant for both the *vangl1* and *vangl2* genes also failed to report such deficits(Qu et al., 2014).

In the forebrain of Foxg1-Cre;Vangl2f/f mice (and Vangl1$^{-/-}$ mice) at P0 (Qu et al., 2014) no axonal guidance defect is observed at the anterior commissure, the corticospinal tract, the internal capsule or the thalamocortical axons.This suggests that Fzd3 and Celsr2-3 guide forebrain axons in a Vangl-independent manner. This is also observed in motor neuron axons projecting into the hindlimb (Chai et al., 2014). In Vangl2$^{-/-}$ embryos, in contrast to Celsr3 or Fzd3 mutants, no hindlimb malformation or motor and peroneal axon projection defect have been observed.

This difference in Vangl2 implication in axonal guidance could be due to a dominant negative activity or an eventual gain of function associated with the Lp mutation. Indeed the Lp allele encodes a mutated Vangl2 protein that may modify the function of the endogenous Vangl2 and/or other PCP signaling proteins.

Role in dendrite outgrowth

Vangl2-depleted neurons exhibit reduced density of presynaptic Synaptophysin puncta, as well as for postsynaptic PSD95, suggesting that Vangl2 has a role on synaptogenesis (Nagaoka et al., 2014b). Lp mutants show a decrease of dendritic spine density in hippocampal neurons. Vangl2-depleted hippocampal neurons have less dendritic spines and abnormal dendritic branching (Hagiwara et al., 2014). These phenotypes are also observed in cultured glutamatergic neurons of the forebrain in Vangl2 knockout mice that present simpler dendrite arbors and less spines (Okerlund et al., 2016) . However in a different Vangl2 cKO mice model, CA1 pyramidal cells present an increased in spine density *in vivo* at P7 and P14 (Thakar et al., 2017).

In vitro, Vangl2-depleted neurons exhibit a reduced average density of PSD95 clusters along the dendrites (Nagaoka and Kishi, 2016). The idea of a precise and complex spatio-temporal function for Vangl2 is critical. Recently, our group showed that in a conditional mutant for Vangl2, where the gene is deleted in postmitotic neurons thus bypassing its developmental function, hippocampal GCs presented smaller spine and a more detailed arborization defect. Interestingly, their proximal part of the dendritic tree is

less complex while the distal part was more ramified than in control GCs (Robert et al., 2020).

Mechanistically, Vangl2 localization in the postsynaptic compartment, and its role on the dendritic spine has been associated with its Cter TSV domain which binds to the third PDZ domain of PSD95, as a Vangl2-ΔTSV is less concentrated in dendritic spine (Torban et al., 2004a; Yoshioka et al., 2013). We and others showed that the association between Vangl2 Cter Prickle-binding domain and N-Cadherin also acts on spine formation through N-cadherin internalization (Dos-Santos Carvalho et al., 2020; Nagaoka et al., 2014b). Intriguingly, Vangl2-ΔTSV and Vangl2-ΔC have only a small effect on dendritic spines, and Vangl2-ΔC significantly increases dendritic development in cultured hippocampal neurons in contrast with the Nterminal region deletion which triggers a significant decrease in spine density (Hagiwara et al., 2014). These results suggest a bidirectional regulation of Vangl2 on spine and dendritic formation.

Finally, a recent study showed that this regulation of spine formation depends on the interaction of Vangl2 with the Ap2m1 protein, which is involved in the regulation of clathrin-mediated endocytosis. Depletion of Ap2m1 in cultured neurons replicates the reduction of spine formation observed in Vangl2 knock-down models (Yasumura et al., 2021). This further establishes the importance of Vangl2 in the regulation of dendritic morphology development.

Role in glia

Very little is known about the role of Vangl2 and other PCP proteins in glial cells. However, a recent study explored a role for Vangl2 in oligodendrocytes (Jarjour et al., 2020). This study shows for the first time that Vangl2 is also expressed in oligodendrocytes and localized in the paranodes of P60 spinal cord neurons, as well as one of his binding partners, Prickle1. In Vangl2 cKO mice, a disruption of the paranode was observed through a loss of Caspr spiral, suggesting that Vangl2 is required for normal adhesion between paranodal loops but not between paranodal loop and axon. This could be due to a mislocalization of Claudin-11, an adhesion protein, observed in Vangl2 cKO mice paranodal tight junctions. The authors also observed that oligodendroglial Vangl2 is essential to maintain the separation between axonal nodal and paranodal domains, and to regulate the axonal diameter in the nervous system.

These observations could be a gateway to a new role of Vangl2, and PCP in general, on cellular organization within the nervous system.

Role in ependymal cells

Ependymal cells are epithelial polarized cells lining the cerebral ventricles surface and are involved in the circulation of cerebrospinal fluid (CSF) thanks to the coordinated movements of their multiple motile cilias (Ohata and Álvarez-Buylla, 2016). Ependymal cells originate from the division and differentiation of radial glia cells during embryonic development (between E14 and E16) (Merkle et al., 2004; Spassky et al., 2005). Alteration of the ependymal cells can result in hydrocephalus with varying degrees of severity. Several studies showed that the PCP pathway and Vangl2 are responsible for the polarization and the organisation of the ependymal cells in the brain. In collaboration with the group of N. Spassky, we showed that Vangl2 has a planar and asymmetrical localization within the ependymal in P4 mice (Guirao et al., 2010). This planar distribution is required for the correct orientation and beating direction of the ependymal cilia in response to CSF flow (Guirao et al., 2010). Vangl2 is also necessary for the polarization of the radial glia cells and the organization of cilia at both the single cell level and the whole tissue level. Loss of polarity of radial glia cells and disorganization of the multiple ependymal cilia were observed in Vangl2 mutants (Boutin et al., 2014). These observations led to the passive flow hypothesis: early hydrodynamic flow of CSF on the surfaces of radial glia cells has been proposed to help guide the initial establishment of planar polarity in these cells and later in the ependymal cells (Mirzadeh et al., 2010; Ohata and Álvarez-Buylla, 2016). The alteration of other proteins could alter the asymmetrical localization of Vangl2 in the ependymal cell cilia and basal body. Mechanosensory proteins Pkd1 and Pkd2 deletion in radial glia cells affects the localization of Vangl2 later in ependymal cells (Herranz-Pérez et al., 2015). Mutants of Celsr1/2/3 proteins, which are known Vangl2 interactors, present an altered expression and a mislocalization of Vangl2, leading to hydrocephalus (Boutin et al., 2014; Tissir et al., 2010). This suggests an interaction between the Wnt/PCP pathway and the Pkd pathway to establish the early polarization of the radial glia cells and the subsequent correct organization and function of the ependymal cells. The PDZ protein NHERF1, which interacts with Vangl2 through its PDZBM, is necessary for its asymmetric localization at the ependymal cell membrane and its deletion leads abnormal Vangl2 localization, affects ependymal ciliogenesis and induces hydrocephalus (Treat et al., 2016). Those studies highlight the importance of

Vangl2 and more globally of PCP signaling in the organization and function of brain ciliated cells, both at the cell and tissue levels.

3.2.5- Functional implication of Vangl2 CNS expression

To this day, only a few studies link the expression of Vangl2 in the brain to functional processes. However, due to the multiple cellular roles of Vangl2, one can expect a more global functional relevance of the expression of the PCP protein. In 2020, Robert et al. showed that Vangl2 participates in the regulation of pattern separation and pattern completion, two processes highly dependent on the DG-CA3 hippocampal circuit. The genetic ablation of *vangl2* in adult mice affected the maturation of DG granule cells, resulting in the destabilization of AMPAR in the synapses located in the molecular layer and in the reduction of LTP. Mutant mice displayed impaired performances in pattern completion tasks, which were rescued after reexpression of Vangl2 in the DG. This study showed that Vangl2 regulates DG activity and specific hippocampal-dependent cognitive processes. Additionally, a collaborative study with the group of N. Abrous showed that adult Vangl2 looptail mutant mice had impaired spatial memory flexibility and accelerated age-related deterioration of memory (Koehl et al., 2022) . This work suggests that altering Vangl2 can have long lasting consequences on cognitive processes. The work of Jarjour et al. showed that altering Vangl2 expression in oligodendrocytes affected the organization of the Ranvier's nodes along myelinated axons in the CNS, resulting in altered action potential threshold and conductivity (Jarjour et al., 2020). This suggests that Vangl2 impact on functional processes could be extended to the whole CNS and not only the hippocampus.

3.2.6-Vangl2 and CNS pathologies

As we saw in the previous sections, Vangl2 is involved in a great variety of processes that are necessary for the correct cerebral development and function, from the cellular level to global circuitry. Because of that, one could assume that Vangl2 might also be involved in various pathologies, from neurodevelopmental to neurodegenerative diseases.

Vangl2 and NTDs

As reported previously, Vangl2 is crucial for CE mechanisms and for neural tube closure. VANGL1 and VANGL2 mutations have been reported in patients with neurodevelopmental pathologies included in the NTDs such as spina bifida, anencephaly and craniorachischisis (Iliescu et al., 2014; Kibar et al., 2011; Lei et al., 2010). A recent study showed that the abnormalities induced by these mutations result from PCP deficits (Humphries et al., 2020). The VANGL2 mutations reported in living patients are all heterozygous, showing that the severe impact of these mutation of VANGL2 during in utero development is probably incompatible with life, and would explain why there is still no association between the VANGL genes and neurodevelopmental disorders such as ASD or ID. However, microduplications of the chromosomal region including VANGL2 gene were found in the Decipher database in patients displaying symptoms commonly associated with ASD and ID such as with microcephaly, delayed speech and language development, stereotypic behaviour and scoliosis. Further studies are needed to understand the implication of Vangl2 in neurodevelopmental disorders.

Vangl2 and Alzheimer's disease

The first gene linked with familial AD (FAD) is the β-amyloid precursor protein (APP). As the precursor of Aβ peptides, APP is at the center of AD neuropathology and is extensively studied in order to better apprehend the onset of AD. Despite the normal physiological function of APP in vivo in the nervous system remaining elusive, there is evidence for a role in cell signaling and endocytosis. The work of Killick and others have shown that APP and Aβ synaptotoxicity in AD is linked to Wnt-PCP signaling (Caricasole et al., 2004; Elliott et al., 2018; Killick et al., 2014; Sellers et al., 2018). Indeed studies have shown that APP is a direct interactor of Vangl2 in both Drosophila and mice (Elliott et al., 2018; Soldano et al., 2013). Mutated versions of APP such as APP_{Swe} bind preferentially to Vangl2, inducing the activation of the Wnt-PCP pathway while reducing the activation of the canonical Wnt-βcatenin pathway, resulting in synaptic loss by both reducing synaptogenesis and enhancing synapse withdrawal, at least in those FAD cases carrying the APP_{Swe} mutation (Elliott et al., 2018). Further studies are necessary to establish if this mechanism applies to other forms of FAD. Wnt-PCP is known for its role in endocytosis and endosomal trafficking, which is a key mechanism in Aβ production. Endosomal trafficking of FAD mutant forms of APP, including APP_{Swe}, has been shown

to differ from that of wild-type APP. It has been shown that the increase of Aβ peptide production resulting from altered APP_{Swe} trafficking is correlated with increased Wnt-PCP signaling activation (Elliott et al., 2018). This suggests that when APP preferentially activates the Wnt-PCP pathway, it is more likely that Aβ production is increased. Increased levels of Aβ peptides have been shown to promote the expression of the protein Dkk1, a regulator of the Wnt signaling pathways. Synaptotoxic forms of Aβ induces the activation of the Wnt-PCP RhoA/ROCK pathway and the inhibition of the canonical Wnt-βcatenin via upregulated levels of Dkk1, leading to synaptotoxicity and altered localization of synaptic proteins (Sellers et al., 2018). Moreover, a recent study showed that Vangl2 participates in the synaptotoxic effect of Aβ oligomers both in vivo and in vitro, via its interactor Ryk (Feng et al., 2021). This suggests that Vangl2 and by extension the Wnt PCP pathway are an interesting therapeutic target for neurodegenerative diseases such as Alzheimer’s disease.

Aims and hypothesis

As outlined in this introductory chapter, the development and maintenance of correct connectivity and function of the hippocampus depends on the fine tuning of a great variety of mechanisms, and a misregulation can have great consequences such as neurodevelopmental and neurodegenerative disorders. Investigating the molecular mechanisms underlying the hippocampal circuits' connectivity is key to understanding these pathologies.

The complex MFB/TE synapse that connects the DG to the CA3 has been shown to be a key element of the hippocampal circuitry. In the hippocampus, mossy fiber boutons (MFB) form these complex giant synapses with the elaborate dendritic spines (called thorny excrescences or TE) of CA3 pyramidal cells in the *stratum lucidum* (*sl*) region. Structural alterations of these connections were shown in mouse models of disorders such as Down syndrome or Alzheimer's disease. The MFB/TE synapse's postnatal morphogenesis depends on cytoskeleton remodeling, specific trans-synaptic complexes and cell-surface molecules such as neurexin/neuroligin or the HSPG cell surface molecules.

Amongst the many regulators of cytoskeleton remodeling, the Wnt/PCP pathway is a conserved signalling pathway known to shape tissues during development via the regulation of adhesion complexes and cytoskeleton dynamics. Recently, our lab showed that the PCP protein Vangl2, known for its role in embryonic morphogenesis, is enriched in the dentate gyrus (DG)/CA3 network of adult mice and that its postnatal deletion affects the DG granule cell maturation. We also showed that Vangl2 controls neuronal outgrowth of young hippocampal neurons via the regulation of the adhesion molecule N-cadherin.

The aim of this thesis was to decipher whether Vangl2-dependent signalling is necessary for regulating the synaptic organizing protein complexes that control MFB/TE synapse development, structural maturation and morphofunctional plasticity throughout life.

The first objective was to establish the role of Vangl2 during the postnatal development of the MFB/TE synapse, thanks to a conditional knock-out model developed in the lab: the Emx1-Vangl2$^{-/-}$ mouse. I characterized the consequences of the early deletion of the protein on the morphology, molecular characteristics and function of the synapse both at

the juvenile and adult stage. I also studied the behavioural consequences of the mutation in adult mice.

Studies have already established a role of Vangl2 in the pathophysiology of Alzheimer's disease, a disorder associated with pathological aging and known to affect the MFB/TE synapse. However, no characterization of the role of Vangl2 during physiological aging has been done. Therefore, the second objective of my thesis was to evaluate the consequences of the early deletion of Vangl2 during physiological aging, with the aim to better know the role of Vangl2 in aged stages.

Chapter II : Methods

Animals

This study was performed according to the European Communities Council Directives (2010/63/EU) with local ethical approval. The conditional knockout line (Emx1-Vangl2$^{-/-}$) was generated by crossing Vangl2 flox/flox animals (Ramsbottom et al., 2014) with Emx1B6.129S2-Emx1tm1(cre)Krj/J (Emx1-Cre) mice. Emx1 is expressed in the entire telencephalon as early as E10.5 (Gorski et al., 2002). The recombination is predicted to produce a premature stop codon that gives rise to a small 8 KDa protein, which lacks the four trans-membrane domains and C-terminal PDZ-binding domain (Dos-Santos Carvalho et al., 2020). Mice were maintained under standard conditions (food and water ad libitum; 23 ± 1°C, 7 h–12 h light–dark cycle, light on at 7:00; experiments were performed between 9:00 and 17:00). Only male mice between 8 and 12-week-old unless specified otherwise were used and they were housed collectively in groups of five to eight in polypropylene cages.

For enriched environment (EE) experiments, sets of Emx1-Vangl2$^{-/-}$ and control males littermates were either kept in normal-sized common cages without additional objects (6-7 mouse per cage; Ctrl conditions), or in large (rat) cages equipped with 2 running wheels per cage, toys, and hiding spaces for exploration (7 mice per cage; EE conditions). The objects in the EE conditions were moved every 2 days and completely changed every week. EE was started at 7 weeks of age, one week after surgery (see methods below) and lasted 5 weeks.

Antibodies

The following antibodies were used in this study: rabbit polyclonal anti-dsRed (Takara-Bio), rabbit polyclonal anti-Vangl2 (Montcouquiol et al., 2006 ; commercialized by Millipore), rabbit polyclonal anti-Synaptoporin (Synaptic Systems), rabbit anti-Synapsin 1 (Synaptic Systems), mouse monoclonal anti-Bassoon (Enzo Life Sciences), rabbit polyclonal anti-GPC4 (Proteintech), rabbit polyclonal anti-GPR158 (Sigma), chicken polyclonal anti-GFP (Abcam), mouse monoclonal anti-HA (Biolegend), mouse monoclonal anti-myc (Covance), mouse monoclonal anti-PSD95 (Thermoscientific).

For c-fos staining, the antibodies used were: anti-c-Fos rabbit polyclonal antibody (Cell Signaling) and biotinylated goat anti-rabbit IgG (Jackson Immunoresearch).

Alexa fluor secondary antibodies were purchased from Jackson Immunoresearch and Invitrogen. For western blot, secondary antibodies goat anti-mouse or anti-rabbit coupled to the horseradish peroxidase (HRP, from Jackson Immunoresearch), donkey anti-guinea pig HRP (Jackson Immunoresearch) and mouse-anti Rabbit HRP (GE Healthcare UK) were used.

Plasmids and virus

The Vangl2-GFP construct is from Montcouquiol et al., 2006. The HA-GRP158, HA-GPC4 constructs were kindly given by Pr. De Wit (VIB-KU Leuven, Belgium) (Condomitti et al., 2018). The GPC4-myc construct was purchased from Origen. The pEGFP-C3 vector used as control was purchased from BD Biosciences Clontech. The pOrange-Vang2-GFP plasmid allowing the tagging of endogenous Vangl2 via CRISPR-Cas9 technology was generated by cloning an insert containing the *vangl2* sequence along with a GFP flanked by Vangl2 target sequence into a vector coding for the Cas9 (Addgene Plasmid #131471).

The adeno-associated viruses AAV2/9-CaMKII (0.4)-mCherry-WPRE and AAV2/9-CamKII(0,4)-mcherry-2A-mVangl2-WPRE were purchased from Vector Biolab (Robert et al., 2020).

Cell culture, transfection and immunocytochemistry

Hippocampal neurons

All the experiments are carried out on 15 mm coverslips coated overnight at 37° C. with 10 µg/ml of poly-L-lysine (PLL) taken up in a borax buffer then they are rinsed with Braun water.

Sprague-Dawley rats at E18.5 were used for mixed cultures of hippocampal neurons. Hippocampi were harvested in a mixture of Hank's balanced salt solution (HBSS, Gibco)/HEPES (Gibco)/penicillin-streptomycin (Gibco, 10 U/ml) and pooled and rinsed with cold hash solution (HBSS/HEPES /Dnase, Dnase (Sigma-Aldrich)). Their enzymatic dissociation is then carried out with a mixture of hot chopping solution with trypsin (Gibco) at 37°C for 12 to 15 min with one or two slow agitation. The action of the trypsin was

stopped with 4 washing in chopping solution then a mechanical dissociation was carried out by gently moving the mixture up and down using a Pasteur pipette with a refined end. The cells were counted and seeded in a culture medium containing neurobasal medium (Gibco), a B27 supplement (50x, Gibco) and 2% FBS at a rate of 106 cells for a 6-well plate and 3 coverslips per well. The neurons were kept in a humidified incubator, at 37°C and with 5% CO2. The middle half is changed to DIV3, DIV7, DIV10, DIV14 and DIV17 with neurobasal medium (Gibco), a B27 supplement (50x, Gibco).

One hour before transfection, the cell medium was removed and replaced with hot DMEM alone.Cells were transfected using calcium phosphate. The different cDNAs were mixed with 12.5 µl of 2M CaCl2 and H2O Braun to a total volume of 100 µl. For the transfection with the pOrangeVgl2 plasmid, the amount of cDNA was used at 12 µg and the transfection carried out DIV7. For the eGFP-C3, GFP-Vgl2, HA-Gpr158 and HA-GPC4 plasmids, the transfection is carried out at DIV15 at a rate of 5 µg, 5 µg, 10 µg and 10 µg respectively.

The CaCl2 cDNA mixture was added dropwise and with stirring to 100 µl of 2x HBS and then incubated for 30 min at room temperature in the dark before being added to the cells. The plates were then placed back in the incubator for 40 min before performing 4 washes in DMEM alone, the last wash being placed in the incubator for 10 min. Then the DMEM was replaced with old culture medium diluted half with new culture medium. Cells were stopped at DIV21 for the pOrange and DIV18 for the other to perform the immunostaining.

COS7 cell line

COS-7 (ATCC-American Type Culture Collection) were cultured with advanced Dublecco's modified Eagle's medium (DMEM, Gibco) supplemented with 10% fetal bovine serum (FBS, Gibco), 1% L-glutamine 200 mM (Gibco) and 1% penicillin-streptomycin (10000 U/ml, Gibco). Cell cultures were grown in a humidified incubator at 37°C with 5% CO2. Subculture procedure was done following the indications of the distributor. For transfecting COS-7, cells were plated onto 6-well plates with 3 coverslips (15 mm) per well in complete DMEM at a suitable dilution to reach 30-40% confluence before transfection. Cells were transfected using calcium phosphate (Piguel et al., 2014). The different cDNAs were prepared with 12.5 µl of CaCl2 and H2O until a total volume of

100 µl. For cDNA quantities, 1µg was used for Pk2, 4 µg for AnkG-480, Scrib and bIV spectrin. These values were kept for double transfections. The resulting mix was applied, dropwise, to 100 µl of HBS 2x incubated for 30 min at room temperature in the dark and applied to the cells. The plates were then placed back in the incubator for 5h. After that, 3 abundant washes with serum-free DMEM were performed and the plate cells in the incubator for 10 minutes. Finally, serum-free DMEM was replaced by complete medium. 24h later, cells were fixed and processed for immunocytochemistry. COS-7 cells were fixed with 4% sucrose 4% PFA for 10 min at RT, permeabilized and blocked with 5% BSA 0.3% triton X-100 in PBS for 1h at RT and incubated with primary antibodies for 1h at RT. After extensive washes, secondary antibodies were incubated for 30 min at RT and coverslips were mounted using Fluoromount-G antifade medium (Electron Microscopy Sciences).

Stereotaxic injections

Stereotaxic viral injection into neonatal mice. Under sterile conditions, mouse pups (P5) were beforehand anesthetized by inhalation of a O_2/Isoflurane mix. The pups were considered anesthetized when all movement stops and no reflexes subsisted. Anesthetized pups were then secured in a digital stereotaxic frame with neonatal mice adaptor (World Precision Instruments, Inc., Sarasota, FL, USA), maintained on O_2/isoflurane inhalation (0.2%). Before performing the surgical incision, 5 µl of lidocaine (5 mg/kg, intradermal) was injected at the incision site for local anesthesia. Holes of the size of the injection needle were drilled with a fine needle into the skull, and injections were distributed using a 30G Nanofil needle attached to a Nanofil syringe (World Precision Instruments, Inc., Sarasota, FL, USA) coupled with a UMP3 UltraMicroPump (WPI). To label DG MF and/or reexpress *vangl2*, 100 nl of AAV2/9-CaMKII (0.4)-mCherry-WPRE virus (titer of 1.9 10^{12} genome copies/ml diluted in sterile PBS, Vector Biolabs) or AAV2/9-CaMKII(0,4)-mcherry-2A-mVangl2-WPRE virus (5,9 x 10^{13} gcp /ml or 1,7 x 10^{13} gcp /ml in sterile PBS, Vector Biolab) were injected bilaterally in the dentate gyrus zone (Y: ~1mm from lambda; X: ±0.75 mm; Z: 1.65 mm). After surgery, neonates were allowed to recover on a warm heating pad and, then, returned to their mother until P25.

Stereotaxic viral injection into adult mice. 6- to 8-weeks-old mice were injected with a buprenorphine solution (0.15mg/kg, intraperitoneal) 15 to 20 min before the start of the procedure. Before the procedure, mice were anesthetized by inhalation of a 4% isoflurane/ air mix. The animals were considered anesthetized when all movement stops and no reflexes subsisted. The area of injection was shaved and disinfected, the eyes protected with drops of a water-based oculo-protectant then the animal was subsequently secured in a digital stereotaxic frame (World Precision Instruments, Inc., Sarasota, FL, USA), maintained on air/isofluorane inhalation (2%). Before performing the surgical incision, 10 µl of lidocaine (5 mg/kg, intradermal) was injected at the incision site for local anesthesia. After the incision of the skin, holes of the size of the injection needle were drilled using a microdrill, and injections were distributed using a 30G Nanofil needle attached to a Nanofil syringe (World Precision Instruments, Inc., Sarasota, FL, USA) coupled with a UMP3 UltraMicroPump (WPI). To label MF and/or rexpress *vangl2*, 300 nl of AAV2/9-CaMKII (0.4)-mCherry-WPRE virus (titer of 1.9 10^{12} genome copies/ml diluted in sterile PBS, Vector Biolabs) or AAV2/9-CamKII(0,4)-mcherry-2A-mVangl2-WPRE virus (5,9 x 10^{13} gcp /ml or 1,7 x 10^{13} gcp /ml in sterile PBS, Vector Biolab) were injected bilaterally in the dentate gyrus zone (coordinates : X=±1.6 Y=-2 Z=-1.9 for mutants, X=±1.25 Y=-2 Z=-2 for controls). After stitching the wound, the animal was injected with warm NaCl solution then allowed to recover in a clean individual cage placed in a heated chamber until full mobility was restored. After 48 hr of post-op observations, the mice were returned to collective housing.

For the EE experiment, one week after surgery, the mice were transferred in normal-sized common cages without additional objects (6-7 mouse per cage; Ctrl conditions), or in large (rat) cages equipped with 2 running wheels per cage, toys, and hiding spaces for exploration (7 mice per cage; EE conditions).

Stereotaxic viral injection into aged mice. 9 months old and 15 months old mice were injected with a buprenorphine solution (0.15mg/kg, intraperitoneal) 15 to 20min before the start of the procedure. Before the procedure, mice were anesthetized by inhalation of a 4% isoflurane/ air mix. The animals were considered anesthetized when all movement stopped and no reflexes subsisted. The area of injection was shaved and disinfected, the eyes protected with drops of a water-based oculo-protectant then the animal was subsequently secured in a digital stereotaxic frame (World Precision Instruments, Inc., Sarasota, FL, USA), maintained on air/isoflurane inhalation (2%). Before performing the

surgical incision, 10µl of lidocaine (5 mg/kg, intradermal) was injected at the incision site for local anesthesia. After the incision of the skin, holes of the size of the injection needle were drilled using a microdrill, and injections were distributed using a 30G Nanofil needle attached to a Nanofil syringe (World Precision Instruments, Inc., Sarasota, FL, USA) coupled with a UMP3 UltraMicroPump (WPI). To label mossy fibers of the dentate gyrus, 500nl of AAV2/9-CaMKII (0.4)-mCherry-WPRE virus (titer of 1.9 1012 genome copies/ml diluted in sterile PBS, Vector Biolabs) were injected bilaterally in the dentate gyrus zone (coordinates: X=±1.5 Y=-1.8 Z=-1.9 for mutants, X=±1.3 Y=-1.9 Z=-2 for controls). After stitching the wound, the animal was injected with warm NaCl solution then allowed to recover in a clean individual cage placed in a heated chamber until full mobility was restored. After 72h of post-op observations, the mice were returned to collective housing.

Immunohistochemistry, fluorescence microscopy and quantification

Immunofluorescence on brain sections. WT and Emx1-Vangl2$^{-/-}$ mice were terminally anesthetized with intraperitoneal administration of pentobarbital (50 mg/kg body weight). For Vangl2 and mCherry immunofluorescence, animals were perfused transcardially with phosphate buffer (PB) followed by 4% paraformaldehyde (PFA) in PB, brains were removed and postfixed in 4% PFA for 2 hr to 24 hr at 4°C. 40-50 µm-coronal vibratome sections (VT1000S vibratome from Leica) were permeabilized with 0.3% Triton X-100 in PBS for 1hr at room temperature (RT) and blocked with 5% bovine serum albumin (BSA) 5% normal goat serum (NGS) - PBS for 2 hr at RT. Primary antibodies were incubated for 12 to 24 hr at 4°C. Alexa fluor secondary antibodies (Jackson Immunoresearch) were diluted in PBS and incubated for 1 hr at RT. Slices were mounted using ProLong Gold antifade medium (Life Technologies) or Fluoromount-G (Electron Microscopy Sciences). For synaptic markers immunofluorescence, animals were perfused transcardially with cold ACSF for 3 to 4 min, brains were removed and frozen in embedding medium (M-1 Embedding Matrix, Thermo Scientific) before being stored at -80°C for at least 12 hr. 20µm brain sections were made using cryostat, slices were mounted and dried for at least 2 hr at 37°C. They were then fixed in either ice cold 4% PFA or -20° methanol for 5min, rinsed, permeabilized in 0.2% Triton X-100 PBS for 1h at RT and blocked with 5% bovine serum albumin (BSA) 5% normal goat serum (NGS) - PBS for 2h at RT. Primary

antibodies were incubated for 12 to 24 hr at 4°C. Alexa fluor secondary antibodies (Jackson Immunoresearch) were diluted in PBS and incubated for 1 hr at RT. Slices were mounted using ProLong Gold antifade medium (Life Technologies).

Epifluorescence imaging. Slides were imaged using a Zeiss AxioImager Z1 (63x / 1.40 NA oil objective) equipped with an AxioCam MRm and the Zen software (Zeiss) and a LED light source Colibri 7 from Zeiss (wavelengths: UV 385/30 nm, V 423/44 nm, B 469/38 nm, C 511/44 nm, G 555/30 nm, Y 590/27 nm, R 631/33 nm).

Image quantification. Our aim was to quantify fluorescence expression for different markers at the sl, which was done using Fiji (https://imagej.nih.gov/ij/). A mask outlining the sl was created in channels. This region of interest (ROI) was then applied to other channels of the same image to measure pixel intensity. To normalize the results, measurements were also taken at the *stratum radiatum* (sr), which was the second ROI. The intensities at sl were normalized to that of sr. Only the normalized integrated pixel density at the sl of stained slices was used for comparison of relative synaptic marker levels between control and mutants.

c-Fos neuroimaging. DAB-revealed c-Fos immunochemistry and counting were performed as previously described (Brayda-Bruno et al., 2013). The trained mice were perfused with 4% PFA 90min after an ultimate trial in the radial maze. Naïve mice who were not submitted to radial maze training were used as controls. After perfusion the brains were post-fixed overnight in 4% PFA at 4°C. The brains were then sliced into 50µm sections. Sections were stocked in a cryoprotectant solution (ethylene glycol/glycerol/PB) until immunohistochemical processing for the visualization of c-Fos. Free-floating sections were washed in PBS, and then incubated in PBS with 0.5% H2O2 for 30 min, followed by incubation in a blocking PBS solution containing 1% BSA, 3% NGS, and 0.2% Triton X-100. Sections were incubated with primary antibody in a PBS 0.3% Triton X-100 solution overnight at 4°C. After extensive washes in PBS 0.3% Triton X-100, sections were incubated with the biotinylated secondary antibody in aPBS 0.3% Triton X-100 solution for 1h30 at RT. After rinsing, sections were then incubated in avidin–biotinylated horseradish peroxidase complex (ABC, Vectastain Elite kit, Vector Laboratories) for 1h30 at RT. Next, the sections were rinsed, and the peroxidase reaction end product was visualized in 0.05 M PB containing 0.025% 3,3′-diaminobenzidine tetrahydrochloride (DAB, Sigma) and 0.03% H2O2. Finally, the sections were rinsed and mounted on

gelatin-coated glass slides before being stained using neutral red coloration. The slides were then dehydrated through a graded series of ethanol, cleared in toluene, and coverslipped with Eukitt mounting medium. For each animal, structures were anatomically defined according to the atlas of Franklin and Paxinos. c-Fos was evaluated in the CA1, CA3 and DG, as well as in the lateral entorhinal cortex. Trained groups were compared to naive groups kept in their home cage but otherwise submitted to the same treatment and feeding conditions as trained mice to evaluate the effect of Vangl2 before behavioral testing. c-Fos levels were expressed as the mean number per animal of c-Fos positive cells per mm2 in each brain structure studied. At least 3–4 slides per structure per animal for each group were analyzed (Biocom Visiolab 2000, V4.50).

Confocal imaging and analysis of infected hippocampi

Confocal image stacks of PFA-fixed brain sections were acquired with a Leica DM2500 TCS SPE laser-scanning microscope with 561 nm excitation wavelength using 63x Leica oil objective. Images of the MF termination zone in the CA3 *sl* region of the hippocampus were captured with an interval of 300 nm in the z-axis. Camera aperture, magnification, light power, and exposure time were fixed for all images. A minimum of 6 stacks from each animal of each genotype and age was acquired randomly. High-resolution 3D stacks were generated using Imaris 9.2.1 software (Bitplane) to characterize and analyze presynaptic terminals as individual objects. For each 3D mossy fiber bouton (MFB), we then determined the volume, the area, and the number of filopodial extensions per MFB. Values are presented as mean ± SEM of n experiments. For statistical analysis, after checking the assumption of Normality, unpaired t-test was used for comparison of two groups. If the normality test failed, the groups were compared using Mann-Whitney test. Statistical differences were considered as significant when $p \leq 0.05$. The quantitative statistical analysis was performed using GraphPad Prism version 8 for Windows.

Serial block face electron microscopy, 3D reconstruction and analysis

P21 male mice were terminally anesthetized by brief inhalation of isoflurane (0.05% in air), followed by an intramuscular injection of ketamine (100 mg/ kg) and xylazine (10 mg/kg). Subsequently mice were perfused intracardially with 1 ml 5000U Heparin

dissolved in phosphate buffer saline (PBS: 0.1 M, pH 7.2), followed by 200ml 2% paraformaldehyde + 2.5% glutaraldehyde in PBS, cooled to 4°C. Then the brain was dissected and placed in the same fixative and stored at 4°C until shipping. For shipping, brains were transferred to 1x PBS + 0.01% Na Azide, at 4°C, and restored to 2% paraformaldehyde + 2.5% glutaraldehyde in PBS at 4°C upon arrival. All procedures were performed in full accordance with recommendations of the European Communities Council Directives (86/609/EEC), the French national Committee (87/848) and the requirements of the United Kingdom Animals (Scientific Procedures) Act 1986, AWERB Newcastle University (ID: 374). Note that, at all times the experimenters were blind to the mouse genotype. The code was only broken once all the modeling and analyses were finalized.

Sectioning was performed on a vibratome (Leica VT1000 S, Leica Biosystems) in PBS, producing 100 µm sections which were trimmed down to include the region of interest (ROI), and stored in glass vials with PBS at 4°C. Osmium impregnation began with rinsing samples in PBS five times for three minutes each, then 3% potassium ferrocyanide in 2% osmium tetroxide in PBS at 4°C for 1 hr. Samples were rinsed in ddH_20 at RT 5 times for 3 min each, and incubated in freshly prepared and filtered 1% (w/v) thiocarbohydrazide (TCH) for no longer than 20 min to avoid crystal formation and precipitation. They were then rinsed 5 times for 3 min each in ddH_20 followed by 2% osmium tetroxide in ddH_2O for 30 min, rinsed 5 times for 3 min and en bloc stained in 1% uranyl acetate in ddH_20, at 4°C overnight. The next day samples were rinsed 5 times for 3 min each in ddH_20, placed in Walton's lead aspartate solution at 60°C for 30 min, then rinsed in ddH_20 as before at RT. Dehydration via a graded ethanol series: 25%, then 10 min at 4°C each change (1 x 50%, 1 x 70%, 1 x 90%, 2 x 100%), followed by 3 times in 100% Acetone for 30 minutes at RT. Samples were infiltrated by embedding in increasing concentrations of TAAB 812 epon resin (TAAB) mixed with acetone, beginning at 50% TAAB 812 resin rising to 70% after 30 minutes and 90% after a further 30 minutes, at RT. The samples were then transferred to aluminum boats filled with 100% TAAB 812 resin for 4 hr at RT. Sections were then flat embedded and polymerized at 60°C for 48 hr. Specimens containing the ROI were then prepared on metal stubs for SBFsEM (Tapia et al. 2012, Wilke et al. 2013). Specimens were imaged on a Zeiss Sigma VP Scanning Electron Microscope with Gatan 3View to gather images using 50 nm z-steps for control samples and 60 nm for Emx1-Vangl2$^{-/-}$ samples measuring the same parameters as in Wilke et al., 2013).

3D models were produced from the SBFSEM image stacks using the publicly available Microscope Image Browser (MIB; http://mib.helsinki.fi) software (Belevich et al., 2016). The resultant 3D profiles were used to produce volumetric reconstructions of, and to provide statistics on the volume of, pre- and postsynaptic structures of interest. A total of 2 datasets were completed. In each dataset postsynaptic dendrites were first traced in their entirety within the block and reconstructed. Then the spines, postsynaptic densities (PSDs), and presynaptic elements were similarly isolated individually and reconstructed. Spines and thorny excrescences (TEs) were defined as a protrusion from the dendritic shaft, typically with a narrow neck. PSDs were defined as an increased electron density and thickening of the postsynaptic membrane at an interface between presynaptic and postsynaptic structures. MFB were defined visually by their structure surrounding the TE/spines isolated previously. Only synapses and structures perpendicular to the plane of sectioning could be reconstructed, and reconstructions were constrained by the edges of the image block. Final 3D models and their morphological measurements were obtained at full resolution through Imaris 9.2.1 software (Bitplane).

Electrophysiology

Slice preparation. Parasagittal hippocampal slices (300µm thick) were obtained in P21 to P32 mice. Animals were anesthetized with 4% isoflurane. After checking their reflexes, decapitation was performed. The brain was quickly removed and immersed in ice-cold cutting solution (the composition is given below). The hemispheres were separated by a sagittal cut in the corpus callosum and each one was glued and mounted onto a Leica VT1200S vibratome. Brain slices were made with a razor blade with an angle of ~17° at 0.09 mm/s. All the preparation was performed under oxygenation (95% 0_2 and 5% CO_2), in an ice-cold cutting solution (in mM): 87 NaCl, 25 $NaHCO_3$, 10 glucose, 75 sucrose, 2.5 KCl, 1.25 NaH_2PO_4, 0.5 $CaCl_2$, and 7 $MgSO_4$. Right after slicing, slices were transferred into a holding chamber at 33°C during 30 minutes to 1 hour for recovery and were then placed at RT for the duration of the experiment. Slices were transferred to a recording chamber in which they were continuously superfused at a rate of 3-4 ml/min with an oxygenated extracellular medium (95% O_2 and 5% CO_2) containing (in mM): 125 NaCl, 2.5 KCl, 2.5 $CaCl_2$, 1.3 $MgSO_4$, 1.25 NaH_2PO_4, 26 $NaHCO_3$, 10 glucose, pH 7.4. Recordings were performed at RT in voltage-clamp from CA3 PC using borosilicate pipettes (Harvard apparatus: 1.5 OD x 0.86 ID) pulled with micropipette puller (P97, Sutter

Instruments, Novato, CA), which had resistances between 4 and 8 MΩ. The patch electrodes were filled with a solution containing (in mM): 140 $CsCH_3SO_3$, 2 $MgCl_2$, 4 NaCl, 5 phospho-creatine, 2 Na_2ATP, 0.2 EGTA, 10 HEPES, 0.33 GTP, pH 7.3 adjusted with CsOH.

All recordings (spontaneous activity, evoked activity, paired pulse ratio and AMPA/NMDA ratio recordings) were performed with the $GABA_A$ receptor antagonist bicuculline methiodide (20 µM) and NMDA receptor antagonist D-APV (50 µM) added to the ACSF.

Evoked EPSCs were recorded in CA3 PCs in the whole-cell patch clamp mode by stimulating with a glass pipette the DG hilus to activate MFs (Marchal and Mulle, 2004). While recording from a CA3 PC, the stimulating electrode was moved to a position where a sharp EPSC with fixed latency was evoked. Stimulation intensity was adjusted just above the sharp threshold for activation of a synaptic response. Using such low minimal stimulations, no prominent polysynaptic activation was observed. MF stimulation was assessed by its large dynamic range of short-term facilitation (40 ms paired pulse ratio > 2 or 1 Hz/0.1 Hz ratio > 4).

For AMPA/NMDA ratio recordings, we first isolated AMPAR/KaïnateR response by recording EPSC amplitudes at -70 mV in presence of NMDA receptor antagonist D-APV (50 µM) added to the ACSF. After 15 minutes of washing D-APV, we added the AMPA/KaïnateR antagonist NBQX (20 mM) to record NMDAR EPSC amplitudes at +40 mV. For each pharmacological condition 30 sweeps were averaged.

To ensure that MF responses were not contaminated by associational/commissural inputs, the metabotropic glutamate receptor agonist (2S,1′R,2′R,3′R)-2-(2,3-dicarboxy cyclopropyl) glycine (DCG-IV; 1 µM) was applied at the end of some of the experiments to block MF responses selectively.

Drugs. All drugs were obtained from Tocris Cookson (Bristol, UK), Sigma (St. Louis, MO), HelloBio **(**Bristol, UK).

Data acquisition and analysis. Recordings were made *via* Patchmaster 2.71 using an EPC10 amplifier (HEKA Elektronik, Lambrecht/ Pfalz, Germany), filtered at 0.5–1 kHz, digitized at 5-10 kHz, and stored on a personal computer. Analysis was performed using Neuromatic 3.0 (www.neuromatic.thinkrandom.com) written within the Igor Pro 6.37 environment (WaveMetrics, Lake Oswego, OR). Data analysis was performed using

GraphPad Prism 8 (GraphPad Software). All values are presented as mean ± SEM. Datasets were tested for normality using D'Agostino and Pearson test. If datasets passed the test, they were analyzed using Student's unpaired t-test with Welch's correction. Otherwise, the datasets were analyzed using nonparametric unpaired t-tests (Mann–Whitney). For paired-pulse ratio experiments, comparisons between two genotypes were performed using two-way ANOVA test (Bonferroni's multiple comparisons test).

No statistical methods were used to predetermine sample sizes, but our sample sizes are similar to those generally employed in the field. N mentioned in the paper represents the number of mice used in an experiment, n mentioned in the paper represents a single measurement from a single cell.

Western blot

For each set of experiments, 2 hippocampi from 3-week-old mice of each genotype were processed as described previously (Moreau et al., 2010). A volume of a solution containing 10 mM PB, pH 7.4, 0.32 M sucrose, 1 mM EDTA, 1 mM NaN3 and protease inhibitors (Roche) was added to the tissues according to their weight. Samples were then homogenized with a polytron (Kinematica PT1200) and sonicated and protein concentration was evaluated twice using BCA analysis (BCA protein Assay Kit from Thermo Scientific). Protein concentration was adjusted for each sample and diluted with 2x SDS loading buffer containing 10% β-mercaptoethanol. Considering the different molecular weights, proteins were loaded on 10%, 8% or 7% acrylamide gels and ran at 120V between 1h30 and 2h in running buffer (25 mM Tris, 192 mM glycine, pH 8.3 – Biorad). Proteins were then transferred to Immobilion-P polyvinylidene fluoride membranes (Millipore) or for 2h30 at 60V in transfer buffer (25 mM Tris, 192 mM glycine, pH 8.3 – Biorad) supplemented with 20% methanol. The membranes were blocked with a 0.05% Tween-TBS (25mM Tris, pH7.5 + 137mM NaCl + KCl 3mM + MilliQ water up to 2L) solution containing 5% non-fat milk for 1h at RT. Primary antibodies were incubated for 1h at RT and extensively washed. Secondary antibodies, coupled to the horseradish peroxidase (HRP), were then incubated for 1h at RT. Membranes were exposed to chemiluminescence kits with different sensitivities (ECL, Thermo Scientific and Bio-Rad) and protein detection was done on Amersham Hyperfilm ECL (GE Healthcare) films with developer and fixer solutions (Carestream Kodak autoradiography GBX). The optic

density (OD)*mm2 was analyzed for each detected band. Quantifications of band intensities were done using the Quantity One software (Bio-Rad).

Behavioural analysis

All experimental manipulations were approved by the Committee on Animal Health and Care of the local governmental body and performed in strict compliance with the EEC recommendations for the care and use of laboratory animals. Experiments were done using control and Emx1-Vangl2−/−littermates. All animals were adult male mice of 10-12 weeks or 16 months of age at the start of behavioral tests that were housed under standard laboratory conditions with a 12 hr light/12 hr dark cycle (light on at 07:00) with food and water supplied ad libitum.

Locomotor activity. Locomotor activity was assessed in photocell-based activity chambers under light-dark environmental conditions, using inter-connected Plexiglas individual chambers equipped with infra-red sensors as published previously (23). Chambers are inter-connected and linked to a computer using an electronic interface (Imetronic, Bordeaux, France). Rearing and horizontal activity data were collected for each mouse over a 3hr time course (response to novelty in 10-min bouts).

Elevated plus-maze. The Plexiglas plus-maze apparatus had two open and two enclosed arms radiating outward from a central open square and was 60 cm above the floor. The maze was illuminated by halogen light at 100 lux in the central open square. Mice were briefly handled for 2 consecutive days prior to elevated plus-maze experiment to habituate them. They were placed in the center of the maze and allowed free access to all arms for 5 min.

Dark/light exploration assay. The dark/light was conducted in a two-chamber shuttle box with an opaque divider in the middle. The walls of the dark chamber were made of black Plexiglas while the light chamber was white and illuminated by halogen light at 300 lux. Mice were first placed into the dark chamber and allowed to freely travel between the chambers for 5 min. For each test, a video tracking system (Ethovision version 11, Noldus Technology, Wageningen, The Netherlands) was used to analyze the mouse movements, the percentage of time spent and the number of entries in the open arms or light chamber.

Spontaneous alternation in the Y maze. Spontaneous alternation was assessed in a grey, plastic Y-maze, placed on a table 80 cm above the floor and located in the middle of a room containing a variety of extra-maze cues. The three arms of the Y-maze were similar in appearance, spaced at 120° from each other and were illuminated with the same light. Mice were placed at the end of one of the arms and allowed to explore the maze for 5 min. Allocation of the start arm was counterbalanced within experimental groups. An entry into one of the arms was scored when all four paws of the animal were placed inside this arm. Spontaneous alternation, expressed as a percentage, refers to the proportion of arm choices differing from the two previous choices. Thus, if an animal made the following sequence of arm choices: A, B, C, B, A, B, C, A, the total number of alternation opportunities would be six (total entries minus two) and the percentage alternation would be 67% (four out of six).

Novel object recognition in L maze. Novel object recognition was assessed in a gray, plastic L maze, placed on a table 80 cm above the floor and located in the middle of a room containing a variety of extra-maze cues. The task has been thoroughly described in Da Cruz et al., 2020. Briefly, the animal is habituated in the empty maze for 9 min on the first day of trial. On the second day, the animal is placed in the L maze with 2 identical objects, one at the end of each arm, for 9 min. The time spent with each object during the session is recorded. 24h later, one of the familiar objects is replaced with a new object, and the animal is placed in the L maze again for 9 min. The time spent with each object during the session is recorded. Exploration of an object is scored when: the animal nose is directly facing the object (< 2 cm). We do an discrimination index analysis (DI), defined as DI = [Timenovel – Timefamiliar)]/[(Timefamiliar) + (Timenovel)] , to evaluated differences in exploration for the different groups. Statistical differences were considered as significant when $p \leq 0.05$. The quantitative statistical analysis was performed using GraphPad Prism version 8 for Windows.

Spatial learning and memory in the Morris water maze. Spatial memory was tested in a circular pool (diameter 150 cm) filled with water maintained at 19-20°C and opaque by the adjunction of a non-toxic cosmetic adjuvant. Mice were trained to swim to a 14 cm diameter platform in order to escape from the water. Data was collected using a video camera fixed to the ceiling of the room and connected to a computerized tracking system (Viewpoint, Lyon, France) located in an adjacent room. To measure performance in hidden trials, the escape latency, distance to the target, and swim speed were analyzed

as outcome measures for each session. During the test, mice were trained for two series of three trials per day: 3 trials in the morning and 3 trials in the afternoon, with a cut-off of 60 s, 5 min intertrials interval and 3 hr interseries interval. If the mice found the platform, they were allowed to remain on it for 15s (reinforcement); mice that failed to find the platform within 60s were led to the platform by the experimenter where they were allowed to stay for 15s. Mice were released from different starting points at each trial, and different sequences of starting points were used each day. Visual training: During 5 consecutive sessions, mice were trained to swim to an unsubmerged platform indicated by a ball suspended with a transparent thread at 7.5cm above the platform. Spatial training: Mice were trained for 10 days to swim to a submerged platform (1.5 cm below the water surface) using spatial cues located in the room (posters on the walls). Probe testing: The probe trials were designed to examine the extent of spatial discrimination learning (spatial bias) at day 10 during the spatial training. To do this, the platform was removed from the pool 24 hr after the last hidden platform training trial. The number of crossings of the platform location, and the time that mice spent swimming in the target quadrant (where the platform was located during hidden platform training) were measured over a 60 s trial.

Relational/Declarative memory in the radial maze. One week before the beginning and until the end of the experiments, mice were subjected to partial food deprivation (82-85% of their free feeding weight) and handled daily. We used three identical fully automatized 8-arm radial-mazes made of grey Plexiglas. Only extra-maze cues were available (posters on the walls). Habituation: Each mouse was submitted to two days of habituation, where all the arms are baited and open, and must visit each arm and eat all the pellets to complete the session. Training: Each mouse was assigned three pairs of adjacent arms for all the training (pairs A, B and C). One arm of each pair is always baited (the right arm for pairs A and B, the left one for pair C). Within each daily training session, the mouse was submitted to 20 successive presentations (trials) of the three pairs, in a pseudo-random order, separated by an inter-trials interval of 20 sec. A trial was considered successful when the mouse chose the baited arm. The training lasted at least 5 days, and ended when a mouse achieved a mean performance of 72.5% on two days for all three pairs. Mice, which failed to complete each daily session in a maximum of one hour, and mice, which did not finish the training in 12 days, were excluded from the analysis (here, 3 control and 3 Emx1-Vangl2−/−mice were excluded). Test. When a mouse completed the training, it was submitted to a test session of 20 trials. During this

session, each mouse was assigned three pairs of arms. One was already known (the pair C, that will serve as a control pair), one was totally new (pair N, composed of two adjacent arms never visited during the training), and one pair was recombined using the unbaited arm of the pair A and the baited arm of the pair B (pair AB). The percentage of performance obtained for this pair AB served as an index of memory flexibility, which is a cardinal characteristic of relational/declarative memory for the animal (Al Abed et al., 2020). Statistical analysis of the behavioural tests. All data were presented as mean ± SEM, and $p \leq 0.05$ was considered statistically significant. When necessary, we have checked the assumption of Normality. One-way ANOVA was used for analyzing the effect of genotype on time spent in each quadrant of the water maze in the probe test. Two-ways ANOVA was used for analyzing the effect of days of training and genotype in the declarative and working memory performance of the radial maze test. The Bonferroni post hoc test was used when appropriate. The Student's t-test was used for comparing control and Emx1-Vangl2−/−mice in the plus-maze; dark/light test; locomotor rearing and Y-maze test and declarative memory. All calculations were performed using GraphPad Prism version 8 for Windows.

Every day-like memory in the radial maze. This task was designed to assess two components of everyday-like memory: retention and organization. It has been thoroughly described in (Al Abed et al., 2016). One week before the beginning and until the end of the experiments, mice were subjected to partial food deprivation (85-90% of their free feeding weight) and handled daily. We used three identical fully automatized 8-arm radial-mazes made of gray Plexiglas. Only extra-maze cues were available (posters on the walls). Habituation. Each mouse was submitted to one day of habituation, as described above. Training. Each mouse was assigned three pairs of adjacent arms for all the training (pairs A, B and C). Within each daily training session, the mouse was submitted to 23 successive presentations (trials) of the three pairs, in a pseudo-random order, separated by a varying inter-trials interval (0s, 10s or 20s). It is important to note that when the ITI is increased, the retention difficulty is increased whereas the organization difficulty is decreased. For the first presentation of each pair, the two arms were baited. Then, for the following presentations, the reward was in the arm not visited during the previous presentation, requiring the mouse to alternate between the arms for each pair. Each trial (n) thus required retention of information (the ability to remember the arm visited at the previous presentation, that depended on the number of trials separating two

presentations of the same pair: n-1 and n; five levels of retention difficulty: 0 to 4), but also organization (the ability to discriminate between the two previous presentations of a pair and make a choice based only on the most recent one, that depended on the number of trials separating the two previous presentations of the same pair: n-2 and n-1; five levels of organization difficulty: 0 to 4). The difficulty of the task was balanced over three days of training, we thus compared the performances between blocks of three days. We performed 4 blocks of training with an Inter-Trial Interval (ITI) of 10 sec, followed by one block with an ITI of 20 sec and one block with an ITI of 0sec. Mice which failed to complete each daily session in a maximum of one hour, were excluded from the analysis.

Unpaired contextual conditioning. We here used an unpaired protocol of contextual fear conditioning, where the tone does not predict the shock, and the context is the only predictor. For the conditioning we used two different chambers. The conditioning chamber is made of transparent Plexiglass (30x24x22 cm), with a floor consisting of stainless-steel rods connected to a shock generator (Imetronic, Talence, France). The neutral chamber is made of opaque gray plastic (30x24x22 cm), with a plastic floor. The first day, mice were placed in the neutral chamber for a 3 min habituation. 24 hr later, mice were placed in the conditioning chamber for the 4 min unpaired protocol: 100 sec after being placed in the chamber, a footshock (0.4 mA, 50Hz, 3s) was presented; then after a 20 sec interval, a tone (65 dB, 1000 Hz) was presented for 15 sec; after a 30 sec interval, the same tone was presented; finally, after a 30 sec interval, the same footshock was presented, and after 20 sec mice were replaced in their home cage. 24 hr later, mice were submitted to 4 tests, 2 hr apart, and freezing behavior was recorded as an index of fear. For the first test, mice were placed in the neutral chamber for 6 min, and the tone (65 dB, 1000 Hz) was presented for 2min after a 2 min delay. 2 hr later, mice were placed in the conditioning chamber for 6 min, with no tone or shock. During the first three minutes the electric grid was hidden under a plastic plate, to prevent its use as a cue. This plastic plate was removed for the end of the test. 2 hr later, mice were placed in the neutral chamber for 6 min, and a tone different from the first one (65 dB, 2000 Hz) was presented for 2 min after a 2 min delay, to assess the generalization of information. In the same goal, 2 hr later, mice were placed in the neutral chamber for 6 min, and a white noise (65 dB) was presented for 2 min after a 2 min delay.

Statistical analysis

Data are shown as mean ± SEM unless specified otherwise. All datasets were tested for normality using D'agostino and Pearson normality test (GraphPad Software). Statistical significance was then determined by the corresponding test, considering the normal distribution of the data and the variance (equal or unequal). Sample sizes are indicated in the figure legends and significance was defined as p*<0.05, p**<0.01, p***<0.001, n.s. – not significant

Chapter III : Results

Project 1:

Vangl2 signalling is necessary for the morpho-functional development and maintenance of the MFB/TE synapse during juvenile and adult stages

In the first part of the results, we explore whether the Wnt/PCP pathway, a conserved signaling pathway known to shape tissues during development via the regulation of adhesion complexes and cytoskeleton, is involved in the post-natal synaptic development and maintenance of the DG-CA3 circuitry via the action of its transmembrane core protein Vangl2. We found that Vangl2 is essential to the development and function of the specific hippocampal MFB/TE synapse. Using 3D reconstruction of both confocal and SBFsEM acquisitions, we show that the early genetic deletion of *vangl2* in mice leads to low complexity of the MFB morphogenesis with long lasting consequences on its structural plasticity. These morphological defects are accompanied by molecular modifications in both pre- and post-synaptic compartments, as well as basal transmission deficits. Lastly, we show that the early loss of Vangl2 leads to specific memory deficits in adult animals. Altogether, our data uncover the importance of the PCP pathway in establishment of hippocampal synaptic connexions and show that Vangl2-dependent mechanisms are critical for the correct postnatal morphogenesis and function of the MFB/TE giant synapse.

Vangl2 is expressed in the DG/CA3 network during its post-natal maturation

Studies showed that the establishment of the MFB/TE giant synapse is progressive during early post-natal stages and MFs make contacts with CA3 pyramidal cells around P7. To test whether Vangl2 plays a role in setting up the MFB/TE synapse, we evaluated the profile of expression of Vangl2 protein at 7 days after birth (P7). We found that Vangl2 is strongly expressed in the hippocampus, notably in the DG and in the developing MF projecting from GCs **(Figure 19B)**. The presynaptic terminals of the MF complexify themselves between 7 and 14 days after birth (P14), and at P14, we observed a specific accumulation of Vangl2 all along the *stratum lucidum*, where MF contact apico-proximal dendrites of CA3 pyramidal cells **(Figure 19B)**. At P21, Vangl2 expression was maintained in the DG-CA3 network regions, with a reduction of the staining in the CA1 region and the GC layer and clear accumulation in MF **(Figure 19B)**. At P21, the synapse is considered structurally mature and Vangl2 is enriched in the sl in the CA3 region.

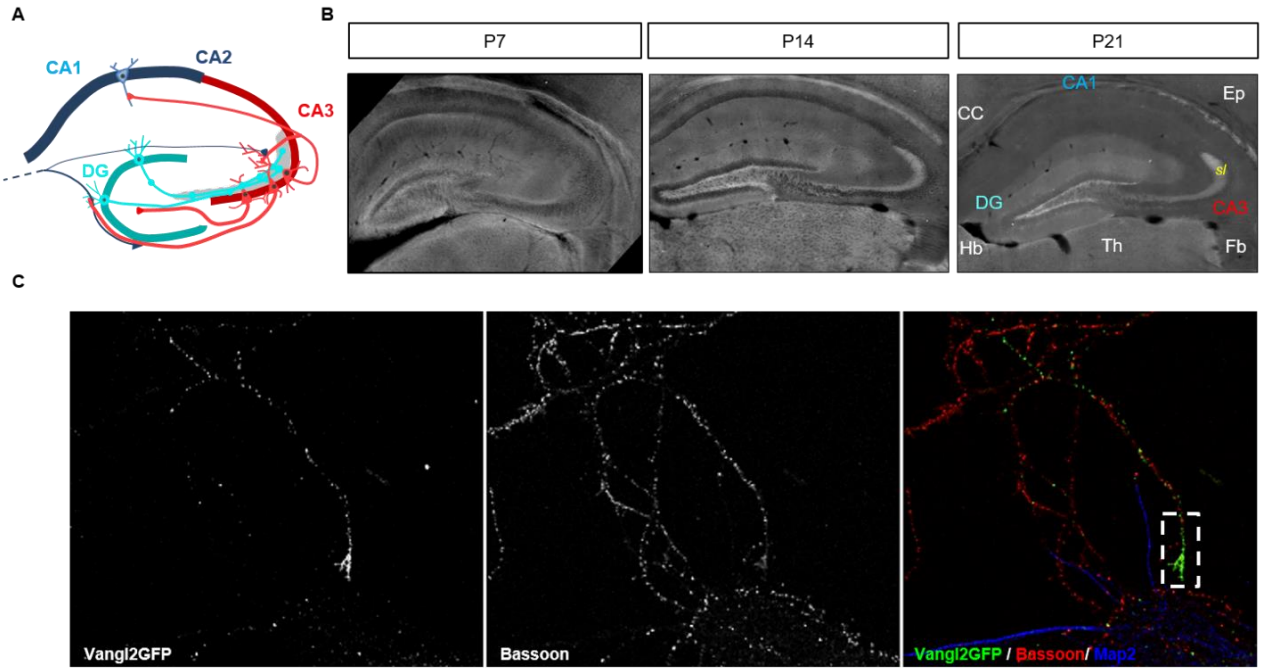

Figure 19: (A) Schematic representation of the hippocampal trisynaptic circuit between the dentate gyrus (DG), Ca3 and CA1. **(B)** Immunostaining against endogenous Vangl2 in P7 mouse brain showing that Vangl2 is expressed across the entire hippocampus, with a specific enrichment in the granular and subgranular layer of the DG, as well as in the mossy fiber projections of the granule cells. This expression pattern is still present in P14 mouse brain, with a strong enrichment in the *stratum lucidum (sl)* of the CA3. At P21 Vangl2 protein expression is more confined than in P14 mice brains and Vangl2 but still enriched in the DG subgranular zone as well as in the *sl*. Note that Vangl2 is also expressed in the corpus callosum (CC), in the ependymal cells lining the ventricules (Ep) as well as in more ventral regions such as the Hb and the Th, but not much in the hippocampal fimbria (Fb). **(C)** Confocal images of DIV21 hippocampal

neurons transfected with pOrange-Vangl2-GFP to label endogenous Vangl2. Vangl2 (green) accumulates in the growth cone region of the axonal projection (white box).

Recently, we showed that Vangl2 controls growth cone velocity by regulating the internal retrograde actin flow in an N-cadherin-dependent fashion in developing neurons (Dos-Santos Carvalho et al., 2020). Using the pORANGE template vector, we designed and generated a GFP-Vangl2 knock-in construct to endogenously label Vangl2 protein in hippocampal neurons. Fluorescence imaging confirmed the expression of Vangl2 in developing neuron growth cones **(Figure 19C)**.

Vangl2 plays a role for the morphogenesis of the pre-synaptic compartments of MFB/TE giant synapse

To assess whether Vangl2 is required for MF pathway development and MFB-TE synaptogenesis, we created a conditional Vangl2 knockout mouse (Emx1-Vangl2$^{-/-}$) to bypass early lethality and anatomical defects typically associated with embryonic deletion of vangl2. This conditional deletion leads to the loss of Vangl2 expression in neuron and glia progenitors during embryogenesis in the dorsal telencephalon, before the formation of the DG-CA3 network. After birth, Vangl2 is no longer present in the hippocampus of Emx1-Vangl2$^{-/-}$ mice while it remains present in the diencephalon. We used a morphometric approach to study the pre-synaptic elements of the MFB/TE synapse and the impact of the early loss of Vangl2. We infected the GC of the DG of post-natal day 5 (P5) Emx1-Vangl2$^{-/-}$ mice, before the development of the MFB, with a AAV carrying a construct allowing the expression of the fluorescent protein mCherry in order to label the MFs and the MFB **(Figure 20A)**. We quantified morphological parameters of 3D reconstructed MFB located in the *sl* at P25 **(Figure 20B-C)**. We observed a significant decrease of the MFB volume (control: 18,21± 0,6272µm^3 , Emx1-Vangl2$^{-/-}$: 12,54±0,3916 µm^3; Mann-Whitney test p<0.0001) and area (control: 160,9± 4,576µm², Emx1-Vangl2$^{-/-}$: 120,4±3,376µm²; Mann-Whitney test p<0.0001) in Emx1-Vangl2$^{-/-}$ mice compared to control **(Figure 2D-E)**. Mature MFB are known to exhibit filopodial extensions that add to their complexity (Lanore et al., 2012). We quantified the number of filopodial extensions per MFB, the percentage of MFB with filopodia. We showed that Emx1-Vangl2$^{-/-}$ mice presented less filopodia's per MFB than controls **(Figure 20F)** (control: 0,7230±0,06207 filopodia per MFB, Emx1-Vangl2$^{-/-}$: 0,3005±0,03581 filopodia per MFB ; Mann-Whitney test p<0.0001). Moreover we observed a reduction of 15% of the number of MFB with

filopodias in P25 Emx1-Vangl2$^{-/-}$ mice compared to controls (control: 36,94 % of total quantified MFB, Emx1-Vangl2$^{-/-}$: 20,91% of total quantified MFB) (Fig.20G). Altogether these results demonstrate that in Emx-Vangl2$^{-/-}$ mice, MFB are structurally smaller and less complex, two characteristics of immature MFB. Our data show that Vangl2 participates in the morphogenesis of the pre-synaptic compartment of the MFB/TE giant synapse.

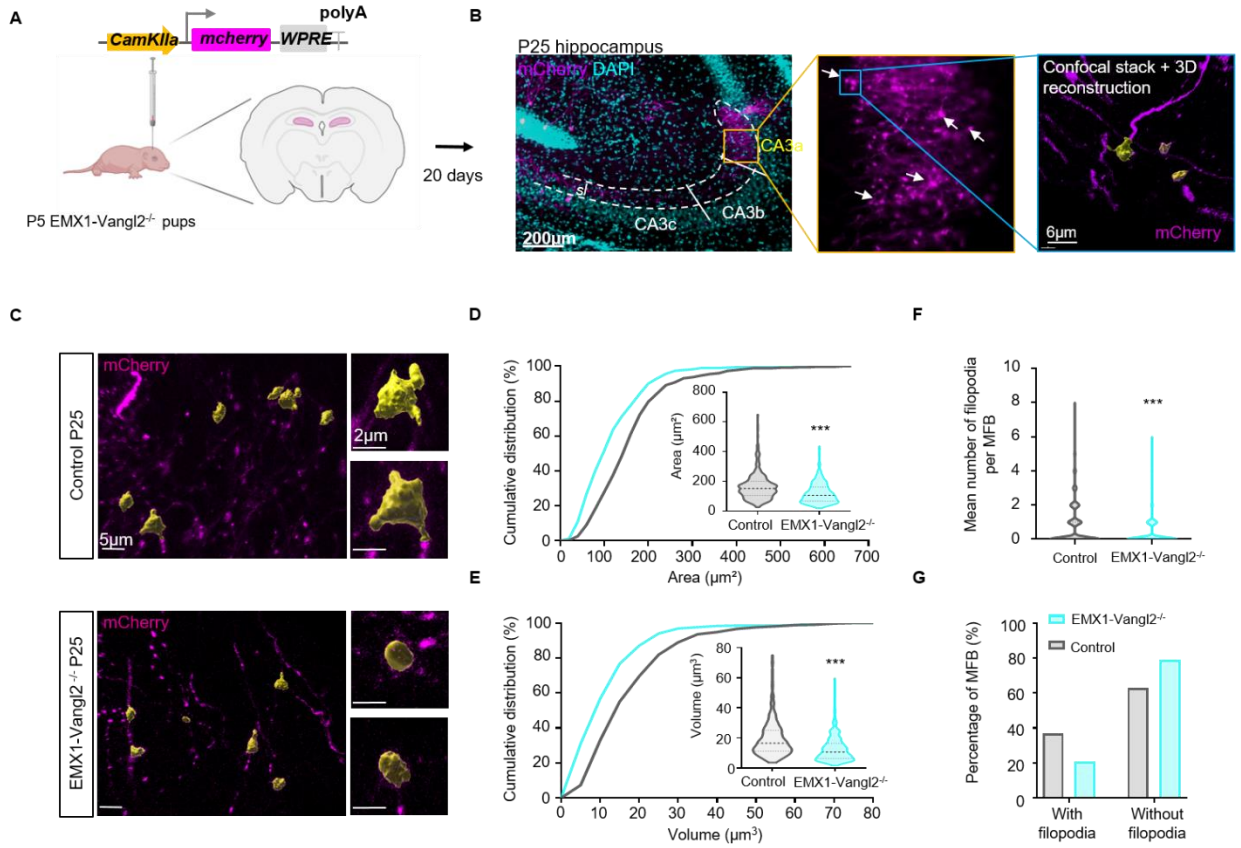

Figure 20: **(A)** Experimental design for stereotaxic virus injection in the DG of P5 pups. **(B)** Representative confocal images of labelled presynaptic MFB in the SL of P25 mice in magenta. **(C)** Representative confocal images of labelled MFB (magenta) with 3D reconstruction (yellow) in the SL of P25 Emx1-Vangl2$^{-/-}$ and control mice. **(D-G)** Quantifications of volume, area, number of filopodia per MFB, and percentage of MFB with filopodia in P25 Emx1-Vangl2$^{-/-}$ and control mice. N control= 351 MFB from 10 mice, N Emx1-Vangl2$^{-/-}$ = 416 MFB from 10 mice. Mann-Whitney test, ***P < 0.001.

Vangl2 plays a role for the morphogenesis of post-synaptic compartments of MFB/TE giant synapse

As the size of the presynaptic compartment influence the size of the post-synapse, we next investigate whether the absence of Vangl2 had an impact on the entire MFB/TE giant synapse. Viral infection in the DG limited the imaging and analysis to the presynaptic side of the MFB/TE junction. To evaluate the impact of vangl2 deletion on the entire

synapse, we used serial block face scanning electron microscopy (SBFsEM), and 3D reconstruction of the whole MFB/TE synapse found in the sl of the CA3a region and quantified the morphological parameters of each synaptic component in control and Emx1-Vangl2$^{-/-}$ P21 mice. We reconstructed the post-synaptic TE elements of the synapse **(Figure 21A)**. On the dendrites we reconstructed, the TE density is not affected by the early deletion of Vangl2 and stays stable between control and Emx1-Vangl2$^{-/-}$ (data not shown).We observed a reduction of the volume of TEs in Emx1-Vangl2-/- mice compared to controls (control: 1,380±0,1518 µm^3 , Emx1-Vangl2-/- : 0,4493±0,05886 µm^3 ; Mann-Whitney test p<0.0001), with a higher number of small TEs (< 0.1 µm^3) in Emx1-Vangl2-/- mice than in controls **(Figure 21A, C)**. Then, we reconstructed the presynaptic MFB, and found a significant decrease in volume between the boutons of Emx1-Vangl2$^{-/-}$ mice and controls (control: 7,001±0,5690 µm^3, Emx1-Vangl2$^{-/-}$: 2,835±0,4051µm^3 ; Mann-Whitney test p<0.0001) **(Figure 21B, D)**. This confirms that the early deletion of Vangl2 impacts the development of the MFB, leading to smaller pre-synaptic boutons, as we previously observed at a lower resolution with confocal microscopy.

The SBFsEM image quality was sufficient to study post-synaptic densities (PSDs). Quantitative analysis of the 3 sets of data showed that in control mice, the TEs we reconstructed had an average of 5,605±0,3612 PSDs while in Emx1-Vangl2$^{-/-}$ mice they had an average of 2,179 ± 0,1945 PSDs **(Figure 21E)**. Thus, the number of PSD per TE was greatly reduced in Emx1-Vangl2$^{-/-}$ mice compared to control **(Figure 21H)**. Unlike the other structures quantified, the PSDs volume was stable in Emx1-Vangl2$^{-/-}$ mice compared to controls (control: 0,005749±0,0001256 µm^3, Emx1-Vangl2$^{-/-}$: 0,005660±0,0001796 µm^3 ; Mann-Whitney test p = 0,7118), however the area of the PSDs was reduced in Emx1-Vangl2$^{-/-}$ mice compared to controls (control: 0,2879±0,005981 µm^2, Emx1-Vangl2$^{-/-}$: 0,2480±0,007023µm^2 ; Mann-Whitney test p = 0,0029) **(Figure 21E-G)**. Taken together, these results show that the early deletion of Vangl2 in the hippocampus affects the morphological development and structure of the entire MFB/TE giant synapse.

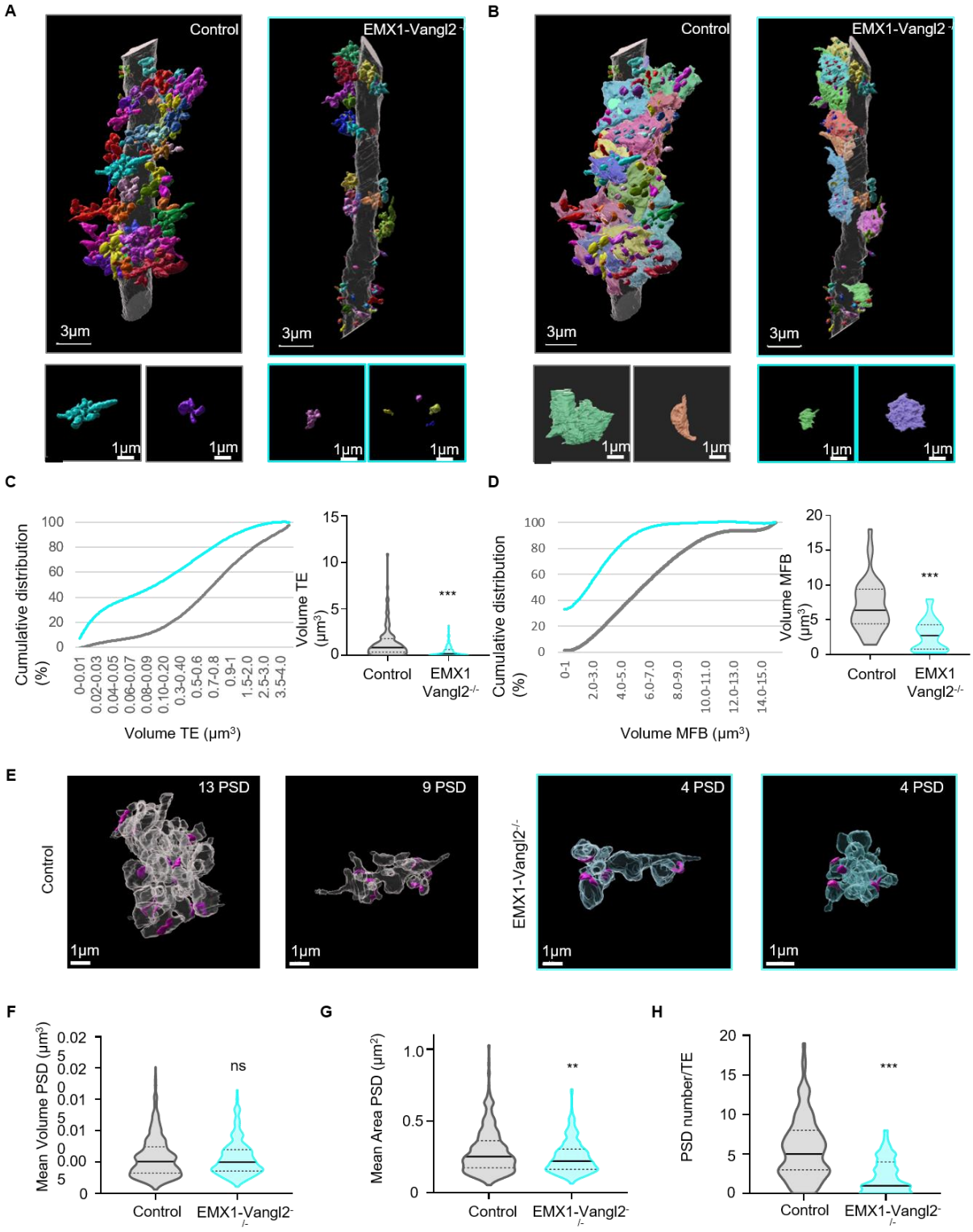

Figure 21: (A-B) Representative 3D rendering of dendrites segmented from SBF-SEM stacks of CA3a in P21 control and Emx1-Vangl2$^{-/-}$ animals. TE are represented in bold colors (A), MFBs are represented in pastel colors (B). **(C-D)** Cumulative distributions and quantifications of 3D reconstructed TEs (C) and MFBs (D) average volumes in P21 control (grey) and Emx1-Vangl2$^{-/-}$ (turquoise) mice. Number of MFBs: control: n=42, Emx1-Vangl2$^{-/-}$: n=30; Number of TEs: Control: n=119, Emx1-Vangl2$^{-/-}$: n=117. Mann-Whitney test, ***p<0.001. **(E)** Representative 3D rendering of PSDs (pink) onto TEs segmented from SBF-SEM stacks in P21 control and Emx1-Vangl2$^{-/-}$ animals. **(F-H)** Quantifications of the mean PSD volume (F), area (G) and number of PSDs per TE (H), for control (grey) and Emx1-Vangl2$^{-/-}$ P21 mice (turquoise). Number of

PSDs: control: n=681, Emx1-Vangl2$^{-/-}$: n=255. Mann-Whitney test, **p<0.01 ***p<0.001.

Early deletion of Vangl2 impairs spontaneous synaptic transmission at mossy fibers-CA3 synapses.

To examine the effect of Vangl2 loss on transmission at MFB/TE synapses, we fisrt recorded CA3 pyramidal neurons in acute hippocampal slices of P21-P32 Emx1-Vangl2$^{-/-}$ mice and control littermates in a whole-cell voltage-clamp configuration. The frequency of spontaneous excitatory postsynaptic currents (sEPSC) was reduced by 57.5% in Emx1-Vangl2$^{-/-}$ mice relative to the control (**Figure 23A-C**; unpaired t-test, p<0.0001). The amplitude of sEPSC was reduced by 19% in Emx1-Vangl2$^{-/-}$ mice compared to the control mice (**Figure 23D-E** ; unpaired t-test p=0.0036). The comparison of sEPSC amplitudes showed a suppression of larger amplitudes events above 30 pA in Emx1-Vangl2$^{-/-}$ mice **(Figure 23F-G)**. We also analyzed decay time of sEPSC that showed no difference between the two genotypes indicating that a loss of Vangl2 didn't modify the electrical properties of the synapse **(Figure 23H)**. MFB/TE inputs are known to give rise to larger amplitudes (Apóstolo et al., 2020; Condomitti et al., 2018; Henze et al., 2002a). When DCG-IV (1 µM), a mGluR2-3 agonist, was added to the bath, we observed that sEPSC frequency of events are no longer different between Emx1-Vangl2$^{-/-}$ mice and control littermates **(Figure 22A-B)**. We also showed that high sEPSC amplitude of control synapses are suppressed leading to no longer difference between the two genotypes **(Figure 22C-D)**. All these results suggest that the loss of Vangl2 leads to an impairment of specifically MFB/TE synaptic transmission.

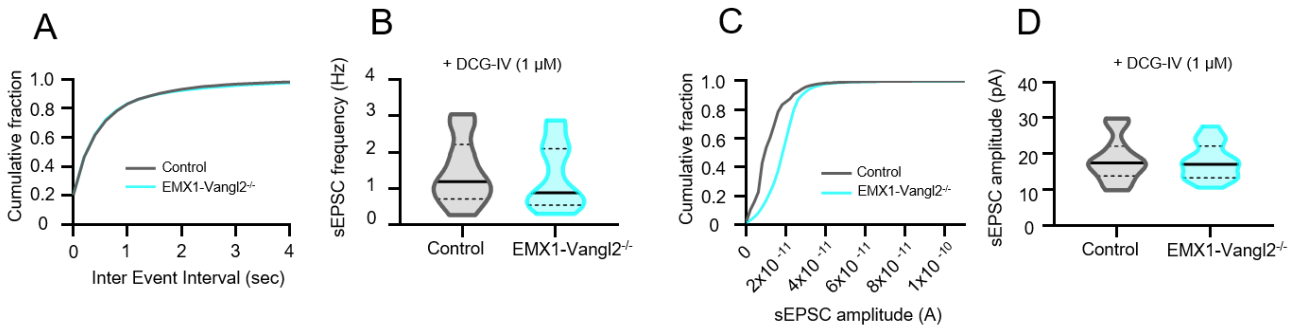

Figure 22: (A) Cumulative distribution of sEPSC inter-event-intervals in control and Emx1-Vangl2$^{-/-}$ neurons with DCG-IV. **(B)** Quantification of sEPSC frequency of control neurons (1,458 ± 0.29 Hz ; n=10 cells) versus Emx1-Vangl2$^{-/-}$ (1.323 ± 0.24 Hz ; n= 14 cells) with DCG-IV. Unpaired t-test with Welch's correction. **(C)** Cumulative distribution of sEPSC amplitudes in control and Emx1-Vangl2$^{-/-}$ neurons with DCG-IV. **(D)** Quantification of sEPSC amplitude of control neurons (18,35 ± 1.908 pA ; n=11 cells) versus Emx1-Vangl2$^{-/-}$ (17,86 ± 0.299 pA ; n= 15 cells) with DCG-IV. Unpaired t-test with Welch's correction.

Next, we wanted to investigate if the synaptic strength of MFB/TE synapses was impaired by the loss of Vangl2. We recorded AMPA/Kainate receptors EPSC and NMDA receptors EPSC in acute hippocampal slices of Emx1-Vangl2$^{-/-}$ mice and control littermates. No significant difference can be highlighted both for AMPAR and NMDAR EPSC response amplitudes (**Figure 23I-N**; ns, p>0.05). These results suggest that a loss of Vangl2 didn't impair the functionality of postsynaptic receptors at MFB/TE synapses.

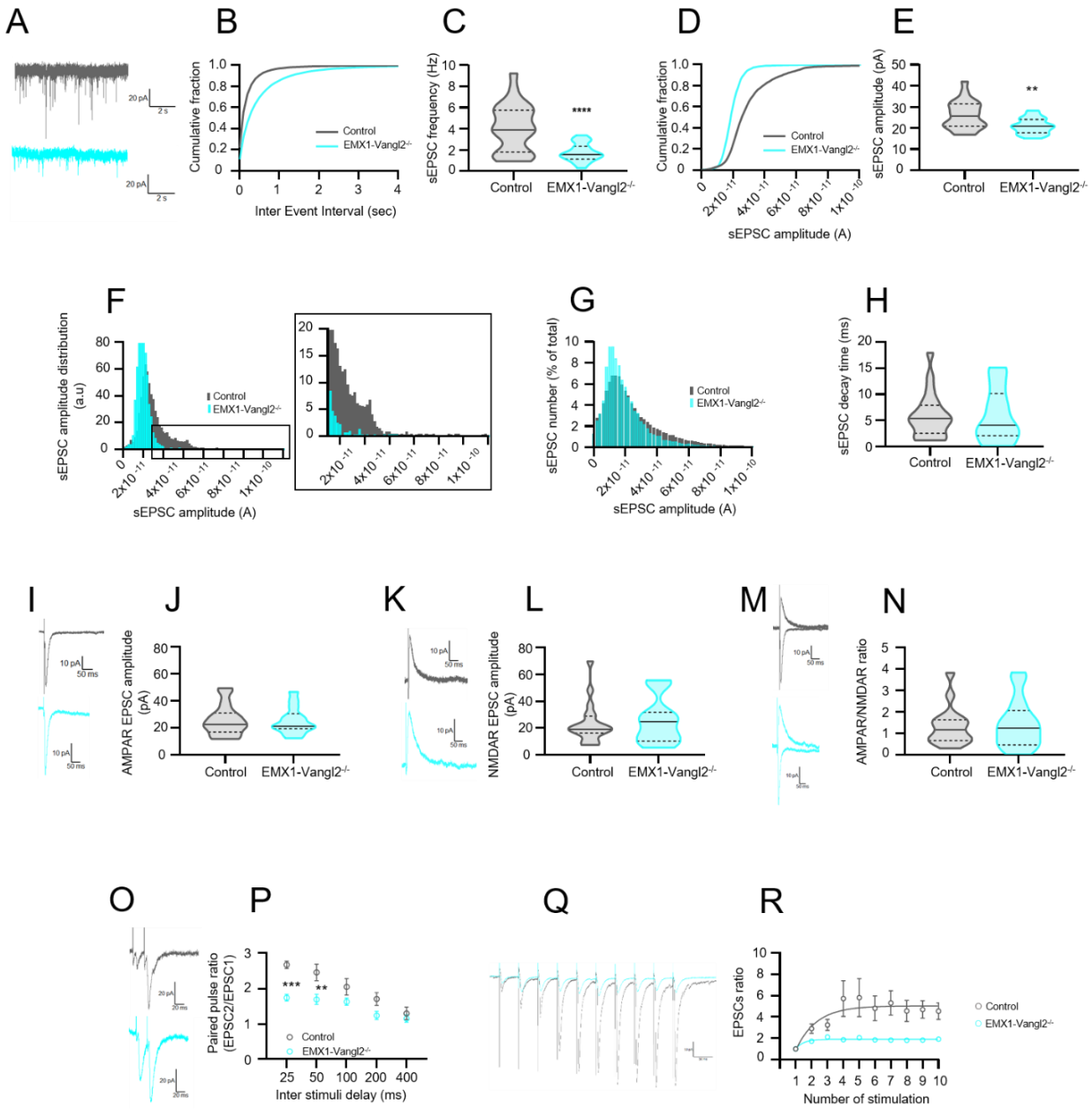

Figure 23: (A) Representative spontaneous EPSC (sEPSC) traces from CA3a pyramidal neurons in P21-P30 control (grey) and Emx1-Vangl2$^{-/-}$ (light blue) acute hippocampal slices. **(B)** Cumulative distribution of sEPSC inter-event-intervals in control and Emx1-Vangl2$^{-/-}$ neurons. **(C)** Quantification of sEPSC frequency of control neurons (4.105 ± 0.46 Hz ; N=16 mice, n=24 cells) versus Emx1-Vangl2$^{-/-}$ (1.745 ± 0.196 Hz ; N=14 mice, n= 19 cells). ****p<0.0001 Unpaired t-test with Welch's correction. **(D)** Cumulative distribution

of sEPSC amplitudes in control and Emx1-Vangl2$^{-/-}$ neurons. **(E)** Quantification of sEPSC amplitude of control neurons (26.02 ± 1.346 pA ; N=16 mice, n=24 cells) versus Emx1-Vangl2$^{-/-}$ (20.96 ± 0.827 pA ; N=14 mice, n= 19 cells). **p=0.0036, Unpaired t-test with Welch's correction. **(F)** sEPSC amplitude distribution in CA3a pyramidal neurons in control (N=16 mice, n =24 cells) versus Emx1-Vangl2$^{-/-}$ (N=14 mice, n =19 cells). The binning size for the amplitude was 2 pA. The rectangle delimits the region were sEPSC above 30 pA are suppressed in Emx1-Vangl2$^{-/-}$ and is enlarged. **(G)** sEPSC number plotted against sEPSC amplitude. **(H)** sEPSC decay time (ms) in CA3a pyramidal neurons in P21-30 control (5.894 ± 0.931 ms ; N=16 mice, n=24 cells) and Emx1-Vangl2$^{-/-}$ acute hippocampal slices (5.969 ± 1.230 ms; N=14 mice, n= 19 cells). ns, p>0.05, two-tailed Mann-Whitney test. **(I)** Representative traces of evoked response of AMPA/Kaïnate receptors recorded at -70 mV from CA3a pyramidal neurons in P21-P30 control (grey) and Emx1-Vangl2$^{-/-}$ (light blue) acute hippocampal slices. **(J)** Quantification of AMPA receptors EPSC amplitudes of MFB/TE synapses in control (N=12 mice, n=16 cells) and Emx1-Vangl2$^{-/-}$ mice (N= 11 mice, n=14 cells). ns, p>0.05 **(K)** Representative traces of evoked response of NMDA receptors recorded at +40 mV from CA3a pyramidal neurons in P21-P30 control (grey) and Emx1-Vangl2$^{-/-}$ (light blue) acute hippocampal slices. **(L)** Quantification of NMDA receptors EPSC amplitudes of MFB/TE synapses in control (N= 12 mice, n= 16 cells) and Emx1-Vangl2$^{-/-}$ mice (N=11 mice, n= 14 cells). ns, p>0.05. **(M)** Representative traces of AMPA/NDMDA ratio from CA3a pyramidal neurons in P21-P30 control (grey) and Emx1-Vangl2$^{-/-}$ (light blue) acute hippocampal slices. **(N)** AMPA/NMDA ratio at MFB/TE synapses in control (N= 12 mice, n= 16 cells) Emx1-Vangl2$^{-/-}$ mice (N= 11 mice, n= 14 cells). ns, p>0.05. **(O)** Representative traces of paired-pulse ratio of MFB/TE synapses of control and Emx1-Vangl2$^{-/-}$ mice. **(P)** Quantification of paired-pulse ratio of MFB/TE synapses in control (N=12 mice, n=14 cells) and Emx1-Vangl2$^{-/-}$ mice (N=12 mice, n=15 cells). ***p<0.001, **p<0.01, 2nd way ANOVA with Bonferronni's multiple comparisons test. **(Q)** Representative traces of train of 10 stimuli at 20 Hz of MFB/TE synapses of control and Emx1-Vangl2$^{-/-}$ mice. **(R)** Analysis of the presynaptic facilitation in trains of 10 stimuli at 20Hz in control and Emx1-Vangl2$^{-/-}$ MFB/TE synapses. Facilitation is represented by the amplitude of the EPSCs normalized by the first EPSC. Two-way ANOVA; control: N= 9 mice, n=11 cells, Emx1-Vangl2$^{-/-}$: N=9 mice, n=11 cells ; p=0.0059.

Then, we analyzed paired-pulse ratio (PPR) to assess the presynaptic function of Emx1-Vangl2$^{-/-}$ MFB/TE synapses **(Figure 23O-P)**. MFB/TE synapses are known to be highly facilitating synapses (Salin et al., 1996). Accordingly, in WT synapses, the amplitude of the second EPSC at 25 ms inter-stimulus interval (ISI) was increased by 267% relative to the first EPSC amplitude ; whereas in Emx1-Vangl2$^{-/-}$ mice, the amplitude of the second EPSC at the same ISI was increased by 174% compared to the first EPSC amplitude (**Figure 23P** ; Two-way ANOVA, p=0.0001). At 50 ms interval, the amplitude of the second EPSC in control synapses was increased by 246% ; whereas in Emx1-Vangl2$^{-/-}$ synapses, the amplitude of the second EPSC at the same ISI was increased by 169% compared to the first EPSC (**Figure 23P** ; Two-way ANOVA, p=0.0039). No significant difference can be highlighted for higher interstimuli intervals. Thus, in Emx1-Vangl2$^{-/-}$ synapses, the increase in PPR was reduced at shorter interstimuli intervals (25 ms and 50 ms) compared to control synapses. We also analyzed the presynaptic facilitation in trains of 10 stimuli at 20Hz in control and Emx1-Vangl2$^{-/-}$ MFB/TE synapses **(Figure 23Q-R)**. We observed that presynaptic facilitation is nearly abolished in Emx1-Vangl2$^{-/-}$ MFB/TE synapses compared to the control (Two-way ANOVA, p=0.0059).

All together these results showed that loss of Vangl2 impairs synaptic transmission and short-term plasticity predominantly at the presynaptic side of mossy fibers synapses in CA3a region of hippocampus.

Presynaptic Vangl2 re-expression rescues the phenotype of MFB/TE synapses in young Emx1-Vangl2$^{-/-}$ mice

To test whether the morphological deficits and the presynaptic short-term plasticity observed in young Emx1-Vangl2$^{-/-}$ mice were indeed dependent on Vangl2 expression, we did a rescue experiment with a AAV virus allowing the expression of Vangl2 in the GC of the DG as well as the expression of mCherry in neo-natal Emx1-Vangl2$^{-/-}$ mice and controls (control^{Resc} and Emx1-Vangl2$^{-/-Resc}$) **(Figure 24A)**. This allowed to re-express Vangl2 in the pre-synaptic compartment just at the start of MFs growth and synapse development. At P25, after synapse maturation, we observe no differences between the MFB of Emx1-Vangl2$^{-/-Resc}$ and control^{Resc} mice **(Figure 24B)**. There was no statistical difference neither in volume (control: 16,43±0,5848 µm^3, Emx1-Vangl2$^{-/-}$: 15,60±0,5046 µm^3 ; Mann-Whitney test p= 0,7637), nor in area (control: 164,7±5,085 µm^2, Emx1-Vangl2$^{-/-}$: 170,0±4,546µm^2 ; Mann-Whitney test p= 0,1670), between the boutons of control^{Resc} and Emx1-Vangl2$^{-/-Resc}$ **(Figure 24D-E)**. Moreover, the number of filopodia per MFB as well as the percentage of MFB without any filopodia were also rescued by Vangl2 re-expression (control: 0,6236±0,05824 filopodia per MFB, Emx1-Vangl2$^{-/-}$: 0,6735±0,06255 filopodia per MFB ; Mann-Whitney test p=0,5969) **(Figure 24F-G)**. Morphological parameters from control^{Resc} mice were compared with those of control mice, and no significant differences were found between the two conditions, showing that the re-expression of exogen Vangl2 does not affect the morphology of the MFB in control conditions (data not shown).

Taken together, these results suggest that Vangl2 re-expression in the GC rescues the morphological deficits induced by the early deletion of Vangl2. This would mean that the correct morphological development and maturation of the MFB/TE giant synapse critically depends upon correct pre-synaptic expression of Vangl2 in the hippocampus.

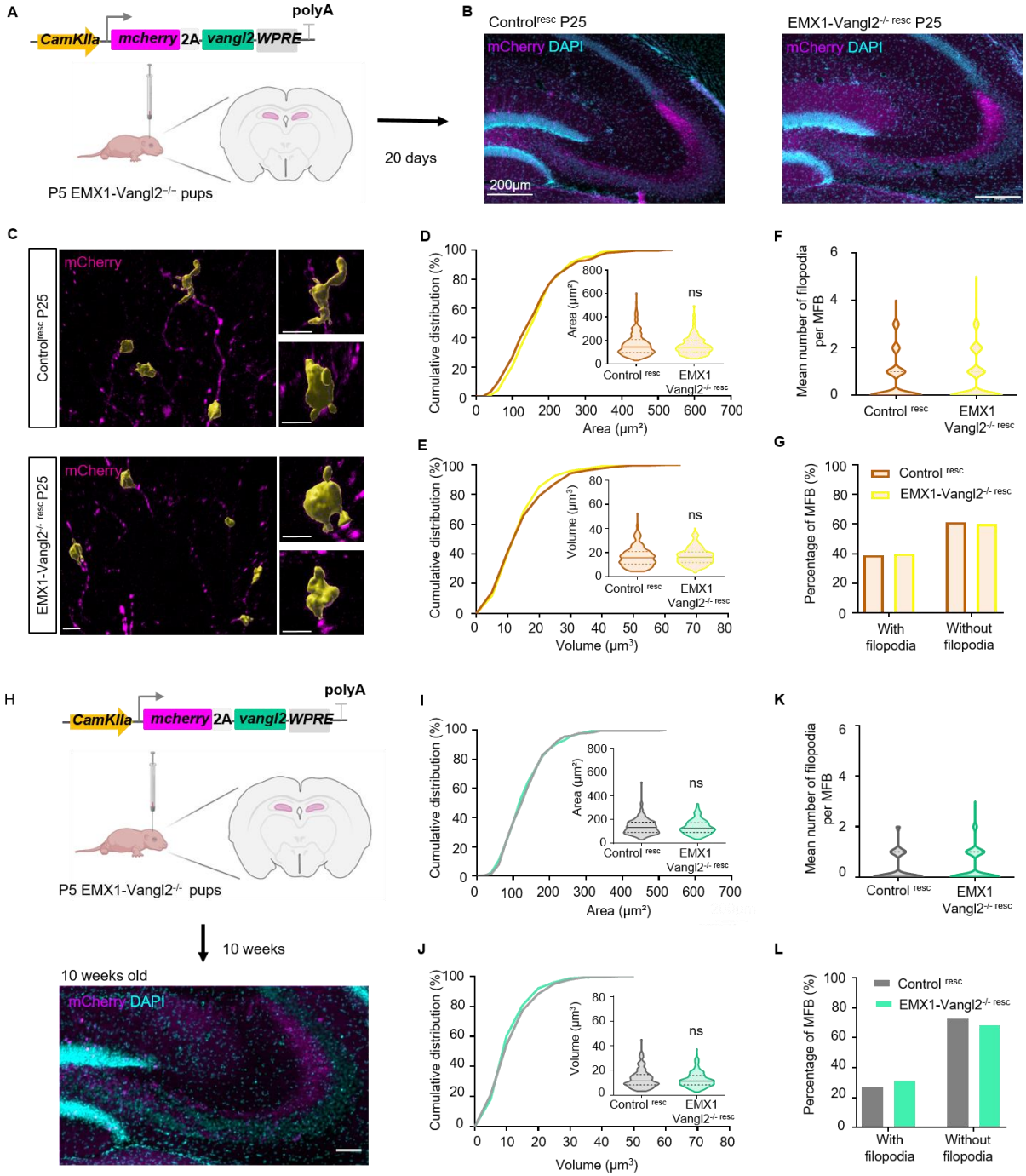

Figure 24: (A) Experimental design for stereotaxic virus injection for the reexpression of Vangl2 in the DG of P5 pups. **(B)** Representative confocal images of labelled presynaptic MFB in the SL of P25 control^{resc} and Emx1-Vangl2$^{-/-\ resc}$ mice in magenta. **(C)** Representative confocal images of labelled MFB (magenta) with 3D reconstruction (yellow) in the SL of P25 Emx1-Vangl2$^{-/-resc}$ and control^{resc} mice. **(D-G)** Quantifications of volume, area, number of filopodia per MFB, and percentage of MFB with filopodia in P25 Emx1-Vangl2$^{-/-\ resc}$ and control^{resc} mice. N control^{resc} = 263 MFB from 8 mice, N Emx1-Vangl2$^{-/-\ resc}$ = 245 MFB from 8 mice. Mann-Whitney test, ns p>0.05. **(H)** Experimental design for stereotaxic virus injection for the reexpression of Vangl2 in the DG of P5 pups and representative confocal images of labelled presynaptic MFB in the SL of 10 weeks old control^{resc} in magenta. **(I-L)** Quantifications of volume, area, number of filopodia per MFB, and percentage of MFB with filopodia in 10 weeks Emx1-Vangl2$^{-/-\ resc}$ (green) and control^{resc} (grey) mice. N control^{resc} = 180 MFB from 6 mice, N Emx1-Vangl2$^{-/-\ resc}$ = 266 MFB from 8 mice. Mann-Whitney test, ns p>0.05

We also tested whether the re-expression of presynaptic Vangl2 has an impact on the MFB/TE synapse of adults. P5 Emx1-Vangl2$^{-/-}$ pups and control littermates were injected in the DG with a virus allowing the re-expression of Vangl2, and the morphology of the presynaptic MFB was observed once they reached 10 weeks of age **(Figure 24H)**. No difference was found between adult control and mutant presynaptic MFB, both in area (control: 140,9±4,857 µm^2, Emx1-Vangl2$^{-/-Resc}$: 138,6±4,084 µm^2 ; Mann-Whitney test p= 0,7635) and volume (control: 13,38±0,5563 µm^3, Emx1-Vangl2$^{-/-Resc}$: 12,57±0,4113 µm^3 ; Mann-Whitney test p= 0,6009) **(Figure 24I-J)**. The number of filopodias per MFB and the percentage of MFB with filopodias is also similar between Emx1-Vangl2$^{-/-}$ and control mice (control: 0,3167±0,04130 filopodia per MFB, Emx1-Vangl2$^{-/-Resc}$: 0,3717±0,03986 filopodia per MFB ; Mann-Whitney test p=0,3547) **(Figure 24K-L)**.

Vangl2 organizes presynaptic markers

In regard of our findings on the morphology and pre-synaptic function of Vangl2, we decided to assess whether the vangl2 early deletion would impact pre-synaptic markers. We did immunohistochemistry on 3-week-old mice brain slices for Bassoon, Synapsin1 and Synaptoporin. We measured the integrated density of the fluorescent signal in the *sl*, normalized it to the integrated density of the signal of the *sr* and calculated the percentage of reduction of this parameter between controls and mutants **(Figure 25B, D and F)**. We observed notably that the fluorescent signals for Synaptoporin, Bassoon and Synapsin 1 were significantly reduced in brain slices of mice lacking the expression of vangl2 (Synaptoporin: -18,11±2,572 %, One sample t-test p=0.0001 ; Bassoon: -10,11±1,564 %, One sample t-test p=0.0002 ; Synapsin 1: -16,70±3,238 %, One sample t-test p= 0,0021) **(Figure 25C-E-G)**. These results indicate that the early loss of vangl2 affects the expression of pre-synaptic proteins in the MFB/TE synapses.

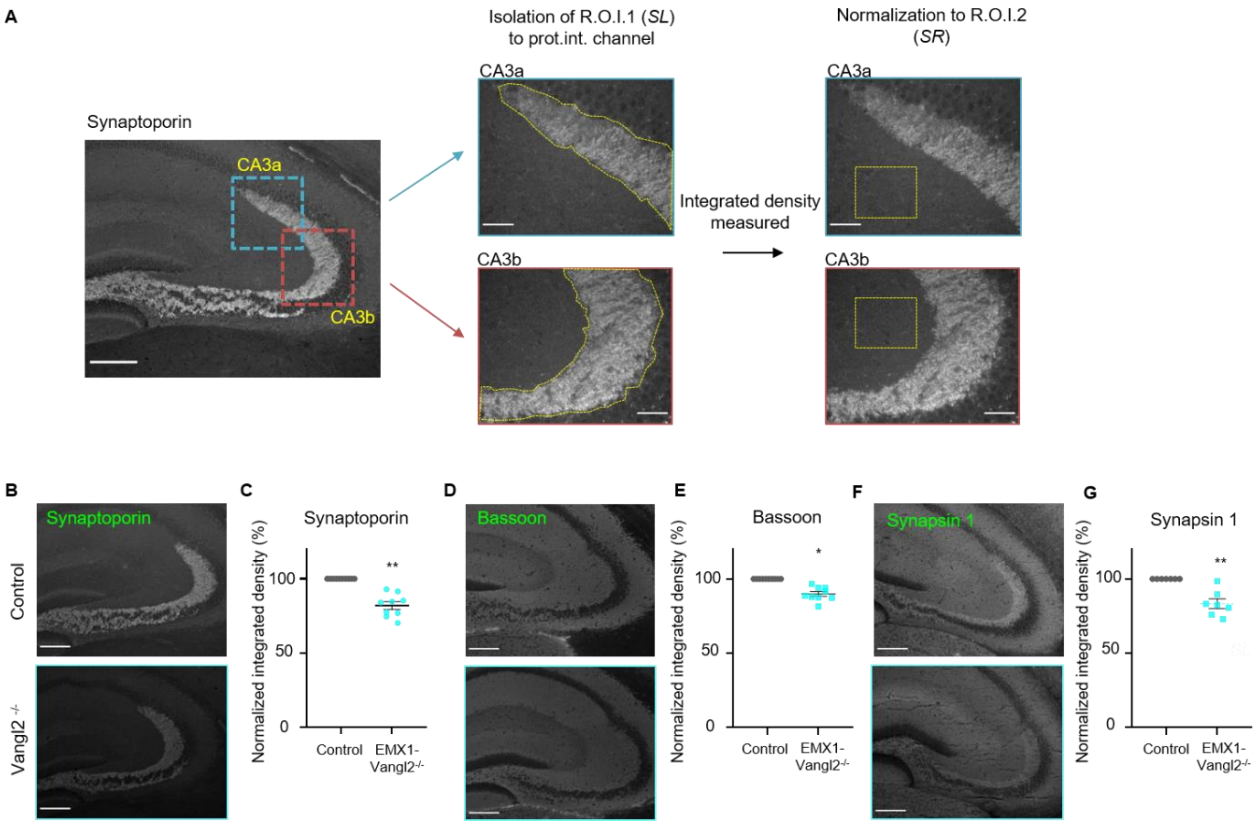

Figure 25: (A) To quantify the intensity of the stainings a mask corresponding to the SL was created in the red channel. This first region of interest (ROI) was applied to the green channel where the integrated density of the protein of interest was measured only in the SL. The results are normalized onto values measured in a second ROI: the *stratum radiatum*. **(B, D, F)** Representative epifluorescence images of the *stratum lucidum* where stainings of Synaptoporin, Bassoon and Synapsin 1 are depicted in P23 Emx1-Vangl2$^{-/-}$ and control mice. Scale bar = 200µm. **(C, E, G)** Quantification of the percentage of reduction of the normalized integrated density for the signal of Synaptoporin, Bassoon and Synapsin 1 in P23 control (grey) and Emx1-Vangl2$^{-/-}$ (turquoise) mice. N control = 10 mice, N Emx1-Vangl2$^{-/-}$ = 9 mice. One sample t-test. **p < 0.01, and ***p < 0.001. Error bars represent SEM.

Vangl2 colocalizes with presynaptic GPC4 to stabilize postsynaptic GPR158

Among the many pre-synaptic proteins that participate to the establishment of the MFB/CA3 giant synapse, the heparan sulfate proteoglycan (HSPG) glypican 4 (GPC4) was recently found to be enriched in MFs (Condomitti et al., 2018). Recently, GPC4 has been found to regulate PCP during convergent extension in zebrafish by influencing the localization of Cadherin 2 (Balaraju et al., 2021) or acting as a co-receptor with Fzd for Wnt to promote Wnt11 function (Ohkawara et al., 2003; Topczewski et al., 2001). To test whether Vangl2 could interact with GPC4 in cis **(Figure 26A)**, we examined the

localization of Vangl2 in COS-7 cells in the absence or presence of GPC4. Single transfection of Vangl2 or GPC4 revealed membrane and vesicular localization in COS-7 cells **(Figure 26B-C)**. When co-transfected, the two proteins colocalized in vesicles or in clusters, and in some domains of the plasma membrane **(Figure 26D)**. When we used a GPC4-myc construct interfering with the glycosylphosphatidylinositol (GPI) anchoring mechanism that is not properly trafficked to the membrane **(Figure 26C)**, we found that Vangl2 was also blocked in intracellular compartments **(Figure 26E)**. We also examined the localization of Vangl2 in presence of the orphan receptor GPR158, a transynaptic interactor of GPC4 (Condomitti et al., 2018). We co-transfected Vangl2 with a HA-GPR158 plasmid in COS-7 cells, and the two proteins do not seem to colocalize outside of the Golgi apparatus **(Figure 26F)**. These results suggest that GPC4 can associate with Vangl2 early in the trafficking pathway and that both protein travel together in clusters to the plasma membrane.

We next assessed if this association between Vangl2 and GPC4 occured in the presynaptic compartment of cultured neurons. We co-transfected cultured rat hippocampal neurons with Vangl2 and GPC4. At DIV17, Vangl2 and GPC4 can both be found partially colocalized at the growth cone in the axon of transfected neurons **(Figure 26G)**. This data suggests that GPC4 and Vangl2 are associated in the presynaptic compartment of neurons during axonal development. We next investigated the impact of Vangl2 early deletion on the level of GPC4 in the organization of synaptic architecture and function of the MFB/TE synapse. Using immunohistochemistry on 3 week-old mice brain slices, we observed that the integrated density of the fluorescent signal for GPC4 was significantly reduced in Emx1-Vangl2$^{-/-}$ mice compared to controls (-25,29±3,503 % , One sample t-test $p<0.0001$) **(Figure 26H-I)**. Since GPC4 binds to the orphan receptor GPR158 to stabilize it at the postsynaptic side, we also quantify GPR158 immunofluorescence in controls and mutant mice. As expected, GPR158 was also significantly reduced in Emx1-Vangl2$^{-/-}$ mice compared to controls (-14.66±4,950 %, One sample t-test $p=0.0143$) **(Figure 26J-K)**.

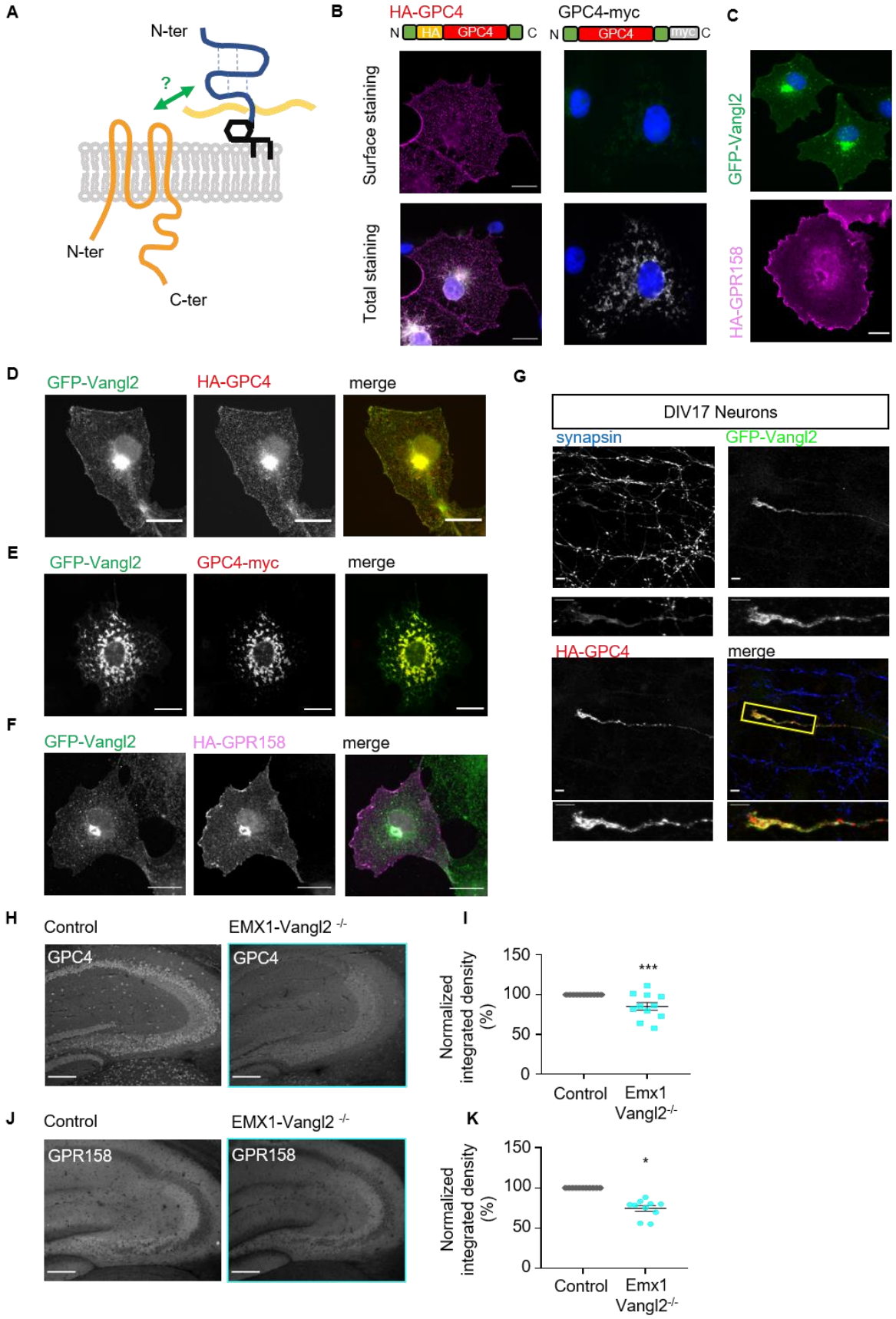

Figure 26: (A) Schematic representation of Vangl2 and GPC4 proteic structures and their potential interaction in cis. **(B)** Representative images of surface and total staining of HA-GPC4 (red) and GPC4-myc (grey) expression in transfected COS-7 cells. **(C)** Representative images of total staining of Vangl2-

GFP (green) and HA-GPR158 (magenta) expression in transfected COS-7 cells. Scale bar = 20µm. **(D-F)** Representative images of total staining of Vangl2-GFP (green), HA-GPC4 (red) , GPC4-myc (red) and HA-GPR158 (magenta) expression in co-transfected COS-7 cells. Scale bar = 20µm. **(G)** Representative image of the expression of synapsin (blue), HA-GPC4 (red) and Vangl2-GFP (green) in the axonal projection of a DIV17 transfected neuron. Scale bar = 5µm. **(H)** Representative epifluorescence images of the *stratum lucidum* with GPC4 staining in P21 Emx1-Vangl2$^{-/-}$ and control mice. Scale bar = 200µm**. (I)** Quantification of the percentage of reduction of the normalized integrated density for the signal of GPC4 in P21 control (grey) and Emx1-Vangl2$^{-/-}$ (turquoise) mice. N control = 11 mice, N Emx1-Vangl2$^{-/-}$ = 11 mice. One sample t-test ***p < 0.001. Error bars represent SEM. **(J)** Representative epifluorescence images of the *stratum lucidum* with GPR158 staining in P21 Emx1-Vangl2$^{-/-}$ and control mice. Scale bar = 200µm**. (K)** Quantification of the percentage of reduction of the normalized integrated density for the signal of GPR158 in P21 control (grey) and Emx1-Vangl2$^{-/-}$ (turquoise) mice. N control = 11 mice, N Emx1-Vangl2$^{-/-}$ = 11 mice. One sample t-test *p < 0.05. Error bars represent SEM.

Early presynaptic structural deficits are compensated in adults but morpho-structural plasticity of the MFB/TE synapse remains affected

We then evaluated if the morphological deficits observed on the MFB/TE synapses of young Emx1-Vangl2$^{-/-}$ mice was maintained in adult mice. 8 weeks old Emx1-Vangl2$^{-/-}$ mice and controls were injected with an AAV virus allowing the expression of the fluorescent protein mCherry in order to label the MFs and the MFB **(Figure 27A)**. After 3D reconstruction, we observed no difference between the different morphological parameters of the presynaptic MFB in 10 weeks old Emx1-Vangl2$^{-/-}$ mice and controls **(Figure 27B)**. There was no statistical difference neither in volume (control: 18,93±0,7454 µm^3, Emx1-Vangl2$^{-/-}$: 18,43±0,7555 µm^3 ; Mann-Whitney test p= 0,5702), nor in area (control: 180,0± 5,834 µm², Emx1-Vangl2$^{-/-}$: 181,6±5,713µm² ; Mann-Whitney test p= 0,6931) between the boutons of control and Emx1-Vangl2$^{-/-}$ **(Figure 27C-D)**. The number of filopodias was also unchanged between mutants and controls (control: 0,6291±0,06343 filopodia per MFB, Emx1-Vangl2$^{-/-}$: 0,7059±0,07059 filopodia per MFB ; Mann-Whitney test p= 0,5522), as well as the proportion of MFB with filopodias **(Figure 27E-F)**. These results suggest that the early presynaptic structural deficits are compensated in adult mice.

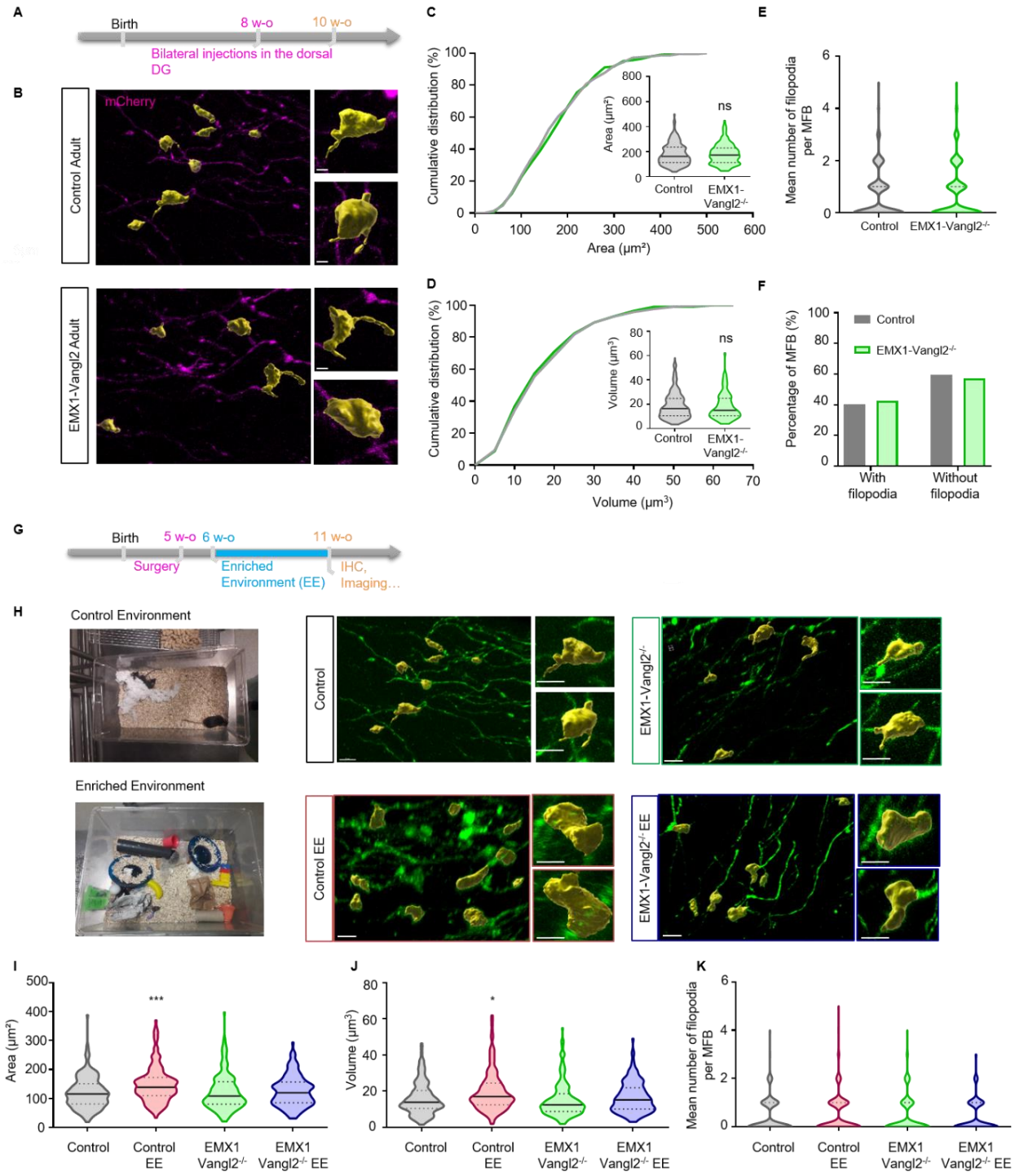

Figure 27: (A) Experimental design for stereotaxic virus injections in the DG of 8 weeks old mice. **(B)** Representative confocal images of labelled MFB (magenta) with 3D reconstruction (yellow) in the SL of 10wo Emx1-Vangl2$^{-/-}$ and control mice. **(C-F)** Quantifications of volume, area, number of filopodia per MFB, and percentage of MFB with filopodia in 10wo Emx1-Vangl2$^{-/-}$ and control mice. N control = 213 MFB from 6 mice, N Emx1-Vangl2$^{-/-}$ = 204 MFB from 6 mice. Mann-Whitney test, ns p>0.05. **(G-H)** Schematic representation of the EE procedure in adult mice. To summarize, 5wo mice are injected with a mcherry expressing virus to label the MFB then placed into enriched (EE) or control (CE) environment for 5 weeks before doing immunohistochemistry and 3D confocal imaging of the MFB. **(H)** 3D reconstruction of presynaptic MFB (yellow) on confocal stacks in the four conditions: control (red) and Emx1-Vangl2$^{-/-}$ (blue) mice in Enriched Environment (EE), Control (grey) and Emx1-Vangl2$^{-/-}$ (green) mice in control environment. **(I-K)** Quantification of the MFB area, volume and number of filopodia per MFB for Emx1-Vangl2$^{-/-}$ and

control mice, after 5 weeks in EE or control environment. N Control = 167 MFB from 7 mice; Emx1-Vangl2$^{-/-}$ ctl = 167 MFB from 6 mice; Control EE = 177 MFB from 6 mice; Emx1-Vangl2$^{-/-}$ EE = 153 MFB from 6 mice. Kruskall-Wallis test, *p<0.05, ***p<0,001.

The MFB/TE giant synapse is prone to morpho-functional plasticity and mice subjected to an enriched environment present an increase of the number and complexity of the boutons as well as a stabilization of their structures (Galimberti et al., 2006; Gogolla et al., 2009). To see whether Vangl2 is necessary for this environment-dependent structural plasticity, we placed Emx1-Vangl2$^{-/-}$ mice and littermate controls in either an enriched environment or a control environment for 5 weeks **(Figure 27G-H)**. After 3D reconstruction of the pre-synaptic MFB **(Figure 27H)**, we confirmed an increase of volume and area of the MFB of control mice placed in EE compared to control environment (Volume control EE: 19,80±0,8251 µm^3, volume control: 16,01±0,6917 µm^3, Kruskal-Wallis test p<0.001 ; Area control EE: 149,4±4,697 µm², Area control: 121,1±4,258 µm², Kruskal-Wallis test p<0.0001). However, no significant difference was found for the area and volume of MFB of Emx1-Vangl2$^{-/-}$ mice place in EE compared to Emx1-Vangl2$^{-/-}$ and control mice placed in a control environment **(Figure 27E-G)**. This show that the early deletion of vangl2 affects the structural plasticity of the MFB/TE synapse in adult mice. These results suggest that even though the effect of early vangl2 loss is morphologically compensated in adult mice, the structural plasticity of the MFB synapse is still impaired in the mutants.

Vangl2 is necessary for memory flexibility assessed by radial-maze spatial discrimination learning

To determine the functional consequence of a loss of *vangl2* in the forebrain, we tested Emx1-Vangl2$^{-/-}$ mice and their littermate controls in a series of tasks measuring emotional, exploratory and cognitive behaviors. We first performed elevated plus-maze and dark/light experiments to test anxiety-like behaviour **(Figure 28A-C)**. Compared to their control littermates, Emx1-Vangl2$^{-/-}$ mice spent a normal amount of time in the open arms of the elevated plus-maze (Unpaired *t*-test, t_{28}=1.66, p>0.05 n.s), as well as a comparable percentage of time in the white box of the dark/light test (Unpaired *t*-test, t_{28}=1.33, p>0.05 n.s) **(Figure 28B-D)**. This means that the Emx1-Vangl2$^{-/-}$ mice did not display alteration of anxiety-like behavior. In addition, locomotion was also unaltered for Emx1-Vangl2$^{-/-}$ mice in an open field session **(Figure 28E)**, which displayed normal

rearing behavior (Unpaired *t*-test, t_{28}=1.16, p>0.05 n.s) and horizontal units of activity (2-way ANOVA, main effect of genotype, $F_{(1,476)} < 1$, p>0.05 n.s) **(Figure 28F-G)**.

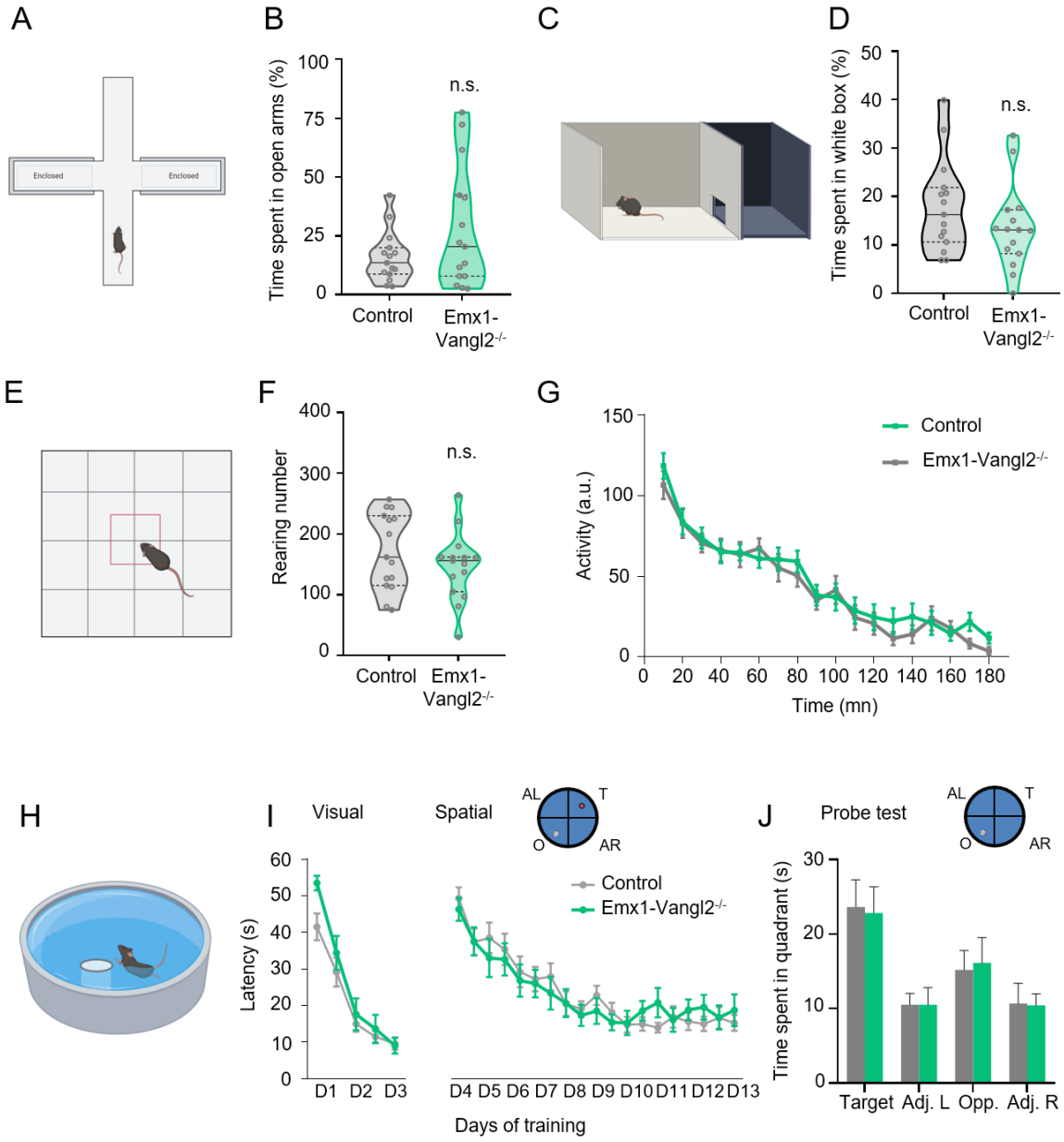

Figure 28: (A) Representation of the plus maze paradigm used to assess anxiety. **(B)** Quantification of the percentage of time spent in the open arms of the plus-maze test. Unpaired t-test, n.s. p>0.05. **(C)** Representation of the dark/light paradigm used to assess anxiety. **(D)** Quantification of the percentage of time spent in the white box of the dark/light test. Unpaired t-test, n.s. p>0.05. **(E)** Representation of the open field paradigm used to assess locomotor activity. **(F)** Quantification of the number of rearings during a 3h session in the open field. Unpaired t-test, n.s. p>0.05. **(G)** Quantification of activity during a 3h session in the open field. 2-way ANOVA. **(H)** Representation of the Morris Water Maze paradigm used to assess spatial learning and memory. **(I)** Latency to escape of the water maze test during the visual, spatial and reversal acquisition. 2-way ANOVA. **(J)** Time spent in the four quadrants of the water maze during the probe test at 10 days during the spatial acquisition. T: target, A.L: adjacent left, O: opposite, A.R: adjacent right. One sample t-test. Number of animals: control: n=15, Emx1-Vangl2$^{-/-}$: n=15.

We next analyzed the effect of Vangl2 loss on spatial learning and memory in the Morris water maze, known as a typical "hippocampus-dependent" test **(Figure 28H)**. During visual acquisition of the task, we found no impairment in the Emx1-Vangl2$^{-/-}$ mice. Similarly, the Emx1-Vangl2$^{-/-}$ mice were also indistinguishable from control during the acquisition of the standard spatial reference memory version of the Morris water maze task **(Figure 28I)**. Analysis of the latency to reach the platform during spatial training revealed that the two groups of mice acquired the task at the same rate (main effect of days, $F_{(18,513)} = 15.25$; $p < 0.0001$; main effect of genotype, $F_{(1,513)} < 1$; n.s; genotype-by days interaction, $F_{(18,513)} < 1$; n.s) **(Figure 28I)**. The performances were also assessed during probe test conducted 24hr after the last trial of the 10th day. Analysis of the distribution of time spent in the four quadrants of the pool revealed a significant effect of quadrant for the probe tests of control mice (2-way ANOVA, $F_{(3,56)} = 28.07$, $p < 0.0001$; target *vs.* others quadrants. Unpaired *t*-test $p < 0.001$) but also for Emx1-Vangl2$^{-/-}$ mice (2-way ANOVA, $F_{(3,56)} = 21.32$, $p < 0.0001$; target *vs.* others quadrants. Unpaired *t*-test $p < 0.001$) **(Figure 28J)**. In this spatial memory task, control and Emx1-Vangl2$^{-/-}$ mice learned the location of the platform to the same extent. Despite the fact that MFB morphology was affected, Emx1-Vangl2$^{-/-}$ displayed normal anxiety-like behavior, activity and spatial learning and memory.

We next tested another aspect of spatial memory, its flexibility taken as a model of reference memory, using a specific version of the 8 arm radial maze task (Al Abed et al., 2020; Etchamendy et al., 2003). The acquisition phase of this task evaluates the capability to learn constant food locations within the maze, i.e. acquisition of reference spatial memory. The maze arms are repeatedly presented by pairs (3 invariant pairs A, B, C), and the test phase evaluates the capability to flexibly express learned information, a distinctive feature of declarative memory, by recombining into a novel pairing two of the pairs learnt in the acquisition phase **(Figure 29A)**. During the acquisition, we found no impairment in the Emx1-Vangl2$^{-/-}$ mice as they reached the learning criterion as quickly as control mice (t-test, t24=1.4) **(Figure 29B)**, and had similar levels of performance during the first five days of training (2-way ANOVA, Days: $F(4,96) = 11.7$; $p < 0.0001$; Genotype: $F(1,96) < 1$; $p>0.05$; Genotype x Days: $F(4,96) < 1$; $p>0.05$) or the last five days of training (2-way ANOVA, Days: $F(4,96) = 35.95$; $p < 0.0001$; Genotype: $F(1,96) < 1$; $p>0.05$; Genotype x Days: $F(4,108) < 1$, $p>0.05$) **(Figure 29C-D)**. Both groups thus

displayed equally good abilities to acquire spatial (reference) memory. To analyze the results of the test, we compared the performance on the last day of training (D-1) to the performance in the test day. There was no difference between D-1 and test whatever the genotype regarding the control pair C (2-way ANOVA; Days: $F(1,48) < 1$; $p>0.05$; Genotype: $F(1,48) = 2.85$; $p>0.05$; Genotype x Days: $F(1,48) < 1$; $p>0.05$) or the novel pair (one group t-test vs. 50%, control $t10 = 1.1$; $p>0.05$; Emx1-Vangl2$^{-/-}$ $t14 = 0.56$; $p>0.05$) **(Figure 29F-G)**. In contrast, regarding the recombined pair AB, the analysis showed that performance significantly declined between the end of acquisition D-1 and the test in Emx1-Vangl2$^{-/-}$ mice only (2-way ANOVA, Days: $F(1,48) = 14.57$; $p < 0.01$; Genotype: $F(1,48) = 1.61$; $p>0.05$; Genotype x Days interaction: $F(1,48) = 4.06$; $p>0.05$; Bonferroni comparison D-1 vs. test: control $p>0.05$; Emx1-Vangl2$^{-/-}$ $p<0.001$) (**Figure 29E)**. Hence, while control mice could flexibly express their memories in a modified testing, Emx1-Vangl2$^{-/-}$ mice failed to do so hence showing memory inflexibility. All together, these data show that Emx1-Vangl2$^{-/-}$ mice are not grossly impaired as they can normally learn and express spatial memories in unvarying situations, but they are not capable to use their spatial memory with flexibility in a changed situation, hence displaying a selective impairment of relational/declarative memory.

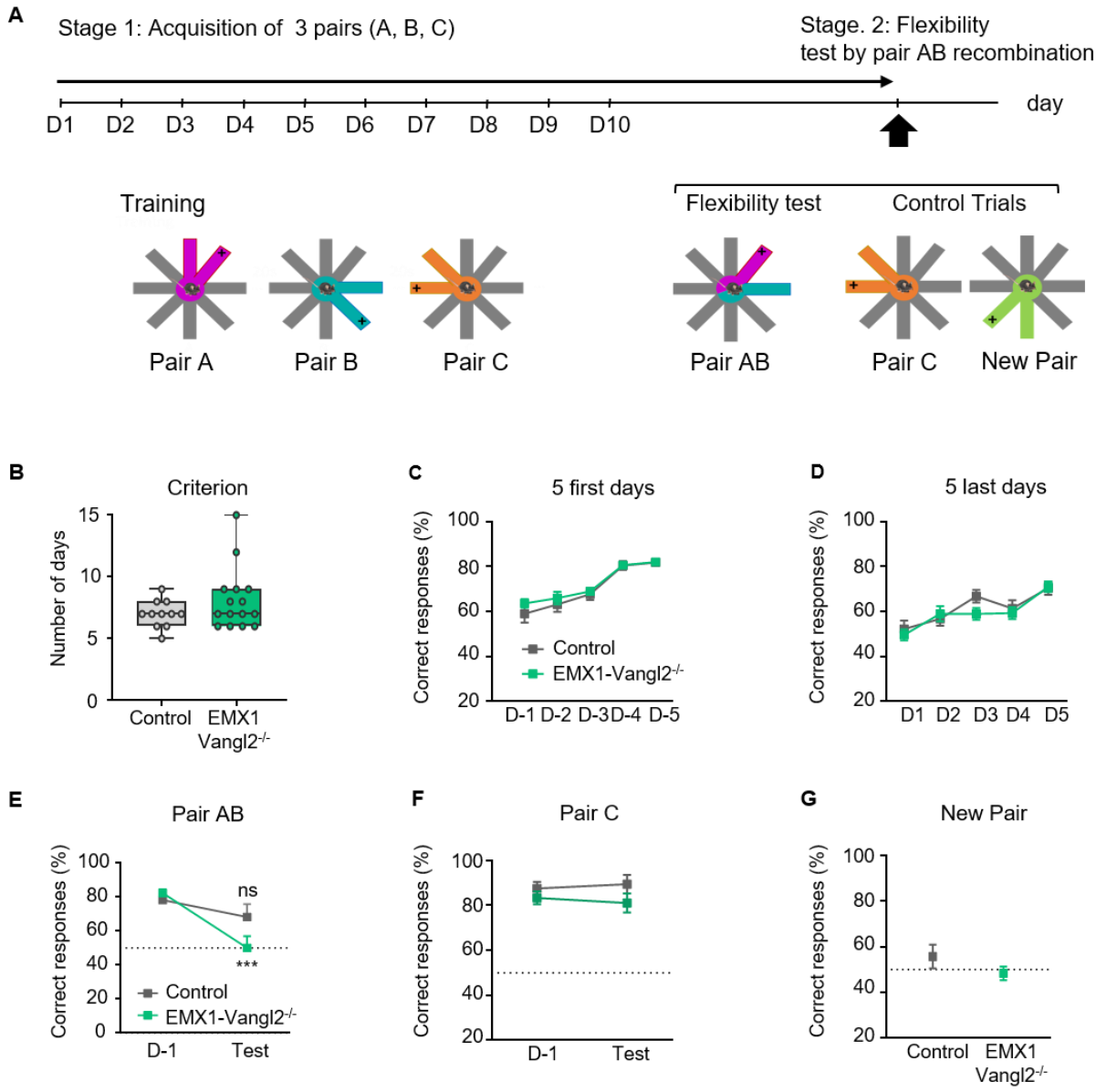

Figure 29: (A) Experimental design for the reference memory in the 8-arm radial maze test. **(B-D)** Quantification of the performance level during the acquisition phase measured by the number of day before reaching the criterion (B), and the percentage of correct response during the 5 first (C) and 5 last days of acquisition (D). N: Control = 11, Emx1-Vangl2$^{-/-}$ = 15. Mann-Whitney and 2-way ANOVA. **(E-G)** Graph of the evolution of percentage of correct responses between the last day of acquisition (D-1) and the Test for the critical pairs (E) (left: Pairs A and B recombined into Pair AB in the Test, representing the critical flexibility probe) and control pairs (F-G) (middle: Pair C is an "known" control; right: New Pair is an "novel" control appearing in Test only). N Control = 11, N Emx1-Vangl2$^{-/-}$ = 15. For Pair AB and Pair C: 2-way ANOVA with Bonferroni comparison, D-1 versus Test. ns $p>0.05$; *** $p<0.001$. For the Novel Pair: Mann-Whitney and One sample t-test vs 50%.

Vangl2 is necessary for working memory

Next, we tested spontaneous alternation in the Y-maze, based on the natural tendency of mice to explore a novel environment **(Figure 30A)**. Alternation can therefore be taken as an index of short-term/working memory. The analysis showed a significant difference between Emx1-Vangl2$^{-/-}$ mice and their control in the percentage of alternation **(Figure 30B)**. The Emx1-Vangl2$^{-/-}$ mice performance was not significantly different than the chance while the control group had an almost 75% alternation score (control: 74.06 %, Emx1-Vangl2$^{-/-}$: 56,09 ; t-test, p=0.0003 ; one sample t-test, control p<0.0001, Emx1-Vangl2$^{-/-}$ p=0.0545) **(Figure 30B)**. These data suggest that the Emx1-Vangl2$^{-/-}$ mice displayed poor spatial working memory.

To go further, we then assessed everyday-like working memory in a radial maze task that allows the testing of two component of memory: retention and organization (Al Abed et al., 2016).The animals were submitted to four blocks of three days of this task, where they add to alternate between the two arms of three pairs of arms. The retention difficulty depends on the number of trials separating two presentations of the same pair of arms (n and n-1), whereas the organizational difficulty (also called proactive interference) depends on the number of trials separating the last two presentations of the same pair of arms (n-1 and n-2) **(Figure 30C)**. Both groups learned the task correctly across the four first blocks of the experiment with an ITI of 10 seconds (Two-way ANOVA, Day x Genotype interaction: F (3, 69) = 1,551, p=0,2092 ; Day: F (3, 69) = 14,95, p<0,0001 ; Genotype: F (1, 23) = 0,03128, p=0,8612) **(Figure 30D)**. Regarding the retention component, the analysis of the four blocks shows that the performance decreases as the retention difficulty increases in both control and Emx1-Vangl2$^{-/-}$ mice (data not shown). When combining the performances of the third and fourth block, when the animals have acquired the task, we found that both the genotype and the level of retention difficulty had an impact on the animals' performance (Two-way ANOVA, retention difficulty x Genotype interaction: F (1, 58) = 0,7134, p=0,4018 ; retention difficulty: F (1, 58) = 41,82, p<0,0001 ; Genotype: F (1, 58) = 4,137 , p=0,0465) **(Figure 30F)**. Regarding the organization component, the five levels of organizational difficulty have been grouped in two levels: High interference (0 or 1 trial between n-1 and n-2 presentations of a pair of arms) and Low interference (2, 3 or 4 trials between n-1 and n-2 presentations of a pair of arms). We found that Emx1-Vangl2$^{-/-}$ mice are impaired when the organization difficulty is high

(Two-way ANOVA, organization difficulty x Genotype interaction: F (1, 23) = 8,812, p=0,0069 ; organization difficulty: F (1, 23) = 1,699, p=0,2053 ; Genotype: F (1, 23) = 1,089, p=0,3074 ; Bonferroni comparison control vs Emx1-Vangl2$^{-/-}$: high difficulty p=0,0397, low difficulty p >0,9999) **(Figure 30E)**. These results showed that Emx1-Vangl2$^{-/-}$ mice have specifics impairments in both retention and organization components of everyday-like working memory.

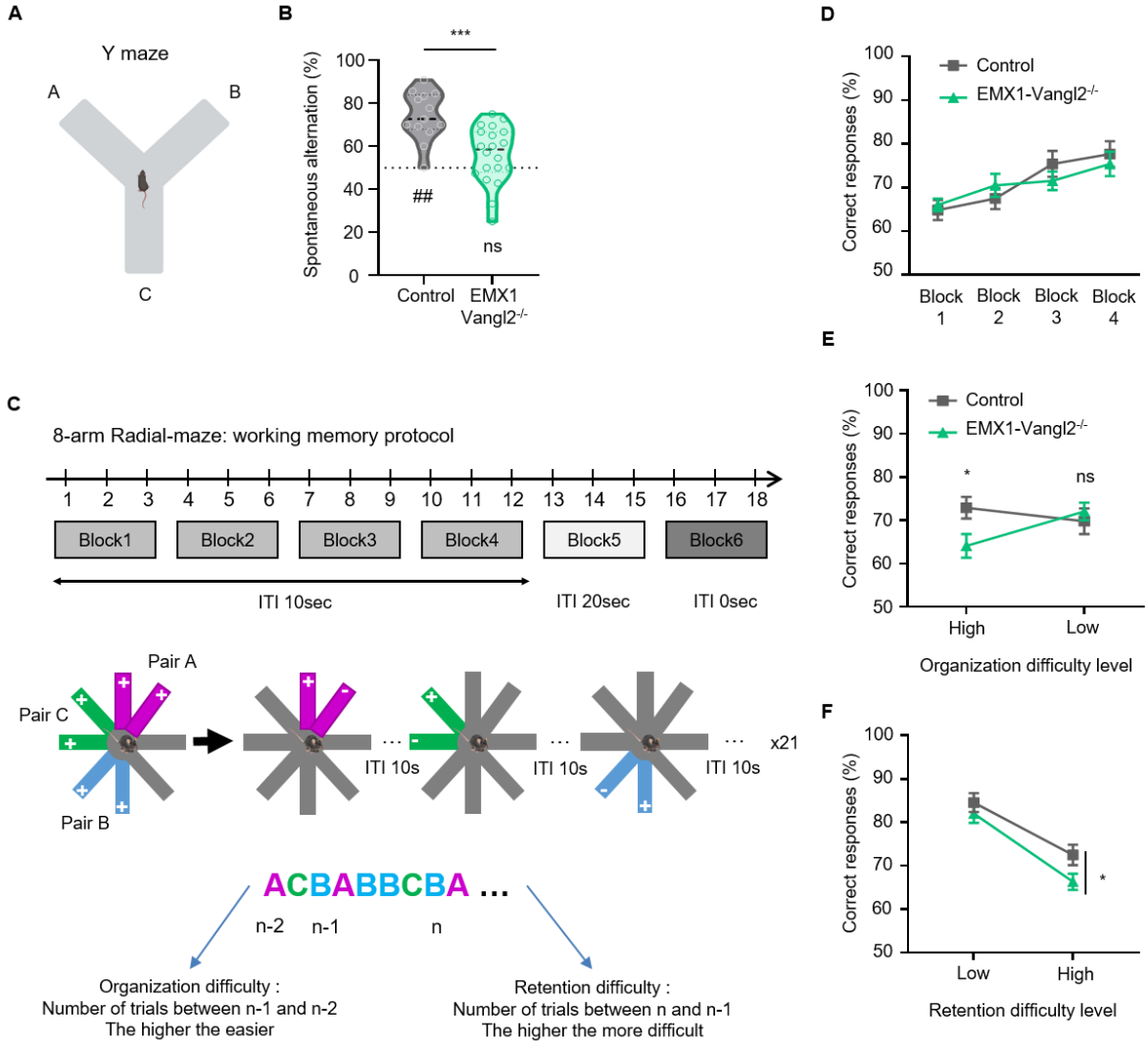

Figure 30: (A) Experimental setup for the spontaneous alternation test in Y maze. **(B)** Mean percentage of spontaneous alternation control (grey) and Emx1-Vangl2$^{-/-}$ adult mice (green) which can be interpreted as a working memory deficit. N Control = 13 mice; N Emx1-Vangl2$^{-/-}$ = 20 mice. Unpaired t-test, ***p<0.001; One sample t-test against 50%, ###p<0.001, ns p>0.05. **(C)** Experimental design for the working memory in the 8-arm radial maze test. **(D)** Quantifications of the percentage of correct response during the first four blocks of the experiment (ITI 10s). N Control=11, N Emx1-Vangl2$^{-/-}$ =15. 2-way ANOVA 2-way. **(E-F)** Quantifications of the percentage of correct response depending on the level of organization (E) and retention (F) difficulty. N Control=11, N Emx1-Vangl2$^{-/-}$ =15. 2-way ANOVA 2-way, *p<0.05.

Vangl2 controls the ability to recollect on information based on relevant contextual cues

To assess what kind of cues the animals use to recollect information, we tested fear memory in an unpaired contextual fear conditioning protocol, which will allow us to assess hippocampal function, in the ability of the animals to focus on distal or tonic contextual cues **(Figure 31A)**. During the first test in the neutral chamber, as expected the level of freezing was low for both control and Emx1-Vangl2$^{-/-}$ mice during the first two minutes, as the neutral chamber is not associated with the shock **(Figure 31B)**. When the tone used for the conditioning phase started, the level of freezing of both genotypes remained low, but it increased after the end of the tone only for the Emx1-Vangl2$^{-/-}$ mice, indicating a wrong association between the tone and the footshock (2-way ANOVA, Time: $F(2,50) = 4.987$; $p=0.0106$; Genotype: $F(1,25) = 0.2451$; $p>0.05$; Genotype x Time: $F(2,50) = 1.361$; $p>0.05$; Bonferroni's multiple comparison test, for control: no significant effect of time, for Emx1-Vangl2$^{-/-}$ mice: significant difference between the last two minutes and the two other time intervals) **(Figure 31B)**. During the second test, in the conditioning chamber, during the first three minutes the electric grid was hidden **(Figure 31A)**. As expected, the control mice displayed a high level of freezing, indicating the right association between the context and the footshock **(Figure 31C)**. On the other hand, Emx1-Vangl2$^{-/-}$ mice displayed a lower level of freezing **(Figure 31C)**. During the last three minutes, when the grid was revealed, the level of freezing of control animals decreased, showing an extinction of the conditioning, whereas the level of freezing of Emx1-Vangl2$^{-/-}$ mice increased, showing that they relied on salient elements of the context rather than on distal cues (2-way ANOVA, Time: $F(1,24) = 0.2023$; $p>0.05$; Genotype: $F(1,24) = 0.2813$; $p>0.05$; Genotype x Time: $F(1,25) = 6.596$; $p=0.0169$; Bonferroni's multiple comparison test, for control: no significant effect of time, for Emx1-Vangl2$^{-/-}$ mice: significant difference between the two time intervals) **(Figure 31C)**. The third test occurs in the neutral chamber, where a tone different from the one used during the conditioning phase is used, to assess a potential partial generalization of information **(Figure 31A)**. Again, as expected the level of freezing was low for both control and Emx1-Vangl2$^{-/-}$ mice during the first two minutes. When the tone started, the level of freezing of Emx1-Vangl2$^{-/-}$ mice increased, and continued to increase after the end of the tone, indicating a partial generalization of the wrong information linking the tone to the footshock (2-way ANOVA, Time: $F(2,50) = 6.8$; $p=0.0024$; Genotype: $F(1,25) = 0.2194$;

p>0.05 ; Genotype x Time: F(2,50) = 3.249; p=0.0471; Bonferroni's multiple comparison test, for control: no significant effect of time, for Emx1-Vangl2$^{-/-}$ mice: significant difference between the first two minutes and the two other time intervals) **(Figure 31D)**. Finally, during the fourth test, in the neutral chamber, mice were submitted to a white noise, to assess a potential global generalization of information **(Figure 31D)**. During the first two minutes of the test, the level of freezing of Emx1-Vangl2$^{-/-}$ mice was low, whereas the one of the control was unexpectedly high, possibly reflecting a loss of conditioning. When the white noise started, the level of freezing of control mice decreased, and the one of Emx1-Vangl2$^{-/-}$ mice remained low, and stayed low for both genotypes after the end of the tone, indicating the absence of association between the white noise and the footshock, and thus no global generalization of information (2-way ANOVA, Time: F(2,50) = 2.669; p>0.05 ; Genotype: F(1,25) = 1.437; p>0.05 ; Genotype x Time: F(2,50) = 6.072; p=0.0044; Bonferroni's multiple comparison test, for control: significant difference between the first two minutes and the two other time intervals, for Emx1-Vangl2$^{-/-}$ mice: no significant effect of time **(Figure 31E)**. These results showed that Emx1-Vangl2$^{-/-}$ mice have do not use the right cues to recollect information, having associated the shock with the sound, which was not predictive of the shock, and with the grid rather with the spatial context which was the predictor of the shock.

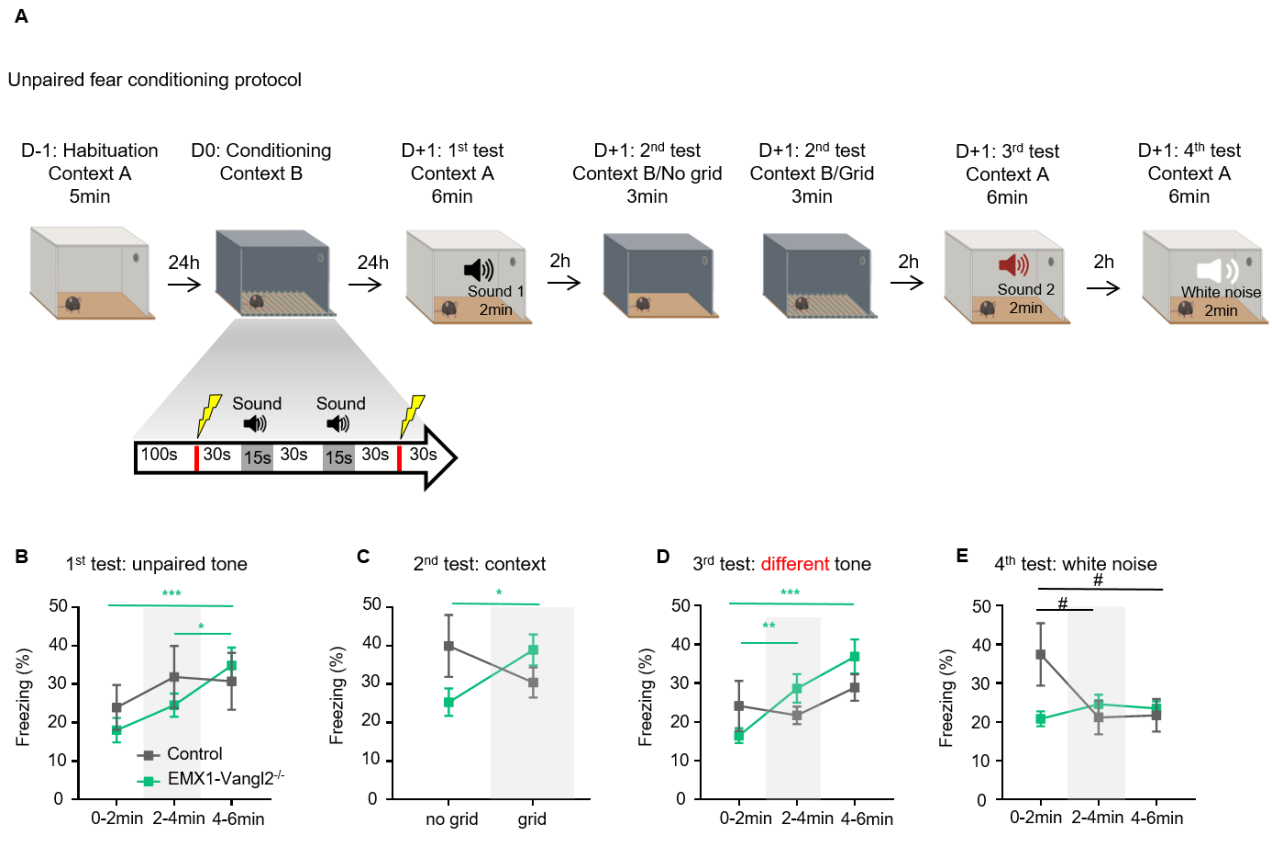

Figure 31: (A) Experimental design for the unpaired contextual fear conditioning protocol. **(B)** Quantification of the percentage of freezing during the first conditioning tone test. N Control=7, N Emx1-Vangl2$^{-/-}$ =20. 2-way ANOVA, *p<0.05 *** p<0.001. **(C)** Quantification of the percentage of freezing during the contextual test. N Control=7, N Emx1-Vangl2$^{-/-}$ =20. 2-way ANOVA, *p<0.05. **(D)** Quantification of the percentage of freezing during the partial generalization test. N Control=7, N Emx1-Vangl2$^{-/-}$ =20. 2-way ANOVA, **p<0.01 *** p<0.001. **(E)** Quantification of the percentage of freezing during the global generalization test. N Control=7, N Emx1-Vangl2$^{-/-}$ =20. 2-way ANOVA, **p<0.01 *** p<0.001.

Project 2:

Vangl2 participates to the morphofunctional degradation of the MFB/TE synapse and alteration of hippocampal-dependent memories during aging

In the second part of the results, we explore the impact of the early deletion of the PCP gene *vangl2* on the DG-CA3 circuit in the context of aging, as it is known to be particularly impacted during both normal and pathological aging. Using 3D reconstruction of confocal acquisitions, we show that the early genetic deletion of *vangl2* in mice has an unexpected protective effect against the aging-related synaptic degradation of the MFB/TE synapse. However, the deficits in presynaptic proteins expression already observed in juvenile mice still persists in aged mutants. We also study the performances of the aged Emx1-Vangl2$^{-/-}$ mice in an array of hippocampal-dependent memory tasks known to be affected during aging. We show that the aged mutant mice have better performances than age-matched controls in spatial learning and memory, novel object recognition and working memory. Altogether, our data show that Vangl2 participates to the degradation of hippocampal circuitry and function during physiological aging and that its early deletion might have a protective effect towards those detrimental effects of age.

Loss of Vangl2 plays a protective role for the morphology of the MFB/TE synapse against the effects of age

Age is correlated with the degradation of the structure of the MFB/TE giant synapses in both rodents and humans (Wilke et al., 2014; Dàs et al., 2019). In the first part of my thesis, I showed that Vangl2 plays a key role for the morphogenesis and the morphological maintenance of the MFB/TE synapse **(see figures 20-21-24)**. Because of these previous observations, we wanted to explore the impact of the early loss of Vangl2 on the morphology of the presynaptic MFB in aged mice. We used a morphometric approach to study the pre-synaptic elements of the mossy fiber bouton/thorny excrescence (MFB/TE) synapse. We infected the GC of the DG of middle aged Emx1-Vangl2$^{-/-}$ mice (15 months old) with a viral construct allowing the expression of the fluorescent protein mCherry in order to label the Mf and the MFB **(Figure 32A)**.

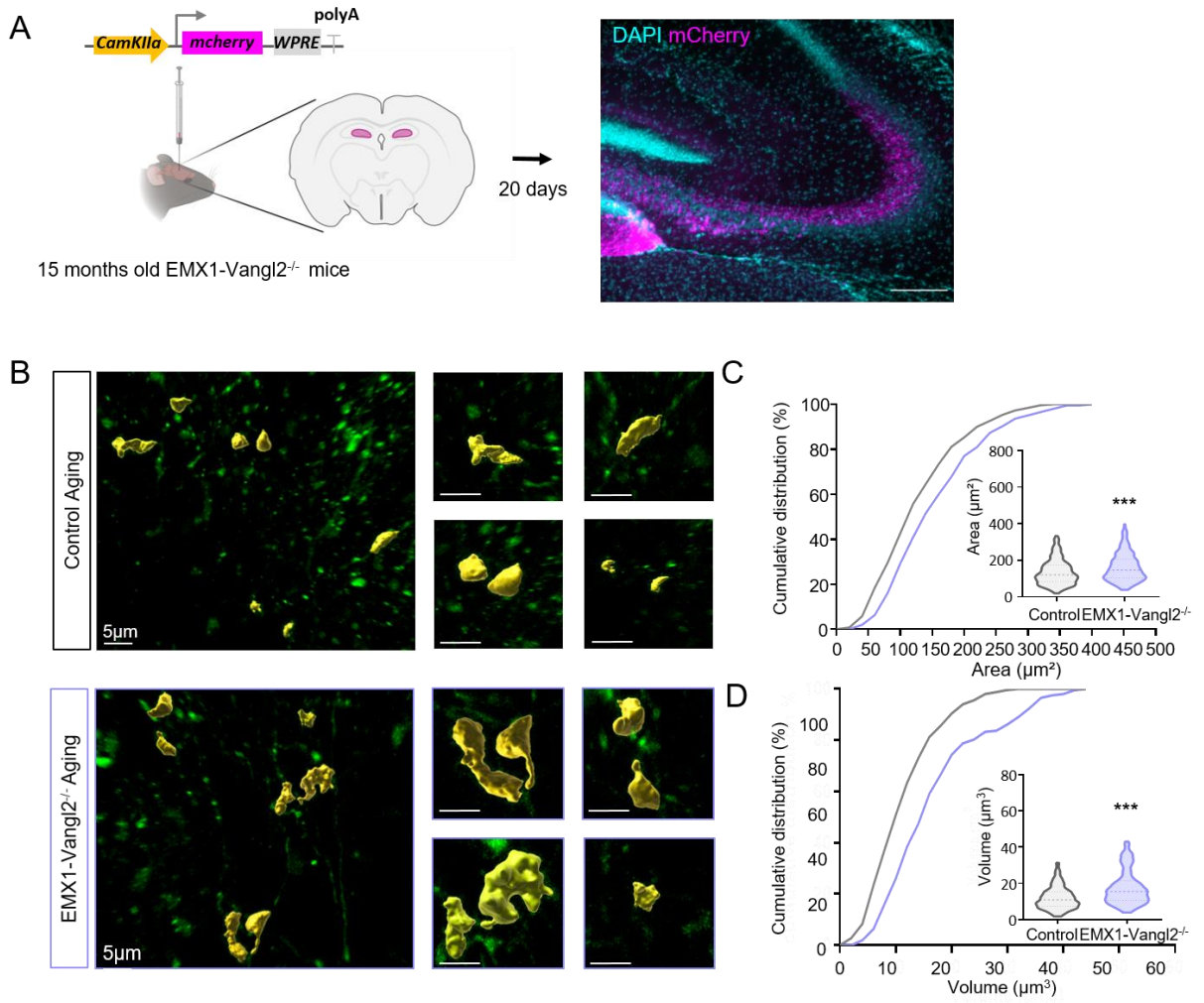

Figure 32: (A) Experimental design for stereotaxic virus injection for the reexpression of Vangl2 in the DG of 15 month old mice. **(B)** Representative confocal images of labelled presynaptic MFB in the SL of 16

month old control mice in magenta. **(C)** Representative confocal images of labelled MFB (green) with 3D reconstruction (yellow) in the SL of 16-17 months old Emx1-Vangl2$^{-/-}$and control mice. **(D-G)** Quantifications of volume, area, number of filopodia per MFB, and percentage of MFB with filopodia in 16-17 months old Emx1-Vangl2$^{-/-}$(purple) and control (grey) mice. N control= 260 MFB from 9 mice, N Emx1-Vangl2$^{-/-}$ = 205 MFB from 7 mice. Mann-Whitney test, ns p>0.05.

We then quantified morphological parameters of 3D reconstructed MFB located in the *stratum lucidum* at 16-17 months old **(Figure 32B)**. Surprisingly, the MFB of aged mutant mice were significantly bigger than the ones of aged control mice, with bigger area (control = 134,1±4,169 µm² ; Emx1-Vangl2$^{-/-}$= 161,3±5,248µm² ; Mann-Whitney test, p<0.001) **(Figure 32C)** and volume (control = 11,95±0,3864 µm^3 ; Emx1-Vangl2$^{-/-}$= 17,53±0,6479 µm^3 ; Mann-Whitney test, p<0.001) **(Figure 32D)**. Altogether these results suggest that Vangl2 expression is still important for the structural dynamics of the MFB/TE giant synapse in aged mice, and that at some point the early deletion of *vangl2* start having a protective effect against the age-linked morphological degradation of the synapse.

Early deletion of Vangl2 does not prevent the alteration of presynaptic proteins expression in MFB/TE synapse

In regard of our finding on the morphology of the MFB/TE giant synapse of aged mice, we decided to assess whether the vangl2 *early* deletion would impact pre-synaptic markers using immunohistochemistry. We did immunohistochemistry on 16-17 months old mice brain slices for Bassoon, Synaptotagmine 7 (Syt7), Synapsin1 and Synaptoporin, which are 4 pre-synaptic proteins present in the pre-synaptic MFB **(Figure 33 A-C-E-G)**. We measured the integrated density of the fluorescent signal in the *SL,* normalized it to the integrated density of the signal of the *SR* and calculated the percentage of reduction of this parameter between controls and mutants **(see figure 24)**. We observed that the fluorescent signals for Synaptoporin (control = 23,49±1,136 u.a. ; Emx1-Vangl2$^{-/-}$= 18,89±0,6450 u.a. ; Welsch's t-test, p=0,0057) , Syt7 (control = 15,34± 0,8100 u.a. ; Emx1-Vangl2$^{-/-}$= 12,81± 0,3255 u.a. ; Welsch's t-test, p=0,0199) and Synapsin 1 (control = 13,03±1,078 u.a. ; Emx1-Vangl2$^{-/-}$= 10,45±0,3091 u.a. ; Welsch's t-test, p= 0,0229) were significantly reduced in brain slices of aged mice lacking the expression of Vangl2 **(Figure 33B-D-F)**. However, the signal for Bassoon was not significantly affected (control = 12,10±0,9185 u.a. ; Emx1-Vangl2$^{-/-}$= 9,860±0,2988 u.a. ; Welsch's t-test, p=0,0519) **(Figure 33H)**. These results indicate that the early loss of

vangl2 still affects the expression of pre-synaptic proteins in the MFB/TE synapses in aged mice, as observed in 3 weeks old animals.

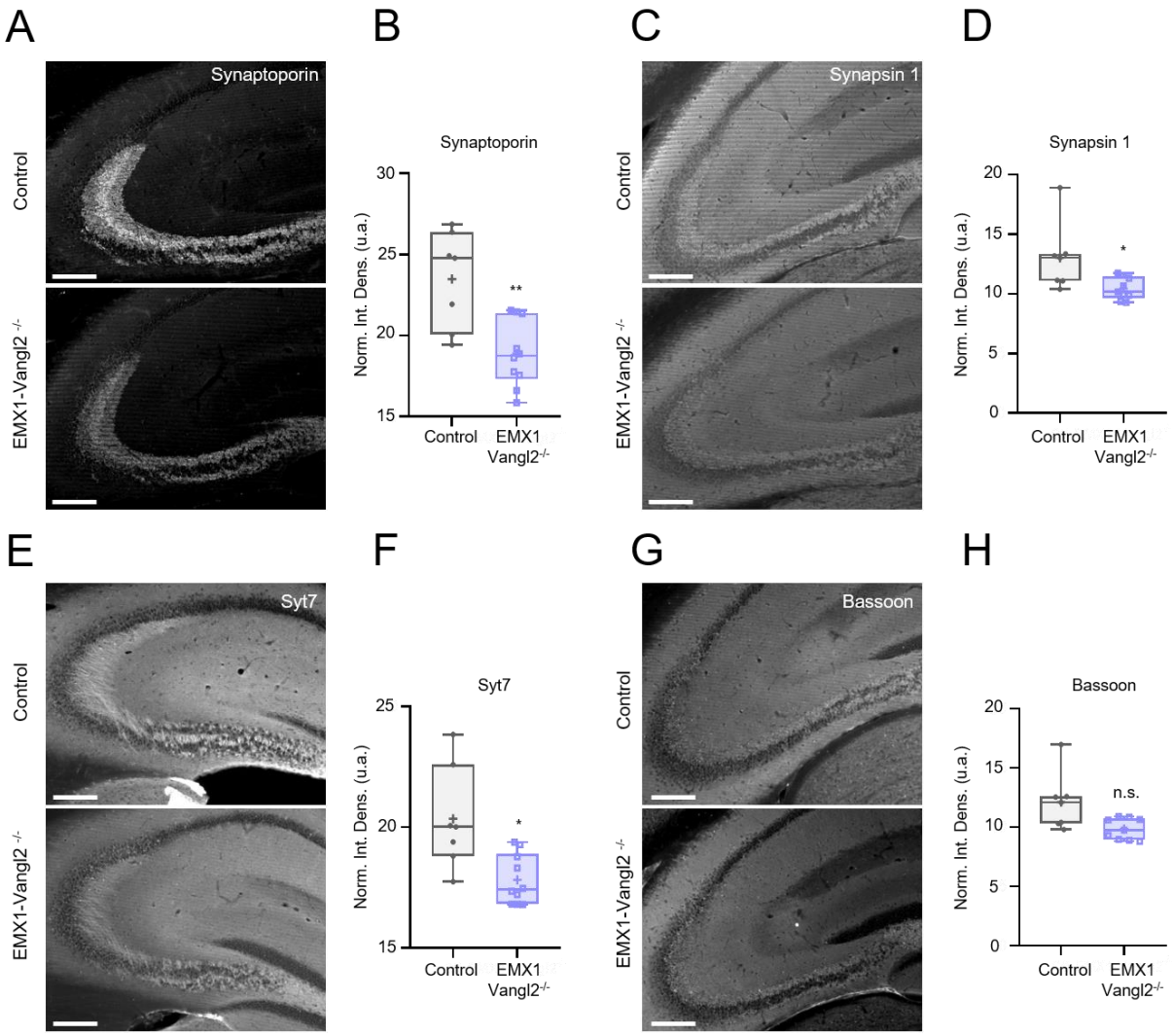

Figure 33: (A, C, E, G) Representative epifluorescence images of the *stratum lucidum* where stainings of Synaptoporin, Bassoon and Synapsin 1 are depicted in 16-17months old Emx1-Vangl2$^{-/-}$ and control mice. Scale bar = 200µm. **(B, D, F, H)** Quantification of the percentage of reduction of the normalized integrated density for the signal of Synaptoporin, Bassoon and Synapsin 1 in P23 control (grey) and Emx1-Vangl2$^{-/-}$ (purple) mice. N control = 7 mice, N Emx1-Vangl2$^{-/-}$ = 9 mice. One sample t-test. **p < 0.01, and ***p < 0.001.

Aged mice that lack Vangl2 expression have better declarative memory performances

We used an array of behavioural tests to assess the functional consequences of the early deletion of *vangl2* on memory performances in aged Emx1-Vangl2$^{-/-}$ and control mice (16 to 18 months old) **(Figure 34)**.

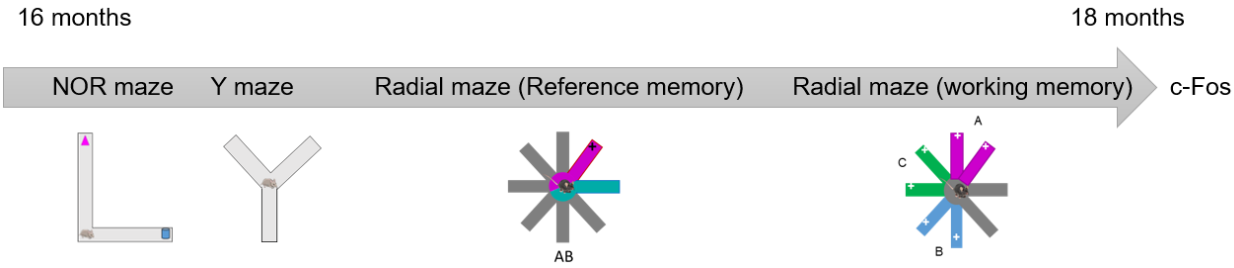

Figure 34: Timeline of the behavioural experiments done in aged Emx1-Vangl2$^{-/-}$ mice.

Spontaneous object recognition (SOR) task procedures are also improved in aged Emx1-Vangl2 mutants

We started our analysis with an L-maze Novel Object Recognition (NOR) task to evaluate object recognition memory, a process often affected during aging. The L-shaped maze has long narrow corridors which minimizes the context surrounding the objects and reduces the weight of other possible cues rather than the objects themselves. The aim is to facilitate the interaction of the animal with the object and to reduce the anxiety related bias normally encountered in open field tests (Da Cruz et al., 2020). The L-maze maximizes the accuracy of the test by enhancing the time of exploration of the objects **(Figure 35A)**. The discrimination index [DI: exploration time novel object – exploration time familiar object / (exploration time novel object + exploration time familiar object)] is measured to evaluate the long term memory, DI significantly above chance (= preference for the novel object) attests of mnemonic retention of the familiar object. We observed that Emx1-Vangl2$^{-/-}$ aged mice had a DI significantly higher than the chance level attesting of recognition memory, whereas aged controls failed to do so (one sample t-test ; control t=1,079, df=8, p=0.3119 ; Emx1-Vangl2$^{-/-}$ t=4,541, df=8, p= 0,0019) **(Figure 35B)**. Previous data from our lab showed that, in 10 weeks old adult mice, both mutant and control groups had significant DI and there was no significant difference based on the genotype (data not shown). Therefore, surprisingly, the loss of Vangl2 appears to counteract the deleterious effect of aging on object recognition memory.

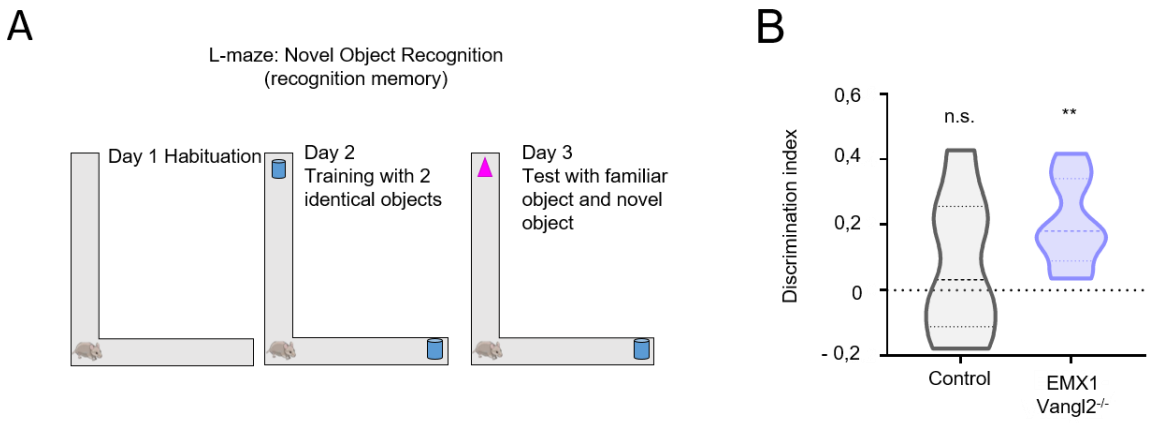

Figure 35: (A) Experimental design of the novel object recognition in L maze. **(B)** Quantification of the discrimination index of 18 month old control (grey) and Emx1-Vangl2$^{-/-}$ (purple) mice. N control = 10, N Emx1-Vangl2$^{-/-}$= 10. One sample t-test, n.s. p>0.05, **p<0.01.

Working memory in the Y-Maze is improved in Emx1-Vangl2 aged mutants

We then proceeded to test working memory performance in our aged mice. First we used spontaneous alternation in a Y maze paradox, which be interpreted as an index of short-term working memory **(Figure 36A)**. Previously we had found that adult Emx1-Vangl2$^{-/-}$ mice had a deficit of spontaneous alternation compared to controls, interpreted as a sign of impaired working memory. Surprisingly, in the aged mice groups, the mutant one had no more deficits of performance and performed significantly better than the control group, who's performance was not different from the chance level (one sample t-test ; control, t=0,2326, df=9, p=0,8213 ; Emx1-Vangl2$^{-/-}$ t=3,566, df=9, p= 0,0061 ; Welsch's t-test, control vs ; Emx1-Vangl2$^{-/-}$ p=0.0496) **(Figure 36B)**.

To further investigate this switch in working memory performances in aged Emx1-Vangl2$^{-/-}$ mice, we used the 8-arm radial maze working memory paradigm **(Figure 37A)**. We studied the global performance level with various demands on retention relative to organization, i.e. under different ITI conditions, 0s, 10s, or 20s-ITI. When looking upon the global performance of the aged mice during the 4 blocks with the 10s ITI, we found that both groups displayed improvement of their performance across training but we already saw that, overall, the aged mutants had significantly better performances than age-matched controls (Two-way ANOVA, Day x Genotype interaction: F (11, 242) = 0,6855, p=0,7518 ; Day: F (11, 242) = 12,42, p<0,0001 ; Genotype: F (1, 22) = 4,703,

p=0,0412) **(Figure 37B)**. However, when we analyse the first block (Day1-3) of each ITI conditions, we observe no effect of the ITI duration on the global performance of both groups (Two-way ANOVA ; Genotype x ITI interaction : F (2, 63) = 0,2697, p=0,7645 ; ITI : F (2, 63) = 2,284, p=0,1103 ; Genotype : F (1, 63) = 5,902, p=0,0180) **(Figure 37C)**.

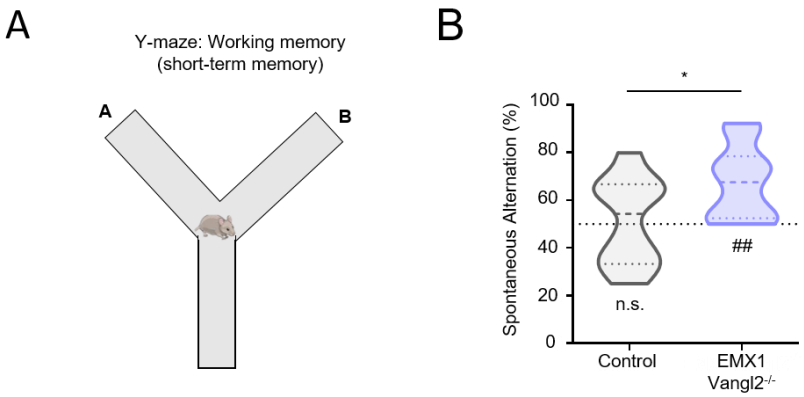

Figure 36: (A) Experimental setup for the spontaneous alternation test in Y maze. **(B)** Mean percentage of spontaneous alternation control (grey) and Emx1-Vangl2$^{-/-}$ adult mice (purple) which can be interpreted as a working memory deficit. N Control = 10 mice; N Emx1-Vangl2$^{-/-}$ = 10 mice. Unpaired t-test, *p<0.05; One sample t-test against 50%, ##p<0.01, ns p>0.05.

We then quantified the level of performance during the 4 ITI-10s blocks in regard of the level of retention and organisation difficulty. Regarding the retention difficulty, both aged group saw their performance affected by the difficulty levels (Two-way ANOVA; Difficulty: F (2, 66) = 20,71, p<0.001). However, Emx1-Vangl2$^{-/-}$ mice had better performances than controls without any relation with the retention difficulty (2-way ANOVA; Genotype x Retention difficulty interaction: F (2, 66) = 0,008818, p=0,9912 ; Genotype: F (1, 66) = 8,387, p=0,0051) **(Figure 37D)**. Similar results can be found for the performance at different levels of organisation difficulty, with an overall decrease of performance when the organisation difficulty increase and a significantly better performance of aged Emx1-Vangl2$^{-/-}$ mice but no interaction between the two parameters (Two-way ANOVA ; Genotype x Difficulty interaction : F (2, 66) = 1,335, p=0,2701 ; Difficulty : F (2, 66) = 4,591, p=0,0136; Genotype : F (1, 66) = 9,582, p=0,0029) **(Figure 37E)**. These results showed that Emx1-Vangl2$^{-/-}$ mice have specifics impairments in both retention and organization components of everyday-like working memory. These results show that the deletion of Vangl2 improves working memory performance in aged mice, disregarding of the retention and organization demand of the task.

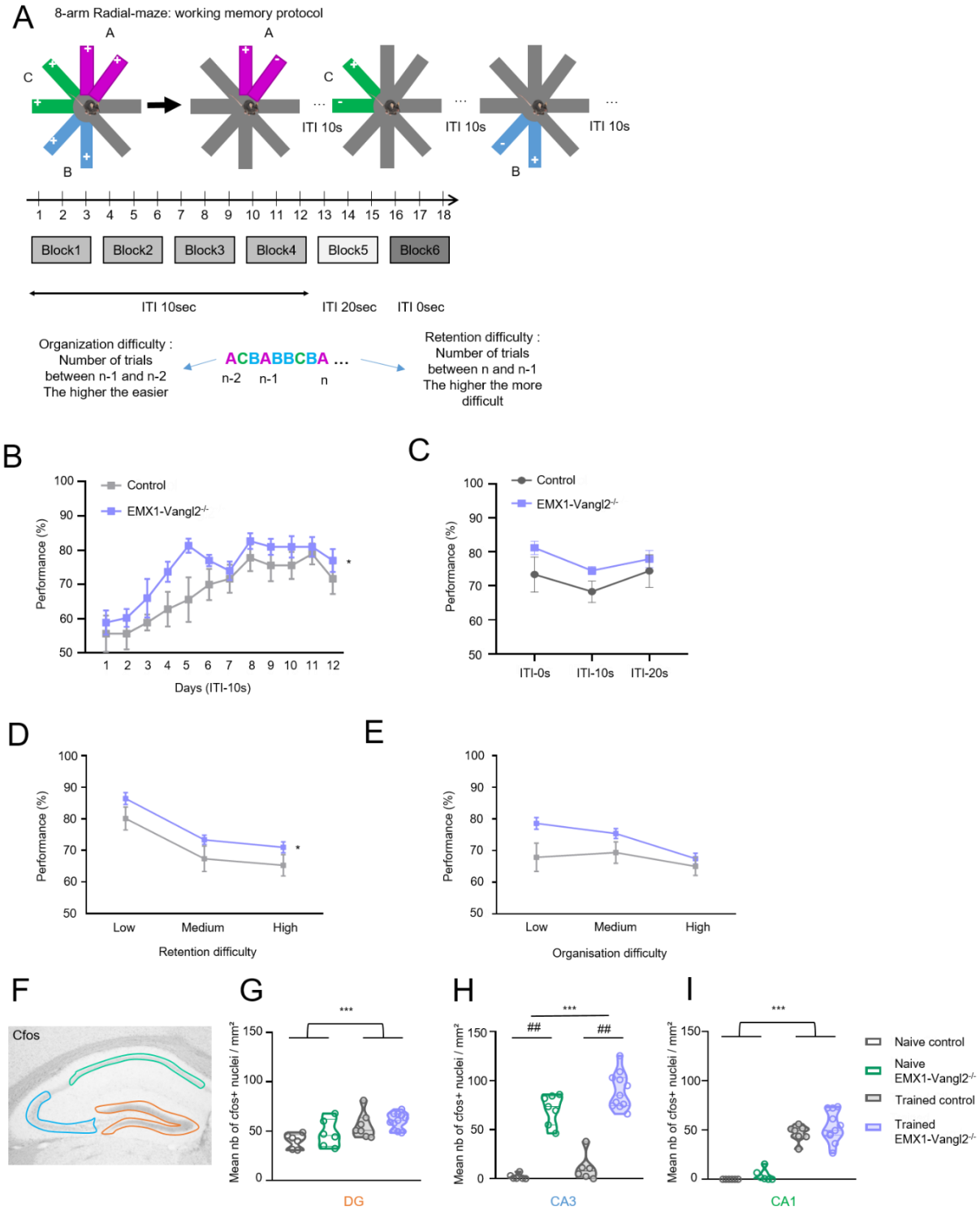

Figure 37: (A) Experimental design for the working memory in the 8-arm radial maze test. **(B)** Mean level of performance (% of correct response) of aged control (grey) and Emx1-Vangl2$^{-/-}$ (purple) mice across the 4 ITI 10s blocks. N control = 9; N Emx1-Vangl2$^{-/-}$ = 15. 2-way ANOVA, *p<0.05. **(C)** Mean level of performance (% of correct response) of aged control (grey) and Emx1-Vangl2$^{-/-}$ (purple) mice with different ITI. N control = 9; N Emx1-Vangl2$^{-/-}$ = 15. 2-way ANOVA. **(D-E)** Quantifications of the percentage of correct response depending on the level of retention (D) and organization € difficulty. N Control=11, N Emx1-Vangl2$^{-/-}$ =15. 2-way ANOVA 2-way, *p<0.05. **(F)** Representative light microscopy image of aged hippocampus with cFos labelling. The regions where the number of cFos positive nucleus was counted are highlighted in orange (DG), blue (CA3) and green (CA1). **(G-H-I)** Quantification of the mean number of

cFos positive nuclei / mm² in different hippocampal regions (G: DG, G: CA3, H: CA1) in trained or naïve aged control and Emx1-Vangl2$^{-/-}$ mice. N control naïve = 6 mice, N Emx1-Vangl2$^{-/-}$ naïve = 6 mice, N control trained = 7 mice, N Emx1-Vangl2$^{-/-}$ trained = 11 mice. 2-way ANOVA, ## p<0.01, ***p<0.001.

Next, we sought to identify potential functional alterations associated with the improvement of working memory in aged Emx1-Vangl2$^{-/-}$ mice. Mice went through a final trial of the WM task in the radial maze and then were sacrificed to perform cFos neuroimaging as an index of neuronal activity. Age-matched naïve mice that never went through the task were used as control. The number of cfos positive nuclei per mm2 was measured in the DG, CA3 and CA1 regions **(Figure 37F)**. As expected, the training increased neuronal activation in all structures observed, both in the control group and the Emx1-Vangl2$^{-/-}$ group (2-way ANOVA ; Training effect : DG= F (1, 26) = 12,67, p=0.0015 ; CA3= F (1, 26) = 172,6, p=<0.0001 ; CA1= F (1, 26) = 139,9, p<0.0001) **(Figure 37G-H-I)**. Interestingly the only structure where the genotype had an effect on the level of neuronal activation, with a higher number of cfos positive cells in both naïve and trained aged Emx1-Vangl2$^{-/-}$ mice compared to controls (2-way ANOVA ; Genotype effect : DG=F (1, 26) = 2,389, p=0,1343 ; CA3=F (1, 26) = 6,229, p=0,0192 ; CA1=F (1, 26) = 1,771, p=0,1949) **(Figure 37H)**. This suggest that the absence of Vangl2 in aged mice is correlated with increased neuronal activity in the CA3, which could explain the improved working memory performances compared to controls.

Spatial memory is also improved in Emx1-Vangl2 mutant mice

Morris Water Maze is a classical task that is used to measure hippocampal-dependent spatial memory in rodents **(Figure 38A)**. Performance is measured by time to locate the platform (escape latency) during training trials before mice reach the platform. For the visual learning tests, controls and mutants performed similarly with a rapid decrease of the latency to reach the platform **(Figure 38B)**. This indicated that the early vangl2 deletion did not affect the mice's motivation to escape the pool, swimming ability and visual acuity. During the spatial acquisition process, no differences were noted between the control and the mutant groups, with a progressive reduction of the latency to reach the platform that stabilizes around the 17th day of training for both groups **(Figure 38C)**. The "all cue" probe test allows for the evaluation of spatial learning by testing the amount of time a mouse spends in each quadrant against the phantom platform area, while all visual clues are still present **(Figure 38A)**. Control groups spent equal amounts of time in the target region in comparison to the other three regions. On the other hand, Emx1-

Vangl2$^{-/-}$ mice spent approximately 45% of the time in the target region and less than 25% of the time on other platform areas (2 way ANOVA; Zone effect: $F(3,68) = 7.875$, $p = 0.0055$; Genotype effect: $F(1,68) = 0.00198$, $p = 0.9647$) **(Figure 38D)**. The “no cue” probe test is a control test, where all indices are removed, and the time spent in each quadrant is measured and expected to be equivalent. It makes it possible to test for the presence of unregistered or unexpected biases, which could appear as ‘spatial-related’ results. When all cues were removed, EMX-Vangl2$^{-/-}$ mice and controls spent equal time in each region. (2 way ANOVA with repeated measures; Zone effect: $F(3,64) = 1.735$, $p = 0.1687$; Genotype effect: $F(1,64) = 0.2851$, $p = 0.5953$) **(Figure 38E)**. Both groups were lost in the no-cue condition **(Figure 38E)**, confirming the requirement for spatial cues to locate the platform. Interestingly, comparing platform latency values of mice in the NC and AC tests showed that there was significant difference between the two probes for the mutants (Welch’s t test; $p = 0.041$) but not for the control (Unpaired t test; $p = 0.781$) **(Figure 38D-E)**. These results suggest that aged mutants had established spatial memory, whereas controls did not.

Another method of estimating spatial memory is through analysis of search strategies employed by the subject in locating the platform in the MWM (Brody and Holtzman, 2006). The swimming strategies are categorized into three distinct groups reflecting the level of spatial learning **(Figure 38F)**. At the beginning of the acquisition tests, we expect more non-spatial strategies to be employed as the mice have not built a spatial map yet, and are primarily trying to escape a stressful situation. With the progression of the learning phase, more spatial memory related strategies, such as focal correct and directed search were used by both groups. There was no remarkable difference found in the type of strategy used by controls vs mutants, and both groups reached the threshold for spatial strategies at 60% on day 22 **(Figure 38G)**.

These data show that the absence of Vangl2 provides partial protection towards age-related impairment of hippocampus-dependent spatial memory in aged mice.

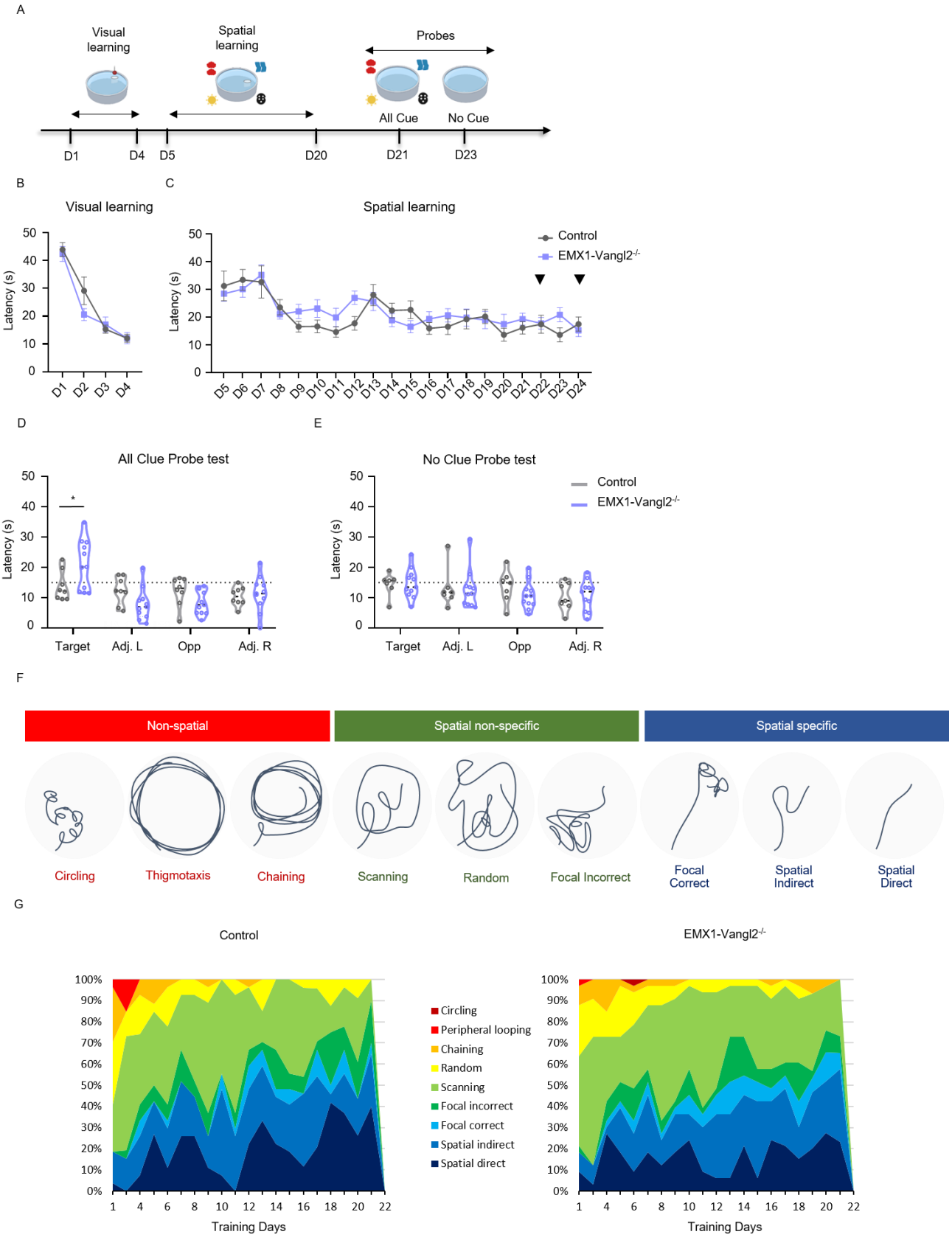

Figure 38: (A) Schematic of experimental set-up and timeline of the spatial memory experiment in a Morris Water Maze paradigm. **(B)** Visual learning and spatial learning in Emx1-Vangl2$^{-/-}$ (violet) and control groups (grey). The latency to reach the platform is measured according to learning sessions. The probe tests are indicated by a black arrow. N = 7 controls and 11 mutants. 2-way ANOVA, n.s. p>0.05. **(C-E)** Quantification

of the time spent in each quadrant of the pool during the all clue (D) and no clue probe (E) tests. N control = 8 mice, N Emx1-Vangl2$^{-/-}$ = 11 mice. 2-way ANOVA, *p<0.05. **(F)** Types of spatial strategies according to Brody and Holtzman, 2006. **(G)** Progressive evolution of the selection of strategies according to the days of learning for control (left) and mutants (right) aged mice

Aged Emx1-Vangl2 mice still display a deficit in flexibility of everyday like reference memory

We next tested another aspect of spatial memory, its flexibility taken as a model of reference memory, using a specific version of the 8 arm radial maze task. The acquisition phase of this task evaluates the capability to learn constant food locations within the maze, i.e. acquisition of reference spatial memory. The maze arms are repeatedly presented by pairs (3 invariant pairs A, B, C), and the test phase evaluates the capability to flexibly express learned information, a distinctive feature of declarative memory, by recombining into a novel pairing two of the pairs learnt in the acquisition phase **(Figure 39A)**. Interestingly during the acquisition, we found an important discrepancy between control and mutant aged mice in their ability to reach criterion with only 45% of control mice reaching the criteria against 75% of Emx1-Vangl2$^{-/-}$ mice **(Figure 39B)**. Control aged mice seem to have difficulties to learn the reference memory task compared to mutants. This must be kept in mind for the interpretation of the following results. To analyze the results of the test, we compared the performance on the last day of training (D-1) to the performance in the test day. There was no difference whatever the genotype regarding the performance in the control pair C at D-1 and test day (2-way ANOVA; Days: $F(1,24) = 1.771$; $p=0.1957$; Genotype: $F(1,24) = 0.6796$; $p=0.7178$; Genotype x Days: $F(1,24)= 0.252$; $p=0.6202$); or the novel pair (unpaired t-test with Welsch's correction; $t=0,4441$, $df=4,593$; $p=0.6771$) **(Figure 39D-E)**. Regarding the recombined pair AB, the analysis showed that performance significantly declined between the end of acquisition D-1 and the test in both groups (2-way ANOVA, Days: $F(1,24) = 32.27$; $p < 0.0001$; Genotype: $F(1,24) = 0.08538$; $p=0,7726$; Genotype x Days interaction: $F(1,24) = 0.143$; $p=7087$; Bonferroni comparison D-1 vs. test: control $p<0.01$; Emx1-Vangl2$^{-/-}$ $p<0.001$) **(Figure 39C)**. Hence, both groups of aged mice failed to show everyday-like reference memory flexibility. This is not surprising as our previous results showed that 10 weeks old Emx1-Vangl2$^{-/-}$ mice already displayed a deficit of spatial memory flexibility, and the literature showed that flexibility of memory performances decrease in aged animals (Al Abed et al., 2016).

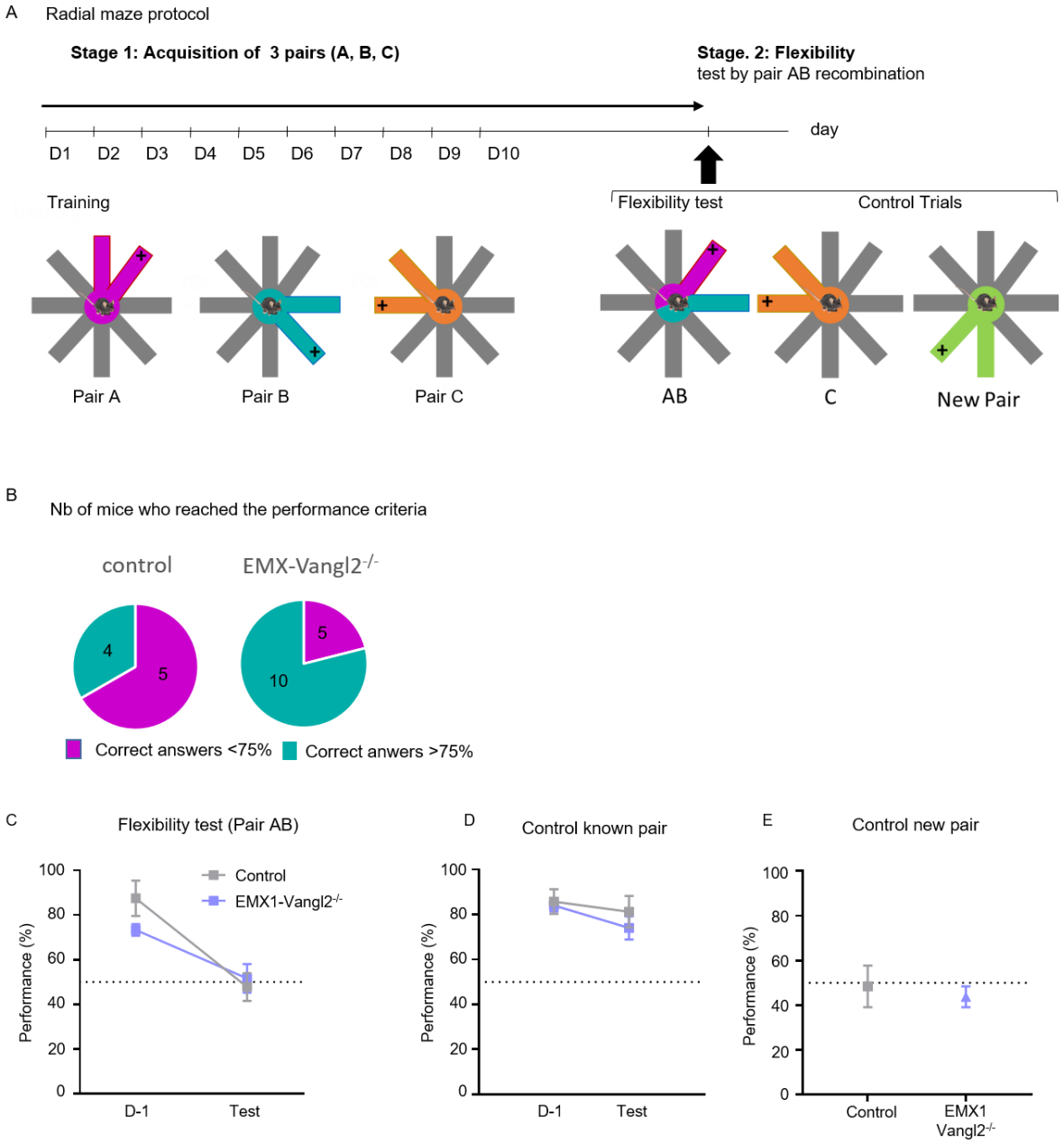

Figure 39: (A) Experimental design for the reference memory in the 8-arm radial maze test. **(B)** Number of mice who reached the performance criteria after 21 days of training. **(C-D-E)** Graph of the evolution of percentage of correct responses between the last day of acquisition (D-1) and the Test for the critical pairs (C) (left: Pairs A and B recombined into Pair AB in the Test, representing the critical flexibility probe) and control pairs (D-E) (middle: Pair C is an "known" control; right: New Pair is an "novel" control appearing in Test only). N Control = 11, N Emx1-Vangl2$^{-/-}$ = 15. For Pair AB and Pair C: 2-way ANOVA with Bonferroni comparison, D-1 versus Test. ns p>0.05. For the Novel Pair: Mann-Whitney and One sample t-test vs 50%.

Chapter IV : Discussion

The aim of this thesis was to decipher whether Vangl2-dependent signalling is necessary for regulating the synaptic organizing protein complexes that control MFB/TE synapse development, structural maturation and morphofunctional plasticity throughout life. Using a cKO model of early *vangl2* deletion, I showed that Vangl2 plays a variety of roles in the hippocampus at the juvenile, adult and aged stages. Using viral injections, confocal and SBFSEM 3D reconstructions, I showed that Vangl2 was necessary for the morphogenesis and structural plasticity of the MFB/TE synapse. With patch-clamp experiments and behavioural tests, I showed that Vangl2 is involved in the MFB/TE synapse's functionality and in the regulation of hippocampal-dependent mnesic processes. Finally, I showed that Vangl2 has a role in the degradation of synaptic and behavioural processes during aging.

Vangl2 is a major modulator of the morpho-functional development and maintenance of the DG-CA3 circuit

Vangl2 is present early on and refines over time in subregions of the hippocampus

Using immunochemistry, I showed that Vangl2 is expressed in the hippocampus at P7, P14 and P21 and particularly enriched in the *stratum lucidum* of the CA3, in the *stratum moleculare* and in the subgranular zone of the DG at P21. This enrichment is present in the developing mossy fibers as early as P7, hinting at a role of Vangl2 in the MFB/TE synapse development in its earliest steps. In the *in vitro* experiments, using the CRISPR/Cas9 technology to label endogenous Vangl2, we show that endogenous Vangl2 localize in the growth cone of the growing axons of cultured hippocampal neurons, suggesting a presynaptic localization of Vangl2 in the mossy fibers, which had also been observed by our group in a recent study (Dos-Santos Carvalho et al., 2020). This presynaptic localization remains to be confirmed *in vivo*. Studies report a postsynaptic colocalization between Vangl2 and PSD95 in PSD fractions thanks to western blot analysis of brain samples (Nagaoka et al., 2014b). This colocalization was also observed using immunochemistry in the spines of CA1 pyramidal neurons and DG granule cells *in vivo* (Robert et al., 2020; Thakar et al., 2017). It is likely that the localization of Vangl2 is tissue-specific, with a strict post-synaptic localization in some structures and a localization in both synaptic compartments in others. Our results suggest that in the MFB/TE synapse Vangl2 is present in both synaptic compartments. I could not detect

colocalization between PSD95 and Vangl2 in the CA3 pyramidal dendrites with immunochemistry *in vivo*, which might be due to either a technical issue or the levels of Vangl2 being too low to be detected in the post-synaptic compartment of the MFB/TE synapse. One possibility to solve the question of the localization of Vangl2 in the MFB/TE synapse would be to use the CRISPR-Cas9 technology that was used for the *in vitro* experiments to label endogenous Vangl2 in the GC or pyramidal cells of mice at different stages, there for by-passing technical limitations linked to the low concentration of Vangl2 in the TE.

Early deletion of vangl2 severely impacts the timeline of morphogenesis of the DG-CA3 synapse

Using powerful high resolution 3D reconstructions of the MFB/TE synapse from both confocal ans SBFSEM images, I show the details of the morphological consequences of the absence of Vangl2 during the postnatal maturation of the synapse in mice. Early deletion of the protein leads to a severe defect of morphogenesis, with smaller and less complex immature synapses at P21 **(Figure 20-21)**. Our morphological study in adult mutant mice show that the morphological deficits observed at an earlier stage are compensated at 10 weeks old, with no difference between controls and mutants at least in the presynaptic bouton **(Figure 24)**. This shows that the early deletion of vangl2 leads to a severe delay of morphogenesis of the MFB/TE synapse. This morphogenesis delay can be compensated by the early presynaptic reexpression of Vangl2 during the first postnatal week **(Figure 24)**. This shows the importance of presynaptic Vangl2 in the synapse at this stage, supporting our claim that Vangl2 is also in the presynaptic mossy fiber bouton. We have to confirm that the presynaptic reexpression of Vangl2 compensate the moprphological delay in the postsynaptic elements of the synapse, but if the morphology of both compartements are restored, this would support the hypothesis that the morphogenesis of MFB/TE synapse depends on transsynaptic cross-talk mechanisms. Globally, these morphological results demonstrate, for the first time, that the early postnatal timing of Vangl2 expression is crucial in the regulation of the MFB/TE synapse establishment, and Vangl2 might regulate different processes at different stages (Robert et al., 2020).

The morphological deficits we observe in our juvenile mutant mice are likely to have important consequences, as morphological immaturity has been associated with synaptic

transmission deficits, and even with pathologies (Condomitti et al., 2018; Witton et al., 2015). However, to our knowledge, no other studies report the effects of a delay of maturation of the MFB/TE synapse such as the one we observe.

Molecular basis of the deficits induced by the early absence of Vangl2

The correct morphogenesis of MFB/TE synapse has been shown to involve many adhesion proteins and cell-surface interactions. PCP proteins are known to regulate adhesion protein dynamics and Vangl2 is no exception, giving us a lead on how Vangl2 participates to the regulation of the MFB/TE synapse morphogenesis. Cell-surface HSPG have been more and more considered as important synaptic regulators. Condomitti et al. showed that the HSPG Glypican 4 and its postsynaptic partner GPR158 are involved in the morphogenesis of the MFB/TE synapse and that affecting this interaction via the deletion of GPR158 resulted in morphologically and functionally immature synapses, very similar to the phenotype observed in Emx1-Vangl2$^{-/-}$ mice. These similar phenotypes lead us to use immunohistochemistry to check the levels of expression of GPC4 and GPR158 in the *stratum lucidum* of our Emx1-Vangl2$^{-/-}$ mutants, where we found that they were significantly decreased compared to control **(Figure 26)**. Our *in vitro* results show that Vangl2 and GPC4 colocalize in COS7 cells and in the presynaptic growth cone of cultured hippocampal neurons, while GPR158 does not seem to colocalize with Vangl2. Vangl2 and GPC4 have been shown to genetically interact, and that in endodermal zebrafish cells GPC4 is necessary for the asymmetric localization of Vangl2 so it is possible that GPC4 is a physical interactor of Vangl2 (Balaraju et al., 2021; Nychyk et al., 2022). Therefore we hypothesize that Vangl2 might physically interact with GPC4, via its GAG domains, in the presynaptic bouton of the MFB/TE synapse, participating in its stabilization at the membrane. Consequently, the absence of Vangl2 in the mutant could lead to the destabilization of the transsynaptic interaction between GPC4 and GPR158, leading to the abnormal development of the MFB/TE synapse. The alteration of the putative Vangl2-GPC4 interaction could also have morphological consequence via their common interactor N-cadherin. GPC4 has been shown to regulate N-cadherin dynamics in endodermal cells of *xenopus* embryos (Balaraju et al., 2021). Vangl2 has been shown to bind N-cadherin in the growth cone of cultured hippocampal neurons as well as in the spines, regulating spines formation and the migration and outgrowth of the axonal structure (Dos-Santos Carvalho et al., 2020; Nagaoka and Kishi, 2016). In the mossy fibers, N-cadherin does not seem to be important for the growth of mossy fibers but plays

an important role in the establishment and complexification of the MFB and the TE, via the formation and stabilisation of puncta adherentia (Bekirov et al., 2008; Mizutani et al., 2021). In the absence of Vangl2, the N-cadherin presence at the membrane and its dynamics in both compartments are likely to be altered, leading to the disruption of puncta adherentia as well as well as altered cytoskeleton dynamics, resulting in the abnormal morphogenesis of the MFB/TE synapse.

Early deletion of vangl2 disrupts MFB/TE synaptic transmission in juvenile mice

When we looked into the functional consequences of the early deletion of Vangl2 at the MFB/TE synapse using whole-cell patch clamp experiments, we found that the spontaneous synaptic transmission activity of the synapse as well as short-term presynaptic potentiation were altered in 3 weeks old mice **(Figure 22-23)**. However, we found no alteration of the AMPA/NMDA ratio in the mutants, meaning that the effect of the early *vangl2* deletion is mostly presynaptic. This functional deficit can be correlated to the morphological deficits observed at the same stage, and further supports our hypothesis that Vangl2 plays an important role in the presynaptic bouton during the early postnatal period. Galimberti et al., showed that MFB/TE synapses that had a large MFB had higher EPSCs amplitude than synapses with a smaller MFB (Galimberti et al., 2006). The size of the presynaptic bouton is also correlated with the number of synaptic vesicles it contains (Rollenhagen and Lübke, 2006). The morphology and size of the presynaptic element have also been shown to have an influence on synaptic vesicles dynamics (Guillaud et al., 2017). It is probable that the size reduction of the MFB/TE synapse in the absence of Vangl2 affects both the size and the dynamics of the different pools of synaptic vesicles, resulting in less vesicles being available for spontaneous release and less short-term potentiation. Our immunochemistry results **(Figure 25)** support also this hypothesis, as we see a reduction of Synaptoporin and Synapsin 1 in the mutants, and those proteins are known to be involved in the traffic dynamics of synaptic vesicles (Knaus et al., 1990; Mirza and Zahid, 2017). The diminution of those synaptic markers could either correspond to a diminution of the number of vesicles, or to an alteration of the trafficking and docking mechanisms necessary for the release of neurotransmitters. Another factor that could be impaired in the Emx1-Vangl2$^{-/-}$ mutants is the recycling of neurotransmitter vesicles via endocytosis. Indeed Vangl2 is known to participate to the endocytosis of cell surface proteins (Dos-Santos Carvalho et al., 2020; Williams et al.,

2012). We can hypothesize that Vangl2 participates to the reuptake of neurotransmitter and the recycling of vesicles at the presynaptic terminals and that the early deletion of *vangl2* leads to less vesicle recycling, diminishing the number of vesicles in the reserve pool. Finally, the last parameter that could explain the presynaptic functional defects is the reduction of the number of active zones. Our SBFSEM results show a drastic decrease of the number of PSD per MFB/TE synapses, dropping from an average of 5 PSD/TE to 1 PSD/TE. The PSD is generally facing the AZ and we assume that the reduction observed for the number of PSDs can be applied to the AZs. A reduction of the AZ means less release sites available for neurotransmitter release, which could explain the presynaptic deficits observed in our mutants. To confirm all of these hypotheses, we could first plan a quantification of the synaptic vesicles present in the MFB of our mutant mice, using a more precise EM technique such as the high pressure cryo-electrotomography (Maus et al., 2020). We could also evaluated the number of release site by quantifying Munc13-1 clusters (Orlando et al., 2021), and evaluate the synaptic vesicles dynamics by performing longer trains of 20-40Hz stimulations in order to evaluate the replenishment rates of the readily releasible pool (Barthet et al., 2018).

Then, still using whole cell patch-clamp, we evaluate the effect of the absence of Vangl2 on the post synaptic response, notably on the AMPA/NMDA ratio. The absence of alteration of postsynaptic response, notably of the AMPA/NMDA ratio in the mutant, is surprising especially given our observations about the PSDs in the Emx1-Vangl2$^{-/-}$ mutants. This means that despite the reduction of the PSD area and numbers, the number and functionality of AMPA and NMDA receptors are unchanged in our mutants compared to controls at P21. This is also in favour of our statement that Vangl2 plays a more important role in the presynaptic MFB than in the postsynaptic TE in the early postnatal stage. However, because we did not block the KAR in our protocol, we cannot exclude the possibility is that the AMPAR numbers are changed but this change is compensated by the KAR. Another possibility is that we see no changes at P21 but that alterations of the postsynaptic response happens earlier in development, leading to functional maturation defects. Such transient phenotypes have been observed in GluK2 mutants which also displayed morphogenesis defects (Lanore et al., 2012). The issue might also be purely technical, and our experimental conditions might not allow us to detect a change of glutamatergic receptor ratio. Such changes are sometimes only detectable in “hyperexcitability” conditions, with a higher concentration of Ca2+. We could

redo the experiments in those conditions to observe an AMPA/NMDA ratio change.

More globally our results report a change of spontaneous activity and short-term plasticity in P21 mice. It would be of interest to study long-term plasticity events to get a complete picture of the effects of Vangl2 on synaptic transmission at the MFB/TE synapse.

Early vangl2 deletion is structurally compensated at DG/CA3 synapse, but structural plasticity is still affected

As stated earlier, we observe a delay of MFB/TE synapse morphogenesis rather than a complete inhibition of the process. It is likely that the effects of the early deletion of Vangl2 are compensated, at least partly, by other regulators of the morphogenesis mechanisms. This kind of delayed morphogenesis in the context of an early *vangl2* deletion have already been observed in another model: the cochlea (Copley et al., 2013). In this study, Dean and collaborators showed that the loss of *vangl2* disturbs the planar polarity orientation of auditory stereociliary bundles in neonatal mice (P0-P3) but this misorientation is corrected in P10-P12 mice. These mice however present hearing deficits, showing that, even if the bundle morphological deficit compensated, the function of the auditory hair cells is still disturbed by an early *vangl2* deletion. This study is consistent with our data in the brain and allowed us to hypothesize that, even if the morphological maturation is only delayed, we could expect functional consequences in adult Emx1-Vangl2$^{-/-}$ mice. We need supplementary analysis to evaluate if the morphological compensation we observe concerns all the elements of the synapse, including the postsynaptic TE and the PSDs or if it only a presynaptic phenomenon. Moreover, we should also replicate the patch-clamp experiments we did at P21 at a later stage of development, to see if the functional effects of *vangl2* deletion are also compensated in adult mice or if it has long lasting consequences as observed in the cochlea (Copley et al., 2013).

Indeed, we observed that even if the global morphology of the MFB/TE synapses was restored in 10 weeks old Emx1-Vangl2$^{-/-}$ mice, they still present some structural plasticity deficits **(Figure 27)**. The MFB/TE synapses are known to undergo structural growth and complexification when the mice are placed in an enriched environment (Galimberti et al., 2006; Gogolla et al., 2009). Using 3D reconstruction of the MFB of Emx1-Vangl2$^{-/-}$ adult mice that were exposed to EE, we show that such plasticity events were not found in our

mutants after we placed them in a sustained enriched environment. This confirms our suspiscion that the effects of Vangl2 absence are not fully compensated in adulthood. An hypothesis is that the mechanisms inducing the delay of morphogenesis of MFB/TE synapses during the first post-natal weeks are still at play in adult mice, and cause a delay of all processes involving a morphological change, including EE-dependent structural plasticity. One way to confirm this hypothesis would be to prolongate the EE period to see if the MFB/TE of Emx1-Vangl2$^{-/-}$ mice eventually undergo structural plasticity and reach the same level of complexity as the control mice. An alteration of synaptic transmission could also participate to the alteration of structural plasticity that we observe in adult mice. Studies show that blocking neurotransmitter release via mGlur2 activation blocks the structural plasticity of the MFB/TE synapse (Galimberti et al., 2006; Nicoll and Schmitz, 2005). LTP has also been shown to induce structural remodelling of MFB/TE synapse (Maruo et al., 2016). If we see an LTP deficit in our Emx1-Vangl2$^{-/-}$ this could also be a lead on the mechanisms underlying the structural plasticity deficits we observed.

Early vangl2 deletion disrupts hippocampal-dependent working and reference memory in adult mice

To further explore the functional consequences of early vangl2 deletion, we used an array of behavioural tasks to investigate the memory performances in our 10 weeks old Emx1-Vangl2$^{-/-}$ mice **(Figure 28-29-30-31)**. Our results show that the early deletion of *vangl2* has long-lasting consequences on some hippocampal-dependent behaviours, namely the flexibility of their spatial reference memory, and spatial working memory. These results confirm that the deficits induced by the early deletion of *vangl2* are compensated only partially, with a recuperation of a normal global morphology but remaining functional and plasticity deficits in the hippocampal circuit. The Emx1-Vangl2$^{-/-}$ mice showed no deficits of spatial learning and recalling in the MWM paradigm. The absence of alteration of spatial memory recalling during the MWM has already been observed in CA3 lesioned rats, meaning that the CA3 is not necessarily required during such a task and the alteration of the MFB/TE connection might not have a detectable impact on that process (Rolls, 2016). However, in a radial maze paradigm, the mutant mice showed a deficit of flexibility of spatial reference memory. This means that some deficits are present in the functionality of the hippocampal circuit under specific conditions when the cognitive flexibility demand is higher. The disruption of the DG-CA3 circuit might be more involved

in the alteration we observed, even though it is difficult to estimate the contribution of the different hippocampal subregions in this spatial reference memory flexibility deficit. Studies report a strong involvement of the DG in some tasks involving spatial flexibility, and increased adult neurogenesis has been linked to improved DG-CA3 activity and improved cognitive flexibility (Anacker and Hen, 2017; Burghardt et al., 2012; Lee and Lee, 2020; Xavier et al., 1999). Moreover, we can argument that the RM test we use for reference memory relies on the effective encoding of different spatial contexts, thanks to DG-dependent pattern separation, and on a combination of both pattern completion for the retrieval and recombination of previously learned pairs and encoding/adjusting of already encoded spatial information in a novel context (the mix of pair A and pair B) which relies on the CA3. On the other hand, the retrieval of consolidated spatial memories relies more on the CA1 and cortical afferences. This could be an explanation of why the alteration of the DG-CA3 network in the early absence of Vangl2 could lead to an alteration of the encoding of new contextual memories and adaptation of learned spatial information, leading to a “rigidity” of spatial reference memory.

The Y maze experiment and the everyday-like radial maze protocol showed that the spatial working memory were selectively impaired in the Emx1-Vangl2$^{-/-}$ mice compared to controls. Emx1-Vangl2$^{-/-}$ displayed lower levels of spontaneous alternation than age-matched control in the Y maze, reflective of hippocampal-dependent short-term/working memory deficit (Hughes, 2004). Kesner showed that the CA3, specifically the CA3a and CA3b subregions, are involved in the encoding and retrieval of spatial short-term memory (R. Kesner, 2013) The interpretation of the spontaneous alternation level in Y maze test as representative of working memory is quite debated, as some consider that it is rather reflective of a highly stereotyped behaviour which can create confusion with some models (Stewart et al., 2011). This is why we confirmed our observation with an “everyday-like” working memory protocol in the 8-arm radial maze protocol. This task put high demand on pattern separation processes to discriminate among highly similar and repetitive events; these processes have been shown to critically rely on the DG-CA3 circuit. We observed a deficit of performance in the mutant mice for the trial with high levels of retention and organizational demand, which means that the early deletion of *vangl2* correlates with specific spatial working memory deficits. A study showed that this task requires the activation of the DG-CA3 circuit and other working memory test done in radial maze showed the involvement of the dorsal dentate gyrus (Al Abed et al., 2016; McLamb

et al., 1988; Walsh et al., 1986). The results of the fear conditioning experiments show that the Emx1-Vangl2$^{-/-}$ mice have an alteration of information retrieval, with the shock being wrongly associated with non-predictive cues. Studies showed that CA3 is involved in the encoding and retrieval of contextual cues while the CA1 and amygdala support the encoding and retrieval of tonic and contextual cues (Hunsaker et al., 2009). The deficits we observe in the *stratum lucidum* of the CA3 might be sufficient to alter the function of the CA3 region, leading to diminished retrieval of contextual clues and an abnormal generalization of non-predictive cues which depend on the CA1/amygdala. Our hypothesis is that the early deletion of vangl2 in the Emx1-Vangl2$^{-/-}$ mice have long term consequences on the function of the MFB/TE synapse, leading to the disruption of the DG-CA3 circuit function and the apparition of a variety of mild impairments of hippocampal-dependent tasks. We focused on the DG-CA3 circuit as Vangl2 expression is particularly enriched in those two regions, leading us to assume that the effect of the deletion would be stronger. The absence of strong cognitive deficits and the fact that spatial learning and memory are normal in our mutants suggest that the CA1 and cortical activity is not impaired, but we cannot exclude that other parts of the hippocampal circuit are impacted too and have a role in the cognitive deficits we report (Etchamendy et al., 2011; Touzani et al., 2003, Mingaud et al., 2007; 2008). One way of confirming that the cognitive deficits we observe are a direct consequence of the early deletion of Vangl2 in the DG-CA3 circuit would be to reexpress Vangl2 selectively in the granule cells or in the CA3 pyramidal neurons via virus injections in Emx1-Vangl2$^{-/-}$ mice, and evaluate their performances in the same array of hippocampal-dependent memory tests. It would also be interesting to evaluate the impact of Vangl2 absence in other regions.

This first part of the work demonstrates the importance of Vangl2 in the DG-CA3 circuit in early postnatal stages. The early morphogenesis delay and functional deficits observed in the absence of early Vangl2 expression in juvenile mice have long lasting consequences on the synapse itself and on the entire hippocampal circuit, leading to selective plasticity and memory impairments.

Vangl2 participates in aging mechanisms affecting the DG-CA3 circuit

The second part of my work focuses on the effect of the early deletion of *vangl2* in the

aged hippocampus. Using 16 to 18 months old Emx1-Vangl2$^{-/-}$ mice, I obtained surprising but interesting results suggesting that Vangl2 is involved in age-related defects of the MFB/TE synapse and hippocampal-dependent mnesic processes, and that the early deletion of *vangl2* had a protective effect toward such degradations linked to aging.

Early vangl2 deletion protects MFB/TE synapses against age-related degradations

First, using viral injections and 3D reconstruction of the MFB of 16-17 months old mice, we report a significant difference of morphology between the MFB of aged Emx1-Vangl2$^{-/-}$ mice compared to aged control, with the mutants having significantly bigger presynaptic boutons than the controls **(Figure 32)**. Although no reduction of MFB/TE size has been reported in aged mice, in humans the size and complexity of the MFB/TE synapse is reduced with age (Das et al., 2019). When comparing our data in adult control mice and aged control mice, we observed a significant reduction of area and volume suggesting that age-dependent morphological degradation is also present in our mice. However, this could be specific of our mice strain, and it would be interesting to quantify the 3D morphological parameters of the MFB/TE synapse in wild type C57Bl6 mice which is the strain from which our Emx1-Vangl2$^{-/-}$ mice are derived. The size of the MFB of 16-17 months old mutant were also slightly reduced compared to 10 weeks old mice, but not as much as in the aged controls. This suggest that the early deletion of *vangl2* protects the MFB/TE synapse against the morphological degradation that accompanies aging, at least presynaptically. As with the 10 weeks old stage, we need additional experiments to evaluate the integrity of the postsynaptic elements of the synapse as well as the synaptic vesicles content and distribution.

Early vangl2 deletion protects aged mice against memory performance loss

Alterations of MFB/TE synapse's function and morphology have been reported repeatedly in mice models of Alzheimer's disease and correlated with deficits of declarative memory processes such as novelty recognition and spatial memory (Decker et al., 2015; Silva et al., 2019; Sydow et al., 2011; Wilke et al., 2014). Progressive alterations of declarative memory have been also described in « normal » physiological aging, both in humans and animal models, with deficits in working memory and other declarative memory processes (Marighetto et al., 1999; Mingaud et al., 2008; O'Shea et

al., 2016). As we observed a modification of MFB morphology in our aged mutants we decided to check onto the behaviour of those mice **(Figure 35 to 39)**. Very interestingly, the aged Emx1-Vangl2$^{-/-}$ mice had significantly better performances than their age-matched controls in a variety of tests assessing hippocampal-dependent memory processes including novel object recognition, spatial learning, and spatial working memory. Although they did not present any difference in spatial learning in the MWM, aged control mice didn't learn the spatial reference and working memory tasks in the radial maze as well as the aged mutants. These results show that the early deletion of Vangl2 has either a protective or an improving effect on hippocampal-dependent mnesic processes against aging-related deficits. This means that Vangl2 participates to the degradation of hippocampal-dependent mnesic processes during aging. Vangl2 being enriched specifically in the DG and the CA3, this could explain why its early deletion might have a protective/improving effect towards processes that highly involve these two hippocampal subregions. The detrimental role of Vangl2 had already been reported in models of neurodegenerative disorders, which are linked with pathological aging. Indeed, Vangl2 has been found to participate to Aβ production and synaptoxicity in different models of AD (Elliott et al., 2018; Feng et al., 2021; Sellers et al., 2018). However, to our knowledge, this thesis is the first work reporting the role of Vangl2 in the deficits linked to normal ageing processes and showing that deleting *vangl2* early can have positive effects on age-related deficits. A way to discriminate between "protection" and "improvement" for the effect of the early *vangl2* deletion would be to do a longitudinal study of the memory performances of Emx1-Vangl2$^{-/-}$ mice, starting at 10 weeks old then later at middle-aged and aged stages. If the memory performances of mutant mice remain stable while the performances of control drop, the effect of Vangl2 absence would be a protective one. If the performances of mutants increase in between stages, then we might talk of an improving effect.

As described in the introduction, pathological and physiological aging both affect many more processes in the hippocampus on top of their effect on synaptic morphology and behaviour. Many studies on aging subjects or models of neurodegenerative pathologies report an increase of neuroinflammation in the hippocampal formation, alterations of myelination and synaptic connectivity as well as deleterious effects on synaptic transmission and adult neurogenesis. To realise an exhaustive characterization of the role of Vangl2 and its contribution to the deleterious effects of aging, we should analyse

the previously listed parameters in Emx1-Vangl2$^{-/-}$ mice.

The multiple “lives” of Vangl2 in the DG-CA3 circuit and therapeutical leads

The results of my work show that the PCP protein Vangl2 plays a wide variety of timing-dependent and localization-dependent roles in the DG-CA3 hippocampal circuit throughout postnatal development and aging in mice.

As Vangl2 is involved in the regulation of different mechanisms, from endocytosis to axonal growth and adhesion, it is most likely that the alteration we observe in juvenile and adult mice are the consequences of an accumulation of morphological and functional developmental defects caused by the early absence of Vangl2. It is complicated to tell the origin point of the defects, as morphogenesis and functionality mutually rely on each other at the MFB/TE synapse. One might consider that everything starts with the misregulation of adhesion proteins and cytoskeleton dynamics because of the known role of Vangl2 in protein endocytosis and turnover in neurons. This kind of early defect of adhesion protein turnover in the absence of Vangl2 has been demonstrated recently in our lab (Dos-Santos Carvalho et al., 2020). This lack of turnover in the mossy fibers of our mutant might lead to aberrant distribution of key adhesion proteins, such as N-cadherin and GPC4, in both presynaptic and postsynaptic compartments, delaying their progressive complexification and maturation after the first contact between mossy fiber and CA3 dendrite. From a purely spatial point of view, the smaller immature MFB/TE synapses are most likely to contain less synaptic vesicles, which partly explain the synaptic transmission deficits. This delayed maturation of the MFB/TE synapse could also affect the stabilization of neurotransmitter receptors, as it was observed in another model of Vangl2 deletion at the GC spines (Robert et al., 2020). In this hypothesis form precedes function and the problems of synaptic transmission are the consequence of the morphogenesis delay of the MFB/TE synapse. Although the global morphology of the synapse is recovered in 10 weeks animals, we still observe some behavioural deficits that are likely resulting from some remaining synaptic transmission deficits in the DG-CA3 circuits. The accumulation of synaptic transmission deficits might not be fully compensated in adult mice, or the absence of Vangl2 at this stage mainly affect the stabilization of the receptors and the liberation of neurotransmitters. However, this

explanation does not fit with our results in aged animals, where the absence of Vangl2 has some clear consequences on both morphological and functional processes of the MFB/TE synapse. It is unlikely that the accumulation of functional deficits ends up having a positive consequence in later stages.

A complementary hypothesis is that the consequence of the early deletion of *vangl2* is the delay of all Vangl2-dependent processes happening in the DG-CA3 circuit. The results of my work and previous studies from the lab demonstrate that the protein Vangl2 has different roles in the DG-CA3 circuit depending on the temporality of its expression. My work shows that in the early postnatal stages, Vangl2 is necessary for the morphological and functional establishment and maturation of the MFB/TE synapse with implication in hippocampal-dependent processes involving some levels of pattern separation and completion. The work of Robert et al. in 2020 shows that in adult mice Vangl2 participates to the maturation and integration of GCs spines, with consequences on the fine tuning of the pattern separation and pattern completion balance. We also show that Vangl2 participates to synaptic and behavioural defects happening during aging. Our data support the postulate that early deletion of Vangl2 delays all Vangl2-dependent processes, disregarding of the temporality. In early postnatal and adult stages, it leads to detrimental consequences with a delay of morphological and functional maturation, which might result with alterations of the structural and functional plasticity mechanisms and correlate with hippocampal-dependent memory deficits. In aged individuals, the delay of Vangl2-dependent mechanisms has positive consequences, with less deteriorated synapses and better memory performances, as the age-linked mechanisms leading to deterioration are delayed.

This timing dependent effect might be an interesting lead for therapeutical strategies for dementia, neurodegenerative and neurodevelopmental disorders. Our results show that deleting Vangl2 improves aging related defects, and studies also showed that it could improves symptoms in AD models where Vangl2 participates to Aβ synaptotoxicity (Feng et al., 2021). After assessing more thoroughly the consequences of Vangl2 early deletion on other aging markers, one interesting perspective would be to pinpoint the adequate timing to have the positive effects of Vangl2 deletion without the negative consequences observed in adult mice, either by disturbing Vangl2 itself or by acting on the activation of the cascade of effectors regulated by Vangl2. This could be done either by selectively deleting Vangl2 or inhibiting its effectors at different time points and in specific

hippocampal regions and regularly assessing behaviour. On the other side of the spectrum, Vangl2 could be a molecule of interest for neurodevelopmental pathology. Heterozygous mutations and microchromosomal changes of *VANGL2* has been linked to symptoms commonly associated with ID and ASD. Some of the behavioural alterations we observe in Emx1-Vangl2$^{-/-}$ mice are similar to what is observed in mice models of ID and in some human patients with ID symptoms, with mild impairments of declarative memory processes that mainly arise when the difficulty of the task increases (Verma et al., 2019; Vicari, 2004; Vicari et al., 2016). The axonal growth alteration and *corpus callosum* agenesis found in Emx1-Vangl2$^{-/-}$ mice are also phenotypes found in ID patients (Accogli et al., 2019; Dos-Santos Carvalho et al., 2020; McFadden and Minshew, 2013). It would be interesting to check levels of Vangl2 in mouse models of ID and see if upregulation of Vangl2 or its effectors can alleviate some of the detrimental phenotypes without causing more deficits.

The objective of this thesis was to better characterize the role of the PCP protein Vangl2 in the development and maintenance of the morphological and functional properties of the DG-CA3 hippocampal circuit throughout postnatal development and aging. I showed that Vangl2 plays a variety of roles in the establishment and maintenance of the MFB/TE synapse and that the early deletion of the vangl2 role as several timing dependent consequences on the morphology, function, molecular composition of the synapse and on related behaviours. These findings establish Vangl2 and possibly its effectors as interesting targets for therapeutical strategies in the context of dementia, neurodegenerative disorders and neurodevelopmental pathologies.

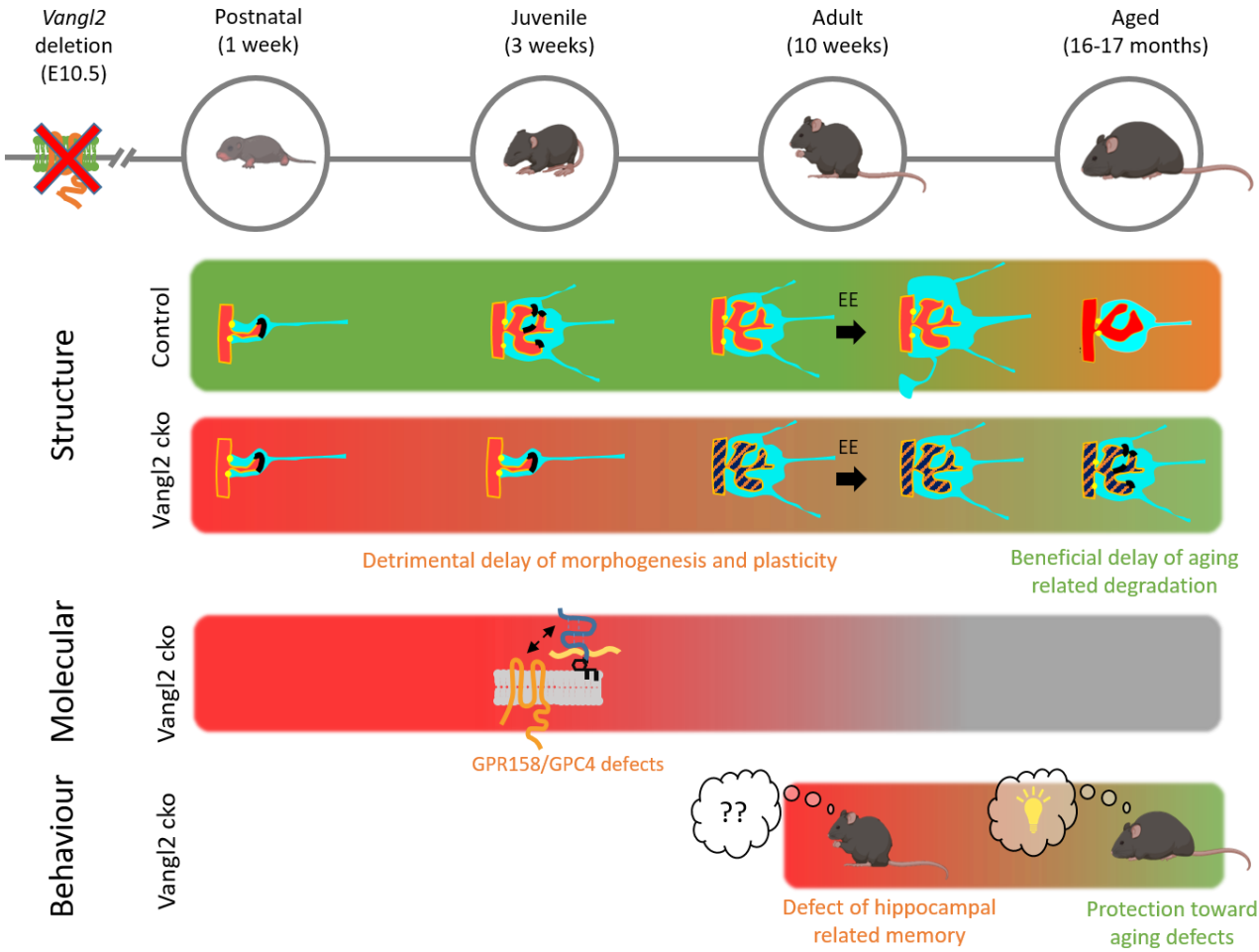

Figure 40: Summary of the consequences of the early deletion of Vangl2 throughout the life of the mouse.

List of references

- A -

Abrous, D.N., Koehl, M., Le Moal, M., 2005. Adult Neurogenesis: From Precursors to Network and Physiology. Physiological Reviews 85, 523–569. https://doi.org/10.1152/physrev.00055.2003

Abulaiti, X., Wang, A., Zhang, H., Su, H., Gao, R., Chen, J., Gao, S., Li, L., 2022. Disrupted mossy fiber connections from defective embryonic neurogenesis contribute to SOX11-associated schizophrenia. Cell. Mol. Life Sci. 79, 180. https://doi.org/10.1007/s00018-022-04206-4

Accogli, A., Calabretta, S., St-Onge, J., Boudrahem-Addour, N., Dionne-Laporte, A., Joset, P., Azzarello-Burri, S., Rauch, A., Krier, J., Fieg, E., Pallais, J.C., Undiagnosed Diseases Network, McConkie-Rosell, A., McDonald, M., Freedman, S.F., Rivière, J.-B., Lafond-Lapalme, J., Simpson, B.N., Hopkin, R.J., Trimouille, A., Van-Gils, J., Begtrup, A., McWalter, K., Delphine, H., Keren, B., Genevieve, D., Argilli, E., Sherr, E.H., Severino, M., Rouleau, G.A., Yam, P.T., Charron, F., Srour, M., 2019. De Novo Pathogenic Variants in N-cadherin Cause a Syndromic Neurodevelopmental Disorder with Corpus Collosum, Axon, Cardiac, Ocular, and Genital Defects. Am J Hum Genet 105, 854–868. https://doi.org/10.1016/j.ajhg.2019.09.005

Acsády, L., Kamondi, A., Sík, A., Freund, T., Buzsáki, G., 1998. GABAergic Cells Are the Major Postsynaptic Targets of Mossy Fibers in the Rat Hippocampus. J. Neurosci. 18, 3386–3403. https://doi.org/10.1523/JNEUROSCI.18-09-03386.1998

Adler, P.N., 2012. Chapter One - The frizzled/stan Pathway and Planar Cell Polarity in the Drosophila Wing, in: Yang, Y. (Ed.), Current Topics in Developmental Biology, Planar Cell Polarity During Development. Academic Press, pp. 1–31. https://doi.org/10.1016/B978-0-12-394592-1.00001-6

Adler, P.N., 2002. Planar Signaling and Morphogenesis in Drosophila. Developmental Cell 2, 525–535. https://doi.org/10.1016/S1534-5807(02)00176-4

Adler, P.N., Wallingford, J.B., 2017. From Planar Cell Polarity to Ciliogenesis and Back: The Curious Tale of the PPE and CPLANE proteins. Trends Cell Biol 27, 379–390. https://doi.org/10.1016/j.tcb.2016.12.001

Ahn, J.H., Lee, T.-K., Park, J.H., Cho, J.H., Kim, I.H., Lee, J.C., Hong, S., Jeon, Y.H., Kang, I.J., Lee, Y.J., Won, M.-H., Lee, C.-H., 2017. Age-dependent differences in myelin basic protein expression in the hippocampus of young, adult and aged gerbils. Lab Anim Res 33, 237–243. https://doi.org/10.5625/lar.2017.33.3.237

Al Abed, A.S., Sellami, A., Brayda-Bruno, L., Lamothe, V., Noguès, X., Potier, M., Bennetau-Pelissero, C., Marighetto, A., 2016. Estradiol enhances retention but not organization of hippocampus-dependent memory in intact male mice. Psychoneuroendocrinology 69, 77–89. https://doi.org/10.1016/j.psyneuen.2016.03.014

Al Abed, A.S., Sellami, A., Potier, M., Ducourneau, E., Gerbeaud-Lassau, P., Brayda-Bruno, L., Lamothe, V., Sans, N., Desmedt, A., Vanhoutte, P., Bennetau-Pelissero, C., Trifilieff, P., Marighetto, A., 2020. Age-related impairment of declarative memory: linking memorization of temporal associations to GluN2B redistribution in dorsal CA1. Aging Cell 19. https://doi.org/10.1111/acel.13243

Altman, J., Bayer, S.A., 1990. Prolonged sojourn of developing pyramidal cells in the intermediate zone of the hippocampus and their settling in the stratum pyramidale. J. Comp. Neurol. 301, 343–364. https://doi.org/10.1002/cne.903010303

Altman, J., Das, G.D., 1965. Autoradiographic and histological evidence of postnatal hippocampal neurogenesis in rats. J Comp Neurol 124, 319–335. https://doi.org/10.1002/cne.901240303

Amaral, D.G., 1979. Synaptic extensions from the mossy fibers of the fascia dentata. Anat Embryol 155, 241–251. https://doi.org/10.1007/BF00317638

Amaral, D.G., Dent, J.A., 1981. Development of the mossy fibers of the dentate gyrus: I. A light and electron microscopic study of the mossy fibers and their expansions. Journal of Comparative Neurology 195, 51–86. https://doi.org/10.1002/cne.901950106

Amaral, D.G., Ishizuka, N., Claiborne, B., 1990. Chapter 1 Chapter Neurons, numbers and the hippocampal network, in: Storm-Mathisen, J., Zimmer, J., Ottersen, O.P. (Eds.), Progress in Brain Research, Understanding the Brain Through the Hippocampus the Hippocampal Region as a Model for Studying Brain Structure and Function. Elsevier, pp. 1–11. https://doi.org/10.1016/S0079-6123(08)61237-6

Anacker, C., Hen, R., 2017. Adult hippocampal neurogenesis and cognitive flexibility — linking memory and mood. Nat Rev Neurosci 18, 335–346. https://doi.org/10.1038/nrn.2017.45

Angevine Jr., J.B., 1965. Time of neuron origin in the hippocampal region: An autoradiographic study in the mouse. Experimental Neurology Suppl. 2, 1–70.

Apóstolo, N., Smukowski, S.N., Vanderlinden, J., Condomitti, G., Rybakin, V., ten Bos, J., Trobiani, L., Portegies, S., Vennekens, K.M., Gounko, N.V., Comoletti, D., Wierda, K.D., Savas, J.N., de Wit, J., 2020. Synapse type-specific proteomic dissection identifies IgSF8 as a hippocampal CA3 microcircuit organizer. Nat Commun 11, 5171. https://doi.org/10.1038/s41467-020-18956-x

Attili, S.M., Silva, M.F.M., Nguyen, T., Ascoli, G.A., 2019. Cell numbers, distribution, shape, and regional variation throughout the murine hippocampal formation from the adult brain Allen Reference Atlas. https://doi.org/10.1101/635201

Axelrod, J.D., 2001. Unipolar membrane association of Dishevelled mediates Frizzled planar cell polarity signaling. Genes Dev 15, 1182–1187. https://doi.org/10.1101/gad.890501

- B -

Bailly, E., Walton, A., Borg, J.-P., 2018. The planar cell polarity Vangl2 protein: From genetics to cellular and molecular functions. Seminars in Cell & Developmental Biology, Cell Polarity and Planar Cell Polarity Proteins 81, 62–70. https://doi.org/10.1016/j.semcdb.2017.10.030

Balaraju, A.K., Hu, B., Rodriguez, J.J., Murry, M., Lin, F., 2021. Glypican 4 regulates planar cell polarity of endoderm cells by controlling the localization of Cadherin 2. Development 148. https://doi.org/10.1242/dev.199421

Barbour, B., Häusser, M., 1997. Intersynaptic diffusion of neurotransmitter. Trends in Neurosciences 20, 377–384. https://doi.org/10.1016/S0166-2236(96)20050-5

Barnes, C.A., 1979. Memory deficits associated with senescence: a neurophysiological and behavioral study in the rat. J Comp Physiol Psychol 93, 74–104. https://doi.org/10.1037/h0077579

Barnes, C.A., Rao, G., Foster, T.C., McNaughton, B.L., 1992. Region-specific age effects on AMPA sensitivity: Electrophysiological evidence for loss of synaptic contacts in hippocampal field CA1. Hippocampus 2, 457–468. https://doi.org/10.1002/hipo.450020413

Barnes, C.A., Rao, G., Houston, F.P., 2000. LTP induction threshold change in old rats at the perforant path–granule cell synapse. Neurobiology of Aging 21, 613–620. https://doi.org/10.1016/S0197-4580(00)00163-9

Barrientos, R.M., Kitt, M.M., Watkins, L.R., Maier, S.F., 2015. Neuroinflammation in the normal aging hippocampus. Neuroscience, Hippocampal vulnerability: from molecules to disease 309, 84–99. https://doi.org/10.1016/j.neuroscience.2015.03.007

Barthet, G., Jordà-Siquier, T., Rumi-Masante, J., Bernadou, F., Müller, U., Mulle, C., 2018. Presenilin-mediated cleavage of APP regulates synaptotagmin-7 and presynaptic plasticity. Nat Commun 9, 4780. https://doi.org/10.1038/s41467-018-06813-x

Bashir, Z.I., Bortolotto, Z.A., Davies, C.H., Berretta, N., Irving, A.J., Seal, A.J., Henley, J.M., Jane, D.E., Watkins, J.C., Collingridge, G.L., 1993. Induction of LTP in the hippocampus needs synaptic activation of glutamate metabotropic receptors. Nature 363, 347–350. https://doi.org/10.1038/363347a0

Bastock, R., Strutt, H., Strutt, D., 2003. Strabismus is asymmetrically localised and binds to Prickle and Dishevelled during Drosophila planar polarity patterning. Development 130, 3007–3014. https://doi.org/10.1242/dev.00526

Baude, A., Nusser, Z., Molnar, E., McIlhinney, R.A.J., Somogyi, P., 1995. High-resolution immunogold localization of AMPA type glutamate receptor subunits at synaptic and non-synaptic sites in rat hippocampus. Neuroscience 69, 1031–1055. https://doi.org/10.1016/0306-4522(95)00350-R

Baude, A., Nusser, Z., Roberts, J.D.B., Mulvihill, E., Mcllhinney, R.A.J., Somogyi, P., 1993. The metabotropic glutamate receptor (mGluRlα) is concentrated at perisynaptic membrane of neuronal subpopulations as detected by immunogold reaction. Neuron 11, 771–787. https://doi.org/10.1016/0896-6273(93)90086-7

Bayer, S.A., 1980. Development of the hippocampal region in the rat I. Neurogenesis examined with3H-thymidine autoradiography. J. Comp. Neurol. 190, 87–114. https://doi.org/10.1002/cne.901900107

Bekirov, I.H., Nagy, V., Svoronos, A., Huntley, G.W., Benson, D.L., 2008. Cadherin-8 and N-cadherin Differentially Regulate Pre- and Postsynaptic Development of the Hippocampal Mossy Fiber Pathway. Hippocampus 18, 349–363. https://doi.org/10.1002/hipo.20395

Bellaïche, Y., Beaudoin-Massiani, O., Stüttem, I., Schweisguth, F., 2004. The planar cell polarity protein Strabismus promotes Pins anterior localization during asymmetric division of sensory organ precursor cells in Drosophila. Development 131, 469–478. https://doi.org/10.1242/dev.00928

Belotti, E., Puvirajesinghe, T.M., Audebert, S., Baudelet, E., Camoin, L., Pierres, M., Lasvaux, L., Ferracci, G., Montcouquiol, M., Borg, J.-P., 2012. Molecular Characterisation of Endogenous Vangl2/Vangl1 Heteromeric Protein Complexes. PLoS One 7. https://doi.org/10.1371/journal.pone.0046213

Bergersen, L., Ruiz, A., Bjaalie, J.G., Kullmann, D.M., Gundersen, V., 2003. GABA and GABAA receptors at hippocampal mossy fibre synapses. European Journal of Neuroscience 18, 931–941. https://doi.org/10.1046/j.1460-9568.2003.02828.x

Binder, D.K., Croll, S.D., Gall, C.M., Scharfman, H.E., 2001. BDNF and epilepsy: too much of a good thing? Trends in Neurosciences 24, 47–53. https://doi.org/10.1016/S0166-2236(00)01682-9

Blackstad, T.W., Kjaerheim, A., 1961. Special axo-dendritic synapses in the hippocampal cortex: electron and light microscopic studies on the layer of mossy fibers. J Comp Neurol 117, 133–159. https://doi.org/10.1002/cne.901170202

Blinkouskaya, Y., Caçoilo, A., Gollamudi, T., Jalalian, S., Weickenmeier, J., 2021. Brain aging mechanisms with mechanical manifestations. Mechanisms of Ageing and Development 200, 111575. https://doi.org/10.1016/j.mad.2021.111575

Bolhuis, J.J., Bijlsma, S., Ansmink, P., 1986. Exponential decay of spatial memory of rats in a radial maze. Behavioral and Neural Biology 46, 115–122. https://doi.org/10.1016/S0163-1047(86)90584-4

Bolós, M., Pallas-Bazarra, N., Terreros-Roncal, J., Perea, J., Jurado-Arjona, J., Ávila, J., Llorens-Martín, M., 2017. Soluble Tau has devastating effects on the structural plasticity of hippocampal granule neurons. Transl Psychiatry 7, 1267. https://doi.org/10.1038/s41398-017-0013-6

Booker, S.A., Vida, I., 2018. Morphological diversity and connectivity of hippocampal interneurons. Cell Tissue Res 373, 619–641. https://doi.org/10.1007/s00441-018-2882-2

Boulland, J.-L., Chaudhry, F.A., 2012. Ontogenetic changes in the distribution of the vesicular GABA transporter VGAT correlate with the excitation/inhibition shift of GABA action. Neurochemistry International, The Glutamatergic Synapse 61, 506–516. https://doi.org/10.1016/j.neuint.2012.03.018

Boutin, C., Labedan, P., Dimidschstein, J., Richard, F., Cremer, H., André, P., Yang, Y., Montcouquiol, M., Goffinet, A.M., Tissir, F., 2014. A dual role for planar cell polarity genes in ciliated cells. Proc Natl Acad Sci U S A 111, E3129–E3138. https://doi.org/10.1073/pnas.1404988111

Boutros, M., Paricio, N., Strutt, D.I., Mlodzik, M., 1998. Dishevelled Activates JNK and Discriminates between JNK Pathways in Planar Polarity and wingless Signaling. Cell 94, 109–118. https://doi.org/10.1016/S0092-8674(00)81226-X

Bouyeure, A., Noulhiane, M., 2020. Chapter 17 - Memory: Normative development of memory systems, in: Gallagher, A., Bulteau, C., Cohen, D., Michaud, J.L. (Eds.), Handbook of Clinical Neurology, Neurocognitive Development: Normative Development. Elsevier, pp. 201–213. https://doi.org/10.1016/B978-0-444-64150-2.00018-6

Brayda-Bruno, L., Mons, N., Yee, B.K., Micheau, J., Abrous, D.N., Nogues, X., Marighetto, A., 2013. Partial loss in septo-hippocampal cholinergic neurons alters memory-dependent measures of brain connectivity without overt memory deficits. Neurobiology of Disease 54, 372–381. https://doi.org/10.1016/j.nbd.2013.01.010

Brody, D.L., Holtzman, D.M., 2006. Morris water maze search strategy analysis in PDAPP mice before and after experimental traumatic brain injury. Exp Neurol 197, 330–340. https://doi.org/10.1016/j.expneurol.2005.10.020

Buckmaster, P.S., 2014. Does mossy fiber sprouting give rise to the epileptic state? Adv Exp Med Biol 813, 161–168. https://doi.org/10.1007/978-94-017-8914-1_13

Buechling, T., Boutros, M., 2011. Wnt signaling signaling at and above the receptor level. Curr Top Dev Biol 97, 21–53. https://doi.org/10.1016/B978-0-12-385975-4.00008-5

Burghardt, N.S., Park, E.H., Hen, R., Fenton, A.A., 2012. Adult-born hippocampal neurons promote cognitive flexibility in mice. Hippocampus 22, 1795–1808. https://doi.org/10.1002/hipo.22013

Burke, S.N., Wallace, J.L., Nematollahi, S., Uprety, A.R., Barnes, C.A., 2010. Pattern separation deficits may contribute to age-associated recognition impairments. Behavioral Neuroscience 124, 559–573. https://doi.org/10.1037/a0020893

Buss, E.W., Corbett, N.J., Roberts, J.G., Ybarra, N., Musial, T.F., Simkin, D., Molina-Campos, E., Oh, K.-J., Nielsen, L.L., Ayala, G.D., Mullen, S.A., Farooqi, A.K., D'Souza, G.X., Hill, C.L., Bean, L.A., Rogalsky, A.E., Russo, M.L., Curlik, D.M., Antion, M.D., Weiss, C., Chetkovich, D.M., Oh, M.M., Disterhoft, J.F., Nicholson, D.A., 2021. Cognitive aging is associated with redistribution of synaptic weights in the hippocampus. Proc. Natl. Acad. Sci. U.S.A. 118, e1921481118. https://doi.org/10.1073/pnas.1921481118

Butler, M.T., Wallingford, J.B., 2018. Spatial and temporal analysis of PCP protein dynamics during neural tube closure. eLife 7, e36456. https://doi.org/10.7554/eLife.36456

- C -

Cadigan, K.M., Liu, Y.I., 2006. Wnt signaling: complexity at the surface. Journal of Cell Science 119, 395–402. https://doi.org/10.1242/jcs.02826

Calabrese, B., Wilson, M.S., Halpain, S., 2006. Development and Regulation of Dendritic Spine Synapses. Physiology 21, 38–47. https://doi.org/10.1152/physiol.00042.2005

Carasatorre, M., Ochoa-Alvarez, A., Velázquez-Campos, G., Lozano-Flores, C., Díaz-Cintra, S.Y., Ramírez-Amaya, V., 2015. Hippocampal Synaptic Expansion Induced by Spatial Experience in Rats Correlates with Improved Information Processing in the Hippocampus. PLoS One 10, e0132676. https://doi.org/10.1371/journal.pone.0132676

Caricasole, A., Copani, A., Caraci, F., Aronica, E., Rozemuller, A.J., Caruso, A., Storto, M., Gaviraghi, G., Terstappen, G.C., Nicoletti, F., 2004. Induction of Dickkopf-1, a Negative Modulator of the Wnt Pathway, Is Associated with Neuronal Degeneration in Alzheimer's Brain. J. Neurosci. 24, 6021–6027. https://doi.org/10.1523/JNEUROSCI.1381-04.2004

Carreira-Barbosa, F., Kajita, M., Morel, V., Wada, H., Okamoto, H., Martinez Arias, A., Fujita, Y., Wilson, S.W., Tada, M., 2009. Flamingo regulates epiboly and convergence/extension movements through cell cohesive and signalling functions during zebrafish gastrulation. Development 136, 383–392. https://doi.org/10.1242/dev.026542

Carta, M., Srikumar, B.N., Gorlewicz, A., Rebola, N., Mulle, C., 2018. Activity-dependent control of NMDA receptor subunit composition at hippocampal mossy fibre synapses. J Physiol 596, 703–716. https://doi.org/10.1113/JP275226

Castillo, P.E., Janz, R., Sdhof, T.C., Tzounopoulos, T., Malenka, R.C., Nicoll, R.A., 1997a. Rab3A is essential for mossy fibre long-term potentiation in the hippocampus. Nature 388, 590–593. https://doi.org/10.1038/41574

Castillo, P.E., Malenka, R.C., Nicoll, R.A., 1997b. Kainate receptors mediate a slow postsynaptic current in hippocampal CA3 neurons. Nature 388, 182–186. https://doi.org/10.1038/40645

Cavazos, J.E., Golarai, G., Sutula, T.P., 1991. Mossy fiber synaptic reorganization induced by kindling: time course of development, progression, and permanence. J. Neurosci. 11, 2795–2803. https://doi.org/10.1523/JNEUROSCI.11-09-02795.1991

Cembrowski, M.S., Spruston, N., 2019. Heterogeneity within classical cell types is the rule: lessons from hippocampal pyramidal neurons. Nat Rev Neurosci 20, 193–204. https://doi.org/10.1038/s41583-019-0125-5

Cerbai, F., Lana, D., Nosi, D., Petkova-Kirova, P., Zecchi, S., Brothers, H.M., Wenk, G.L., Giovannini, M.G., 2012. The Neuron-Astrocyte-Microglia Triad in Normal Brain Ageing and in a Model of Neuroinflammation in the Rat Hippocampus. PLOS ONE 7, e45250. https://doi.org/10.1371/journal.pone.0045250

Cès, A., Burg, T., Herbeaux, K., Héraud, C., Bott, J.-B., Mensah-Nyagan, A.G., Mathis, C., 2018. Age-related vulnerability of pattern separation in C57BL/6J mice. Neurobiology of Aging 62, 120–129. https://doi.org/10.1016/j.neurobiolaging.2017.10.013

Chai, G., Zhou, L., Manto, M., Helmbacher, F., Clotman, F., Goffinet, A.M., Tissir, F., 2014. Celsr3 is required in motor neurons to steer their axons in the hindlimb. Nat. Neurosci. 17, 1171–1179. https://doi.org/10.1038/nn.3784

Chaudhry, F.A., Reimer, R.J., Bellocchio, E.E., Danbolt, N.C., Osen, K.K., Edwards, R.H., Storm-Mathisen, J., 1998. The Vesicular GABA Transporter, VGAT, Localizes to Synaptic Vesicles in Sets of Glycinergic as Well as GABAergic Neurons. J. Neurosci. 18, 9733–9750. https://doi.org/10.1523/JNEUROSCI.18-23-09733.1998

Chauhan, P., Jethwa, K., Rathawa, A., Chauhan, G., Mehra, S., 2021. The Anatomy of the Hippocampus, in: Pluta, R. (Ed.), Cerebral Ischemia. Exon Publications, Brisbane (AU).

Chen, J., Park, C.S., Tang, S.-J., 2006. Activity-dependent Synaptic Wnt Release Regulates Hippocampal Long Term Potentiation*. Journal of Biological Chemistry 281, 11910–11916. https://doi.org/10.1074/jbc.M511920200

Chiba, A.A., Kesner, R.P., Reynolds, A.M., 1994. Memory for spatial location as a function of temporal lag in rats: Role of hippocampus and medial prefrontal cortex. Behavioral and Neural Biology 61, 123–131. https://doi.org/10.1016/S0163-1047(05)80065-2

Chicurel, M.E., Harris, K.M., 1992. Three-dimensional analysis of the structure and composition of CA3 branched dendritic spines and their synaptic relationships with mossy fiber boutons in the rat hippocampus. Journal of Comparative Neurology 325, 169–182. https://doi.org/10.1002/cne.903250204

Chierzi, S., Stachniak, T.J., Trudel, E., Bourque, C.W., Murai, K.K., 2012. Activity maintains structural plasticity of mossy fiber terminals in the hippocampus. Molecular and Cellular Neuroscience 50, 260–271. https://doi.org/10.1016/j.mcn.2012.05.004

Christensen, K.R., Beach, T.G., Serrano, G.E., Kanaan, N.M., 2019. Pathogenic tau modifications occur in axons before the somatodendritic compartment in mossy fiber and Schaffer collateral pathways. Acta Neuropathol Commun 7, 29. https://doi.org/10.1186/s40478-019-0675-9

Colas, J.-F., Schoenwolf, G.C., 2001. Towards a cellular and molecular understanding of neurulation. Developmental Dynamics 221, 117–145. https://doi.org/10.1002/dvdy.1144

Condomitti, G., de Wit, J., 2018. Heparan Sulfate Proteoglycans as Emerging Players in Synaptic Specificity. Frontiers in Molecular Neuroscience 11.

Condomitti, G., Wierda, K.D., Schroeder, A., Rubio, S.E., Vennekens, K.M., Orlandi, C., Martemyanov, K.A., Gounko, N.V., Savas, J.N., de Wit, J., 2018. An Input-Specific Orphan Receptor GPR158-HSPG Interaction Organizes Hippocampal Mossy Fiber-CA3 Synapses. Neuron 100, 201-215.e9. https://doi.org/10.1016/j.neuron.2018.08.038

Conner-Kerr, T.A., Simmons, D.R., Peterson, G.M., Terrian, D.M., 1993. Evidence for the Corelease of Dynorphin and Glutamate from Rat Hippocampal Mossy Fiber Terminals. Journal of Neurochemistry 61, 627–636. https://doi.org/10.1111/j.1471-4159.1993.tb02167.x

Contractor, A., Swanson, G., Heinemann, S.F., 2001. Kainate Receptors Are Involved in Short- and Long-Term Plasticity at Mossy Fiber Synapses in the Hippocampus. Neuron 29, 209–216. https://doi.org/10.1016/S0896-6273(01)00191-X

Copley, C.O., Duncan, J.S., Liu, C., Cheng, H., Deans, M.R., 2013. Postnatal Refinement of Auditory Hair Cell Planar Polarity Deficits Occurs in the Absence of Vangl2. J. Neurosci. 33, 14001–14016. https://doi.org/10.1523/JNEUROSCI.1307-13.2013

Copp, A.J., Greene, N.D.E., Murdoch, J.N., 2003. The genetic basis of mammalian neurulation. Nature Reviews Genetics 4, 784–793. https://doi.org/10.1038/nrg1181

Corti, C., Aldegheri, L., Somogyi, P., Ferraguti, F., 2002. Distribution and synaptic localisation of the metabotropic glutamate receptor 4 (mGluR4) in the rodent CNS. Neuroscience 110, 403–420. https://doi.org/10.1016/S0306-4522(01)00591-7

Courbard, J.-R., Djiane, A., Wu, J., Mlodzik, M., 2009. The apical/basal-polarity determinant Scribble cooperates with the PCP core factor Stbm/Vang and

functions as one of its effectors. Developmental Biology 333, 67–77. https://doi.org/10.1016/j.ydbio.2009.06.024

Crawford, I.L., Connor, J.D., 1973. Localization and Release of Glutamic Acid in Relation to the Hippocampal Mossy Fibre Pathway. Nature 244, 442–443. https://doi.org/10.1038/244442a0

Curtin, J.A., Quint, E., Tsipouri, V., Arkell, R.M., Cattanach, B., Copp, A.J., Henderson, D.J., Spurr, N., Stanier, P., Fisher, E.M., Nolan, P.M., Steel, K.P., Brown, S.D.M., Gray, I.C., Murdoch, J.N., 2003. Mutation of Celsr1 disrupts planar polarity of inner ear hair cells and causes severe neural tube defects in the mouse. Curr Biol 13, 1129–1133. https://doi.org/10.1016/s0960-9822(03)00374-9

- D -

Da Cruz, J.F.O., Gomis-Gonzalez, M., Maldonado, R., Marsicano, G., Ozaita, A., Busquets-Garcia, A., 2020. An Alternative Maze to Assess Novel Object Recognition in Mice. Bio Protoc 10, e3651. https://doi.org/10.21769/BioProtoc.3651

Dailey, M., Buchanan, J., Bergles, D., Smith, S., 1994. Mossy fiber growth and synaptogenesis in rat hippocampal slices in vitro. J. Neurosci. 14, 1060–1078. https://doi.org/10.1523/JNEUROSCI.14-03-01060.1994

Darken, R.S., Scola, A.M., Rakeman, A.S., Das, G., Mlodzik, M., Wilson, P.A., 2002. The planar polarity gene strabismus regulates convergent extension movements in Xenopus. EMBO J 21, 976–985. https://doi.org/10.1093/emboj/21.5.976

Das, G., Jenny, A., Klein, T.J., Eaton, S., Mlodzik, M., 2004. Diego interacts with Prickle and Strabismus/Van Gogh to localize planar cell polarity complexes. Development 131, 4467–4476. https://doi.org/10.1242/dev.01317

Das, S.C., Chen, D., Callor, W.B., Christensen, E., Coon, H., Williams, M.E., 2019. Analysis of synapse-level neuronal morphology in human post-mortem brain tissue (preprint). Neuroscience. https://doi.org/10.1101/558817

Davey, C.F., Moens, C.B., 2017. Planar cell polarity in moving cells: think globally, act locally. Development 144, 187–200. https://doi.org/10.1242/dev.122804

de Fiebre, N.C., Sumien, N., Forster, M.J., de Fiebre, C.M., 2006. Spatial learning and psychomotor performance of C57BL/6 mice: age sensitivity and reliability of individual differences. AGE 28, 235–253. https://doi.org/10.1007/s11357-006-9027-3

Decker, J.M., Krüger, L., Sydow, A., Zhao, S., Frotscher, M., Mandelkow, E., Mandelkow, E.-M., 2015. Pro-aggregant Tau impairs mossy fiber plasticity due to structural changes and Ca++ dysregulation. Acta Neuropathologica Communications 3, 23. https://doi.org/10.1186/s40478-015-0193-3

Deguchi, Y., Donato, F., Galimberti, I., Cabuy, E., Caroni, P., 2011. Temporally matched subpopulations of selectively interconnected principal neurons in the hippocampus. Nat Neurosci 14, 495–504. https://doi.org/10.1038/nn.2768

Delaunay, D., Cortay, V., Patti, D., Knoblauch, K., Dehay, C., 2014. Mitotic Spindle Asymmetry: A Wnt/PCP-Regulated Mechanism Generating Asymmetrical Division in Cortical Precursors. Cell Reports 6, 400–414. https://doi.org/10.1016/j.celrep.2013.12.026

Delgorio, P.L., Hiscox, L.V., Daugherty, A.M., Sanjana, F., Pohlig, R.T., Ellison, J.M., Martens, C.R., Schwarb, H., McGarry, M.D.J., Johnson, C.L., 2021. Effect of Aging on the Viscoelastic Properties of Hippocampal Subfields Assessed with High-Resolution MR Elastography. Cereb Cortex 31, 2799–2811. https://doi.org/10.1093/cercor/bhaa388

Devenport, D., 2014. The cell biology of planar cell polarity. Journal of Cell Biology 207, 171–179. https://doi.org/10.1083/jcb.201408039

Di Benedetto, S., Müller, L., 2019. Aging, Immunity, and Neuroinflammation: The Modulatory Potential of Nutrition, in: Mahmoudi, M., Rezaei, N. (Eds.), Nutrition and Immunity. Springer International Publishing, Cham, pp. 301–322. https://doi.org/10.1007/978-3-030-16073-9_14

Dillon, S.E., Tsivos, D., Knight, M., McCann, B., Pennington, C., Shiel, A.I., Conway, M.E., Newson, M.A., Kauppinen, R.A., Coulthard, E.J., 2017. The impact of ageing reveals distinct roles for human dentate gyrus and CA3 in pattern separation and object recognition memory. Sci Rep 7, 14069. https://doi.org/10.1038/s41598-017-13853-8

Dos-Santos Carvalho, S., Moreau, M.M., Hien, Y.E., Garcia, M., Aubailly, N., Henderson, D.J., Studer, V., Sans, N., Thoumine, O., Montcouquiol, M., 2020. Vangl2 acts at the interface between actin and N-cadherin to modulate mammalian neuronal outgrowth. eLife 9, e51822. https://doi.org/10.7554/eLife.51822

Doudney, K., Moore, G.E., Stanier, P., Ybot-Gonzalez, P., Paternotte, C., Greene, N.D.E., Copp, A.J., Stevenson, R.E., 2005. Analysis of the planar cell polarity gene Vangl2 and its co-expressed paralogue Vangl1 in neural tube defect patients. American Journal of Medical Genetics Part A 136A, 90–92. https://doi.org/10.1002/ajmg.a.30766

Driscoll, I., Hamilton, D.A., Petropoulos, H., Yeo, R.A., Brooks, W.M., Baumgartner, R.N., Sutherland, R.J., 2003. The Aging Hippocampus: Cognitive, Biochemical and Structural Findings. Cerebral Cortex 13, 1344–1351. https://doi.org/10.1093/cercor/bhg081

Driscoll, I., Howard, S.R., Stone, J.C., Monfils, M.H., Tomanek, B., Brooks, W.M., Sutherland, R.J., 2006. The aging hippocampus: A multi-level analysis in the rat. Neuroscience 139, 1173–1185. https://doi.org/10.1016/j.neuroscience.2006.01.040

Dudchenko, P.A., 2004. An overview of the tasks used to test working memory in rodents. Neurosci Biobehav Rev 28, 699–709. https://doi.org/10.1016/j.neubiorev.2004.09.002

Dupret, D., Revest, J.-M., Koehl, M., Ichas, F., De Giorgi, F., Costet, P., Abrous, D.N., Piazza, P.V., 2008. Spatial relational memory requires hippocampal adult neurogenesis. PLoS One 3, e1959. https://doi.org/10.1371/journal.pone.0001959

- E -

Edler, M.K., Munger, E.L., Meindl, R.S., Hopkins, W.D., Ely, J.J., Erwin, J.M., Mufson, E.J., Hof, P.R., Sherwood, C.C., Raghanti, M.A., 2020. Neuron loss associated with age but not Alzheimer's disease pathology in the chimpanzee brain. Philosophical Transactions of the Royal Society B: Biological Sciences 375, 20190619. https://doi.org/10.1098/rstb.2019.0619

Ehninger, D., Kempermann, G., 2008. Neurogenesis in the adult hippocampus. Cell Tissue Res 331, 243–250. https://doi.org/10.1007/s00441-007-0478-3

Eichenbaum, H., 1999. The hippocampus and mechanisms of declarative memory. Behavioural Brain Research 103, 123–133. https://doi.org/10.1016/S0166-4328(99)00044-3

Eisenmann, D.M., 2005. Wnt signaling. WormBook 1–17. https://doi.org/10.1895/wormbook.1.7.1

Elliott, C., Rojo, A.I., Ribe, E., Broadstock, M., Xia, W., Morin, P., Semenov, M., Baillie, G., Cuadrado, A., Al-Shawi, R., Ballard, C.G., Simons, P., Killick, R., 2018. A role for APP in Wnt signalling links synapse loss with β-amyloid production. Transl Psychiatry 8. https://doi.org/10.1038/s41398-018-0231-6

Escobedo, N., Contreras, O., Muñoz, R., Farías, M., Carrasco, H., Hill, C., Tran, U., Pryor, S.E., Wessely, O., Copp, A.J., Larraín, J., 2013. Syndecan 4 interacts genetically with Vangl2 to regulate neural tube closure and planar cell polarity. Development 140, 3008–3017. https://doi.org/10.1242/dev.091173

Etchamendy, N., Enderlin, V., Marighetto, A., Pallet, V., Higueret, P., Jaffard, R., 2003. Vitamin A deficiency and relational memory deficit in adult mice: relationships with changes in brain retinoid signalling. Behav Brain Res 145, 37–49. https://doi.org/10.1016/s0166-4328(03)00099-8

Etheridge, S.L., Ray, S., Li, S., Hamblet, N.S., Lijam, N., Tsang, M., Greer, J., Kardos, N., Wang, J., Sussman, D.J., Chen, P., Wynshaw-Boris, A., 2008. Murine Dishevelled 3 Functions in Redundant Pathways with Dishevelled 1 and 2 in Normal Cardiac Outflow Tract, Cochlea, and Neural Tube Development. PLOS Genetics 4, e1000259. https://doi.org/10.1371/journal.pgen.1000259

Evstratova, A., Tóth, K., 2014. Information processing and synaptic plasticity at hippocampal mossy fiber terminals. Front. Cell. Neurosci. 8. https://doi.org/10.3389/fncel.2014.00028

- F -

Fan, X., Wheatley, E.G., Villeda, S.A., 2017. Mechanisms of Hippocampal Aging and the Potential for Rejuvenation. Annu. Rev. Neurosci. 40, 251–272. https://doi.org/10.1146/annurev-neuro-072116-031357

Fanselow, M.S., Dong, H.-W., 2010. Are the Dorsal and Ventral Hippocampus Functionally Distinct Structures? Neuron 65, 7–19. https://doi.org/10.1016/j.neuron.2009.11.031

Faulkner, R.L., Jang, M.-H., Liu, X.-B., Duan, X., Sailor, K.A., Kim, J.Y., Ge, S., Jones, E.G., Ming, G., Song, H., Cheng, H.-J., 2008. Development of hippocampal mossy fiber synaptic outputs by new neurons in the adult brain. Proc Natl Acad Sci U S A 105, 14157–14162. https://doi.org/10.1073/pnas.0806658105

Feng, B., Freitas, A.E., Gorodetski, L., Wang, J., Tian, R., Lee, Y.R., Grewal, A.S., Zou, Y., 2021. Planar cell polarity signaling components are a direct target of β-amyloid–associated degeneration of glutamatergic synapses. Science Advances 7, eabh2307. https://doi.org/10.1126/sciadv.abh2307

Feng, X., Guo, J., Sigmon, H.C., Sloan, R.P., Brickman, A.M., Provenzano, F.A., Small, S.A., for the Alzheimer's Disease Neuroimaging Initiative, 2020. Brain regions vulnerable and resistant to aging without Alzheimer's disease. PLoS ONE 15, e0234255. https://doi.org/10.1371/journal.pone.0234255

Fenstermaker, A.G., Prasad, A.A., Bechara, A., Adolfs, Y., Tissir, F., Goffinet, A., Zou, Y., Pasterkamp, R.J., 2010. Wnt/Planar Cell Polarity Signaling Controls the Anterior–Posterior Organization of Monoaminergic Axons in the Brainstem. J Neurosci 30, 16053–16064. https://doi.org/10.1523/JNEUROSCI.4508-10.2010

Fernandes, H.B., Catches, J.S., Petralia, R.S., Copits, B.A., Xu, J., Russell, T.A., Swanson, G.T., Contractor, A., 2009. High-Affinity Kainate Receptor Subunits Are Necessary for Ionotropic but Not Metabotropic Signaling. Neuron 63, 818–829. https://doi.org/10.1016/j.neuron.2009.08.010

Frahm, C., Engel, D., Piechotta, A., Heinemann, U., Draguhn, A., 2000. Presence of γ-aminobutyric acid transporter mRNA in interneurons and principal cells of rat hippocampus. Neuroscience Letters 288, 175–178. https://doi.org/10.1016/S0304-3940(00)01217-9

Frankland, P.W., Bontempi, B., 2005. The organization of recent and remote memories. Nat Rev Neurosci 6, 119–130. https://doi.org/10.1038/nrn1607

Fritschy, J.-M., Weinmann, O., Wenzel, A., Benke, D., 1998. Synapse-specific localization of NMDA and GABAA receptor subunits revealed by antigen-

retrieval immunohistochemistry. Journal of Comparative Neurology 390, 194–210. https://doi.org/10.1002/(SICI)1096-9861(19980112)390:2<194::AID-CNE3>3.0.CO;2-X

Fu, Y., Yu, Y., Paxinos, G., Watson, C., Rusznák, Z., 2015. Aging-dependent changes in the cellular composition of the mouse brain and spinal cord. Neuroscience 290, 406–420. https://doi.org/10.1016/j.neuroscience.2015.01.039

Funayama, N., Fagotto, F., McCrea, P., Gumbiner, B.M., 1995. Embryonic axis induction by the armadillo repeat domain of beta-catenin: evidence for intracellular signaling. Journal of Cell Biology 128, 959–968. https://doi.org/10.1083/jcb.128.5.959

- G -

Galimberti, I., Bednarek, E., Donato, F., Caroni, P., 2010. EphA4 Signaling in Juveniles Establishes Topographic Specificity of Structural Plasticity in the Hippocampus. Neuron 65, 627–642. https://doi.org/10.1016/j.neuron.2010.02.016

Galimberti, I., Gogolla, N., Alberi, S., Santos, A.F., Muller, D., Caroni, P., 2006. Long-Term Rearrangements of Hippocampal Mossy Fiber Terminal Connectivity in the Adult Regulated by Experience. Neuron 50, 749–763. https://doi.org/10.1016/j.neuron.2006.04.026

Gao, B., Song, H., Bishop, K., Elliot, G., Garrett, L., English, M.A., Andre, P., Robinson, J., Sood, R., Minami, Y., Economides, A.N., Yang, Y., 2011. Wnt Signaling Gradients Establish Planar Cell Polarity by Inducing Vangl2 Phosphorylation through Ror2. Developmental Cell 20, 163–176. https://doi.org/10.1016/j.devcel.2011.01.001

Garad, M., Edelmann, E., Leßmann, V., 2021. Long-term depression at hippocampal mossy fiber-CA3 synapses involves BDNF but is not mediated by p75NTR signaling. Sci Rep 11, 8535. https://doi.org/10.1038/s41598-021-87769-9

Gemma, C., Bachstetter, A., 2013. The role of microglia in adult hippocampal neurogenesis. Frontiers in Cellular Neuroscience 7.

Giese, A.P., Ezan, J., Wang, L., Lasvaux, L., Lembo, F., Mazzocco, C., Richard, E., Reboul, J., Borg, J.-P., Kelley, M.W., Sans, N., Brigande, J., Montcouquiol, M., 2012. Gipc1 has a dual role in Vangl2 trafficking and hair bundle integrity in the inner ear. Development 139, 3775–3785. https://doi.org/10.1242/dev.074229

Gogolla, N., Galimberti, I., Deguchi, Y., Caroni, P., 2009. Wnt Signaling Mediates Experience-Related Regulation of Synapse Numbers and Mossy Fiber Connectivities in the Adult Hippocampus. Neuron 62, 510–525. https://doi.org/10.1016/j.neuron.2009.04.022

Golgi, C., 1903. Opera omnia, Camillo Golgi. Ulrico Hoepli.

Golgi, C., 1886. Sulla fina anatomia degli organi centrali del sistema nervoso. U. Hoepli, Milano.

Gómez-Lira, G., Trillo, E., Ramírez, M., Asai, M., Sitges, M., Gutiérrez, R., 2002. The Expression of GABA in Mossy Fiber Synaptosomes Coincides with the Seizure-Induced Expression of GABAergic Transmission in the Mossy Fiber Synapse. Experimental Neurology 177, 276–283. https://doi.org/10.1006/exnr.2002.7986

Gonçalves, J.T., Schafer, S.T., Gage, F.H., 2016. Adult Neurogenesis in the Hippocampus: From Stem Cells to Behavior. Cell 167, 897–914. https://doi.org/10.1016/j.cell.2016.10.021

Gorski, J.A., Talley, T., Qiu, M., Puelles, L., Rubenstein, J.L.R., Jones, K.R., 2002. Cortical Excitatory Neurons and Glia, But Not GABAergic Neurons, Are Produced in the Emx1-Expressing Lineage. J Neurosci 22, 6309–6314. https://doi.org/10.1523/JNEUROSCI.22-15-06309.2002

Goto, T., Keller, R., 2002. The planar cell polarity gene strabismus regulates convergence and extension and neural fold closure in Xenopus. Dev Biol 247, 165–181. https://doi.org/10.1006/dbio.2002.0673

Gould, E., Beylin, A., Tanapat, P., Reeves, A., Shors, T.J., 1999. Learning enhances adult neurogenesis in the hippocampal formation. Nat Neurosci 2, 260–265. https://doi.org/10.1038/6365

Greene, N.D.E., Gerrelli, D., Van Straaten, H.W.M., Copp, A.J., 1998. Abnormalities of floor plate, notochord and somite differentiation in the loop-tail (Lp) mouse: a model of severe neural tube defects. Mechanisms of Development 73, 59–72. https://doi.org/10.1016/S0925-4773(98)00029-X

Griego, E., Galván, E.J., 2020. Metabotropic Glutamate Receptors at the Aged Mossy Fiber – CA3 Synapse of the Hippocampus. Neuroscience. https://doi.org/10.1016/j.neuroscience.2019.12.016

Grosse, G., Tapp, R., Wartenberg, M., Sauer, H., Fox, P.A., Grosse, J., Gratzl, M., Bergmann, M., 1998. Prenatal hippocampal granule cells in primary cell culture form mossy fiber boutons at pyramidal cell dendrites. Journal of Neuroscience Research 51, 602–611. https://doi.org/10.1002/(SICI)1097-4547(19980301)51:5<602::AID-JNR7>3.0.CO;2-J

Grove, E.A., Tole, S., 1999. Patterning Events and Specification Signals in the Developing Hippocampus. Cerebral Cortex 9, 551–561. https://doi.org/10.1093/cercor/9.6.551

Gu, Y., Arruda-Carvalho, M., Wang, J., Janoschka, S.R., Josselyn, S.A., Frankland, P.W., Ge, S., 2012. Optical controlling reveals time-dependent roles for adult-born dentate granule cells. Nat Neurosci 15, 1700–1706. https://doi.org/10.1038/nn.3260

Guillaud, L., Dimitrov, D., Takahashi, T., 2017. Presynaptic morphology and vesicular composition determine vesicle dynamics in mouse central synapses. eLife 6, e24845. https://doi.org/10.7554/eLife.24845

Guirao, B., Meunier, A., Mortaud, S., Aguilar, A., Corsi, J.-M., Strehl, L., Hirota, Y., Desoeuvre, A., Boutin, C., Han, Y.-G., Mirzadeh, Z., Cremer, H., Montcouquiol, M., Sawamoto, K., Spassky, N., 2010. Coupling between hydrodynamic forces and planar cell polarity orients mammalian motile cilia. Nat Cell Biol 12, 341–350. https://doi.org/10.1038/ncb2040

- H -

Hagiwara, A., Yasumura, M., Hida, Y., Inoue, E., Ohtsuka, T., 2014. The planar cell polarity protein Vangl2 bidirectionally regulates dendritic branching in cultured hippocampal neurons. Mol Brain 7. https://doi.org/10.1186/s13041-014-0079-5

Hainmueller, T., Bartos, M., 2020. Dentate gyrus circuits for encoding, retrieval and discrimination of episodic memories. Nat Rev Neurosci 21, 153–168. https://doi.org/10.1038/s41583-019-0260-z

Hakanen, J., Ruiz-Reig, N., Tissir, F., 2019. Linking Cell Polarity to Cortical Development and Malformations. Front Cell Neurosci 13. https://doi.org/10.3389/fncel.2019.00244

Hallermann, S., Pawlu, C., Jonas, P., Heckmann, M., 2003. A large pool of releasable vesicles in a cortical glutamatergic synapse. Proc Natl Acad Sci U S A 100, 8975–8980. https://doi.org/10.1073/pnas.1432836100

Hanson, J.E., Blank, M., Valenzuela, R.A., Garner, C.C., Madison, D.V., 2007. The functional nature of synaptic circuitry is altered in area CA3 of the hippocampus in a mouse model of Down's syndrome. J Physiol 579, 53–67. https://doi.org/10.1113/jphysiol.2006.114868

Hara, Y., Morrison, J.H., 2014. Chapter Ten - Synaptic Correlates of Aging and Cognitive Decline, in: Pickel, V., Segal, M. (Eds.), The Synapse. Academic Press, Boston, pp. 301–342. https://doi.org/10.1016/B978-0-12-418675-0.00010-9

Harris, E.W., Cotman, C.W., 1986. Long-term potentiation of guinea pig mossy fiber responses is not blocked by N-methyl D-aspartate antagonists. Neurosci Lett 70, 132–137. https://doi.org/10.1016/0304-3940(86)90451-9

Harris, K.M., Stevens, J.K., 1989. Dendritic spines of CA 1 pyramidal cells in the rat hippocampus: serial electron microscopy with reference to their biophysical characteristics. J. Neurosci. 9, 2982–2997. https://doi.org/10.1523/JNEUROSCI.09-08-02982.1989

Harrison, C., Shao, H., Strutt, H., Strutt, D., 2020. Molecular mechanisms mediating asymmetric subcellular localisation of the core planar polarity pathway proteins.

Biochemical Society Transactions 48, 1297–1308. https://doi.org/10.1042/BST20190404

Hastings, N.B., Gould, E., 1999. Rapid extension of axons into the CA3 region by adult-generated granule cells. Journal of Comparative Neurology 413, 146–154. https://doi.org/10.1002/(SICI)1096-9861(19991011)413:1<146::AID-CNE10>3.0.CO;2-B

Hayashi, K., Kubo, K., Kitazawa, A., Nakajima, K., 2015. Cellular dynamics of neuronal migration in the hippocampus. Frontiers in Neuroscience 9.

Henderson, D.J., Conway, S.J., Greene, N.D., Gerrelli, D., Murdoch, J.N., Anderson, R.H., Copp, A.J., 2001. Cardiovascular defects associated with abnormalities in midline development in the Loop-tail mouse mutant. Circ Res 89, 6–12. https://doi.org/10.1161/hh1301.092497

Henderson, D.J., Long, D.A., Dean, C.H., 2018. Planar cell polarity in organ formation. Current Opinion in Cell Biology, Differentiation and disease 55, 96–103. https://doi.org/10.1016/j.ceb.2018.06.011

Hendricks, W.D., Westbrook, G.L., Schnell, E., 2019. Early detonation by sprouted mossy fibers enables aberrant dentate network activity. Proceedings of the National Academy of Sciences 116, 10994–10999. https://doi.org/10.1073/pnas.1821227116

Henze, D.A., McMahon, D.B.T., Harris, K.M., Barrionuevo, G., 2002a. Giant Miniature EPSCs at the Hippocampal Mossy Fiber to CA3 Pyramidal Cell Synapse Are Monoquantal. Journal of Neurophysiology 87, 15–29. https://doi.org/10.1152/jn.00394.2001

Henze, D.A., Urban, N.N., Barrionuevo, G., 2000. The multifarious hippocampal mossy fiber pathway: a review. Neuroscience 98, 407–427. https://doi.org/10.1016/S0306-4522(00)00146-9

Henze, D.A., Wittner, L., Buzsáki, G., 2002b. Single granule cells reliably discharge targets in the hippocampal CA3 network in vivo. Nat Neurosci 5, 790–795. https://doi.org/10.1038/nn887

Herranz-Pérez, V., Boletta, A., García-Verdugo, J.M., Álvarez-Buylla, A., 2015. Mechanosensory Genes Pkd1 and Pkd2 Contribute to the Planar Polarization of Brain Ventricular Epithelium. J Neurosci 35, 11153–11168. https://doi.org/10.1523/JNEUROSCI.0686-15.2015

Holahan, M.R., Rekart, J.L., Sandoval, J., Routtenberg, A., 2006. Spatial learning induces presynaptic structural remodeling in the hippocampal mossy fiber system of two rat strains. Hippocampus 16, 560–570. https://doi.org/10.1002/hipo.20185

Holahan, M.R., Routtenberg, A., 2011. Lidocaine injections targeting CA3 hippocampus impair long-term spatial memory and prevent learning-induced

mossy fiber remodeling. Hippocampus 21, 532–540. https://doi.org/10.1002/hipo.20786

Holtmaat, A.J.G.D., Gorter, J.A., Wit, J.D., Tolner, E.A., Spijker, S., Giger, R.J., Lopes da Silva, F.H., Verhaagen, J., 2003. Transient downregulation of sema3a mrna in a rat model for temporal lobe epilepsy: A novel molecular event potentially contributing to mossy fiber sprouting. Experimental Neurology 182, 142–150. https://doi.org/10.1016/S0014-4886(03)00035-9

Hsia, A.Y., Salin, P.A., Castillo, P.E., Aiba, A., Abeliovich, A., Tonegawa, S., Nicoll, R.A., 1995. Evidence against a role for metabotropic glutamate receptors in mossy fiber LTP: the use of mutant mice and pharmacological antagonists. Neuropharmacology 34, 1567–1572. https://doi.org/10.1016/0028-3908(95)00115-M

Hua, Z.L., Jeon, S., Caterina, M.J., Nathans, J., 2014. Frizzled3 is required for the development of multiple axon tracts in the mouse central nervous system. Proc Natl Acad Sci U S A 111, E3005–E3014. https://doi.org/10.1073/pnas.1406399111

Hughes, R.N., 2004. The value of spontaneous alternation behavior (SAB) as a test of retention in pharmacological investigations of memory. Neuroscience & Biobehavioral Reviews 28, 497–505. https://doi.org/10.1016/j.neubiorev.2004.06.006

Humphries, A.C., Narang, S., Mlodzik, M., 2020. Mutations associated with human neural tube defects display disrupted planar cell polarity in Drosophila. eLife 9, e53532. https://doi.org/10.7554/eLife.53532

Hunsaker, M.R., Kesner, R.P., 2013. The operation of pattern separation and pattern completion processes associated with different attributes or domains of memory. Neuroscience & Biobehavioral Reviews 37, 36–58. https://doi.org/10.1016/j.neubiorev.2012.09.014

Hunsaker, M.R., Tran, G.T., Kesner, R.P., 2009. A behavioral analysis of the role of CA3 and CA1 subcortical efferents during classical fear conditioning. Behav Neurosci 123, 624–630. https://doi.org/10.1037/a0015455

Hunt, D.L., Puente, N., Grandes, P., Castillo, P.E., 2013. Bidirectional NMDA receptor plasticity controls CA3 output and heterosynaptic metaplasticity. Nat Neurosci 16, 1049–1059. https://doi.org/10.1038/nn.3461

- I -

Iliescu, A., Gravel, M., Horth, C., Gros, P., 2014. Independent mutations at Arg181 and Arg274 of Vangl proteins that are associated with neural tube defects in humans decrease protein stability and impair membrane targeting. Biochemistry 53, 5356–5364. https://doi.org/10.1021/bi500400g

Imig, C., López-Murcia, F.J., Maus, L., García-Plaza, I.H., Mortensen, L.S., Schwark, M., Schwarze, V., Angibaud, J., Nägerl, U.V., Taschenberger, H., Brose, N., Cooper, B.H., 2020. Ultrastructural Imaging of Activity-Dependent Synaptic Membrane-Trafficking Events in Cultured Brain Slices. Neuron 108, 843-860.e8. https://doi.org/10.1016/j.neuron.2020.09.004

Ito, I., 1991. Roles of glutamate receptors in long-term potentiation at hippocampal mossy fiber synapses. NeuroReport 2, 333–336.

Ivanco, T.L., Greenough, W.T., 2002. Altered mossy fiber distributions in adult Fmr1 (FVB) knockout mice. Hippocampus 12, 47–54. https://doi.org/10.1002/hipo.10004

Iwata, T., Hevner, R.F., 2009. Fibroblast growth factor signaling in development of the cerebral cortex. Development, Growth & Differentiation 51, 299–323. https://doi.org/10.1111/j.1440-169X.2009.01104.x

- J -

Jarjour, A.A., Velichkova, A.N., Boyd, A., Lord, K.M., Torsney, C., Henderson, D.J., ffrench-Constant, C., 2020. The formation of paranodal spirals at the ends of CNS myelin sheaths requires the planar polarity protein Vangl2. Glia n/a. https://doi.org/10.1002/glia.23809

Jessen, J.R., Topczewski, J., Bingham, S., Sepich, D.S., Marlow, F., Chandrasekhar, A., Solnica-Krezel, L., 2002. Zebrafish trilobite identifies new roles for Strabismus in gastrulation and neuronal movements. Nat Cell Biol 4, 610–615. https://doi.org/10.1038/ncb828

Jessen, T.N., Jessen, J.R., 2019. VANGL2 protein stability is regulated by integrin αv and the extracellular matrix. Exp. Cell Res. 374, 128–139. https://doi.org/10.1016/j.yexcr.2018.11.017

Jin, S.-X., Liu, L., Li, S., Meunier, A.L., Selkoe, D.J., 2022. Aβ oligomers from human brain impair mossy fiber LTP in CA3 of hippocampus, but activating cAMP-PKA and cGMP-PKG prevents this. Neurobiol Dis 172, 105816. https://doi.org/10.1016/j.nbd.2022.105816

Jin, X., 2016. The role of neurogenesis during development and in the adult brain. European Journal of Neuroscience 44, 2291–2299. https://doi.org/10.1111/ejn.13251

Jonas, P., Major, G., Sakmann, B., 1993a. Quantal components of unitary EPSCs at the mossy fibre synapse on CA3 pyramidal cells of rat hippocampus. J Physiol 472, 615–663.

Jonas, P., Major, G., Sakmann, B., 1993b. Quantal components of unitary EPSCs at the mossy fibre synapse on CA3 pyramidal cells of rat hippocampus. J Physiol 472, 615–663.

Jones, C., Qian, D., Kim, S.M., Li, S., Ren, D., Knapp, L., Sprinzak, D., Avraham, K.B., Matsuzaki, F., Chi, F., Chen, P., 2014. Ankrd6 is a mammalian functional homolog of Drosophila planar cell polarity gene diego and regulates coordinated cellular orientation in the mouse inner ear. Dev Biol 395, 62–72. https://doi.org/10.1016/j.ydbio.2014.08.029

- K -

Kakegawa, W., Tsuzuki, K., Yoshida, Y., Kameyama, K., Ozawa, S., 2004. Input- and subunit-specific AMPA receptor trafficking underlying long-term potentiation at hippocampal CA3 synapses. European Journal of Neuroscience 20, 101–110. https://doi.org/10.1111/j.1460-9568.2004.03461.x

Kamimura, K., Maeda, N., 2021. Glypicans and Heparan Sulfate in Synaptic Development, Neural Plasticity, and Neurological Disorders. Front Neural Circuits 15. https://doi.org/10.3389/fncir.2021.595596

Kamiya, H., Ozawa, S., 2000. Kainate receptor-mediated presynaptic inhibition at the mouse hippocampal mossy fibre synapse. The Journal of Physiology 523, 653–665. https://doi.org/10.1111/j.1469-7793.2000.t01-1-00653.x

Kerr, A.M., Jonas, P., 2008. The Two Sides of Hippocampal Mossy Fiber Plasticity. Neuron 57, 5–7. https://doi.org/10.1016/j.neuron.2007.12.015

Kesner, R., 2013. A process analysis of the CA3 subregion of the hippocampus. Frontiers in Cellular Neuroscience 7.

Kesner, R.P., 2013. An analysis of the dentate gyrus function. Behavioural Brain Research, SI:Medial Temporal Lobe Memory Networks 254, 1–7. https://doi.org/10.1016/j.bbr.2013.01.012

Kesner, R.P., Novak, J.M., 1982. Serial Position Curve in Rats: Role of the Dorsal Hippocampus. Science 218, 173–175. https://doi.org/10.1126/science.7123228

Khalaf-Nazzal, R., Francis, F., 2013. Hippocampal development – Old and new findings. Neuroscience 248, 225–242. https://doi.org/10.1016/j.neuroscience.2013.05.061

Kibar, Z., Salem, S., Bosoi, C.M., Pauwels, E., De Marco, P., Merello, E., Bassuk, A.G., Capra, V., Gros, P., 2011. Contribution of VANGL2 mutations to isolated neural tube defects. Clin Genet 80, 76–82. https://doi.org/10.1111/j.1399-0004.2010.01515.x

Kibar, Z., Vogan, K.J., Groulx, N., Justice, M.J., Underhill, D.A., Gros, P., 2001. Ltap , a mammalian homolog of Drosophila Strabismus/Van Gogh , is altered in the mouse neural tube mutant Loop-tail. Nature Genetics 28, 251–255. https://doi.org/10.1038/90081

Kienzler, F., Norwood, B.A., Sloviter, R.S., 2009. Hippocampal injury, atrophy, synaptic reorganization, and epileptogenesis after perforant pathway stimulation-

induced status epilepticus in the mouse. Journal of Comparative Neurology 515, 181–196. https://doi.org/10.1002/cne.22059

Killick, R., Ribe, E.M., Al-Shawi, R., Malik, B., Hooper, C., Fernandes, C., Dobson, R., Nolan, P.M., Lourdusamy, A., Furney, S., Lin, K., Breen, G., Wroe, R., To, A.W.M., Leroy, K., Causevic, M., Usardi, A., Robinson, M., Noble, W., Williamson, R., Lunnon, K., Kellie, S., Reynolds, C.H., Bazenet, C., Hodges, A., Brion, J.-P., Stephenson, J., Paul Simons, J., Lovestone, S., 2014. Clusterin regulates β-amyloid toxicity via Dickkopf-1-driven induction of the wnt–PCP–JNK pathway. Mol Psychiatry 19, 88–98. https://doi.org/10.1038/mp.2012.163

Klein, R., 2009. Bidirectional modulation of synaptic functions by Eph/ephrin signaling. Nat Neurosci 12, 15–20. https://doi.org/10.1038/nn.2231

Knaus, P., Marquèze-Pouey, B., Scherer, H., Betzt, H., 1990. Synaptoporin, a novel putative channel protein of synaptic vesicles. Neuron 5, 453–462. https://doi.org/10.1016/0896-6273(90)90084-S

Knierim, J.J., 2015. The hippocampus. Current Biology 25, R1116–R1121. https://doi.org/10.1016/j.cub.2015.10.049

Knoth, R., Singec, I., Ditter, M., Pantazis, G., Capetian, P., Meyer, R.P., Horvat, V., Volk, B., Kempermann, G., 2010. Murine Features of Neurogenesis in the Human Hippocampus across the Lifespan from 0 to 100 Years. PLOS ONE 5, e8809. https://doi.org/10.1371/journal.pone.0008809

Kobayashi, K., 2009. Targeting the Hippocampal Mossy Fiber Synapse for the Treatment of Psychiatric Disorders. Mol Neurobiol 39, 24. https://doi.org/10.1007/s12035-008-8049-5

Kobayashi, K., Manabe, T., Takahashi, T., 1996. Presynaptic Long-Term Depression at the Hippocampal Mossy Fiber—CA3 Synapse. Science 273, 648–650. https://doi.org/10.1126/science.273.5275.648

Koehl, M., Ladevèze, E., Montcouquiol, M., Abrous, D.N., 2022. Vangl2, a Core Component of the WNT/PCP Pathway, Regulates Adult Hippocampal Neurogenesis and Age-Related Decline in Cognitive Flexibility. Frontiers in Aging Neuroscience 14.

Kolomeets, N.S., Orlovskaya, D.D., Rachmanova, V.I., Uranova, N.A., 2005. Ultrastructural alterations in hippocampal mossy fiber synapses in schizophrenia: A postmortem morphometric study. Synapse 57, 47–55. https://doi.org/10.1002/syn.20153

Kolomeets, N.S., Orlovskaya, D.D., Uranova, N.A., 2007. Decreased numerical density of CA3 hippocampal mossy fiber synapses in schizophrenia. Synapse 61, 615–621. https://doi.org/10.1002/syn.20405

Kovac, S., Walker, M.C., 2013. Neuropeptides in epilepsy. Neuropeptides 47, 467–475. https://doi.org/10.1016/j.npep.2013.10.015

Koyama, R., Yamada, M.K., Nishiyama, N., Matsuki, N., Ikegaya, Y., 2004. Developmental switch in axon guidance modes of hippocampal mossy fibers in vitro. Developmental Biology 267, 29–42. https://doi.org/10.1016/j.ydbio.2003.11.008

Kozareva, D.A., Cryan, J.F., Nolan, Y.M., 2019. Born this way: Hippocampal neurogenesis across the lifespan. Aging Cell 18, e13007. https://doi.org/10.1111/acel.13007

Kraeuter, A.-K., Guest, P.C., Sarnyai, Z., 2019. The Y-Maze for Assessment of Spatial Working and Reference Memory in Mice. Methods Mol Biol 1916, 105–111. https://doi.org/10.1007/978-1-4939-8994-2_10

Krzisch, M., Fülling, C., Jabinet, L., Armida, J., Gebara, E., Cassé, F., Habbas, S., Volterra, A., Hornung, J.-P., Toni, N., 2017. Synaptic Adhesion Molecules Regulate the Integration of New Granule Neurons in the Postnatal Mouse Hippocampus and their Impact on Spatial Memory. Cerebral Cortex 27, 4048–4059. https://doi.org/10.1093/cercor/bhw217

Kuhn, H., Dickinson-Anson, H., Gage, F., 1996. Neurogenesis in the dentate gyrus of the adult rat: age-related decrease of neuronal progenitor proliferation. J Neurosci 16, 2027–2033. https://doi.org/10.1523/JNEUROSCI.16-06-02027.1996

Kumar, A., Foster, T.C., 2019. Alteration in NMDA Receptor Mediated Glutamatergic Neurotransmission in the Hippocampus During Senescence. Neurochem Res 44, 38–48. https://doi.org/10.1007/s11064-018-2634-4

Kvajo, M., McKellar, H., Drew, L.J., Lepagnol-Bestel, A.-M., Xiao, L., Levy, R.J., Blazeski, R., Arguello, P.A., Lacefield, C.O., Mason, C.A., Simonneau, M., O'Donnell, J.M., MacDermott, A.B., Karayiorgou, M., Gogos, J.A., 2011. Altered axonal targeting and short-term plasticity in the hippocampus of Disc1 mutant mice. Proc Natl Acad Sci U S A 108, E1349–E1358. https://doi.org/10.1073/pnas.1114113108

Kwon, H.-B., Castillo, P.E., 2008. Role of Glutamate Autoreceptors at Hippocampal Mossy Fiber Synapses. Neuron 60, 1082–1094. https://doi.org/10.1016/j.neuron.2008.10.045

- L -

Labat-de-Hoz, L., Alonso, M.A., 2021. Formins in Human Disease. Cells 10, 2554. https://doi.org/10.3390/cells10102554

Lake, B.B., Sokol, S.Y., 2009. Strabismus regulates asymmetric cell divisions and cell fate determination in the mouse brain. J Cell Biol 185, 59–66. https://doi.org/10.1083/jcb.200807073

Lanore, F., Labrousse, V.F., Szabo, Z., Normand, E., Blanchet, C., Mulle, C., 2012. Deficits in Morphofunctional Maturation of Hippocampal Mossy Fiber Synapses

in a Mouse Model of Intellectual Disability. J. Neurosci. 32, 17882–17893. https://doi.org/10.1523/JNEUROSCI.2049-12.2012

Lau, E.O.-C., Damiani, D., Chehade, G., Ruiz-Reig, N., Saade, R., Jossin, Y., Aittaleb, M., Schakman, O., Tajeddine, N., Gailly, P., Tissir, F., 2021. DIAPH3 deficiency links microtubules to mitotic errors, defective neurogenesis, and brain dysfunction. eLife 10, e61974. https://doi.org/10.7554/eLife.61974

Lee, A.-R., Kim, J.-H., Cho, E., Kim, M., Park, M., 2017. Dorsal and Ventral Hippocampus Differentiate in Functional Pathways and Differentially Associate with Neurological Disease-Related Genes during Postnatal Development. Front Mol Neurosci 10, 331. https://doi.org/10.3389/fnmol.2017.00331

Lee, C.-H., Lee, I., 2020. Impairment of Pattern Separation of Ambiguous Scenes by Single Units in the CA3 in the Absence of the Dentate Gyrus. J. Neurosci. 40, 3576–3590. https://doi.org/10.1523/JNEUROSCI.2596-19.2020

Lee, J., Andreeva, A., Sipe, C.W., Liu, L., Cheng, A., Lu, X., 2012. PTK7 Regulates Myosin II Activity to Orient Planar Polarity in the Mammalian Auditory Epithelium. Current Biology 22, 956–966. https://doi.org/10.1016/j.cub.2012.03.068

Lee, S.H., Kim, K.-R., Ryu, S.-Y., Son, S., Hong, H.S., Mook-Jung, I., Lee, S.-H., Ho, W.-K., 2012. Impaired Short-Term Plasticity in Mossy Fiber Synapses Caused by Mitochondrial Dysfunction of Dentate Granule Cells Is the Earliest Synaptic Deficit in a Mouse Model of Alzheimer's Disease. J Neurosci 32, 5953–5963. https://doi.org/10.1523/JNEUROSCI.0465-12.2012

Lee, S.H., Lutz, D., Drexler, D., Frotscher, M., Shen, J., 2020. Differential modulation of short-term plasticity at hippocampal mossy fiber and Schaffer collateral synapses by mitochondrial Ca2+. PLOS ONE 15, e0240610. https://doi.org/10.1371/journal.pone.0240610

Lee, S.M., Tole, S., Grove, E., McMahon, A.P., 2000. A local Wnt-3a signal is required for development of the mammalian hippocampus. Development 127, 457–467. https://doi.org/10.1242/dev.127.3.457

Lei, S., McBain, C.J., 2002. Distinct NMDA Receptors Provide Differential Modes of Transmission at Mossy Fiber-Interneuron Synapses. Neuron 33, 921–933. https://doi.org/10.1016/S0896-6273(02)00608-6

Lei, Y.-P., Zhang, T., Li, H., Wu, B.-L., Jin, L., Wang, H.-Y., 2010. VANGL2 Mutations in Human Cranial Neural-Tube Defects. New England Journal of Medicine 362, 2232–2235. https://doi.org/10.1056/NEJMc0910820

Leung, V., Iliescu, A., Jolicoeur, C., Gravel, M., Apuzzo, S., Torban, E., Cayouette, M., Gros, P., 2016. The planar cell polarity protein Vangl2 is required for retinal axon guidance. Dev Neurobiol 76, 150–165. https://doi.org/10.1002/dneu.22305

Lin, X., Amalraj, M., Blanton, C., Avila, B., Holmes, T.C., Nitz, D.A., Xu, X., 2021. Noncanonical projections to the hippocampal CA3 regulate spatial learning and memory by modulating the feedforward hippocampal trisynaptic pathway. PLOS Biology 19, e3001127. https://doi.org/10.1371/journal.pbio.3001127

Lindqvist, M., Horn, Z., Bryja, V., Schulte, G., Papachristou, P., Ajima, R., Dyberg, C., Arenas, E., Yamaguchi, T.P., Lagercrantz, H., Ringstedt, T., 2010. Vang-like protein 2 and Rac1 interact to regulate adherens junctions. J Cell Sci 123, 472–483. https://doi.org/10.1242/jcs.048074

Lituma, P.J., Kwon, H.-B., Alviña, K., Luján, R., Castillo, P.E., 2021. Presynaptic NMDA receptors facilitate short-term plasticity and BDNF release at hippocampal mossy fiber synapses. eLife 10, e66612. https://doi.org/10.7554/eLife.66612

Lods, M., Pacary, E., Mazier, W., Farrugia, F., Mortessagne, P., Masachs, N., Charrier, V., Massa, F., Cota, D., Ferreira, G., Abrous, D.N., Tronel, S., 2021. Adult-born neurons immature during learning are necessary for remote memory reconsolidation in rats. Nat Commun 12, 1778. https://doi.org/10.1038/s41467-021-22069-4

Lonart, G., Janz, R., Johnson, K.M., Südhof, T.C., 1998. Mechanism of Action of rab3A in Mossy Fiber LTP. Neuron 21, 1141–1150. https://doi.org/10.1016/S0896-6273(00)80631-5

Longo, B., Covolan, L., Chadi, G., Mello, L.E.A.M., 2003. Sprouting of mossy fibers and the vacating of postsynaptic targets in the inner molecular layer of the dentate gyrus. Experimental Neurology 181, 57–67. https://doi.org/10.1016/S0014-4886(02)00046-8

Love, A.M., Prince, D.J., Jessen, J.R., 2018. Vangl2-dependent regulation of membrane protrusions and directed migration requires a fibronectin extracellular matrix. Development 145. https://doi.org/10.1242/dev.165472

Lu, Q., Adler, P.N., 2015. The diaphanous Gene of Drosophila Interacts Antagonistically with multiple wing hairs and Plays a Key Role in Wing Hair Morphogenesis. PLOS ONE 10, e0115623. https://doi.org/10.1371/journal.pone.0115623

Lu, X., Borchers, A.G.M., Jolicoeur, C., Rayburn, H., Baker, J.C., Tessier-Lavigne, M., 2004. PTK7/CCK-4 is a novel regulator of planar cell polarity in vertebrates. Nature 430, 93–98. https://doi.org/10.1038/nature02677

Luján, R., Nusser, Z., Roberts, J.D.B., Shigemoto, R., Somogyi, P., 1996. Perisynaptic Location of Metabotropic Glutamate Receptors mGluR1 and mGluR5 on Dendrites and Dendritic Spines in the Rat Hippocampus. European Journal of Neuroscience 8, 1488–1500. https://doi.org/10.1111/j.1460-9568.1996.tb01611.x

Lyuksyutova, A.I., Lu, C.-C., Milanesio, N., King, L.A., Guo, N., Wang, Y., Nathans, J., Tessier-Lavigne, M., Zou, Y., 2003. Anterior-posterior guidance of commissural axons by Wnt-frizzled signaling. Science 302, 1984–1988. https://doi.org/10.1126/science.1089610

- M -

Ma, K.-G., Hu, H.-B., Zhou, J.-S., Ji, C., Yan, Q.-S., Peng, S.-M., Ren, L.-D., Yang, B.-N., Xiao, X.-L., Ma, Y.-B., Wu, F., Si, K.-W., Wu, X.-L., Liu, J.-X., 2022. Neuronal Glypican4 promotes mossy fiber sprouting through the mTOR pathway after pilocarpine-induced status epilepticus in mice. Experimental Neurology 347, 113918. https://doi.org/10.1016/j.expneurol.2021.113918

Maingret, V., Barthet, G., Deforges, S., Jiang, N., Mulle, C., Amédée, T., 2017. PGE2-EP3 signaling pathway impairs hippocampal presynaptic long-term plasticity in a mouse model of Alzheimer's disease. Neurobiology of Aging 50, 13–24. https://doi.org/10.1016/j.neurobiolaging.2016.10.012

Manzoni, O.J., Weisskopf, M.G., Nicoll, R.A., 1994. MCPG antagonizes metabotropic glutamate receptors but not long-term potentiation in the hippocampus. Eur J Neurosci 6, 1050–1054. https://doi.org/10.1111/j.1460-9568.1994.tb00599.x

Marighetto, A., Etchamendy, N., Touzani, K., Torrea, C.C., Yee, B.K., Rawlins, J.N., Jaffard, R., 1999. Knowing which and knowing what: a potential mouse model for age-related human declarative memory decline. Eur J Neurosci 11, 3312–3322. https://doi.org/10.1046/j.1460-9568.1999.00741.x

Marlow, F., Zwartkruis, F., Malicki, J., Neuhauss, S.C., Abbas, L., Weaver, M., Driever, W., Solnica-Krezel, L., 1998. Functional interactions of genes mediating convergent extension, knypek and trilobite, during the partitioning of the eye primordium in zebrafish. Dev Biol 203, 382–399. https://doi.org/10.1006/dbio.1998.9032

Martin, E.A., Muralidhar, S., Wang, Z., Cervantes, D.C., Basu, R., Taylor, M.R., Hunter, J., Cutforth, T., Wilke, S.A., Ghosh, A., Williams, M.E., 2015. The intellectual disability gene Kirrel3 regulates target-specific mossy fiber synapse development in the hippocampus. eLife 4, e09395. https://doi.org/10.7554/eLife.09395

Martin, E.A., Woodruff, D., Rawson, R.L., Williams, M.E., 2017. Examining Hippocampal Mossy Fiber Synapses by 3D Electron Microscopy in Wildtype and Kirrel3 Knockout Mice. eNeuro 4. https://doi.org/10.1523/ENEURO.0088-17.2017

Martinez, S., Scerbo, P., Giordano, M., Daulat, A.M., Lhoumeau, A.-C., Thomé, V., Kodjabachian, L., Borg, J.-P., 2015. The PTK7 and ROR2 Protein Receptors Interact in the Vertebrate WNT/Planar Cell Polarity (PCP) Pathway. J Biol Chem 290, 30562–30572. https://doi.org/10.1074/jbc.M115.697615

Maruo, T., Mandai, K., Takai, Y., Mori, M., 2016. Activity-dependent alteration of the morphology of a hippocampal giant synapse. Molecular and Cellular Neuroscience 71, 25–33. https://doi.org/10.1016/j.mcn.2015.12.005

Mashima, R., Okuyama, T., Ohira, M., 2022. Physiology and Pathophysiology of Heparan Sulfate in Animal Models: Its Biosynthesis and Degradation. Int J Mol Sci 23, 1963. https://doi.org/10.3390/ijms23041963

Maus, L., Lee, C., Altas, B., Sertel, S.M., Weyand, K., Rizzoli, S.O., Rhee, J., Brose, N., Imig, C., Cooper, B.H., 2020. Ultrastructural Correlates of Presynaptic Functional Heterogeneity in Hippocampal Synapses. Cell Rep 30, 3632-3643.e8. https://doi.org/10.1016/j.celrep.2020.02.083

McBain, C.J., 2008. Differential mechanisms of transmission and plasticity at mossy fiber synapses. Prog Brain Res 169, 225–240. https://doi.org/10.1016/S0079-6123(07)00013-1

McCarthy, J.B., Walker, M., Pierce, J., Camp, P., White, J.D., 1998. Biosynthesis and Metabolism of Native and Oxidized Neuropeptide Y in the Hippocampal Mossy Fiber System. Journal of Neurochemistry 70, 1950–1963. https://doi.org/10.1046/j.1471-4159.1998.70051950.x

McFadden, K., Minshew, N.J., 2013. Evidence for dysregulation of axonal growth and guidance in the etiology of ASD. Front Hum Neurosci 7, 671. https://doi.org/10.3389/fnhum.2013.00671

McGonigal, R., Tabatadze, N., Routtenberg, A., 2012. Selective presynaptic terminal remodeling induced by spatial, but not cued, learning: a quantitative confocal study. Hippocampus 22, 1242–1255. https://doi.org/10.1002/hipo.20998

McLamb, R.L., Mundy, W.R., Tilson, H.A., 1988. Intradentate colchicine disrupts the acquisition and performance of a working memory task in the radial arm maze. Neurotoxicology 9, 521–528.

McNaughton, B.L., Morris, R.G.M., 1987. Hippocampal synaptic enhancement and information storage within a distributed memory system. Trends in Neurosciences 10, 408–415. https://doi.org/10.1016/0166-2236(87)90011-7

Merkle, F.T., Tramontin, A.D., García-Verdugo, J.M., Alvarez-Buylla, A., 2004. Radial glia give rise to adult neural stem cells in the subventricular zone. Proc Natl Acad Sci U S A 101, 17528–17532. https://doi.org/10.1073/pnas.0407893101

Merte, J., Jensen, D., Wright, K., Sarsfield, S., Wang, Y., Schekman, R., Ginty, D.D., 2010. Sec24b selectively sorts Vangl2 to regulate planar cell polarity during neural tube closure. Nat Cell Biol 12, 41–46; sup pp 1-8. https://doi.org/10.1038/ncb2002

Micheau, J., Vimeney, A., Normand, E., Mulle, C., Riedel, G., 2014. Impaired hippocampus-dependent spatial flexibility and sociability represent autism-like phenotypes in GluK2 mice. Hippocampus 24, 1059–1069. https://doi.org/10.1002/hipo.22290

Mineur, Y.S., Sluyter, F., de Wit, S., Oostra, B.A., Crusio, W.E., 2002. Behavioral and neuroanatomical characterization of the Fmr1 knockout mouse. Hippocampus 12, 39–46. https://doi.org/10.1002/hipo.10005

Mingaud, F., Mormede, C., Etchamendy, N., Mons, N., Niedergang, B., Wietrzych, M., Pallet, V., Jaffard, R., Krezel, W., Higueret, P., Marighetto, A., 2008. Retinoid Hyposignaling Contributes to Aging-Related Decline in Hippocampal Function in Short-Term/Working Memory Organization and Long-Term Declarative Memory Encoding in Mice. J Neurosci 28, 279–291. https://doi.org/10.1523/JNEUROSCI.4065-07.2008

Mirza, F.J., Zahid, S., 2017. The Role of Synapsins in Neurological Disorders. Neurosci Bull 34, 349–358. https://doi.org/10.1007/s12264-017-0201-7

Mirzadeh, Z., Han, Y.-G., Soriano-Navarro, M., García-Verdugo, J.M., Alvarez-Buylla, A., 2010. Cilia Organize Ependymal Planar Polarity. J Neurosci 30, 2600–2610. https://doi.org/10.1523/JNEUROSCI.3744-09.2010

Mizoguchi, A., Nakanishi, H., Kimura, K., Matsubara, K., Ozaki-Kuroda, K., Katata, T., Honda, T., Kiyohara, Y., Heo, K., Higashi, M., Tsutsumi, T., Sonoda, S., Ide, C., Takai, Y., 2002. Nectin. J Cell Biol 156, 555–565. https://doi.org/10.1083/jcb.200103113

Mizutani, K., Miyata, M., Shiotani, H., Kameyama, T., Takai, Y., 2021. Nectins and Nectin-like molecules in synapse formation and involvement in neurological diseases. Molecular and Cellular Neuroscience 115, 103653. https://doi.org/10.1016/j.mcn.2021.103653

Monday, H.R., Kharod, S.C., Yoon, Y.J., Singer, R.H., Castillo, P.E., 2022. Presynaptic FMRP and local protein synthesis support structural and functional plasticity of glutamatergic axon terminals. Neuron. https://doi.org/10.1016/j.neuron.2022.05.024

Montcouquiol, M., Jones, J.M., Sans, N., 2008. Detection of Planar Polarity Proteins in Mammalian Cochlea, in: Vincan, E. (Ed.), Wnt Signaling: Pathway Methods and Mammalian Models, Methods in Molecular Biology™. Humana Press, Totowa, NJ, pp. 207–219. https://doi.org/10.1007/978-1-59745-249-6_16

Montcouquiol, M., Kelley, M.W., 2020. Development and Patterning of the Cochlea: From Convergent Extension to Planar Polarity. Cold Spring Harb Perspect Med 10, a033266. https://doi.org/10.1101/cshperspect.a033266

Montcouquiol, M., Rachel, R.A., Lanford, P.J., Copeland, N.G., Jenkins, N.A., Kelley, M.W., 2003. Identification of Vangl2 and Scrb1 as planar polarity genes in mammals. Nature 423, 173–177. https://doi.org/10.1038/nature01618

Montcouquiol, M., Sans, N., Huss, D., Kach, J., Dickman, J.D., Forge, A., Rachel, R.A., Copeland, N.G., Jenkins, N.A., Bogani, D., Murdoch, J., Warchol, M.E., Wenthold, R.J., Kelley, M.W., 2006. Asymmetric Localization of Vangl2 and Fz3 Indicate Novel Mechanisms for Planar Cell Polarity in Mammals. J Neurosci 26, 5265–5275. https://doi.org/10.1523/JNEUROSCI.4680-05.2006

Moon, R.T., Campbell, R.M., Christian, J.L., McGrew, L.L., Shih, J., Fraser, S., 1993. Xwnt-5A: a maternal Wnt that affects morphogenetic movements after overexpression in embryos of Xenopus laevis. Development 119, 97–111. https://doi.org/10.1242/dev.119.1.97

Moreau, M.M., Piguel, N., Papouin, T., Koehl, M., Durand, C.M., Rubio, M.E., Loll, F., Richard, E.M., Mazzocco, C., Racca, C., Oliet, S.H.R., Nora Abrous, D., Montcouquiol, M., Sans, N., 2010. The Planar Polarity Protein Scribble1 Is Essential for Neuronal Plasticity and Brain Function. J Neurosci 30, 9738–9752. https://doi.org/10.1523/JNEUROSCI.6007-09.2010

Moser, M.-B., Moser, E.I., 1998. Functional differentiation in the hippocampus. Hippocampus 8, 608–619. https://doi.org/10.1002/(SICI)1098-1063(1998)8:6<608::AID-HIPO3>3.0.CO;2-7

Moser, M.B., Moser, E.I., Forrest, E., Andersen, P., Morris, R.G., 1995. Spatial learning with a minislab in the dorsal hippocampus. Proc Natl Acad Sci U S A 92, 9697–9701. https://doi.org/10.1073/pnas.92.21.9697

Mulle, C., Sailer, A., Pérez-Otaño, I., Dickinson-Anson, H., Castillo, P.E., Bureau, I., Maron, C., Gage, F.H., Mann, J.R., Bettler, B., Heinemann, S.F., 1998. Altered synaptic physiology and reduced susceptibility to kainate-induced seizures in GluR6-deficient mice. Nature 392, 601–605. https://doi.org/10.1038/33408

Muñoz, R., Moreno, M., Oliva, C., Orbenes, C., Larraín, J., 2006. Syndecan-4 regulates non-canonical Wnt signalling and is essential for convergent and extension movements in Xenopus embryos. Nat Cell Biol 8, 492–500. https://doi.org/10.1038/ncb1399

Murdoch, J.N., Doudney, K., Paternotte, C., Copp, A.J., Stanier, P., 2001. Severe neural tube defects in the loop-tail mouse result from mutation of Lpp1, a novel gene involved in floor plate specification. Hum Mol Genet 10, 2593–2601. https://doi.org/10.1093/hmg/10.22.2593

Murray, K.D., Liu, X.-B., King, A.N., Luu, J.D., Cheng, H.-J., 2020. Age-Related Changes in Synaptic Plasticity Associated with Mossy Fiber Terminal Integration during Adult Neurogenesis. eNeuro 7, ENEURO.0030-20.2020. https://doi.org/10.1523/ENEURO.0030-20.2020

- N -

Nadal, L., Coupé, P., Helmer, C., Manjon, J.V., Amieva, H., Tison, F., Dartigues, J.-F., Catheline, G., Planche, V., 2020. Differential annualized rates of hippocampal subfields atrophy in aging and future Alzheimer's clinical syndrome. Neurobiology of Aging 90, 75–83. https://doi.org/10.1016/j.neurobiolaging.2020.01.011

Nagaoka, T., Furuse, M., Ohtsuka, T., Tsuchida, K., Kishi, M., 2019. Vangl2 interaction plays a role in the proteasomal degradation of Prickle2. Sci Rep 9. https://doi.org/10.1038/s41598-019-39642-z

Nagaoka, T., Inutsuka, A., Begum, K., Hafiz, K. musabbir bin, Kishi, M., 2014a. Vangl2 Regulates E-Cadherin in Epithelial Cells. Sci Rep 4, 6940. https://doi.org/10.1038/srep06940

Nagaoka, T., Kishi, M., 2016. The planar cell polarity protein Vangl2 is involved in postsynaptic compartmentalization. Neuroscience Letters 612, 251–255. https://doi.org/10.1016/j.neulet.2015.12.009

Nagaoka, T., Ohashi, R., Inutsuka, A., Sakai, S., Fujisawa, N., Yokoyama, M., Huang, Y.H., Igarashi, M., Kishi, M., 2014b. The Wnt/Planar Cell Polarity Pathway Component Vangl2 Induces Synapse Formation through Direct Control of N-Cadherin. Cell Reports 6, 916–927. https://doi.org/10.1016/j.celrep.2014.01.044

Nagaoka, T., Tabuchi, K., Kishi, M., 2015. PDZ interaction of Vangl2 links PSD-95 and Prickle2 but plays only a limited role in the synaptic localisation of Vangl2. Sci Rep 5, 12916. https://doi.org/10.1038/srep12916

Nakahira, E., Yuasa, S., 2005. Neuronal generation, migration, and differentiation in the mouse hippocampal primoridium as revealed by enhanced green fluorescent protein gene transfer by means of in utero electroporation. J. Comp. Neurol. 483, 329–340. https://doi.org/10.1002/cne.20441

Nakashiba, T., Cushman, J.D., Pelkey, K.A., Renaudineau, S., Buhl, D.L., McHugh, T.J., Barrera, V.R., Chittajallu, R., Iwamoto, K.S., McBain, C.J., Fanselow, M.S., Tonegawa, S., 2012. Young Dentate Granule Cells Mediate Pattern Separation whereas Old Granule Cells Contribute to Pattern Completion. Cell 149, 188–201. https://doi.org/10.1016/j.cell.2012.01.046

Navajas Acedo, J., Voas, M.G., Alexander, R., Woolley, T., Unruh, J.R., Li, H., Moens, C., Piotrowski, T., 2019. PCP and Wnt pathway components act in parallel during zebrafish mechanosensory hair cell orientation. Nat Commun 10, 3993. https://doi.org/10.1038/s41467-019-12005-y

Newman, E.L., Hasselmo, M.E., 2014. CA3 Sees the Big Picture while Dentate Gyrus Splits Hairs. Neuron 81, 226–228. https://doi.org/10.1016/j.neuron.2014.01.004

Nicoll, R.A., Schmitz, D., 2005. Synaptic plasticity at hippocampal mossy fibre synapses. Nature Reviews Neuroscience 6, 863–876. https://doi.org/10.1038/nrn1786

Nobis, L., Manohar, S.G., Smith, S.M., Alfaro-Almagro, F., Jenkinson, M., Mackay, C.E., Husain, M., 2019. Hippocampal volume across age: Nomograms derived from over 19,700 people in UK Biobank. Neuroimage Clin 23, 101904. https://doi.org/10.1016/j.nicl.2019.101904

Nusse, R., 2005. Wnt signaling in disease and in development. Cell Res 15, 28–32. https://doi.org/10.1038/sj.cr.7290260

Nusse, R., Clevers, H., 2017. Wnt/β-Catenin Signaling, Disease, and Emerging Therapeutic Modalities. Cell 169, 985–999. https://doi.org/10.1016/j.cell.2017.05.016

Nychyk, O., Galea, G.L., Molè, M., Savery, D., Greene, N.D.E., Stanier, P., Copp, A.J., 2022. Vangl2–environment interaction causes severe neural tube defects, without abnormal neuroepithelial convergent extension. Dis Model Mech 15, dmm049194. https://doi.org/10.1242/dmm.049194

- O -

Ohata, S., Álvarez-Buylla, A., 2016. Planar organization of multiciliated ependymal (E1) cells in the brain ventricular epithelium. Trends Neurosci 39, 543–551. https://doi.org/10.1016/j.tins.2016.05.004

Ohkawara, B., Yamamoto, T.S., Tada, M., Ueno, N., 2003. Role of glypican 4 in the regulation of convergent extension movements during gastrulation in *Xenopus laevis*. Development 130, 2129–2138. https://doi.org/10.1242/dev.00435

Ojo, B., Davies, H., Rezaie, P., Gabbott, P., Colyer, F., Kraev, I., Stewart, M.G., 2013. Age-Induced Loss of Mossy Fibre Synapses on CA3 Thorns in the CA3 Stratum Lucidum. Neuroscience Journal 2013, e839535. https://doi.org/10.1155/2013/839535

O'Keefe, J., Dostrovsky, J., 1971. The hippocampus as a spatial map. Preliminary evidence from unit activity in the freely-moving rat. Brain Res 34, 171–175. https://doi.org/10.1016/0006-8993(71)90358-1

Okerlund, N.D., Stanley, R.E., Cheyette, B.N.R., 2016. The Planar Cell Polarity Transmembrane Protein Vangl2 Promotes Dendrite, Spine and Glutamatergic Synapse Formation in the Mammalian Forebrain. MNP 2, 107–114. https://doi.org/10.1159/000446778

Olson, I.R., Moore, K.S., Stark, M., Chatterjee, A., 2006a. Visual working memory is impaired when the medial temporal lobe is damaged. J Cogn Neurosci 18, 1087–1097. https://doi.org/10.1162/jocn.2006.18.7.1087

Olson, I.R., Page, K., Moore, K.S., Chatterjee, A., Verfaellie, M., 2006b. Working memory for conjunctions relies on the medial temporal lobe. J Neurosci 26, 4596–4601. https://doi.org/10.1523/JNEUROSCI.1923-05.2006

Olton, D.S., Becker, J.T., Handelmann, G.E., 1979. Hippocampus, space, and memory. Behavioral and Brain Sciences 2, 313–322. https://doi.org/10.1017/S0140525X00062713

Olton, D.S., Samuelson, R.J., 1976. Remembrance of places passed: Spatial memory in rats. Journal of Experimental Psychology: Animal Behavior Processes 2, 97–116. https://doi.org/10.1037/0097-7403.2.2.97

O'Reilly, K.C., Flatberg, A., Islam, S., Olsen, L.C., Kruge, I.U., Witter, M.P., 2015. Identification of dorsal–ventral hippocampal differentiation in neonatal rats. Brain Struct Funct 220, 2873–2893. https://doi.org/10.1007/s00429-014-0831-8

Orlando, M., Dvorzhak, A., Bruentgens, F., Maglione, M., Rost, B.R., Sigrist, S.J., Breustedt, J., Schmitz, D., 2021. Recruitment of release sites underlies chemical presynaptic potentiation at hippocampal mossy fiber boutons. PLOS Biology 19, e3001149. https://doi.org/10.1371/journal.pbio.3001149

O'Shea, A., Cohen, R., Porges, E., Nissim, N., Woods, A., 2016. Cognitive Aging and the Hippocampus in Older Adults. Frontiers in Aging Neuroscience 8.

- P -

Palotai, M., Schregel, K., Nazari, N., Merchant, J.P., Taylor, W.M., Guttmann, C.R.G., Sinkus, R., Young-Pearse, T.L., Patz, S., 2022. Magnetic resonance elastography to study the effect of amyloid plaque accumulation in a mouse model. J Neuroimaging 32, 617–628. https://doi.org/10.1111/jon.12996

Pan, C.-L., Howell, J.E., Clark, S.G., Hilliard, M., Cordes, S., Bargmann, C.I., Garriga, G., 2006. Multiple Wnts and frizzled receptors regulate anteriorly directed cell and growth cone migrations in Caenorhabditis elegans. Dev Cell 10, 367–377. https://doi.org/10.1016/j.devcel.2006.02.010

Park, M., Moon, R.T., 2002. The planar cell-polarity gene stbm regulates cell behaviour and cell fate in vertebrate embryos. Nature Cell Biology 4, 20–25. https://doi.org/10.1038/ncb716

Parra, P., Gulyás, A.I., Miles, R., 1998. How Many Subtypes of Inhibitory Cells in the Hippocampus? Neuron 20, 983–993. https://doi.org/10.1016/S0896-6273(00)80479-1

Pasaoglu, T., Schikorski, T., 2016. Presynaptic size of associational/commissural CA3 synapses is controlled by fibroblast growth factor 22 in adult mice. Hippocampus 26, 151–160. https://doi.org/10.1002/hipo.22499

Pelkey, K.A., Chittajallu, R., Craig, M.T., Tricoire, L., Wester, J.C., McBain, C.J., 2017. Hippocampal GABAergic Inhibitory Interneurons. Physiol Rev 97, 1619–1747. https://doi.org/10.1152/physrev.00007.2017

Perea, G., Navarrete, M., Araque, A., 2009. Tripartite synapses: astrocytes process and control synaptic information. Trends Neurosci 32, 421–431. https://doi.org/10.1016/j.tins.2009.05.001

Phillips, R.G., LeDoux, J.E., 1992. Differential contribution of amygdala and hippocampus to cued and contextual fear conditioning. Behav Neurosci 106, 274–285. https://doi.org/10.1037//0735-7044.106.2.274

Piekema, C., Fernández, G., Postma, A., Hendriks, M.P.H., Wester, A.J., Kessels, R.P.C., 2007. Spatial and non-spatial contextual working memory in patients with diencephalic or hippocampal dysfunction. Brain Res 1172, 103–109. https://doi.org/10.1016/j.brainres.2007.07.066

Popov, V.I., Kleschevnikov, A.M., Klimenko, O.A., Stewart, M.G., Belichenko, P.V., 2011. Three-dimensional synaptic ultrastructure in the dentate gyrus and hippocampal area CA3 in the Ts65Dn mouse model of down syndrome. Journal of Comparative Neurology 519, 1338–1354. https://doi.org/10.1002/cne.22573

Porcher, L., Bruckmeier, S., Burbano, S.D., Finnell, J.E., Gorny, N., Klett, J., Wood, S.K., Kelly, M.P., 2021. Aging triggers an upregulation of a multitude of cytokines in the male and especially the female rodent hippocampus but more discrete changes in other brain regions. Journal of Neuroinflammation 18, 219. https://doi.org/10.1186/s12974-021-02252-6

- Q -

Qu, Y., Huang, Y., Feng, J., Alvarez-Bolado, G., Grove, E.A., Yang, Y., Tissir, F., Zhou, L., Goffinet, A.M., 2014. Genetic evidence that Celsr3 and Celsr2, together with Fzd3, regulate forebrain wiring in a Vangl-independent manner. Proc Natl Acad Sci U S A 111, E2996–E3004. https://doi.org/10.1073/pnas.1402105111

- R -

Ramon y Cajal, S., 1911. Histologie du système nerveux de l'Homme et des vertébrés, Maloine. ed. Paris.

Ramsbottom, S.A., Sharma, V., Rhee, H.J., Eley, L., Phillips, H.M., Rigby, H.F., Dean, C., Chaudhry, B., Henderson, D.J., 2014. Vangl2-Regulated Polarisation of Second Heart Field-Derived Cells Is Required for Outflow Tract Lengthening during Cardiac Development. PLoS Genet 10, e1004871. https://doi.org/10.1371/journal.pgen.1004871

Rebola, N., Carta, M., Lanore, F., Blanchet, C., Mulle, C., 2011. NMDA receptor–dependent metaplasticity at hippocampal mossy fiber synapses. Nature Neuroscience 14, 691–693. https://doi.org/10.1038/nn.2809

Rebola, N., Carta, M., Mulle, C., 2017. Operation and plasticity of hippocampal CA3 circuits: implications for memory encoding. Nat Rev Neurosci 18, 208–220. https://doi.org/10.1038/nrn.2017.10

Rebola, N., Lujan, R., Cunha, R.A., Mulle, C., 2008. Adenosine A2A Receptors Are Essential for Long-Term Potentiation of NMDA-EPSCs at Hippocampal Mossy Fiber Synapses. Neuron 57, 121–134. https://doi.org/10.1016/j.neuron.2007.11.023

Reichel, J. m., Bedenk, B. t., Czisch, M., Wotjak, C. t., 2017. Age-related cognitive decline coincides with accelerated volume loss of the dorsal but not ventral hippocampus in mice. Hippocampus 27, 28–35. https://doi.org/10.1002/hipo.22668

Rickmann, M., Amaral, D.G., Cowan, W.M., 1987. Organization of radial glial cells during the development of the rat dentate gyrus. Journal of Comparative Neurology 264, 449–479. https://doi.org/10.1002/cne.902640403

Robain, O., Barbin, G., Billette de Villemeur, T., Jardin, L., Jahchan, T., Ben-Ari, Y., 1994. Development of mossy fiber synapses in hippocampal slice culture. Brain Res Dev Brain Res 80, 244–250. https://doi.org/10.1016/0165-3806(94)90109-0

Robert, B.J.A., Moreau, M.M., Dos Santos Carvalho, S., Barthet, G., Racca, C., Bhouri, M., Quiedeville, A., Garret, M., Atchama, B., Al Abed, A.S., Guette, C., Henderson, D.J., Desmedt, A., Mulle, C., Marighetto, A., Montcouquiol, M., Sans, N., 2020. Vangl2 in the Dentate Network Modulates Pattern Separation and Pattern Completion. Cell Reports 31, 107743. https://doi.org/10.1016/j.celrep.2020.107743

Rodríguez, J.J., Yeh, C.-Y., Terzieva, S., Olabarria, M., Kulijewicz-Nawrot, M., Verkhratsky, A., 2014. Complex and region-specific changes in astroglial markers in the aging brain. Neurobiology of Aging 35, 15–23. https://doi.org/10.1016/j.neurobiolaging.2013.07.002

Roh, J.D., Choi, Su-Yeon, Cho, Y.S., Choi, T.-Y., Park, J.-S., Cutforth, T., Chung, W., Park, H., Lee, D., Kim, M.-H., Lee, Y., Mo, S., Rhee, J.-S., Kim, H., Ko, J., Choi, Se-Young, Bae, Y.C., Shen, K., Kim, E., Han, K., 2017. Increased Excitatory Synaptic Transmission of Dentate Granule Neurons in Mice Lacking PSD-95-Interacting Adhesion Molecule Neph2/Kirrel3 during the Early Postnatal Period. Front Mol Neurosci 10, 81. https://doi.org/10.3389/fnmol.2017.00081

Rollenhagen, A., Lübke, J.H.R., 2006. The morphology of excitatory central synapses: from structure to function. Cell Tissue Res 326, 221–237. https://doi.org/10.1007/s00441-006-0288-z

Rollenhagen, A., Sätzler, K., Rodríguez, E.P., Jonas, P., Frotscher, M., Lübke, J.H.R., 2007. Structural Determinants of Transmission at Large Hippocampal Mossy Fiber Synapses. J. Neurosci. 27, 10434–10444. https://doi.org/10.1523/JNEUROSCI.1946-07.2007

Rolls, E.T., 2018. The storage and recall of memories in the hippocampo-cortical system. Cell Tissue Res 373, 577–604. https://doi.org/10.1007/s00441-017-2744-3

Rolls, E.T., 2016. Pattern separation, completion, and categorisation in the hippocampus and neocortex. Neurobiology of Learning and Memory, Pattern Separation and Pattern Completion in the Hippocampal System 129, 4–28. https://doi.org/10.1016/j.nlm.2015.07.008

Roszko, I., Sawada, A., Solnica-Krezel, L., 2009. Regulation of convergence and extension movements during vertebrate gastrulation by the Wnt/PCP pathway. Semin Cell Dev Biol 20, 986–997. https://doi.org/10.1016/j.semcdb.2009.09.004

Ruediger, S., Vittori, C., Bednarek, E., Genoud, C., Strata, P., Sacchetti, B., Caroni, P., 2011. Learning-related feedforward inhibitory connectivity growth required for memory precision. Nature 473, 514–518. https://doi.org/10.1038/nature09946

- S -

Sai, K., Wang, S., Kaito, A., Fujiwara, T., Maruo, T., Itoh, Y., Miyata, M., Sakakibara, S., Miyazaki, N., Murata, K., Yamaguchi, Y., Haruta, T., Nishioka, H., Motojima, Y., Komura, M., Kimura, K., Mandai, K., Takai, Y., Mizoguchi, A., 2017. Multiple roles of afadin in the ultrastructural morphogenesis of mouse hippocampal mossy fiber synapses. Journal of Comparative Neurology 525, 2719–2734. https://doi.org/10.1002/cne.24238

Saied-Santiago, K., Bülow, H.E., 2018. Diverse Roles for Glycosaminoglycans in Neural Patterning. Dev Dyn 247, 54–74. https://doi.org/10.1002/dvdy.24555

Salin, P.A., Scanziani, M., Malenka, R.C., Nicoll, R.A., 1996. Distinct short-term plasticity at two excitatory synapses in the hippocampus. Proc Natl Acad Sci U S A 93, 13304–13309.

Salin, P.A., Weisskopf, M.G., Nicoll, R.A., 1995. A comparison of the role of dynorphin in the hippocampal mossy fiber pathway in guinea pig and rat. J. Neurosci. 15, 6939–6945. https://doi.org/10.1523/JNEUROSCI.15-10-06939.1995

Sandler, R., Smith, A.D., 1991. Coexistence of GABA and glutamate in mossy fiber terminals of the primate hippocampus: An ultrastructural study. Journal of Comparative Neurology 303, 177–192. https://doi.org/10.1002/cne.903030202

Sans, N., Ezan, J., Moreau, M.M., Montcouquiol, M., 2016. Planar Cell Polarity Gene Mutations in Autism Spectrum Disorder, Intellectual Disabilities, and Related Deletion/Duplication Syndromes, in: Neuronal and Synaptic Dysfunction in Autism Spectrum Disorder and Intellectual Disability. Elsevier, pp. 189–219. https://doi.org/10.1016/B978-0-12-800109-7.00013-3

Sarrazin, S., Lamanna, W.C., Esko, J.D., 2011. Heparan Sulfate Proteoglycans. Cold Spring Harb Perspect Biol 3, a004952. https://doi.org/10.1101/cshperspect.a004952

Schambony, A., Wedlich, D., 2007. Wnt-5A/Ror2 regulate expression of XPAPC through an alternative noncanonical signaling pathway. Dev Cell 12, 779–792. https://doi.org/10.1016/j.devcel.2007.02.016

Scharkowski, F., Frotscher, M., Lutz, D., Korte, M., Michaelsen-Preusse, K., 2018. Altered Connectivity and Synapse Maturation of the Hippocampal Mossy Fiber Pathway in a Mouse Model of the Fragile X Syndrome. Cerebral Cortex 28, 852–867. https://doi.org/10.1093/cercor/bhw408

Scheff, S.W., Price, D.A., Schmitt, F.A., Mufson, E.J., 2006. Hippocampal synaptic loss in early Alzheimer's disease and mild cognitive impairment. Neurobiol Aging 27, 1372–1384. https://doi.org/10.1016/j.neurobiolaging.2005.09.012

Schreurs, A., Sabanov, V., Balschun, D., 2017. Distinct Properties of Long-Term Potentiation in the Dentate Gyrus along the Dorsoventral Axis: Influence of Age and Inhibition. Sci Rep 7, 5157. https://doi.org/10.1038/s41598-017-05358-1

Scoville, W.B., Milner, B., 1957. Loss of recent memory after bilateral hippocampal lesions. 1957. J Neuropsychiatry Clin Neurosci 12, 103–113. https://doi.org/10.1176/jnp.12.1.103

Sellers, K.J., Elliott, C., Jackson, J., Ghosh, A., Ribe, E., Rojo, A.I., Jarosz-Griffiths, H.H., Watson, I.A., Xia, W., Semenov, M., Morin, P., Hooper, N.M., Porter, R., Preston, J., Al-Shawi, R., Baillie, G., Lovestone, S., Cuadrado, A., Harte, M., Simons, P., Srivastava, D.P., Killick, R., 2018. Amyloid β synaptotoxicity is Wnt-PCP dependent and blocked by fasudil. Alzheimers Dement 14, 306–317. https://doi.org/10.1016/j.jalz.2017.09.008

Seo, H.-S., Habas, R., Chang, C., Wang, J., 2017. Bimodal regulation of Dishevelled function by Vangl2 during morphogenesis. Hum Mol Genet 26, 2053–2061. https://doi.org/10.1093/hmg/ddx095

Shafer, B., Onishi, K., Lo, C., Colakoglu, G., Zou, Y., 2011. Vangl2 promotes Wnt/Planar Cell Polarity-like signaling by antagonizing Dvl1-mediated feedback inhibition in growth cone guidance. Dev Cell 20, 177–191. https://doi.org/10.1016/j.devcel.2011.01.002

Shepherd, G.M.G., Harris, K.M., 1998. Three-Dimensional Structure and Composition of CA3→CA1 Axons in Rat Hippocampal Slices: Implications for Presynaptic Connectivity and Compartmentalization. J. Neurosci. 18, 8300–8310. https://doi.org/10.1523/JNEUROSCI.18-20-08300.1998

Shigemoto, R., Kinoshita, A., Wada, E., Nomura, S., Ohishi, H., Takada, M., Flor, P.J., Neki, A., Abe, T., Nakanishi, S., Mizuno, N., 1997. Differential Presynaptic Localization of Metabotropic Glutamate Receptor Subtypes in the Rat

Hippocampus. J Neurosci 17, 7503–7522. https://doi.org/10.1523/JNEUROSCI.17-19-07503.1997

Shima, A., Nitta, N., Suzuki, F., Laharie, A.-M., Nozaki, K., Depaulis, A., 2015. Activation of mTOR signaling pathway is secondary to neuronal excitability in a mouse model of mesio-temporal lobe epilepsy. European Journal of Neuroscience 41, 976–988. https://doi.org/10.1111/ejn.12835

Shimada, Y., Usui, T., Yanagawa, S., Takeichi, M., Uemura, T., 2001. Asymmetric colocalization of Flamingo, a seven-pass transmembrane cadherin, and Dishevelled in planar cell polarization. Current Biology 11, 859–863. https://doi.org/10.1016/S0960-9822(01)00233-0

Shimizu, K., Sato, M., Tabata, T., 2011. The Wnt5/Planar Cell Polarity Pathway Regulates Axonal Development of the Drosophila Mushroom Body Neuron. J Neurosci 31, 4944–4954. https://doi.org/10.1523/JNEUROSCI.0154-11.2011

Shindo, A., 2018. Models of convergent extension during morphogenesis. WIREs Developmental Biology 7, e293. https://doi.org/10.1002/wdev.293

Shindo, A., Inoue, Y., Kinoshita, M., Wallingford, J.B., 2019. PCP-dependent transcellular regulation of actomyosin oscillation facilitates convergent extension of vertebrate tissue. Developmental Biology 446, 159–167. https://doi.org/10.1016/j.ydbio.2018.12.017

Sierra, A., Gottfried-Blackmore, A.C., McEwen, B.S., Bulloch, K., 2007. Microglia derived from aging mice exhibit an altered inflammatory profile. Glia 55, 412–424. https://doi.org/10.1002/glia.20468

Silva, S.V. da, Zhang, P., Haberl, M.G., Labrousse, V., Grosjean, N., Blanchet, C., Frick, A., Mulle, C., 2019. Hippocampal Mossy Fibers Synapses in CA3 Pyramidal Cells Are Altered at an Early Stage in a Mouse Model of Alzheimer's Disease. J. Neurosci. 39, 4193–4205. https://doi.org/10.1523/JNEUROSCI.2868-18.2019

Singh, J., Mlodzik, M., 2012. Planar cell polarity signaling: coordination of cellular orientation across tissues. WIREs Developmental Biology 1, 479–499. https://doi.org/10.1002/wdev.32

Sloviter, R.S., Dichter, M.A., Rachinsky, T.L., Dean, E., Goodman, J.H., Sollas, A.L., Martin, D.L., 1996. Basal expression and induction of glutamate decarboxylase GABA in excitatory granule cells of the rat and monkey hippocampal dentate gyrus. Journal of Comparative Neurology 373, 593–618. https://doi.org/10.1002/(SICI)1096-9861(19960930)373:4<593::AID-CNE8>3.0.CO;2-X

Smith, G.K., Kesner, R.P., Korenberg, J.R., 2014. Dentate Gyrus Mediates Cognitive Function in the Ts65Dn/DnJ Mouse Model of Down Syndrome. Hippocampus 24, 354–362. https://doi.org/10.1002/hipo.22229

Smith, P., Azzam, M., Hinck, L., 2017. Extracellular Regulation of the Mitotic Spindle and Fate Determinants Driving Asymmetric Cell Division. Results Probl Cell Differ 61, 351–373. https://doi.org/10.1007/978-3-319-53150-2_16

Sokol, S.Y., 1996. Analysis of Dishevelled signalling pathways during Xenopus development. Curr Biol 6, 1456–1467. https://doi.org/10.1016/s0960-9822(96)00750-6

Soldano, A., Okray, Z., Janovska, P., Tmejová, K., Reynaud, E., Claeys, A., Yan, J., Atak, Z.K., Strooper, B.D., Dura, J.-M., Bryja, V., Hassan, B.A., 2013. The Drosophila Homologue of the Amyloid Precursor Protein Is a Conserved Modulator of Wnt PCP Signaling. PLOS Biology 11, e1001562. https://doi.org/10.1371/journal.pbio.1001562

Spassky, N., Merkle, F.T., Flames, N., Tramontin, A.D., García-Verdugo, J.M., Alvarez-Buylla, A., 2005. Adult Ependymal Cells Are Postmitotic and Are Derived from Radial Glial Cells during Embryogenesis. J Neurosci 25, 10–18. https://doi.org/10.1523/JNEUROSCI.1108-04.2005

Spencer, R.L., Bland, S.T., 2019. Hippocampus and Hippocampal Neurons, in: Stress: Physiology, Biochemistry, and Pathology. Elsevier, pp. 57–68. https://doi.org/10.1016/B978-0-12-813146-6.00005-9

Squire, L.R., Zola, S.M., 1996. Structure and function of declarative and nondeclarative memory systems. Proc Natl Acad Sci U S A 93, 13515–13522. https://doi.org/10.1073/pnas.93.24.13515

Stagni, F., Magistretti, J., Guidi, S., Ciani, E., Mangano, C., Calzà, L., Bartesaghi, R., 2013. Pharmacotherapy with Fluoxetine Restores Functional Connectivity from the Dentate Gyrus to Field CA3 in the Ts65Dn Mouse Model of Down Syndrome. PLoS One 8, e61689. https://doi.org/10.1371/journal.pone.0061689

Stahley, S.N., Basta, L.P., Sharan, R., Devenport, D., 2021. Celsr1 adhesive interactions mediate the asymmetric organization of planar polarity complexes. eLife 10, e62097. https://doi.org/10.7554/eLife.62097

Stephens, M.L., Quintero, J.E., Pomerleau, F., Huettl, P., Gerhardt, G.A., 2011. Age-related changes in glutamate release in the CA3 and dentate gyrus of the rat hippocampus. Neurobiology of Aging 32, 811–820. https://doi.org/10.1016/j.neurobiolaging.2009.05.009

Stewart, S., Cacucci, F., Lever, C., 2011. Which memory task for my mouse? A systematic review of spatial memory performance in the Tg2576 Alzheimer's mouse model. J Alzheimers Dis 26, 105–126. https://doi.org/10.3233/JAD-2011-101827

Strong, L.C., Hollander, W.F., 1949. HEREDITARY LOOP-TAIL IN THE HOUSE MOUSEAccompanied by Imperforate Vagina and with Lethal Craniorachischisis When Homozygous. J Hered 40, 329–334. https://doi.org/10.1093/oxfordjournals.jhered.a105976

Struhl, G., Casal, J., Lawrence, P.A., 2012. Dissecting the molecular bridges that mediate the function of Frizzled in planar cell polarity. Development 139, 3665–3674. https://doi.org/10.1242/dev.083550

Strutt, D., Strutt, H., 2007. Differential activities of the core planar polarity proteins during Drosophila wing patterning. Dev. Biol. 302, 181–194. https://doi.org/10.1016/j.ydbio.2006.09.026

Strutt, D., Warrington, S.J., 2008. Planar polarity genes in the Drosophila wing regulate the localisation of the FH3-domain protein Multiple Wing Hairs to control the site of hair production. Development 135, 3103–3111. https://doi.org/10.1242/dev.025205

Strutt, D.I., 2001. Asymmetric Localization of Frizzled and the Establishment of Cell Polarity in the Drosophila Wing. Molecular Cell 7, 367–375. https://doi.org/10.1016/S1097-2765(01)00184-8

Strutt, D.I., Weber, U., Mlodzik, M., 1997. The role of RhoA in tissue polarity and Frizzled signalling. Nature 387, 292–295. https://doi.org/10.1038/387292a0

Strutt, H., Strutt, D., 2021. How do the Fat–Dachsous and core planar polarity pathways act together and independently to coordinate polarized cell behaviours? Open Biology 11, 200356. https://doi.org/10.1098/rsob.200356

Strutt, H., Strutt, D., 2009. Asymmetric localisation of planar polarity proteins: Mechanisms and consequences. Seminars in Cell & Developmental Biology, Imaging in Cell and Developmental Biology 20, 957–963. https://doi.org/10.1016/j.semcdb.2009.03.006

Sun, Q., Sotayo, A., Cazzulino, A.S., Snyder, A.M., Denny, C.A., Siegelbaum, S.A., 2017. Proximodistal heterogeneity of hippocampal CA3 pyramidal neuron intrinsic properties, connectivity and reactivation during memory recall. Neuron 95, 656-672.e3. https://doi.org/10.1016/j.neuron.2017.07.012

Suto, F., Tsuboi, M., Kamiya, H., Mizuno, H., Kiyama, Y., Komai, S., Shimizu, M., Sanbo, M., Yagi, T., Hiromi, Y., Chédotal, A., Mitchell, K.J., Manabe, T., Fujisawa, H., 2007. Interactions between Plexin-A2, Plexin-A4, and Semaphorin 6A Control Lamina-Restricted Projection of Hippocampal Mossy Fibers. Neuron 53, 535–547. https://doi.org/10.1016/j.neuron.2007.01.028

Sutula, T., Cascino, G., Cavazos, J., Parada, I., Ramirez, L., 1989. Mossy fiber synaptic reorganization in the epileptic human temporal lobe. Ann Neurol 26, 321–330. https://doi.org/10.1002/ana.410260303

Sydow, A., Jeugd, A.V. der, Zheng, F., Ahmed, T., Balschun, D., Petrova, O., Drexler, D., Zhou, L., Rune, G., Mandelkow, E., D'Hooge, R., Alzheimer, C., Mandelkow, E.-M., 2011. Tau-Induced Defects in Synaptic Plasticity, Learning, and Memory Are Reversible in Transgenic Mice after Switching Off the Toxic Tau Mutant. J. Neurosci. 31, 2511–2525. https://doi.org/10.1523/JNEUROSCI.5245-10.2011

- T -

Takai, Y., Shimizu, K., Ohtsuka, T., 2003. The roles of cadherins and nectins in interneuronal synapse formation. Current Opinion in Neurobiology 13, 520–526. https://doi.org/10.1016/j.conb.2003.09.003

Takumi, Y., Ramírez-León, V., Laake, P., Rinvik, E., Ottersen, O.P., 1999. Different modes of expression of AMPA and NMDA receptors in hippocampal synapses. Nature Neuroscience 2, 618–624. https://doi.org/10.1038/10172

Tanaka, J., Okuma, Y., Tomobe, K., Nomura, Y., 2005. The Age-Related Degeneration of Oligodendrocytes in the Hippocampus of the Senescence-Accelerated Mouse (SAM) P8: A Quantitative Immunohistochemical Study. Biological and Pharmaceutical Bulletin 28, 615–618. https://doi.org/10.1248/bpb.28.615

Tashiro, A., Sandler, V.M., Toni, N., Zhao, C., Gage, F.H., 2006. NMDA-receptor-mediated, cell-specific integration of new neurons in adult dentate gyrus. Nature 442, 929–933. https://doi.org/10.1038/nature05028

Tawarayama, H., Yoshida, Y., Suto, F., Mitchell, K.J., Fujisawa, H., 2010. Roles of semaphorin-6B and plexin-A2 in lamina-restricted projection of hippocampal mossy fibers. J Neurosci 30, 7049–7060. https://doi.org/10.1523/JNEUROSCI.0073-10.2010

Taylor, J., Abramova, N., Charlton, J., Adler, P.N., 1998. Van Gogh: A New Drosophila Tissue Polarity Gene. Genetics 150, 199–210.

Thakar, S., Wang, L., Yu, T., Ye, M., Onishi, K., Scott, J., Qi, J., Fernandes, C., Han, X., Yates, J.R., Berg, D.K., Zou, Y., 2017. Evidence for opposing roles of Celsr3 and Vangl2 in glutamatergic synapse formation. Proc Natl Acad Sci U S A 114, E610–E618. https://doi.org/10.1073/pnas.1612062114

Thomas, C., Strutt, D., 2012. The roles of the cadherins Fat and Dachsous in planar polarity specification in Drosophila. Developmental Dynamics 241, 27–39. https://doi.org/10.1002/dvdy.22736

Thompson, L.T., Best, P.J., 1990. Long-term stability of the place-field activity of single units recorded from the dorsal hippocampus of freely behaving rats. Brain Res 509, 299–308. https://doi.org/10.1016/0006-8993(90)90555-p

Tissir, F., Bar, I., Jossin, Y., De Backer, O., Goffinet, A.M., 2005. Protocadherin Celsr3 is crucial in axonal tract development. Nat Neurosci 8, 451–457. https://doi.org/10.1038/nn1428

Tissir, F., Goffinet, A.M., 2006. Expression of planar cell polarity genes during development of the mouse CNS. European Journal of Neuroscience 23, 597–607. https://doi.org/10.1111/j.1460-9568.2006.04596.x

Tissir, F., Qu, Y., Montcouquiol, M., Zhou, L., Komatsu, K., Shi, D., Fujimori, T., Labeau, J., Tyteca, D., Courtoy, P., Poumay, Y., Uemura, T., Goffinet, A.M.,

2010. Lack of cadherins Celsr2 and Celsr3 impairs ependymal ciliogenesis, leading to fatal hydrocephalus. Nature Neuroscience 13, 700–707. https://doi.org/10.1038/nn.2555

Toni, N., Laplagne, D.A., Zhao, C., Lombardi, G., Ribak, C.E., Gage, F.H., Schinder, A.F., 2008. Neurons born in the adult dentate gyrus form functional synapses with target cells. Nat Neurosci 11, 901–907. https://doi.org/10.1038/nn.2156

Toni, N., Schinder, A.F., 2016. Maturation and Functional Integration of New Granule Cells into the Adult Hippocampus. Cold Spring Harb Perspect Biol 8, a018903. https://doi.org/10.1101/cshperspect.a018903

Topczewski, J., Sepich, D.S., Myers, D.C., Walker, C., Amores, A., Lele, Z., Hammerschmidt, M., Postlethwait, J., Solnica-Krezel, L., 2001. The Zebrafish Glypican Knypek Controls Cell Polarity during Gastrulation Movements of Convergent Extension. Developmental Cell 1, 251–264. https://doi.org/10.1016/S1534-5807(01)00005-3

Torban, E., Iliescu, A., Gros, P., 2012. Chapter Ten - An Expanding Role of Vangl Proteins in Embryonic Development, in: Yang, Y. (Ed.), Current Topics in Developmental Biology, Planar Cell Polarity During Development. Academic Press, pp. 237–261. https://doi.org/10.1016/B978-0-12-394592-1.00005-3

Torban, E., Kor, C., Gros, P., 2004a. Van Gogh-like2 (Strabismus) and its role in planar cell polarity and convergent extension in vertebrates. Trends in Genetics 20, 570–577. https://doi.org/10.1016/j.tig.2004.09.003

Torban, E., Patenaude, A.-M., Leclerc, S., Rakowiecki, S., Gauthier, S., Andelfinger, G., Epstein, D.J., Gros, P., 2008. Genetic interaction between members of the Vangl family causes neural tube defects in mice. Proc Natl Acad Sci U S A 105, 3449–3454. https://doi.org/10.1073/pnas.0712126105

Torban, E., Wang, H.-J., Groulx, N., Gros, P., 2004b. Independent Mutations in Mouse Vangl2 That Cause Neural Tube Defects in Looptail Mice Impair Interaction with Members of the Dishevelled Family. J. Biol. Chem. 279, 52703–52713. https://doi.org/10.1074/jbc.M408675200

Torban, E., Wang, H.-J., Patenaude, A.-M., Riccomagno, M., Daniels, E., Epstein, D., Gros, P., 2007. Tissue, cellular and sub-cellular localization of the Vangl2 protein during embryonic development: effect of the Lp mutation. Gene Expr Patterns 7, 346–354. https://doi.org/10.1016/j.modgep.2006.07.007

Toth, K., Suares, G., Lawrence, J.J., Philips-Tansey, E., McBain, C.J., 2000. Differential Mechanisms of Transmission at Three Types of Mossy Fiber Synapse. J Neurosci 20, 8279–8289. https://doi.org/10.1523/JNEUROSCI.20-22-08279.2000

Toyoshima, D., Mandai, K., Maruo, T., Supriyanto, I., Togashi, H., Inoue, T., Mori, M., Takai, Y., 2014. Afadin regulates puncta adherentia junction formation and

presynaptic differentiation in hippocampal neurons. PLoS One 9, e89763. https://doi.org/10.1371/journal.pone.0089763

Treat, A.C., Wheeler, D.S., Stolz, D.B., Tsang, M., Friedman, P.A., Romero, G., 2016. The PDZ Protein Na+/H+ Exchanger Regulatory Factor-1 (NHERF1) Regulates Planar Cell Polarity and Motile Cilia Organization. PLoS One 11. https://doi.org/10.1371/journal.pone.0153144

Tremblay, M.-È., Riad, M., Chierzi, S., Murai, K.K., Pasquale, E.B., Doucet, G., 2009. Developmental course of EphA4 cellular and subcellular localization in the postnatal rat hippocampus. Journal of Comparative Neurology 512, 798–813. https://doi.org/10.1002/cne.21922

Trinchero, M.F., Herrero, M., Monzón-Salinas, M.C., Schinder, A.F., 2019. Experience-Dependent Structural Plasticity of Adult-Born Neurons in the Aging Hippocampus. Front Neurosci 13, 739. https://doi.org/10.3389/fnins.2019.00739

Tronel, S., Belnoue, L., Grosjean, N., Revest, J.-M., Piazza, P.-V., Koehl, M., Abrous, D.N., 2012. Adult-born neurons are necessary for extended contextual discrimination. Hippocampus 22, 292–298. https://doi.org/10.1002/hipo.20895

Tronel, S., Fabre, A., Charrier, V., Oliet, S.H.R., Gage, F.H., Abrous, D.N., 2010. Spatial learning sculpts the dendritic arbor of adult-born hippocampal neurons. Proc Natl Acad Sci U S A 107, 7963–7968. https://doi.org/10.1073/pnas.0914613107

Tulving, E., 2002. Episodic Memory: From Mind to Brain. Annual Review of Psychology 53, 1–25. https://doi.org/10.1146/annurev.psych.53.100901.135114

- U -

Urban, N.N., Henze, D.A., Barrionuevo, G., 2001. Revisiting the role of the hippocampal mossy fiber synapse. Hippocampus 11, 408–417. https://doi.org/10.1002/hipo.1055

- V -

van Strien, N.M., Cappaert, N.L.M., Witter, M.P., 2009. The anatomy of memory: an interactive overview of the parahippocampal–hippocampal network. Nat Rev Neurosci 10, 272–282. https://doi.org/10.1038/nrn2614

Vandael, D., Borges-Merjane, C., Zhang, X., Jonas, P., 2020. Short-Term Plasticity at Hippocampal Mossy Fiber Synapses Is Induced by Natural Activity Patterns and Associated with Vesicle Pool Engram Formation. Neuron 107, 509-521.e7. https://doi.org/10.1016/j.neuron.2020.05.013

VanGuilder, H.D., Yan, H., Farley, J.A., Sonntag, W.E., Freeman, W.M., 2010. Aging alters the expression of neurotransmission-regulating proteins in the

hippocampal synaptoproteome. Journal of Neurochemistry 113, 1577–1588. https://doi.org/10.1111/j.1471-4159.2010.06719.x

Vaughn, J.E., Matthews, D.A., Barber, R.P., Wimer, C.C., Wimer, R.E., 1977. Genetically-associated variations in the development of hippocampal pyramidal neurons may produce differences in mossy fiber connectivity. Journal of Comparative Neurology 173, 41–51. https://doi.org/10.1002/cne.901730104

Veldsman, M., Nobis, L., Alfaro-Almagro, F., Manohar, S., Husain, M., 2021. The human hippocampus and its subfield volumes across age, sex and APOE e4 status. Brain Communications 3, fcaa219. https://doi.org/10.1093/braincomms/fcaa219

Verma, V., Paul, A., Amrapali Vishwanath, A., Vaidya, B., Clement, J.P., 2019. Understanding intellectual disability and autism spectrum disorders from common mouse models: synapses to behaviour. Open Biol 9, 180265. https://doi.org/10.1098/rsob.180265

Viana da Silva, S., Haberl, M.G., Zhang, P., Bethge, P., Lemos, C., Gonçalves, N., Gorlewicz, A., Malezieux, M., Gonçalves, F.Q., Grosjean, N., Blanchet, C., Frick, A., Nägerl, U.V., Cunha, R.A., Mulle, C., 2016. Early synaptic deficits in the APP/PS1 mouse model of Alzheimer's disease involve neuronal adenosine A2A receptors. Nat Commun 7, 11915. https://doi.org/10.1038/ncomms11915

Vicari, S., 2004. Memory development and intellectual disabilities. Acta Paediatrica 93, 60–63. https://doi.org/10.1111/j.1651-2227.2004.tb03059.x

Vicari, S., Costanzo, F., Menghini, D., 2016. Chapter Four - Memory and Learning in Intellectual Disability, in: Hodapp, R.M., Fidler, D.J. (Eds.), International Review of Research in Developmental Disabilities, Fifty Years of Research in Intellectual and Developmental Disabilities. Academic Press, pp. 119–148. https://doi.org/10.1016/bs.irrdd.2016.05.003

Vichas, A., Zallen, J.A., 2011. Translating cell polarity into tissue elongation. Semin Cell Dev Biol 22, 858–864. https://doi.org/10.1016/j.semcdb.2011.09.013

Villanueva-Castillo, C., Tecuatl, C., Herrera-López, G., Galván, E.J., 2017. Aging-related impairments of hippocampal mossy fibers synapses on CA3 pyramidal cells. Neurobiology of Aging 49, 119–137. https://doi.org/10.1016/j.neurobiolaging.2016.09.010

Vinet, J., Lemieux, P., Tamburri, A., Tiesinga, P., Scafidi, J., Gallo, V., Sík, A., 2010. Subclasses of oligodendrocytes populate the mouse hippocampus. European Journal of Neuroscience 31, 425–438. https://doi.org/10.1111/j.1460-9568.2010.07082.x

Vinson, C.R., Adler, P.N., 1987. Directional non-cell autonomy and the transmission of polarity information by the frizzled gene of Drosophila. Nature 329, 549–551. https://doi.org/10.1038/329549a0

Vivancos, V., Chen, P., Spassky, N., Qian, D., Dabdoub, A., Kelley, M., Studer, M., Guthrie, S., 2009. Wnt activity guides facial branchiomotor neuron migration, and involves the PCP pathway and JNK and ROCK kinases. Neural Development 4, 7. https://doi.org/10.1186/1749-8104-4-7

Von Bohlen und Halbach, O., Unsicker, K., 2002. Morphological alterations in the amygdala and hippocampus of mice during ageing. European Journal of Neuroscience 16, 2434–2440. https://doi.org/10.1046/j.1460-9568.2002.02405.x

Vorhees, C.V., Williams, M.T., 2014. Assessing Spatial Learning and Memory in Rodents. ILAR J 55, 310–332. https://doi.org/10.1093/ilar/ilu013

- W -

Wallingford, J.B., 2012. Planar cell polarity and the developmental control of cell behavior in vertebrate embryos. Annu Rev Cell Dev Biol 28, 627–653. https://doi.org/10.1146/annurev-cellbio-092910-154208

Walsh, T.J., Schulz, D.W., Tilson, H.A., Schmechel, D.E., 1986. Colchicine-induced granule cell loss in rat hippocampus: selective behavioral and histological alterations. Brain Res 398, 23–36. https://doi.org/10.1016/0006-8993(86)91246-1

Wang, J., Hamblet, N.S., Mark, S., Dickinson, M.E., Brinkman, B.C., Segil, N., Fraser, S.E., Chen, P., Wallingford, J.B., Wynshaw-Boris, A., 2006. Dishevelled genes mediate a conserved mammalian PCP pathway to regulate convergent extension during neurulation. Development 133, 1767–1778. https://doi.org/10.1242/dev.02347

Wang, M., de Marco, P., Capra, V., Kibar, Z., 2019. Update on the Role of the Non-Canonical Wnt/Planar Cell Polarity Pathway in Neural Tube Defects. Cells 8, 1198. https://doi.org/10.3390/cells8101198

Wang, Y., Nathans, J., 2007. Tissue/planar cell polarity in vertebrates: new insights and new questions. Development 134, 647–658. https://doi.org/10.1242/dev.02772

Wang, Y., Thekdi, N., Smallwood, P.M., Macke, J.P., Nathans, J., 2002. Frizzled-3 Is Required for the Development of Major Fiber Tracts in the Rostral CNS. J. Neurosci. 22, 8563–8573. https://doi.org/10.1523/JNEUROSCI.22-19-08563.2002

Wansleeben, C., Feitsma, H., Montcouquiol, M., Kroon, C., Cuppen, E., Meijlink, F., 2010. Planar cell polarity defects and defective Vangl2 trafficking in mutants for the COPII gene Sec24b. Development 137, 1067–1073. https://doi.org/10.1242/dev.041434

Watanabe, M., Fukaya, M., Sakimura, K., Manabe, T., Mishina, M., Inoue, Y., 1998. Selective scarcity of NMDA receptor channel subunits in the stratum lucidum

(mossy fibre-recipient layer) of the mouse hippocampal CA3 subfield. European Journal of Neuroscience 10, 478–487. https://doi.org/10.1046/j.1460-9568.1998.00063.x

Weinberger, D.R., 1999. Cell biology of the hippocampal formation in schizophrenia. Biol Psychiatry 45, 395–402. https://doi.org/10.1016/s0006-3223(98)00331-x

Weisskopf, M.G., Zalutskyt, R.A., NicoHt, R.A., 1993. The opioid peptide dynorphin mediates heterosynaptic depression of hippocampal mossy fibre synapses and modulates long-term potentiation 362, 5.

Weng, F.-J., Garcia, R.I., Lutzu, S., Alviña, K., Zhang, Y., Dushko, M., Ku, T., Zemoura, K., Rich, D., Garcia-Dominguez, D., Hung, M., Yelhekar, T.D., Sørensen, A.T., Xu, W., Chung, K., Castillo, P.E., Lin, Y., 2018. Npas4 Is a Critical Regulator of Learning-Induced Plasticity at Mossy Fiber-CA3 Synapses during Contextual Memory Formation. Neuron 97, 1137-1152.e5. https://doi.org/10.1016/j.neuron.2018.01.026

West, M.J., 1993. Regionally specific loss of neurons in the aging human hippocampus. Neurobiol Aging 14, 287–293. https://doi.org/10.1016/0197-4580(93)90113-p

Wiera, G., Mozrzymas, J.W., 2015. Extracellular proteolysis in structural and functional plasticity of mossy fiber synapses in hippocampus. Front Cell Neurosci 9, 427. https://doi.org/10.3389/fncel.2015.00427

Wilke, S.A., Antonios, J.K., Bushong, E.A., Badkoobehi, A., Malek, E., Hwang, M., Terada, M., Ellisman, M.H., Ghosh, A., 2013. Deconstructing complexity: serial block-face electron microscopic analysis of the hippocampal mossy fiber synapse. J. Neurosci. 33, 507–522. https://doi.org/10.1523/JNEUROSCI.1600-12.2013

Wilke, S.A., Raam, T., Antonios, J.K., Bushong, E.A., Koo, E.H., Ellisman, M.H., Ghosh, A., 2014. Specific disruption of hippocampal mossy fiber synapses in a mouse model of familial Alzheimer's disease. PLoS ONE 9, e84349. https://doi.org/10.1371/journal.pone.0084349

Williams, B.B., Cantrell, V.A., Mundell, N.A., Bennett, A.C., Quick, R.E., Jessen, J.R., 2012. VANGL2 regulates membrane trafficking of MMP14 to control cell polarity and migration. J. Cell. Sci. 125, 2141–2147. https://doi.org/10.1242/jcs.097964

Williams, M.E., Wilke, S.A., Daggett, A., Davis, E., Otto, S., Ravi, D., Ripley, B., Bushong, E.A., Ellisman, M.H., Klein, G., Ghosh, A., 2011. Cadherin-9 regulates synapse-specific differentiation in the developing hippocampus. Neuron 71, 640–655. https://doi.org/10.1016/j.neuron.2011.06.019

Wilson, I.A., Ikonen, S., Gallagher, M., Eichenbaum, H., Tanila, H., 2005. Age-Associated Alterations of Hippocampal Place Cells Are Subregion Specific. J. Neurosci. 25, 6877–6886. https://doi.org/10.1523/JNEUROSCI.1744-05.2005

Wisden, W., Seeburg, P., 1993. A complex mosaic of high-affinity kainate receptors in rat brain. J Neurosci 13, 3582–3598. https://doi.org/10.1523/JNEUROSCI.13-08-03582.1993

Witter, M.P., Kleven, H., Flatmoen, A.K., 2017. Comparative Contemplations on the Hippocampus. BBE 90, 15–24. https://doi.org/10.1159/000475703

Witton, J., Padmashri, R., Zinyuk, L.E., Popov, V.I., Kraev, I., Line, S.J., Jensen, T.P., Tedoldi, A., Cummings, D.M., Tybulewicz, V.L.J., Fisher, E.M.C., Bannerman, D.M., Randall, A.D., Brown, J.T., Edwards, F.A., Rusakov, D.A., Stewart, M.G., Jones, M.W., 2015. Hippocampal circuit dysfunction in the Tc1 mouse model of Down syndrome. Nat Neurosci 18, 1291–1298. https://doi.org/10.1038/nn.4072

Wolff, T., Rubin, G.M., 1998. Strabismus, a novel gene that regulates tissue polarity and cell fate decisions in Drosophila. Development 125, 1149–1159.

Wong, L.L., Adler, P.N., 1993. Tissue polarity genes of Drosophila regulate the subcellular location for prehair initiation in pupal wing cells. J Cell Biol 123, 209–221. https://doi.org/10.1083/jcb.123.1.209

Wu, J., Klein, T.J., Mlodzik, M., 2004. Subcellular Localization of Frizzled Receptors, Mediated by Their Cytoplasmic Tails, Regulates Signaling Pathway Specificity. PLoS Biol 2, e158. https://doi.org/10.1371/journal.pbio.0020158

- X -

Xavier, G.F., Oliveira-Filho, F.J., Santos, A.M., 1999. Dentate gyrus-selective colchicine lesion and disruption of performance in spatial tasks: difficulties in “place strategy” because of a lack of flexibility in the use of environmental cues? Hippocampus 9, 668–681. https://doi.org/10.1002/(SICI)1098-1063(1999)9:6<668::AID-HIPO8>3.0.CO;2-9

Xie, Y., Miao, H., Blankenship, J.T., 2018. Membrane trafficking in morphogenesis and planar polarity. Traffic 19, 679–689. https://doi.org/10.1111/tra.12580

- Y -

Yan, J., Lu, Q., Fang, X., Adler, P.N., 2009. Rho1 has multiple functions in Drosophila wing planar polarity. Dev Biol 333, 186–199. https://doi.org/10.1016/j.ydbio.2009.06.027

Yang, W., Garrett, L., Feng, D., Elliott, G., Liu, X., Wang, N., Wong, Y.M., Choi, N.T., Yang, Y., Gao, B., 2017. Wnt-induced Vangl2 phosphorylation is dose-dependently required for planar cell polarity in mammalian development. Cell Research 27, 1466. https://doi.org/10.1038/cr.2017.127

Yao, R., Natsume, Y., Noda, T., 2004. MAGI-3 is involved in the regulation of the JNK signaling pathway as a scaffold protein for frizzled and Ltap. Oncogene 23, 6023–6030. https://doi.org/10.1038/sj.onc.1207817

Yassa, M.A., Mattfeld, A.T., Stark, S.M., Stark, C.E.L., 2011. Age-related memory deficits linked to circuit-specific disruptions in the hippocampus. Proceedings of the National Academy of Sciences 108, 8873–8878. https://doi.org/10.1073/pnas.1101567108

Yasumura, M., Hagiwara, A., Hida, Y., Ohtsuka, T., 2021. Planar cell polarity protein Vangl2 and its interacting protein Ap2m1 regulate dendritic branching in cortical neurons. Genes to Cells 26, 987–998. https://doi.org/10.1111/gtc.12899

Yates, L.L., Papakrivopoulou, J., Long, D.A., Goggolidou, P., Connolly, J.O., Woolf, A.S., Dean, C.H., 2010. The planar cell polarity gene Vangl2 is required for mammalian kidney-branching morphogenesis and glomerular maturation. Hum Mol Genet 19, 4663–4676. https://doi.org/10.1093/hmg/ddq397

Yeckel, M.F., Berger, T.W., 1990. Feedforward excitation of the hippocampus by afferents from the entorhinal cortex: redefinition of the role of the trisynaptic pathway. Proc. Natl. Acad. Sci. U.S.A. 87, 5832–5836. https://doi.org/10.1073/pnas.87.15.5832

Yokoi, M., Kobayashi, K., Manabe, T., Takahashi, T., Sakaguchi, I., Katsuura, G., Shigemoto, R., Ohishi, H., Nomura, S., Nakamura, K., Nakao, K., Katsuki, M., Nakanishi, S., 1996. Impairment of Hippocampal Mossy Fiber LTD in Mice Lacking mGluR2. Science 273, 645–647. https://doi.org/10.1126/science.273.5275.645

Yoshioka, T., Hagiwara, A., Hida, Y., Ohtsuka, T., 2013. Vangl2, the planner cell polarity protein, is complexed with postsynaptic density protein PSD-95. FEBS Letters 587, 1453–1459. https://doi.org/10.1016/j.febslet.2013.03.030

Yu, D.X., Marchetto, M.C., Gage, F.H., 2014. How to make a hippocampal dentate gyrus granule neuron. Development 141, 2366–2375. https://doi.org/10.1242/dev.096776

- Z -

Zhang, P., Lu, H., Peixoto, R.T., Pines, M.K., Ge, Y., Oku, S., Siddiqui, T.J., Xie, Y., Wu, W., Archer-Hartmann, S., Yoshida, K., Tanaka, K.F., Aricescu, A.R., Azadi, P., Gordon, M.D., Sabatini, B.L., Wong, R.O.L., Craig, A.M., 2018. Heparan Sulfate Organizes Neuronal Synapses through Neurexin Partnerships. Cell 174, 1450-1464.e23. https://doi.org/10.1016/j.cell.2018.07.002

Zhao, C., Teng, E.M., Summers, R.G., Ming, G., Gage, F.H., 2006. Distinct Morphological Stages of Dentate Granule Neuron Maturation in the Adult Mouse Hippocampus. J Neurosci 26, 3–11. https://doi.org/10.1523/JNEUROSCI.3648-05.2006

Zhao, S., Studer, D., Chai, X., Graber, W., Brose, N., Nestel, S., Young, C., Rodriguez, E.P., Saetzler, K., Frotscher, M., 2012. Structural plasticity of hippocampal mossy fiber synapses as revealed by high-pressure freezing. Journal of Comparative Neurology 520, 2340–2351. https://doi.org/10.1002/cne.23040

Zucker, R.S., Regehr, W.G., 2002. Short-Term Synaptic Plasticity. Annu. Rev. Physiol. 64, 355–405. https://doi.org/10.1146/annurev.physiol.64.092501.114547

Rôle de la voie de la polarité planaire dans les fonctions cognitives dans le contexte du développement post-natal et du vieillissement

Résumé: La mauvaise compréhension de la formation et du fonctionnement du système nerveux central nous freine dans la prise en charge des troubles cognitifs. Comprendre ces mécanismes et comment ils modifient les propriétés des neurones et de leurs synapses en fonction de l'environnement et de l'âge est donc essentiel. Mon projet aborde cette problématique par l'étude originale de la protéine de la voie de la polarité planaire cellulaire (PCP) Vangl2, qui régule les dynamiques du cytosquelette pendant le développement et participe à la morphogenèse de nombreux tissus. J'étudie son rôle dans le circuit hippocampique, structure cérébrale impliquée dans la mémoire épisodique et la discrimination de contexte, dont le dysfonctionnement entraine des troubles cognitifs. Je montre que Vangl2 joue un rôle dans le développement et le maintien d'une connexion spécifique au sein de l'hippocampe : la synapse formée entre les cellules granulaires du DG et les neurones pyramidaux du CA3. A l'aide d'un modèle murin de délétion précoce de Vangl2 et de techniques d'injections virales et d'imagerie, je montre que l'absence de Vangl2 retarde le développement de la synapse et affecte sa plasticité structurale chez l'adulte. De plus, à l'aide de tests comportementaux, je montre que l'absence de Vangl2 induit des troubles de certains processus mnésiques hippocampaux dépendant chez la souris adulte. Mes résultats préliminaires montrent également un rôle de Vangl2 dans les effets du vieillissement physiologique sur le circuit DG/CA3, avec un potentiel effet protecteur de la délétion précoce de vangl2 vis à vis des altérations morphofonctionelles dues au vieillissement. Les résultats obtenus au cours de ce projet de thèse permettent donc d'établir un premier lien entre la voie de la PCP, le développement et la fonction synaptique de l'hippocampe, et la régulation des processus cognitifs au cours de la vie.

Mots clés : hippocampe, mémoire, polarité planaire, plasticité, processus cognitifs

Role of the planar polarity pathway in cognitive functions in the context of postnatal development and aging

Abstract: Lack of knowledge on the mechanisms of development and function of the central nervous system are slowing our efforts to take care of people suffering from cognitive disorders. Understanding those mechanisms and their role in the modification of neuronal and synaptic properties induced by the environment during life and aging is therefore necessary. My PhD research project tackles this issue through the study of the planar cell polarity protein Vangl2, which is known to regulate cytoskeleton dynamics during development. I study the role of this protein in the hippocampus, a cerebral structure involved in episodic memory and context discrimination, which is known to be affected in some cognitive disorders. Preliminary data from the lab showed that Vangl2 is enriched postnatally in the network formed by 2 sub-regions of the hippocampus: the dentate gyrus and the CA3. My work shows that Vangl2 plays a crucial role in the development and maintenance of a specific synaptic connection in this network: the synapse formed between the granular cell of the DG and the pyramidal neurons of the CA3. Using a mice model for an early deletion of Vangl2 and techniques of virus injections and microscopy, I show that the early loss of Vangl2 delays the development of the synapse and affects its structural plasticity in adults. Using behavioural experiments, I show that the early loss of Vangl2 induces defects in some memory processes involving the hippocampus in adult mice. Interestingly, data in aging mutant mice show that the early loss of Vangl2 in the hippocampus has protective effects against the functional and morphological degradation of the DG/CA3 network linked to aging. These results show the importance of Vangl2 in the morphofunctional properties of the DG/CA3 network across development and aging and establish a link between the planar cell polarity pathway, the synaptic development and function in the hippocampus, and cognitive processes through life.

Keywords: hippocampus, memory, planar polarity, plasticity, cognitive processes

---

Neurocentre Magendie, INSERM U1215
146 rue Léo Saignat 33077 Bordeaux